UNIVERSITY OF BIRMINGHAM

DEVELOPMENT AND USES OF *IN VITRO* HEPATIC MODELS IN TOXICOLOGY STUDIES

By

NICHOLAS JAMES COLTMAN

A thesis submitted to the University of Birmingham

for the degree of

DOCTOR OF PHILOSOPHY

College of Life and Environmental Sciences
University of Birmingham
December 2021

ABSTRACT

The central role of the human liver in normal physiology gives rise to organ susceptibility in terms of the on and off-target effects of xenobiotics. The most widely used models for the study of liver biology are one of either *in vivo* murine origin or *in vitro* cell culture models; however, as is often the case, these models do not translate adequately enough to humans and thus chemical exposure risk is missed, underpredicted or underreported. Accordingly, in Chapters 2 – 3 we implemented a HepG2/C3A spheroid model generated using an optimised forced-aggregate approach, into a series of *in vitro (*geno)- toxicology and hepatotoxicity studies. Uniform spheroids, formed over 7 days, were produced with enhanced basal mRNA expression of key ADME (Nuclear receptors, *CYP450s, UGTs, SULTs*) and liver related gene sets (*ALB, CPS1, HNF4A*), when compared to monolayers of cells. Exposure to pro-genotoxicants benzo[a]pyrene, 2-aminoanthracene and 2-amino-1-methyl-6-phenylimidazo[4,5-b]pyridine revealed increased ADME and DNA damage response In spheroids versus monolayers at both the transcriptional (qRT-PCR) and phenotypical level (comet assay, quantification of γH2AX foci). In Chapter 4 we focussed on robust methods to assess single spheroid metabolism to support Chapter 5, and to reveal that cellular mitochondrial metabolism changed as a function of spheroid cell number and time. Chapter 5 therefore revealed that cellular-mitochondrial respiration was significantly altered in HepG2/C3A spheroids by extracellular flux analysis. Cells were forced to rely more heavily on oxidative phosphorylation and mitochondrial respiratory pathways than monolayers of cells, suggesting HepG2/C3A spatial geometry enhances heavier glycolytic flux usage, associated with differentiated hepatocytes, in contrast to the original cancer cell line from which they were derived. Chapter 5 further demonstrated that these metabolic changes continued in

spheroids over time, although histological and flow-cytometric analysis of spheroids indicated that the overall viability of HepG2/C3A spheroids was reduced after 28 days in culture. Given these observations, Chapter 5 further assessed the impact over 7 days of repeat dosing of 4 genotoxic and 12 well-characterised hepatotoxic compounds. Revealing that such regimens had better sensitivity at much lower dose exposure than has been reported previously. Given the utility of HepG2/C3A spheroids in long-term assays, not achievable with 2D monolayers, we looked to assess how these models diverged over time. Therefore, in Chapter 6, we acquired a large transcriptomic dataset, using paired-end RNA-sequencing, of HepG2/C3A cells cultured in monolayer form and compared their transcriptomic profile to 3D spheroids grown for 7 (500 DEGs), 14 (1024 DEGs), 21 (1298 DEGs) and 28 days (1526 DEGs). RNA-Seq analysis revealed clear divergence of HepG2/C3A spheroids from monolayers, and further inter-spheroid divergence over the culture periods tested, suggesting transcriptional transformation in spheroids, not evident in monolayers. Differential gene expression analyses revealed a series of upregulated gene clusters relating to: cholesterol metabolism and bile acid synthesis; xenobiotic metabolism; and pathways related to the remodelling of extracellular matrices. Conversely, downregulated gene sets specifically related to cell-cycle repression, DNA repair and attenuation of apoptosis. In conclusion, this thesis has improved our understanding of the biological cues that HepG2/C3A cells take when transitioning from monolayers to spheroids and demonstrated their novel use and relative sensitivities within *in* vitro toxicological studies.

DEDICATION

Dedicated to the ever-beautiful Henry Anton Alexander McLeod

Born sleeping 31st October 2021

Sincere thanks to my esteemed colleagues that support the ongoing clinical research concerned with stillbirth and pregnancy loss, and to the charity SANDS for whom we'll be eternally grateful for the support you offer to those families in need.

ACKNOWLEDGEMENTS

The upmost thanks are firstly given to Dr Nikolas John Hodges who over these last four years has allowed me all the freedoms possible to pursue my own research goals, interests, and collaborations. The greatest thanks are given to Dr Patricia Lalor within the Centre for Liver and Gastrointestinal Research, University of Birmingham for the additional supervision they have offered me, alongside the opportunity to interact with those esteemed researchers working at the cutting edge of advanced liver research. Additional thanks are given to Dr Emma Shepherd, also of the CLGR – the doggedness with which you approach research and the environment within which we work is nothing short of inspiring! I wish to spread additional gratitude and hope for future collaborations to all my co-authors and collaborators at the University of Birmingham, particularly Dr Jonathan Barlow within the Centre for Mitochondrial Profiling and Dr Alessandro di Maio within the Advanced Imaging Hub.

One cannot underestimate the other support that is required to bring a project of this kind to fruition, I'm therefore especially grateful to all those research and admin support teams that have the University running, particularly in hostile times – hats off to Mr Shrikant Jondhale to this end. Furthermore, this work was realised by not only the financial support of the BBSRC, and Specifically the Midlands Integrated Biosciences Training Programme, but the skill sets gained within the first year of this research project. This PhD thesis really does only scratch the surface of the upskilling I have gained over the last four years; through teaching, current and future collaborations, I will look to ensure that these are used to serve benefit to others.

As always, significant applause is given to my wife, Rosie for supporting what has been a highly self-indulgent activity over the last four years! To Ma, Pa and mon frère – thanks for your continued support!

PUBLICATIONS AND CONFERENCE COMMUNICATIONS

Publications during this PhD (2017 – 2021):

Coltman, N. J., Coke, B. A., Chatzi, K., Shepherd, E. L., Lalor, P. F., Schulz-Utermoehl, T. and Hodges, N. J. (2021) 'Application of HepG2/C3A liver spheroids as a model system for genotoxicity studies', *Toxicology Letters,* 345, pp. 34-45.

Coltman, N. J., Rochford, G., Hodges, N. J., Ali-Boucetta, H. and Barlow, J. P. (2021) 'Optimised protocols to explore mitochondrial energy metabolism in spheroids using Agilent Seahorse Extracellular Flux Analysis', *[Accepted to Journal of Visual experimentation,* awaiting pre-print]

Melidis, L., Hill, H. J., Coltman, N. J*., Davies, S. P., Winczura, K., Chauhan, T., Craig, J. S., Garai, A., Hooper, C. A. J., Egan, R. T., McKeating, J. A., Hodges, N. J., Stamataki, Z., Grzechnik, P. and Hannon, M. J. (2021) 'Supramolecular Cylinders Target Bulge Structures in the 5' UTR of the RNA Genome of SARS-CoV-2 and Inhibit Viral Replication*', *Angewandte Chemie International Edition England,* 60(33), pp. 18144-18151.
*Jointly awarded the Atassi Research Prize

Lanne, A., Cui, Y., Browne, E., Craven, P. G. E., Cundy, N. J., Coltman, N. J., Dale, K., Feula, A., Frampton, J., Goff, A., Hama Salih, M. A., Lang, X., Li, X., Moon, C. W., Morton, M., Pascoe, J., Peng, X., Portman, V., Press, C., Schulz-Utermoehl, T., Tortorella, M., Tu, Z., Underwood, Z. E., Wang, C., Yoshizawa, A., Zhang, T., Waddell, S. J., Bacon, J., Neagoie, C., Fossey, J. S. and Alderwick., L. J. (2020) 'Azetidines kill Mycobacterium tuberculosis without detectable resistance by blocking mycolate assembly', *bioRxiv*, pp. 2020.09.03.281170 [*also submitted to J. Med Chem].*

Higgs, E. B., Godschalk, R., Coltman, N. J., Stewart, G. S., van Schooten, F. J. and Hodges, N. J. (2020) 'Induction of apoptosis in Ogg1-null mouse embryonic fibroblasts by GSH depletion is independent of DNA damage', *Toxicology Letters,* 332, pp. 27-35.

Submitted manuscripts and those in preparation:

Coltman, N.J., Lalor, P. F ., and Hodges, N.J (2021) 'Global transcriptomic profiling of HepG2/C3A spheroids by RNA-seq analysis', [*Manuscript in preparation].*

Bellili, S., Coltman, N.J., Hodges, N.J. and Allouche, F. (2021) 'Study of the reactivity of aminocyanopyrazoles and evaluation of mitochondrial reductive function of some products', [*Submitted to Heterocyclic Communications]*

Data generated during postgraduate study has resulted in the following conference communications:

Metabolism users meeting (Agilent technologies, BMG Labtech & Promega), online conference – September 2021. ‘Uses and metabolic alterations of spheroid-cultured hepatic cells’

British Toxicology Society Annual Congress, online conference – April 2021. 'Application of HepG2/C3A liver spheroids as a model system for genotoxicity studies
Institute of Immunology and Immunotherapy symposium, Birmingham, UK - November 2018. ‘Development of 3D culture systems to model liver disease’.

Drug Metabolism Discussion Group Annual Meeting - September 2018. ‘Development of a hepatic liability panel of assays to study drug-induced livery injury’

BBSRC Student Symposium, Warwick, UK – September 2018 . ‘The staged development of liver spheroids for toxicology and discovery DMPK’

TABLE OF CONTENTS

LIST OF FIGURES

LIST OF TABLES

LIST OF ABBREVIATIONS

2D	two-dimensional
3D	three-dimensional
2AA	2-amino anthracene
2D monolayer	cells grown on a flat surface, typically a cell culture flask/plate
4NQO	4-nitroquinoline-1-oxide
ABC transporter	ATP binding cassette protein
ADME	absorption, distribution, metabolism, and extraction (xenobiotics)
ALD	alcoholic liver disease
AMD	amiodarone
ANOVA	analysis of variance
APAP	acetaminophen
APOPB	apolipoprotein
AQP	aquaporin protein family
ATCC	American Type Culture Collection
ATP	adenosine triphosphate
ATRV	atorvastatin
B[a]P	benzo [a] pyrene
BAM (file)	binary sequence alignment map format, NGS data file type
BSEP	bile salt export pump
Cmax	maximum plasma concentration (*in vivo*)
CPM	counts per million
CYP(450)	cytochromes P450 enzymes
DCF	diclofenac
DDR	DNA damage response
DEG	differentially expressed gene
DILI	drug-induced liver injury
DMEM	Dulbecco's Modified Eagles Medium
DMSO	dimethly sulphoxide
DNA	deoxyribose nucleic acid
DSB	DNA double strand break
dsDNA	double stranded DNA
ECACC	European Collection of Cell Cultures
ECAR	extracellular acidification rate
ECM	extracellular matrix
(7)-EC	7-ethoxycoumarin
EDTA	ethylene diamine tetra acetic acid
EGTA	ethylene glycol-bis tetra acetic acid
ENA	European nucleotide archive
EROD	Ethoxyresorufin O-deethylation
ETC	electron transport chain
FASTQ (file)	"fast all" qualitative file, nucleotide sequence file for NGS data
FBS	foetal bovine serum
FDR	false discovery rate

FIJI	FIJI is just imageJ
FITC	fluorescein isothiocyante
FMO	flavin monooxygenase enzyme
FPKM	fragments per kilobase, per million
GC (content %)	guanine-cytosine content
GO (term)	gene ontology pathway
GRCh38	human reference genome, version 38
GSH	glutathione
GST	gluthathione S-transferase enzyme
GTF	genome transfer file
HSC	hepatic stellate cells
IC50	concentration required to inhibit activity by 50 %
iPSC	Induced pluripotent stem cells
ISZ	isoniazid
ITG	integrin family of proteins
KETO	ketoconazole
KRB	Krebs-Ringer buffer
LiGEP	Liver gene expression panel
LMPA	low melting agarose
LOT	liquid overlay technique (agarose)
LPS	lipopolysaccharide
LSC	liver stellate cells
LSEC	liver endothelial cells
MRP	multidrug resistance associated protein
NAFLD	non-alcoholic fatty liver disease
NAPQI	N-acetyl-p-benzoquinone
NASH	non-alcoholic steatohepatitis
NAT	n-acetyl transferase enzyme
NGS	next generation sequencing
NMPA	normal melting agarose
NPC	non-parenchymal cells
OCR	oxygen consumption rate
Padj	*P* value adjusted for multiple statistical testing
PBS	phosphate buffered saline
PCA	principle component analysis
PER	proton efflux rate
PHH	primary human hepatocytes
PHiP	2-amino-1-methyl-6-phenylimidazo[4,5-b]pyridine
PHRED	phred quality score applied to nucleobases in NGS FASTQ files
PI	Propidium iodide
PKPD	pharmacokinetic – pharmacodynamic
PMA	phorbol myristate acetate
qPCR	quantitative (real-time) polymerase chain reaction
RIPA	radio-immunoprecipitation assay buffer
RLT	RNA extraction lysis buffer

RNA	ribonucleic acid
RNA-seq	RNA sequencing, transcriptomics
RNS	reactive nitrogen species
ROS	reactive oxygen species
RPMI	Roswell Park Memorial Institute tissue culture medium
RT	room temperature
RW1	RNA extraction wash buffer
SAM (file)	sequence alignment/map format, NGS data file type
SDS	sodium dodecyl sulphate
SLC	solute carrier protein family
SLD	sulindac
SMA	smooth muscle actin
SRA	NCBI sequence read archive
SRC	spare respiratory capacity
SSB	DNA single strand break
SULT	sulfotransferase enzyme
TCA	tricarboxylic acid
TCR	tacrine
TE (buffer)	tris-EDTA buffer
TGF	transforming growth factor
TGZ	troglitazone
TLR	toll-like receptor
TNF	tumour necrosis factor
TRV	trovafloxacin
UGT	glucuronosyltransferase enzyme
VER	verapamil
VPA	valproic acid
XF (analyses)	extracellular flux analyses, (Agilent seahorse)
γH2AX	gamma H2AX
Z score (gene counts)	overall average of raw gene counts abundance, divided by the standard deviation of all the measured gene counts

Chapter 1. GENERAL INTRODUCTION

1.1. Introduction

The central role of the human liver in normal physiology, makes it susceptible to both on and off-target effects of xenobiotic, alcohol, and infection-induced damage. Humans are exposed to a multitude of xenobiotics or *foreign substances* daily, these include both pharmaceutical, and environment chemicals collectively referred to as xenobiotics. Xenobiotics may be detoxified to inactive metabolites by the liver; on the other hand, many xenobiotics are bio-transformed by the liver to active components. In the case of pharmaceuticals, hepatic drug metabolism may be beneficial in the activation of prodrugs to elicit pharmacological effects whereas conversely, many xenobiotics derived from environmental chemical exposure are metabolised by the liver to toxic moieties potentially leading to adverse outcomes such as carcinogenesis in the case of genotoxins. Despite recent advances in clinical medicine and public health interventions, acute and chronic liver injury, and disease, continue to be the greatest burden to western health organisations (Pimpin et al., 2018). In addition, hepatotoxicity, and drug induced-liver injury (DILI) is a predominant reason for drug attrition, market withdrawals, and restricted use of drugs through black-box warnings (Baze et al., 2018). Together, the need to de-risk novel chemical entities is a requirement, both preclinically and regulatory. Under current guidelines any chemical for which human exposure, whether directly or indirectly, is a potential hazard, requires rigorous assessment (Fischer et al., 2020, Krewski et al., 2020), with the aim of being able to define the *no observed adverse effect level* (NOAEL). That is the ability to define a margin or window in which human exposure is considered *safe* (Parasuraman, 2011); in the case of pharmaceuticals this could also be defining this margin as the difference between exposure considered therapeutic and toxic.

1.2. Anatomy and physiology of the human liver

In mammals the liver constitutes the largest organ, contributing up to 5 % of total adult human body weight, approximately 1.5 Kg. The liver is a lobular organ physically separated into left and right lobes by the falciform ligament, but functionally separated by the middle hepatic vein (Figure 1.1A). The left lobe sits in the upper central region of the abdomen and its convex structure found moulded to the diaphragm; the right lobe is approximately 6 times larger than the left and is further subdivided within its left posterior region into to physiologically independent lobes called the *caudate* and quadrate The liver is a highly vascularised organ, receiving blood via the hepatic artery from the aorta (approximately 20 %) and hepatic portal vein (remaining 80 %) which supplies blood from neighbouring organs such as the gallbladder, spleen, pancreas and intestines, in a poorly-oxygenated form. Hepatic hili around the portal vein also convey the lymphatic system and bile ducts out of the liver (Lalor et al., 2002); the bile ducts drain bile produced by the liver, and collected by bile canaliculi, into the gall bladder and/or duodenum.

The liver lobule is the anatomical subunit of the liver and is a hexagonal structure approximately 1-2 mm^2, comprising the central vein at the core and the hepatic portal triad around the peripheral vertices (Figure 1.1D). The portal triad describes the arrangement of the hepatic artery, portal vein and bile duct, in addition to substructures such as lymphatic vessels and vagus nerve (Figure 1.1B). These vessels are further sub-divided into sinusoids (Figure 1.1**Error! Reference source not found.**C). which serve as a channel for blood flow between hepatic plates and portal tracts, leading to lobules. Each liver lobe comprises approximately 1 x 10^6 lobules; each lobule is arranged into 3 physiologically-distinct zones (Gebhardt, 1992). Zone 3 is a region closest to the central vein and is thus subjected to a

lower oxygen concentration and nutrient supply compared to the periportal zone 1 which is much more highly vascularised and exposed to higher concentrations of oxygenated blood and nutrients. Zone 2 represents a transitional region which sits between the two. The zonation of the liver into lobes, and further functional and physiological zonation at the lobule level, reveals a wide array of different functions at both the organ level, and in cells occupying different lobule zones.

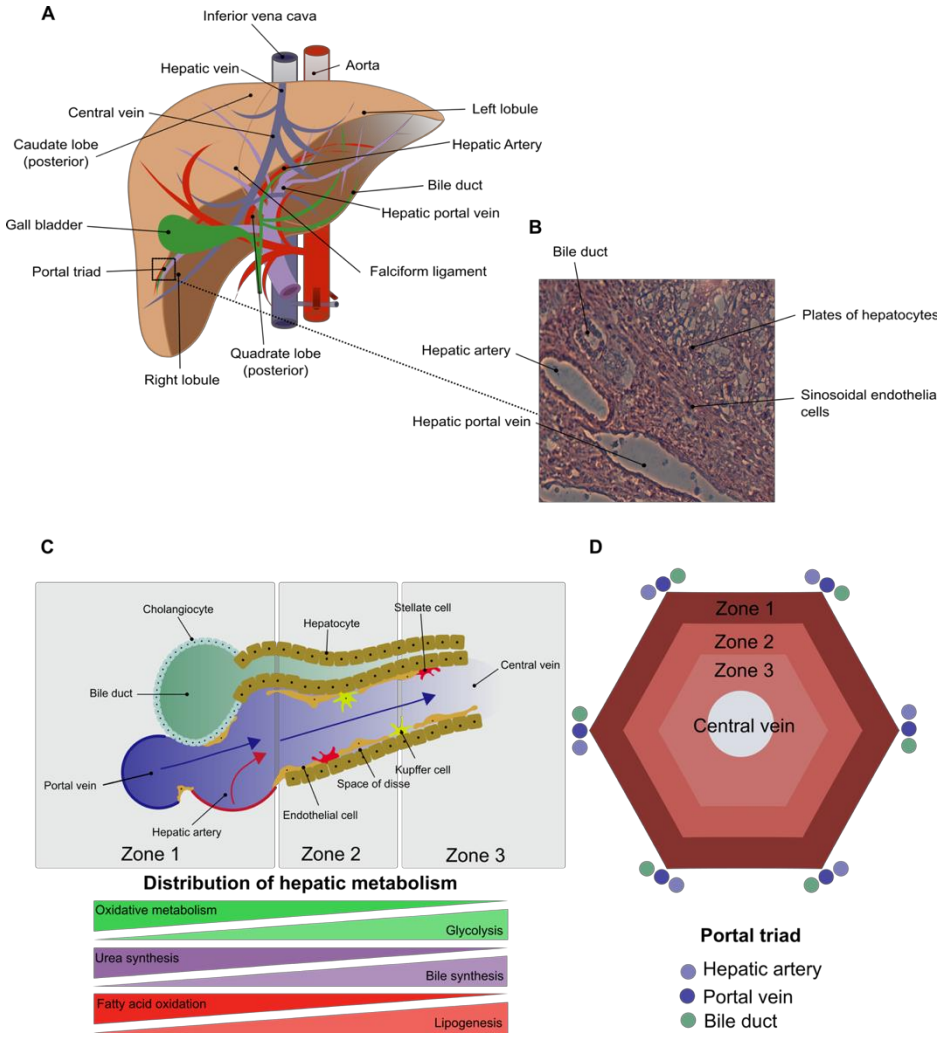

Figure 1.1. Anatomy and physiology of the human liver. *The liver is a large organ with (A) gross anatomy of human liver displaying vascular and biliary system, separated into lobules; (B) histology stain of human liver highlighting hepatic portal triad of portal vein, hepatic artery and biliary duct systems; (C) Schematic of the liver sinusoid and cell types of human liver; (D) Illustration of the hepatic lobule separated into functional zones. Figures hand-*

drawn in Inkscape open-source software and adapted from Trefts et al. (2017). Panel B human tissue used was collected at the Liver and Hepatobiliary Unit, Queen Elizabeth Hospital, Birmingham, with prior written informed patient consent and local research ethics committee approval (06/Q2702/61).

1.3. Subdivision of the liver into different cell types and the orchestration of liver damage and repair

Histology shows that the liver is subdivided into parenchymal cells (hepatocytes) which constitute the majority of liver cell types, occupying up to 80 % total liver volume and approximately two-thirds of total cell number, and non-parenchymal representing the remaining third of cell number but less than 10 % of total liver volume; each cell group being uniquely responsible for processes that balance the liver between homeostasis and injury (Kmiec, 2001). The primary role of hepatocytes depends on their position throughout the liver structure. For example, those distributed around the periportal region of the liver (Zone 1, Figure 1.1) are more likely to be involved in oxidative metabolism, urea synthesis (Mavri-Damelin et al., 2008, Mavri-Damelin et al., 2007, Su et al., 2018) and the metabolism of fatty acids (Trefts et al., 2017) whereas those closer to the central vein are more likely to involved in the synthesis of lipids, bile and utilise glycolysis for respiratory metabolism (Jungermann and Kietzmann, 1997) and synthesis of serum proteins such as albumin (Wencel et al., 2021). The distribution of hepatocytes throughout liver zones dictates their metabolic profile whereby polarised hepatocytes, with both an apical and basal membrane, typically utilise glycolysis to produce cellular ATP synthesis whereas those in a non-differentiated state rely more heavily on oxidative phosphorylation (Fu et al., 2013).

1.4. Liver parenchyma and drug metabolism

Hepatocytes (PHHs) are functionally-polarised epithelial cells are seated within plates along the hepatic lobules, flanked laterally and basally by liver sinusoids, providing a blood supply through the capillary network (Zhou et al., 2016). Gap junctions provide cytoplasmic channels between adjacent hepatocytes whereas tight junctions prevent extracellular leakage between neighbouring cells, allowing the formation of bile canaliculi. Hepatocytes transport endogenous and exogenous, lipophilic molecules with a molecular weight ≥ 500 Da, across the sinusoidal, lateral and apical membranes (Faber et al., 2003). Hepatocellular uptake (Phase 0) is typically orchestrated by organic anion or cation transporter proteins (OATs/OCTs), *e.g.* OATP1B1 for acidic molecules (Faber et al., 2003); parent molecules are subjected to redox or hydrolysis reactions (Phase I), primally through cytochromes P450 enzymes (CYPs), *e.g.* CYP2E1 for alcohol or CYP3A4/CYP2D6 for common xenobiotics (Foti and Dalvie, 2016), or flavin monooxygenases (FMO) (Huang et al., 2021) . Prior to the final excretion, conjugation reactions, yield molecules with greater hydrophilicity (Phase II), *e.g.* glucuronidation (Bradshaw et al., 2020), sulfation, glutathionylation or conjugation to amino acids (Westerink and Schoonen, 2007). Conjugated molecules are then either excreted into the bile by ABC transporters including multidrug resistance-associated protein-2 (ABCC2, MRP2) or via the bile salt export pump (ABCB1, BSEP), or directly into the blood across the sinusoids by MRP3/MRP4 proteins (Phase III), (Faber et al., 2003, Schinkel and Jonker, 2003). Without xenobiotic stimulus, these hepatocyte mechanisms are critical for the control of influx and efflux mechanisms of steroids, bile acids and lipid-soluble molecules such as vitamins (Boyer, 2013, Russell, 2009), and also include the involvement of other proteins such as aquaporins to maintain liver osmolality (Jung et al., 2021, Masyuk and LaRusso,

2006). Genetic polymorphisms of Absorption Distribution Metabolism Excretion (ADME) proteins are highly-associated with hepatoxic events, for example alterations in CYP2E1 and N-acetyl transferase (NAT) function is associated with isoniazid anti-tuberculosis drug toxicity (Nicoletti et al., 2021, Yang et al., 2019, Huang et al., 2003) and CYP2C9 polymorphisms are associated with the disposition of common NSAIDs (Krasniqi et al., 2016). Notwithstanding their role in ADME, hepatocytes are also a key inflammatory cell type in the innate immune response to liver injury (*e.g.* bacterial infection), by acting as both a receiver and responder to hepatic inflammatory stimuli (Zhou et al., 2016). In hepatic injury, hepatocytes help to regulate the host immune-inflammatory response by interacting with non-parenchymal and immune cells, and by the production of innate immune proteins such as bactericidal proteins; detecting and responding to pathogen and damage associated molecular patterns (PAMPs/DAMPs). Not limited to non-parenchymal cells (NPCs), PHHs have also been found to express toll-like receptor proteins (TLRs) which are the most important family of receptor proteins in the innate immune response (Soares et al., 2010).

Biliary epithelial cells (cholangiocytes)

Lining the hepatic bile ducts and comprising approximately 3-5 % of hepatic cells, cholangiocytes are an epithelial cell type that contribute a variety of roles including supporting biliary and hepatic transport processes (Pauli-Magnus et al, 2006) and form a major part of the hepatic biliary tree. Alongside hepatocytes, cholangiocytes represent a secondary polarised cell type with an apical and basal membrane supporting hepatic reabsorption and secretion processes (Beneditti et al, 1997, Pauli-Magnus et al, 2006), and cell-cell gap junctions that orchestrate inter-cellular communication (Banales, et al 2019). In

prominent hepatic diseases, cholangiocytes can be activated by inflammatory cytokines via the toll-like receptor axis to mediate cellular crosstalk between the hepatic adaptive and innate immune response and influence the deposition of hepatic ECM as well as supporting compromised hepatocyte regeneration in disease biology (Banales, et al 2019). As excretion into the bile is one of the major routes of export for small molecules of molecular weight 300 - 500 Da, the role of cholangiocytes in drug-metabolism and toxicology is of particular interest alongside hepatocytes. Bile-salt mediated solubilisation of hepatic phospholipids and excretion into the bile duct via BSEP and MRP2 is associated with the protection of cholangiocytes (Benedetti, et al 1997, Visentin, et al 2018) whereas impaired function of basolateral and apical transporters and continued perturbation of normal cholangiocytes biology is associated with several hepatic pathologies, mostly associated with sclerosis of biliary ducts. For example, the xenobiotic drug, sulindac has been shown to induce hypercholeresis (Bolder et al, 1999), leading to drug induced bile duct injury (Visentin, et al 2018), which without therapeutic intervention or resolution can lead to hepatic fibrosis and cirrhosis, and hepatic failure as a primary endpoint.

1.4.1. Non-parenchymal cells in the liver

NPCs represent the remaining 30-40 % of cells within the liver and are responsible for the maintenance of liver functionality, homeostasis and also contribute to its physiological structure through the production of extracellular matrices. Furthermore, NPC orchestrate the balance between liver damage and regeneration, by balancing tolerance and immune responses. NPC are further subdivided into liver sinusoidal endothelial cells (LSEC, 60 %),

liver stellate cells (LSC, 15 %) and resident liver macrophages called Kupffer cells (KC, 20 %), (Friedman and Roll, 1987, Kmiec, 2001). LSEC serve as an interface between the liver and systemic circulation, lining liver capillaries at the sinusoids, and directing blood flow from the hepatic artery and portal vein to the hepatocytes beyond. LSEC are well-positioned at this interface for the removal and recycling of macromolecules such as proteins, hormones, lipids, toxins and viruses (Shetty et al., 2018, Poisson et al., 2017), through fenestrae 'molecular sieves', triggering the immuno-inflammatory processes and driving liver regeneration through interactions with other hepatic cell types such as LSCs (DeLeve, 2013, Balaphas et al., 2019).

KCs are resident hepatic macrophages, which line the liver sinusoids, migrate around the liver and are exposed to the gastrointestinal tract (Bouwens et al., 1986). Their key role is in the elimination of cellular debris, microorganisms, the detoxification of alcohols (*e.g.* ethanol) as well as endotoxins; for example, the interaction between KCs and lipopolysaccharides (LPS) released from bacteria, are indicated as being the key molecular initiating event (MIE) for hepatotoxicity in various forms of liver injury, particularly alcohol-induced liver injury (Dixon et al., 2013, Kolios et al., 2006, Wheeler, 2003) and acetaminophen-induced liver injury (Laskin, 1990, Ju et al., 2003), via tumour necrosis – reactive oxygen species pathways (Kolios et al., 2006). LSCs are located in the sinusoidal space of Disse and serve multiple roles in liver physiology through their strategic location to interact with HCs, LSEC and KCs (Hautekeete and Geerts, 1997). Under normal liver function, LSC display a *quiescent* phenotype, serve as a master reservoir for hepatic retinoids (e.g. vitamin A) as lipid droplets and are slowly proliferating and are the primary synthesis site for

hepatic extracellular matrix (Hautekeete and Geerts, 1997, Tsuchida and Friedman, 2017), and therefore serve a central role in hepatic fibrosis and the formation of scar tissue.

1.4.2. Liver toxicity in context using the paracetamol paradigm

Drug-induced hepatotoxicity and liver injury (DILI) describes a pattern of liver injury associated effects of therapeutics taken by patients for the treatment of disease but could be similarly applied to any foreign xenobiotic e.g., through environmental exposures. Toxic exposure to such agents can lead to liver damage, injury and can even organ failure. The pathogenesis of drug-induced hepatotoxicity is broad; in terms of its study as an adverse outcome pathway, it stretches from clinical observations monitoring systemic liver enzyme levels at one end, to a molecular initiating event at the other which could be the bio-generation of a drug metabolite forming haptens and liver protein adducts; the processes along the way leading to the impairment of the organ are diverse (see Table 1.1 for overview). Using acetaminophen as an example, resident liver enzyme, once other metabolic pathways are saturated, CYP2E1, bio-transforms acetaminophen to a reactive NAPQI intermediate (N-acteyl-p-benzoquinone). NAPQI depletes hepatic parenchymal pools of glutathione antioxidants (GSH) leading to the generation of reactive oxygen species (ROS) leading to mitochondrial damage. Reactive metabolites also bind covalently with macromolecules throughout the liver and form haptens thus eliciting antibody production and the release of inflammatory cytokines throughout the liver. This acute immune response triggers the activation of liver non-parenchymal cells which continue to orchestrate the immune-inflammatory response and begin the process of liver repair and regeneration in acute liver injury, or towards the formation of scar tissue in chronic liver damage.

Although liver injury through xenobiotics can be both on- and off-target, hepatotoxicity and liver injury, is most likely not associated with the registered pharmaceutical mode of action.

For example, liver toxicity from acetaminophen (paracetamol) – a common over the counter pain relief medication, is the most common cause of liver injury in the United Kingdom (Newsome et al., 2001) and (Hinson et al., 2010), due to off-target toxicity in the liver. Aside from its clinical burden in Western medicine, DILI is one of the principal cause for drug attritions, market withdrawals and flagged-warnings, and a bottle neck for the pharmaceutical industry, leading to poor research and development productivity and the early closure of drug discovery programmes due to safety risks (DiMasi et al., 2016). All these outcomes are incredibly costly for both patients in terms of health outcomes, and the pharmaceutical industry in terms of the financial burden. Therefore, there is an innovation gap that needs to be bridged to bring safer medicines to patients and accurately assess the toxicological hazards associated with chemicals already in existence for which human risk is poorly understood or was missed before approval. Therefore, methods and models that can better predict DILI are required (see Figure 1.2)

The most widely used models for the study of liver toxicity and biology are one of either *in vivo* rodent origin (e.g., murine lethal dose studies, to define LD_{50}) or simplified *in vitro* cell culture models (e.g., basic cytotoxicity to determine IC_{50} in terms of cellular viability). However, as is often the case, these models do not translate adequately enough to man. Despite its extensive use, the limited physiological relevance of 2D cell culture restricts our ability to model perturbations to normal liver physiology, effectively *in vitro*. Recent advances within the last 10-15 years in tissue culture techniques, utilising both primary and immortalised cells, show promise for recapitulating *in vivo* physiological responses to that of human liver, particularly hepatic 3D spheroid models for deployment in the study of

genotoxicity and hepatotoxicity. Table 1.1 reviews hepatotoxic compounds commonly tested *in vitro* toxicology studies.

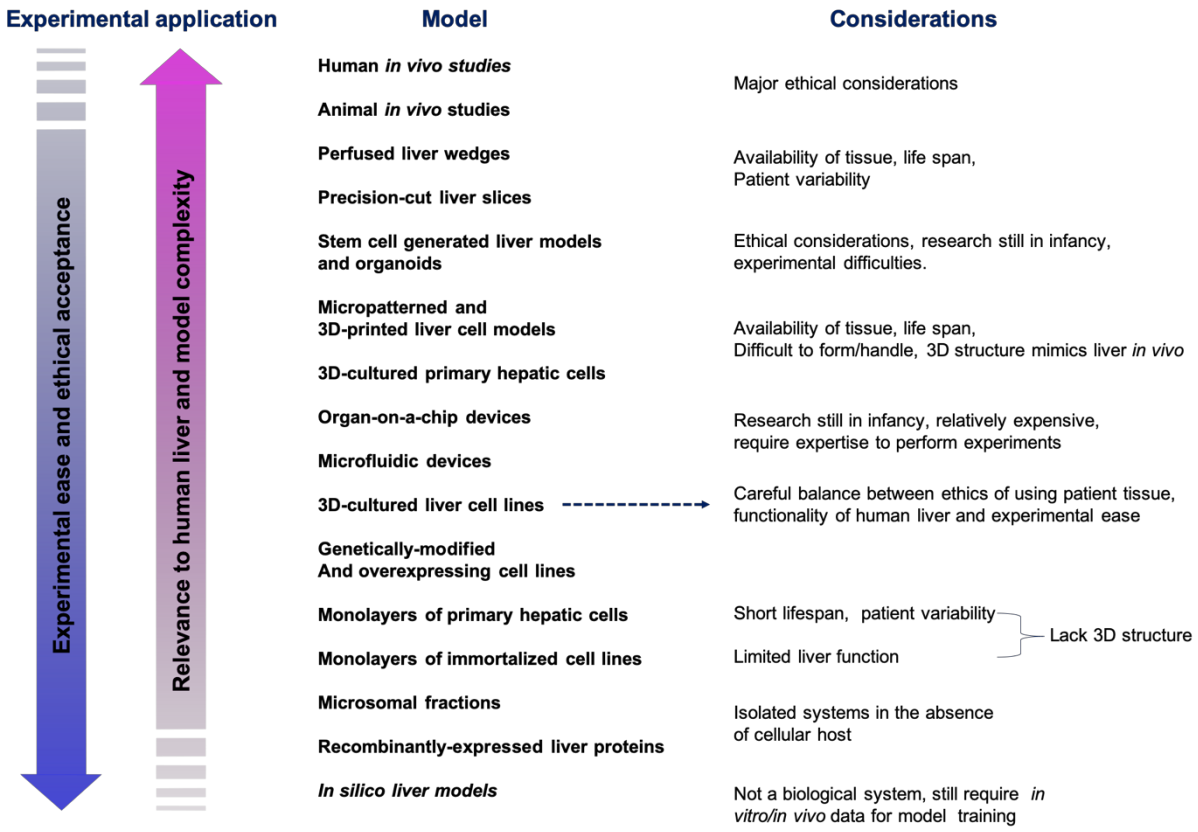

Figure 1.2. The current landscape of complex liver models for toxicological research. *In recent years, the complexity, applicability, and availability of liver models for both academic and industrial research, has greatly increased, however the selection of the right model for employment in toxicology studies has become even harder.*

Table 1.1. Overview of the toxicological mechanisms associated with hepatotoxic compounds commonly reviewed and deployed in hepatic toxicological studies using a combination of 2D and 3D approaches

Compound (Abbreviation)	DILI ranking*	Pattern of injury	Deduced mechanism of action (incl. metabolism routes)	Selective references
Acetaminophen; APAP **Analgesic**	Low	Hepatocellular toxicity	Metabolism via CYP2E1 and CYP1A; formation of NAPQI metabolite, forming protein adducts. Alcohol induction of CYP2E1 drives excess metabolism to NAPQI. Mitochondrial toxicity and oxidative stress reveal induction of apoptosis/necrosis hepatic cell death pathways, alongside elevation in excess Ca^{+} ion accumulation.	(Caparrotta et al., 2018, Ramachandran and Jaeschke, 2018, McGill and Jaeschke, 2013, Hinson et al., 2010)
Amiodarone; AMD **Antiarrhythmic**	Severe	Phospholipidosis/ steatosis	Metabolised by CYP3A4 routes and therefore liable to drug-drug interactions through concomitant use of other 3A4 induces, e.g., warfarin. Excess accumulation of metabolites in hepatic lysosomes which can progress to phospholipidosis - steatosis and eventual liver cirrhosis. Parent and metabolites shown to be potent inactivators of major CYP450 families including CYP1A2, 2C9 and 2D6	(Chatterjee et al., 2014); (Wu et al., 2021, Goldman et al., 1985)
Atorvastatin; ATRV **Antilipemic**	High	Hepatocellular toxicity	Mechanisms controversial as is hepatotoxicity of statins in general as users are typically co-medicating with other pharmaceuticals. Mechanism is suggested to be related to its high lipophilicity and extensive metabolism by CYP3A4 routes, accompanied by high oral dosing regimens. Induction of autoimmune hepatic response	(Yu et al., 2014) ; (Bjornsson, 2017); (Chen et al., 2013)
Diclofenac; DCF **Non-steroidal anti-inflammatory drug**	High	Hepatocellular toxicity	Metabolism mediated by CYP2C family (2C9/2C8) followed by glucuronidation via UGT2B family (2B7 mainly). MRP2 drug transporter may be implicated. Glucuronidation generates reactive quinonimines and circulating, unstable acyl-glucuronides capable of forming antigen-haptens adducts potentially leading to immune response. Mitochondrial dysfunction and hepatocellular stress also implicated. Route of metabolism highly polymorphic which may account of idiosyncrasy in some patients.	(Lazarska et al., 2018, Sarkar et al., 2017, Daly et al., 2007, Aithal, 2004, Ponsoda et al., 1995); (Walles et al., 2020)
Cinchophen; CNCH **Non-steroidal anti-inflammatory drug**	High	Hepatocellular toxicity	Little is known as first NSAID synthesised but quickly removed from market due to liver toxicity in human participants; still used in veterinary medicine. Steatotic and necrotic liver was observed in patients within 6-12 hours of administration. Structure is carboxylic acid-based so glucuronidation likely major route of metabolism potentially leading to formation of reactive acyl glucuronides thus mechanism of toxicity may be similar to that of idiosyncratic DCF toxicity or bromfenac. CYP1A and CYP2C hydroxylation also likely	(Rabinowitz, 1930, Reichle, 1929); (Lassila et al., 2015); (Walles et al., 2020); (Enlo-Scott et al., 2017)
Ketoconazole; KTZ **Anti-fungal**	Severe	Hepatocellular toxicity	Mechanism is currently unknown, however KTZ is a potent CYP3A4 inhibitor and hence is implicated in a number of serious drug-drug interactions with those other pharmaceuticals requiring metabolism via the major CYP3A4 thus may cause indirect hepatotoxicity by increasing serum levels on those xenobiotics. In addition, the CYP3A family (3A4, 3A5 and 3A7) are involved in hepatic sterol synthesis thus inhibition may have other downstream consequences such as repression of bile acid synthesis pathways.	(Li et al., 2021a, Kim et al., 2017, Greenblatt and Greenblatt, 2014, Rodriguez, 1999)
Isoniazid; ISZ **Antimicrobial**	Severe	Hepatocellular toxicity	Mechanism of hepatotoxicity not clear however suggested route of metabolism is via CYP2E1 and NAT2 reactions followed by GST conjugation. It is possible that acetylation of the hydrazine yields reactive adducts that covalently bind to hepatic proteins, inducing immune response. Some suggestion that auto-metabolism via oxidative routes may be possible through residual ROS in liver. Suggestion that NAT2-associated genetic polymorphisms may be the driver for idiosyncratic DILI in some patients	(Nicoletti et al., 2021, Khan et al., 2019, Wang et al., 2016, Metushi et al., 2016, Metushi et al., 2012)
Sulindac; SLD **Non-steroidal anti-inflammatory drug**	High	Hepatocellular toxicity	Incidences of SLD toxicity are relatively idiosyncratic and hence mechanisms are unclear. Principal metabolic route is via oxidation to its sulfone or reduction its sulfide active form via CYP1A2 (mainly) but also CYP1B1 and 3A4. Patterns of injury closely aligned with other NSAIDs such as DCF. Sulfide metabolite likely more toxic that parent or sulfone metabolite, suggested to behave as a mitochondrial uncoupler thus diminishing mitochondrial function in hepatocytes. SLD likely to interact with LPS to induce inflammatory cytokine production in liver macrophages to activate haemostatic systems in liver, deposition of fibrin and disruption of vascular flow leading to hypoxia induction.	(Brunell et al., 2011, Zou et al., 2009, Leite et al., 2006, Tarazi et al., 1993)

Tacrine; TCR **Acetylcholinesterase inhibitor**	High	Hepatocellular toxicity	Mechanisms currently considered are controversial. Major route of metabolism is via CYP1A2 hydroxylation to protein-reactive intermediates, however hepatotoxicity has also been seen in rat models (lacking CYP1A2 activity). Metabolomics revealed that tacrine perturbed hepatic glycolysis and gluconeogenesis pathways, triggering induction of mitochondrial dysfunction, ROS release to induce oxidative stress and cell death.	(Lou et al., 2015, Zientek et al., 2008, Madden et al., 1993)
Troglitazone; TGX **Antilipemic**	Severe	Hepatocellular cholestasis (mainly); hepatotoxicity	Major routes of metabolism are typically via CYP3A4 followed by sulphation (mainly SUKT1A family) to form TGZ-sulphate as an active/toxic metabolite; UGT-metabolism also thought to be involved. TGZ-metabolite known to inhibit the excretion of bile acids via BSEP and MRP2 leading to cholestasis. Mitochondrial toxicity is also implicated by induction of pro-apoptotic pathways. Minor metabolism routes may also reveal highly-reactive moieties, e.g., unstable epoxides within ring structures leading to excess accumulation of ROS which further drives mechanisms relating to mitochondrial dysfunction	(Ogimura et al., 2011, Lauer et al., 2009, Smith, 2003, Funk et al., 2001, Loi et al., 1999)
Trovafloxacin; TRV **Antimicrobial**	Severe	Hepatocellular toxicity	Glucuronidation via UGT1A1 considered major route of metabolism, possibly yielding reactive acyl-glucuronide intermediates. Several immune-related mechanisms induced on TRV exposure including CXCL2 chemokine inducing apoptotic cell death in hepatocytes. Nuclear translocation of NFKB is induced by lipopolysaccharide/tumour necrosis factor which drives apoptosis mechanisms and cell death.	(Giustarini et al., 2020, Giustarini et al., 2019, Mitsugi et al., 2016, Beggs et al., 2014, Lucena et al., 2000)
Valproic acid; VPA **Anticonvulsant**	Severe	Hepatocellular toxicity	VPA is a carboxylic acid derivative and therefore shares similar metabolic routes with other similar molecules, conjugation to glucuronide therefore major route of metabolism but some evidence to suggest that CYP2C family is involved thus highly polymorphic CYP2C9 might be implicated in metabolic route to 4-ene VPA. Mechanism of hepatotoxicity have been linked to inhibition of beta-oxidation pathways in mitochondria, leading to oxidative stress and mitochondrial dysfunction. Production of ROS, a depletion in hepatic GSH pools and rapid loss of lysosomal membrane integrity likely to lead to hepatic microvesicular steatosis. Alcohol-CYP2E1-ROS axis may be implicated.	(Neuman et al., 2001); (Meseguer et al., 2021); (Kiang et al., 2006); (Pourahmad et al., 2012)
Verapamil; VER **Vasodilator**	Low	Hepatocellular cholestasis	VER is of low-DILI concern, however it is a chemical derivative of the alkaloid papaverine which is implicated in auto-immune hepatitis. Major route of metabolism includes CYP2C family as well as 3A5, and 3A4 hence liable to drug-drug interactions through concomitant use of other 3A4 induces, e.g., warfarin. Likely mechanisms of hepatotoxicity are idiosyncratic and probably related to immunologic reactions or may be associated with off-target toxicity relating to its interactions with other CYP3A4 substrates, for example	(Tracy et al., 1999); (Sampaziotis et al., 2015, Lin et al., 2012, Reder-Hilz et al., 2004)

DILI ranking* taken from curated databases including liver toxicology knowledge database (Thakkar et al., 2018); DIList (Thakkar et al., 2020)

1.5. Overview of hepatic cell types commonly employed in toxicological studies

1.5.1. HepG2

HepG2 cells are an epithelial cell line (grow as flat-planar cells) extensively deployed for use within *in vitro* ADME and toxicological studies for more than 40 years (Arzumanian et al., 2021). Despite being isolated from hepatic carcinoma tissue, they have been routinely shown to maintain several of the functions of 'normal' hepatic tissues, including major plasma proteins (e.g., albumin, lipoproteins) for which the *in vivo* liver is the principal site of synthesis (Knowles et al., 1980). Owing to maintained and competent tumour suppressor gene p53 status, they have been extensively employed for the testing of potential carcinogenic chemicals (Boehme et al., 2010, Park et al., 2006).

However, basal expression of ADME enzymes is inherently poor in HepG2, particularly CYP450 enzymes and hence they serve limited use for the detection of metabolism-mediated toxicity (Donato et al., 2008, Westerink and Schoonen, 2007, Dai et al., 1993). Interestingly, enrichment of amino acid cell culture medium compositions, to levels much higher than in standard tissue culture conditions, has been shown to boost CYP450 expression to levels to those similar of primary hepatocytes (Boon et al., 2020). Alternatively of course then HepG2 cells are highly amenable to genetic engineering in which ADME function can be returned to the cell line (Herzog et al., 2016, Hashizume et al., 2010, Hashizume et al., 2009).

1.5.2. HepG2/C3A

HepG2/C3A cells are subtype/derivative of the parental HepG2 cell line, originally isolated for attributes associated with contact inhibition when grown, compared with the highly

proliferative parent (Kelly, 1994). Originally employed for use within bioartificial liver devices, they have many more favourable characteristics compared to HepG2 (Shvartsman et al., 2009, Mavri-Damelin et al., 2008). The original depositor of the HepG2/C3A cell line claimed *AFP* and albumin (*ALB*) secretion were higher in C3A versus the HepG2 parent (Kelly, 1994). C3A cells are thought to produce urea but not via the detoxification of ammonia, which is the principle hepatic mechanism (Iyer et al., 2010, Mavri-Damelin et al., 2008, Mavri-Damelin et al., 2007).Leroy et al. (2021) showed that the expression of connexin 43, which is typically upregulated in HCC, was found to be repressed in HepG2/C3A cells to a similar extent as primary human hepatocytes with the promotion of gap junction formation when compared to other HCC derived cell lines over time (Leroy et al., 2021). This therefore suggests that HepG2/C3A perhaps obtain a more differentiated phenotype and growth status that is more like PHHs than other carcinoma derived cell lines (Nelson et al., 2017), and hence might be more suitable for the growth of hepatic spheroids.

1.5.3. Huh7

Huh7 are immortalised hepatic cell line that is sparingly used in toxicological studies. Huh7 were found to be very similar to HepG2 in a direct comparison for the expression of over 200 ADME genes between Huh7, primary hepatocytes, HepG2 and other models such as THLE2 (Guo et al., 2011). However, for some specific targets such as aldehyde dehydrogenase enzymes (*ADH1A, ADH5*), Huh7 were significantly more correlated to primary cells versus HepG2 whereas other studies have indicated that AhR-mediated CYP1A1, CYP1A2 activity was equivalent to HepG2 (Terashima et al., 2015a). Elsewhere, Huh7 have also been reported to express hepatic liver makers such as *HNF4A, ALB,* and *alpha-antitrypsin (AATR)* -

(Sainz et al., 2009). However due to extensive proliferation, induction of hypoxia inducing factors, and pro-apoptotic mechanisms, they may not be suitable for growth as spheroids (Jung et al., 2017), by comparison to HepG2/C3A.

1.5.4. HepaRG

HepaRG is also a hepatoma-derived cell line (Aninat et al., 2006) which is capable of being differentiated towards primary human hepatocyte-like status, including the re-expression of several CYP450 enzymes such as *CYP7A1, CYP3A4*, and *CYP2E1, UGT* enzymes and hepatic nuclear receptors (Kanebratt and Andersson, 2008). Over a period of differentiation, HepaRG cells have been shown to form cells akin to that of the biliary epithelium *in vivo* (Wang et al., 2019) and attain hepatocyte-like status including markers of cellular polarisation such as drug transporter proteins (MRP2, BSEP) - (Kanebratt and Andersson, 2008, Guillouzo et al., 2007). By comparison to HepG2/C3A for example, they have been shown to possess superior xenobiotic metabolism potential, enhanced sensitivity to hepatotoxicants (Nelson et al., 2017). Similarly, HepaRG were considered as more appropriate to the inclusion of bioartificial liver devices in terms of liver functionality, such as lactate production, detoxification of ammonia and drug metabolism (van Wenum et al., 2016).Regulatory transcription factors *CAR* and *PXR*, were found to be significantly enhanced in HepaRG cells grown in 2D compared to HepG2 (Guillouzo et al., 2007). However, unlike HepG2 or HepG2/C3A cells, the cultivation of HepaRG cells typically require the extensive use of specialist culture mediums for differentiation, in addition to their limited use beyond the academic setting without licence.

1.5.5. Primary human hepatocytes (PHHs)

PHHs are considered the *gold standard* for deployment in toxicological and drug metabolism studies. Owing to their primary status, direct from human tissue donors, PHHs maintain many of the functions attained from the original organ progenitor such as extensive drug metabolism ability (Wilkening, 2003, Boess et al., 2003), production of hepatic nuclear factors such as *HNF4A* and *HNF1A* (Kamiyama et al., 2007), and extensive production of hepatic serum proteins, metabolism of fatty acids and the production of bile acid proteins (Gerlach et al., 2003). However, compared to immortalised cell lines, accessibility is limited, and their isolation direct from human tissue is a considerable bottleneck, although this has been improved with commercial sources of PHHs, though not necessarily a viable option for all researchers. In addition, on isolation, PHHs rapidly lose their differentiated status when grown on stiff plastic under standard tissue culture conditions and undergo de-differentiation (Oliva-Vilarnau et al., 2020), and lose proliferative status by comparison to HepG2 for example and are forced into a quiescent phenotype, i.e. normal cell-cycle is stalled. Because of this, the viability of PHHs is subsequently reduced, therefore PHHs are often grown on extracellular matrices such as sandwich cultures (Bell et al., 2018a, Yang et al., 2016, Tuschl et al., 2009) in order to force PHHs to re-polarise and differentiate (Zeigerer et al., 2017).

1.6. The expanded use of hepatic 3D spheroid models in the literature

The quest to circumvent the use of animal in toxicology experiments is one that has been ongoing since the inception of such regulatory processes some 50 years ago under the 3R's principle (Beken et al., 2016). In addition, toxicological studies are often poorly translated

between experiments conducted using basic in vitro cell culture models (Section 1.5), and regulatory animal studies. In this way, advanced cell culture models, particularly the use of spheroids, have shown great promise in recapitulating many of the functions that are lost in basic cell culture models, including hepatic metabolism (e.g., bile acid production, cholesterol metabolism, production of albumin) and restoration of ADME function. Those most extensively evaluated have been hepatic spheroid models borne from PHHs (Kanebratt et al., 2021b, Riede et al., 2021, Hendriks et al., 2020a, Bell et al., 2020), HepaRG (Ramaiahgari et al., 2017, Wang et al., 2015, Darnell et al., 2011) and HepG2, including the C3A derivative (Stampar et al., 2019, Ramaiahgari et al., 2014, Wrzesinski et al., 2013, Gaskell et al., 2016). Although, there is also emerging utility for other advanced models that have been significantly evaluated for deployment in toxicological studies (**Figure 1.2).**These include the optimisation of dynamic microfluidic and liver-chip devices (Petreus et al., 2021, Chao et al., 2020, Busche et al., 2020); precision-cut liver slices (Gupta et al., 2021, Boess et al., 2003, Lerche-Langrand and Toutain, 2000) and multicellular microtissues (Hafiz et al., 2021, Kermanizadeh et al., 2019, Rowe et al., 2018).

The research progress in hepatic 3D spheroid models can be exemplified using a literature retrieval strategy using Boolean and Mesh terms, in which the number of publications relating to hepatic spheroids has increased considerably in the last decade, detailed in Figure 1.3. It is therefore of no surprise that the development of hepatic 3D models appears to correlate with an increase in the number of formalised programmes and initiatives tasked with assessing and implementing such strategies. The development, assessment, and deployment of

advanced haptic models throughout all levels of research, therefore, represents a significant harmonised approach, not achievable by one model or approach alone.

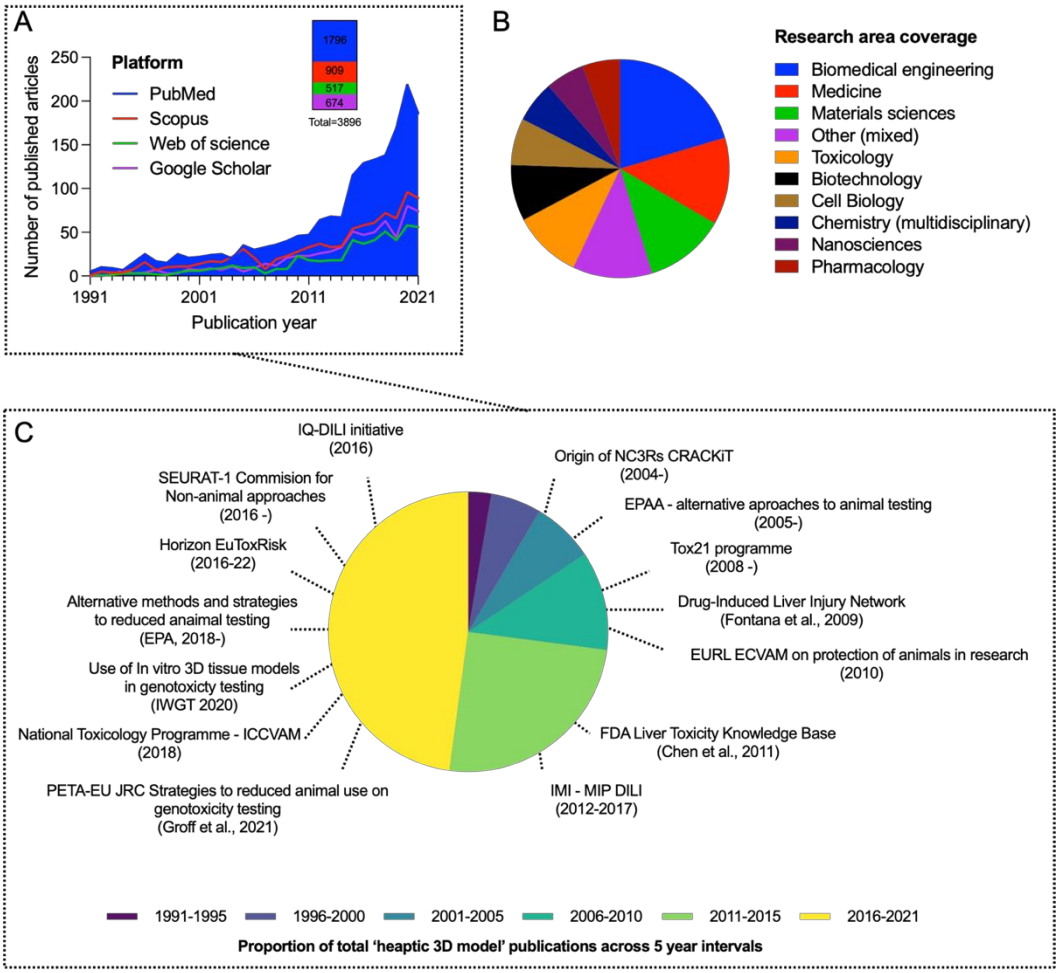

Figure 1.3. Literature retrieval strategy to exemplify the increased use of hepatic spheroid models 1991-2021. *Publication records from the last thirty years of articles pertaining to hepatic spheroids were retrieved by systematic literature searching and text-mining approach. (A) The number of publications archived between 1991 and 2021 using systematic text and Boolean search terms through four repositories. (B) Research area coverage of published articles across liver spheroid fields by proportion of archived publications. (C) Proportion of total retrieved articles published in segmented 5-year intervals, mapped to the origins of key consortia, working groups and programmes concerned with the use of alternative models for geno- and hepatotoxicity testing.*

The use of *in vitro* spheroids models for use in ADME and toxicological studies is extensively reviewed as part of **Chapter 3** of thesis, therefore **Table 1.2** offers an overview of many of the attributes that are associated with culturing hepatic cells in three-dimensions. In addition, a comprehensive overview of the limitations associated with spheroid cell culture models is presented in **Chapter 4**.

Table 1.2. *Summary* of the phenotypic transformations *when* hepatic cells *are* cultured as spheroids for deployment within in vitro toxicological and ADME studies

Hepatic cell type	Biological observation when transformed into 3D spheroid model	References
HepG2	• PXR upregulated in spheroids cultured by hanging drop • CAR activation • Adapted for use in micronuclei assay for detection of genotoxicants • Confounding data for both enhanced and repressed albumin secretion in cell culture medium • CYP1A family is significantly expressed in 3D versus 2D • Hepatic nuclear receptors induced (*AhR, CAR, HNF1*) • Poor formation of spheroids and proteome poorly reflects 'functional ADME enrichment' • Confounding data to show that HepG2 3D proteome is diverged over time from monolayers • Evidence for bile-canaliculi formation in spheroids • Sensitive to single stranded DNA breaks as detected by comet assay • Suitability for repeat dose studies	(Yokobori et al., 2017); (Yokobori et al., 2019); (Conway et al., 2020); (Elje et al., 2019b); (Ellero et al., 2021); (Nishikawa et al., 2017); (Ramaiahgari et al., 2014); (Shah et al., 2018a); (Štampar et al., 2021); (Hurrell et al., 2019)
HepG2/C3A	• Active urea cycle (e.g., *CPS1, ARG1*) though not attributed to ammonia detoxification • Increased secretion of hepatic serum proteins such as ALB, ApoB/APEOE, AFP • 'Contact-inhibition' properties and expression of cell-cell gap junction (connexins) proteins promotes inter-cellular contact and deposition of ECM • Repressed proliferation • Cells appear to polarise and form functional bile-canaliculi • Several CYP450 proteins upregulated (CYP1A2, 2E1, 3A4, 2D6) • Increased sensitivity to commonly assessed hepatotoxicants • Xenobiotic metabolism activity (CYP450-mediated, some evidence of phase II) • Enhanced sensitivity to pro-genotoxicants (i.e., requiring CYP1A metabolism • Functionality over 28 days of culture • ADME functionality continues even in disaggregated spheroids • Maintenance of spheroid structure allows them to be cultured using stirred-bioreactors • Higher sensitivity to hepatotoxicants versus HepaRG	(Leroy et al., 2021); (Basharat et al., 2020); (Biazi et al., 2020); (Calitz et al., 2019); (Fey et al., 2020); (Gaskell et al., 2016); (Jia et al., 2020); (Iyer et al., 2010); (Pluta et al., 2020); (Stampar et al., 2020); (Wrzesinski et al., 2013)

	• Capable of modulating the hepatic glucose-insulin axis	
Huh7	• Induction of hypoxia leading to apoptosis thus may not be suitable for spheroid formation • Large suite of CYP450 enzymes induced in Huh7 spheroids • Deployable for screening for pharmacological intervention of hepatic viruses • Some evidence that nuclear transcription factors upregulated in 3D (e.g., PXR) • Enhanced *CYP1A1* and *CYP1A2* mRNA expression • Huh7 spheroids mimic aggressive hepatic carcinoma malignancy	(Sainz et al., 2009); (Jung et al., 2017); (Terashima et al., 2015b)
HepaRG	• Enhanced sensitivity to genotoxicants (AFB, B[a]P) • Less sensitive than HepG2/C3A for detection of DILI positive compounds • High inducibility of CYP1A enzymes, also CYP3A4 • Evidence of CYP2B6 activity • Proteome closely aligned with PHHs • Detection of genotoxicants in chronic dosing studies • Significant sensitivity to DILI positive compounds such as APAP, KETO, TRV • Deployed for used in CYP3A4 drug-drug interaction studies/CYP inhibition • Secretion of apolipoproteins • Spheroid can mimic liver zonation and oxygen gradients • Extrapolation of pharmacokinetics to *in vivo* • Utility for high-throughout, multiplexed in vitro studies	(Takahashi et al., 2015); (Wang et al., 2015); (Basharat et al., 2020); (Tascher et al., 2019); (Rose et al., 2021); (Mandon et al., 2019); (Ramaiahgari et al., 2017); (Shin et al., 2018); (Ahn et al., 2019); (Zhang et al., 2020); (Ott et al., 2017)
PHHs	• Metabolic stability over several weeks, evidenced by both transcriptomics and metabolomics • Expression of all major CYP450 isoforms for metabolism of common pharmaceuticals (CYP1A2, CYP2C9, CYP2C19, CYP3A4, CYP2D6) • Co-culture with non-parenchymal cells for improved hepatic functionality (e.g., elicit immune response against DCF toxicity) • Enhanced sensitivity to small molecule compounds with cholestatic liabilities • Significantly enhanced CYP450 and UGT function • Readily deployed in screening cascades for DILI • Functional ammonia detoxification system, unlike HepG2 • mRNA expression of ADME proteins is maintained over prolonged periods of growth • Albumin secretion akin to that of hepatocytes in native tissue • Sensitivity to hepatotoxicants allows screening at more physiologically relevant concentrations • PHHs re-differentiated in 3D through inhibition of p53 via the WNT/beta-catenin pathway • Sensitive to inflammatory cytokines such as TNF-alpha • Suitable for modelling drug-induced steatosis	(Hendriks et al., 2016); (Granitzny et al., 2017); (Baze et al., 2018); (Vorrink et al., 2017); (Schofield et al., 2021); (Kanebratt et al., 2021a); (Oliva-Vilarnau et al., 2020); (Peng et al., 2018); (Kozyra et al., 2018b); (Messner et al., 2018); (Bell et al., 2018b); (Bell et al., 2017)

1.7. Utilising commercially available sources to generate advanced liver models

Most 3D hepatic models in the literature use the forced-aggregate approach for formation of both immortalised and primary hepatic models which are considerably easier, and cheaper to implement in toxicological screening strategies compared to advanced systems available commercially in 'ready-to-use' formats. Moreover, early estimates suggest that the liquid overlay technique to generate cell-repellent microplates, utilised extensively in the literature (Kyffin et al., 2019, Dorst et al., 2014, Carlsson and Yuhas, 1984, Costa et al., 2014), could generate spheroid microplates for as little as £0.90 per plate however microplates sourced commercially can be sourced for anywhere between £5 (Greiner Bio One) – £15 (Corning, Thermo Fisher Scientific), depending on vendor. Commercial plates have been shown to be suitable for the cultivation of monocultured hepatic cells including HepG2, PHH and HepaRG (Ingelman-Sundberg and Lauschke, 2021, Rose et al., 2021, Hurrell et al., 2019) , as well as multi-cellular spheroids with maintained viability and expressed function (Li et al., 2020, Kozyra et al., 2018a, Baze et al., 2018). However, given their cost versus the liquid agarose overlay technique, or indeed homemade hanging drop approaches such as those used by Shah et al. (2018b) in HepG2 spheroids, it is difficult to see how they might outperform other approaches. Notwithstanding these observations, commercially sought modalities may help bridge development-gaps in the pharmaceutical setting where the need for high-throughput of datasets and guaranteed reproducibility, outweighs the development of cheaply implemented alternatives.

Where development of hepatic spheroid models represents a bottleneck in terms of method development or the use of primary human tissue presents poor reproducibility of datasets,

then a number of vendors including Corning, Thermo Fish and BioIVT repositories have a range of batch-certified PHHs that have qualified ADME status and the ability to form spheroids (BioIVT, 2021, Corning Life Sciences Inc, 2018, Thermo Fisher Scientific, 2021), with greater sensitivity compared to monolayers of the same cells, guaranteed. InSightLiver spheroids and microplate from InSphero are another example of this but available in several species formats, integrating primary hepatocytes derived from rodent models, dog and primates in a 96-well format with other liver cell types (Messner et al., 2018, Proctor et al., 2017). The microtissues maintained viability over 28 days of cultivation, with the continued expression of liver specific markers such as albumin and CYP450 activity, with some evidence for the induction of cellular polarity (Proctor et al., 2017) and drug transporter activity (Messner et al., 2018). The HepaPredict system of pre-prepared spheroids have been shown to express the common suite of P450 enzymes (Bell et al., 2016), associated with the metabolism of most pharmaceuticals, functional biliary secretion systems and long-term stability (Vorrink et al., 2017), but more importantly, availability of different batches of hepatocytes in this system may potentially allow for idiosyncratic drug reactions and metabolism to be studied (Hendriks et al., 2020b). Elsewhere, other commercial hepatic models include the OrganoPlate which supports the use several different hepatic models in a 96-array format including spheroids and cell lines and is extensively reviewed by Jang et al. (2015).

Several liver-on-chip devices are available commercially where fluid flow dynamics and shear stress like that observed in the human liver, has been shown to improve the overall vitality and functionality of hepatic models. In particular, it is well observed that medium flow has

been shown to upregulate nuclear-receptor mediated drug metabolism in hepatic cells, e.g., AhR-CYP1A1 activity in HepG2 monolayers (Mufti et al., 1995), and in HepG2/C3A models (Shvartsman et al., 2009), thus demonstrating that recapitulation of hepatic-fluid flow may regulate hepatic function.

For example HepaRG cells were differentiated using a liver-chip device to recapitulate impaired liver function related to disease, e.g., repressed CYP1A2 function (Jang et al., 2019) whereas (Tsamandouras et al., 2017) performed in vitro – in vivo extrapolations using a series of different hepatocyte donors on a similar perfused chip device assessing population-level drug metabolism (e.g., phenacetin CY1A activity) potential in PHH spheroid batches. Use of a multi-compartment bioreactor fluidic modality from Kirkstall Ltd improved CYP1A2 and CYP2D6 functionality in hepatocytes derived from iPSCs under fluid-shear stress (Rashidi et al., 2016), with reduction of immature hepatocyte markers, however serum albumin secretion and expression of CPS1 (relating to the urea cycle) was also depleted suggesting loss of viability. Furthermore, this mini-bioreactor was found to have improved the functionality of the commercially transfected hepatic cell model, Upcyte (Ramachandran et al., 2015) in-long term xenobiotic exposure studies.

1.8. Liver organoids

The development of techniques, technologies and approaches to generate human-relevant hepatic organoids has gathered much attention in recent years for evaluation of hepatotoxic drugs, xenobiotic metabolism, and disease modelling (Prior et al., 2019). Organoids are 3D structures formed from several different cell types which could include induced pluripotent (iPSCs), naïve embryonic stem cells or possibly even mature adult cells, e.g., those from liver

resections or biopsies (Xie et al., 2021) that are typically grown on or in matrix- and growth hormone-supplemented hydrogels, e.g., Corning Matrigel (Huch et al., 2015). Evidence indicates that cultivation of hepatic stem cells with Wnt controls the proliferation and differentiation of stem cells towards the preferred terminal lineage, e.g., hepatocyte (Oliva-Vilarnau et al., 2020, Huch et al., 2013, Hay et al., 2008b, Hay et al., 2008a) whereas other growth hormones such as hepatocyte growth factor may be important for other cell types such as cholangiocytes and hepatobiliary cells.

ADME gene expression profiles and vascularisation are essential functions of the human liver *in vivo.* Early organoid work from Takebe et al. (2013) showed that iPSCs could be used in order to generate functional liver organoids with recapitulated ADME gene expression profiles and evidence of zonal-vascularisation in implantable human organoids in murine models but later updated enabling the production of liver bud organoids without the need for transplantation (Takebe et al., 2017). Compared to some hepatic *in vitro* models, the xenobiotic metabolic potential of liver organoids is considerable (Lancaster and Huch, 2019). In some cases the generation of organoids direct from hepatic tissue cells has been found to have drug metabolism ability greater than that of the original tissue (Park et al., 2019). Scalable liver organoids were formed from human cells to reveal models that was strikingly aligned to the human liver *in vivo* (Mun et al., 2019) including inducibility of drug metabolism exemplified by significant CYP3A4 activity and evidence of phase II drug metabolism as well as having structural similarities to the liver. Hepatotoxicity screening revealed increased sensitivity to DILI-registered drugs such as APAP and troglitazone compared to PHHs in 2D through multiple endpoints including detection of reactive oxygen

species at clinically-relevant exposures (C_{max}) (Mun et al., 2019). Maintenance of oxygen gradient across the hepatic parenchyma is critical to liver drug metabolism capabilities, revealing functional zones throughout the liver (Farzaneh et al., 2020). Knowledge and selection of key transcriptional pathways could be advantageous for generating 'tuneable' organoids and possibly even recapitulate patient polymorphisms such as those associated with key CYP enzymes such as the 2D6* family.

There is emerging evidence that liver organoids may also serve a role in genotoxicology studies (Caipa Garcia et al., 2021) however their applicability in such studies is still gathering attention (Guo et al., 2020). Liver organoids are showing significant promise for use in cross-species toxicological studies (Augustyniak et al., 2019). Further data is scarce in liver organoids, and this may be because of inadequate DNA repair competency – one of the principal drivers as to why immortalised cell lines are used favourably in genotoxicity testing. Hence the use of liver organoids in genotoxicity studies represents a very early area of development that is currently being discussed by such working groups as the International Workshop on Genotoxicity Testing (IWGT) - (Pfuhler et al., 2020). Hence, this thesis principally focuses on the use of the readily-available and well characterised HepG2/C3A cell line for deployment in a range of *in* vitro toxicological studies.

1.9. A critical perspective on the use of hepatic 3D models in *in vitro* genotoxicity experiments

The use of advanced cell culture models such as 3D spheroids have been gathering traction in several toxicological fields including genotoxicity assessment (Guo et al., 2020, Pfuhler et

al., 2020) however they are behind in terms of the considerable developments that have been made regarding the use of advanced hepatic models in hepatotoxicity studies. Although, considering that many of those small molecules typically studied in *in vitro genetic toxicology screens* share considerable chemical similarity to commonly prescribed pharmaceuticals, it seems strange that there hasn't been more of an overlap between these parties. For example, PAHs or aromatic amines which are common structural motifs found within pharmaceutical agents (Bradshaw et al., 2018), e.g., tolcapone. Biazi et al. (2020) used HepG2/C3A spheroids and monolayers for investigating the genotoxicity potential of naturally derived alkaloids but failed to provide a thorough comparison between 2D and 3D responses (i.e., comet assay was only performed in 2D monolayers). Several assays that are traditionally performed in monolayers of cells or cell suspensions such as the comet assay (Elje et al., 2019a) or micronucleus assay (Sommer et al., 2020, Conway et al., 2020), have proved effective in spheroid models but clearly require further development, particularly in terms of applicability and approaches to methodologies. In a similar vein to the Mechanism-Based Integrated Systems for the Prediction of Drug-Induced Liver Injury (IMI MIP-DILI) project, one could envisage a multi-centre approach to generate a series of data packages in this model types that could be questioned and examined empirically using a training set of compounds (Dragovic et al., 2016); this approach was taken in the recent development of a high-throughput comet assay for use in genotoxicity studies which utilised a training set of compounds from the National Toxicology Programme, USA (Sykora et al., 2018).

Most of the published spheroid models that detail approaches to assessing genetic toxicity mainly use endpoint-based assessments; as such the IWGT intends to assemble a series of

robust protocols that could be deployed in organoid models to test a battery of prototypical genotoxicants and thus may be directly appropriate to adoption in a regulatory sense (Pfuhler et al., 2020). One area of particular concern is the development of 3D hepatic assays capable of assessing potential substances for gene mutation capacity such as PAHs (Kirkland et al., 2016). It is therefore clear that use of 3D spheroid models for use in genotoxicity testing is gathering attention, however the robustness, reproducibility of validity of such approaches requires much attention to ensure assays are fit for purpose and capable of offering 'value added alternatives' to those models currently employed.

Table 1.3. Overview of the toxicological mechanisms associated with (geno)-toxicants commonly deployed in in vitro toxicology studies using a combination of 2D and 3D hepatic cell models.

Compound	Typical human exposure routes	IARC Class*; Associated damage caused	Deduced mechanism of action (incl. metabolism routes)	Selected references
2-Aminoanthracene; 2-AA **2-actetly aminofluorene; 2-AAF** **2-amino-3-methylimidazo [4,5-f]quinoline; IQ**	Occupational carcinogens likely found in dyes/inks, plastic manufacturing	IARC Group 2A carcinogen. Hepatocarcinogenesis but also other tumours likely.	Model aromatic amines. Likely route of metabolism is via CYP1A family through N-hydroxylation to hydroxylamine. Some evidence that other hepatic phase I enzymes may also be involved such as FMOs. Hydroxylamine metabolites capable of reacting with DNA. Alternatively, NAT1/2 acetylation to yields electrophilic nitrenium ion which binds directly to DNA. In the case of IQ the ester formation most likely carcinogenic moiety. Reactive moieties bind to nucleophilic DNA bases inducing oxidative stress, potentially inducing mutagenic events	(Weisburger and Weisburger, 1973, Rendic and Guengerich, 2012); (Means et al., 2003); (Rodrigues et al., 1994); (Moller et al., 2002)
Aflotoxin B1; **AFB1**	Exposure to molds and fungi, e.g., aspergillus family	IARC Group 1 carcinogen. Necrosis of the liver leading to cirrhosis and eventual carcinoma; intestinal tumours	Hepatic CYP1A2 and 3A4 activate AFB1 to form reactive metabolite epoxide, but possibly CYP2A family members also. Which may be detoxified via GST routes. CYP450s hydrolyse AFB1 to DNA-reactive diol epoxide which intercalates DNA through covalent binding. DNA adducts formed through alkylation with guanine bases forming mutation to p53 tumour suppressor gene through transversions. If not repaired by nuclear excision repair system then altered p53 state triggers downstream events such as cell-cycle stalling, cell death (apoptosis), leading to carcinogenesis events. ROS and oxidative stress mechanism implicated.	(Cai et al., 2020, Benkerroum, 2020, Rushing and Selim, 2019, Dohnal et al., 2014)
Benzo[a]pyrene; B[a]P	Incomplete combustion sources; cigarette smoke; cured foods, e.g., smoked salmon	IARC Group 2A carcinogen; Hepatocarcinogenesis Plus multiple tumours	Pro-genotoxicant induces CYP1A1 via AhR with major metabolic route via CYP1A1 and CYP1B1 to unstable diol-epoxide. Metabolite intercalates covalently with DNA and undergoes electrophilic substitution with guanine or thymidine bases forming bulky lesions. Affinity with tumour suppressor gene regions (p53), triggering carcinogenesis events as with AFB1. Recent evidence suggests that B[a]P may be capable of inducing metabolic reprograming (Warburg effect) in mitochondria towards hepatic cell survival and reversal of carcinogenic mechanisms. Evidence that B[a]P may induce drug exporter proteins e.g., MRP2 as a potential route of excretion in liver. ROS and oxidative stress mechanism implicated.	(Hardonniere et al., 2016, Schults et al., 2014, Park et al., 2006, Schwarz et al., 2001); (Faber et al., 2003)
2-amino-1-methyl-6-phenylimidazo [4,5-b]pyridine; PhiP	Mostly food borne sources	IARC Group 2B carcinogen. Mostly haematopoetic tumours	Heterocyclic aryl amine with major route of metabolism is through N-hydroxylation by CYP1A family. DNA and protein-reactive deoxyguanosine moieties formed by further esterification by NAT and SULT routes.	(Muckel et al., 2002, Rendic and Guengerich, 2012); (Davis et al., 1993); (Snyderwine et al., 1992)
4-Nitroquinoline-*N*-oxide; 4-NQO	Limited occurrences in natural environment, most manufactured sources	Mostly adenocarcinomas of lung and oral carcinogenesis	Direct acting DNA alkylating agent. 4-NQO is potentially detoxified by glutathione thus ROS is implicated as a potential mechanism of toxicity in the liver. Thought to be hepatically cleared and detoxified by conjugation of the reactive hydroxyaminoquinoline metabolites. Both parent and hydroxy metabolite bind with DNA (and proteins) causing mutagenicity and genotoxicity if DNA lesions not repaired. Some evidence that 4-NQO may induce DNA breaks via induction of topoisomerases.	(Peklak-Scott et al., 2005, Arima et al., 2006); (Arima et al., 2006); (Miao et al., 2006)

*** IARC (International Agency for Research on Cancer). Classification of compounds as (Kirkland et al., 2016)**

1.10. Considerations for the inclusion of advanced *in vitro* models in nonclinical safety evaluations

The use of advanced *in vitro* models for use in toxicological studies has gained significant attention in the last 10 years. For example, as a representative parameter of the situation, the 3D cell culture market alone is thought to grow by between 10 -15 % in the years 2019 – 2028 (Grand View Research, 2021, Allied Market Research, 2020); the main market contributor to this is those involved in drug discovery and chemical safety assessment. It is clear that 3D cell culture models are making a significant contribution to a number of research areas, however there is a general concern that the velocity with which these developments are being made (e.g., commercial white papers, number of peer-reviewed publications using advanced *in vitro* platforms) is potentially transcending critical applicability and robustness evaluation (Anklam et al., 2021). Thus there remains a sincere need to develop evaluation strategies as to the applicability of 3D cell culture models for regulatory toxicology use (Lee et al., 2020, Guo et al., 2020) or for general deployment for preclinical research (Weaver et al., 2020) – see Figure 1.3. Several programmes such as the IMI-MIP DILI consortium have sort to undertake significant reproducibility and robustness assessments of such models. In order to reduce the number of false-positive results in toxicity studies and more reliable translation from *in vitro* to *in vivo* predictions, the best *in vitro* model for both geno – hepatotoxicity studies would ideally be metabolically active, represent *in vivo* liver function (Lee et al., 2020, Jia et al., 2020, Kuna et al., 2018) , be p53 competent and therefore be DNA-repair proficient (Kirkland et al., 2007, Guo et al., 2020), and demonstrate that an *in vitro* derived endpoints, are clinically relevant.

1.11. Emerging modalities for the characterisation of toxicological models and safety assessment of chemicals using alternative approach methodologies

All industries concerned with the manufacture of chemical entities for example agriculture (e.g., pesticides, animal feeds), cosmeceuticals, drug discovery, and pharmaceutical research, are required to undertake a series of integrated, mandatory risk assessments relating to the likelihood of a given novel chemical entity (NCE) being genotoxic (Thybaud et al., 2017, Hartwig et al., 2020) or hepatotoxic (Daston et al., 2015, European Medicines Agency, 2010). The Committee on Mutagenicity of Chemicals in Food, Consumer Products and the Environment (COM), International Council for Harmonisation of Technical Requirements for Pharmaceuticals for Human Use (ICH) whereas the Organisation for Economic Co-operation and Development (OECD), outline a tiered strategy for the genotoxicity testing of chemical substances (OECD, 2017). As well as these studies being mandatory, the early identification of chemical hazards is of particular benefit to industries for the development of new pharmaceuticals where hazardous chemistry is not only of high risk to humans exposed to these medicines, but also to the pharmaceutical industry in terms of the financial burden associated with the early termination of drug discovery programmes due to safety concerns (Hartwig et al., 2020). Regulatory agencies are still heavily reliant upon data collected from *in vivo* animal studies to predict human health risks in terms of individual organ and whole host response, yet translation from animal to man often prove difficult when considering genetic and species differences (Ingber, 2020). Therefore, many events, such as chemically-induced genotoxicity or drug toxicity, are more likely to be missed or at best, underpredicted. Ethical approval for use of *in vivo* animal models and welfare considerations are also implicated in toxicity studies under the UK [Animals (Scientific

Procedures) Act 1986] and in the EU [Directive on the protection of animals used for scientific procedures (2010/63/EU)], as well as the economic burden that typical *in vivo* studies carry. Current *in vitro* systems are used in isolation as part of the core battery of tests in toxicity studies, but fail to mimic the biological environments seen *in vivo* and lack the reporting power to be able to reliably extrapolate across to predict the hazards in humans exposed to toxic chemicals but may prove useful in being able to assemble adverse outcome pathways.

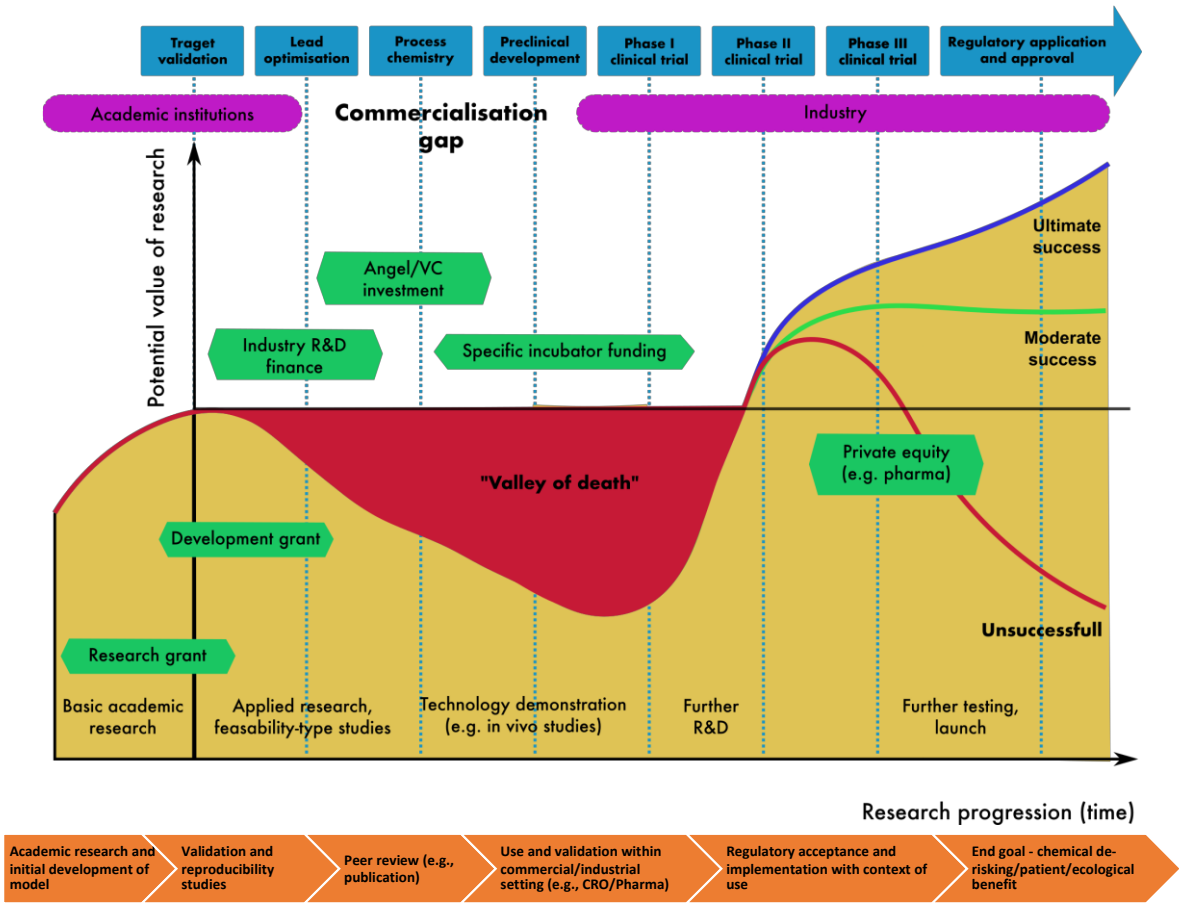

Figure 1.4. The journey for acceptance of novel models (e.g., 3D spheroids) from academia into regulatory testing pipelines within the context of the drug discovery innovation process. *A figure modelled on (Fernandez-Moure, 2016, Linton and Xu, 2020).*

1.11.1. Potential for the integration of advanced 3D models with NAMs

The use of computational learning modalities such as *deep learning, machine learning or AI* have been introduced to toxicological testing pipelines (Minerali et al., 2020); some of the earliest approaches were made over 10 years ago in a study used QSAR data and that derived from toxicogenomic screens to identify potential nongenotoxic molecules with carcinogenic potential in the liver (Liu et al., 2011), however the greatest traction for use of such models has really been made in the last 3-5 years. Put simply, these approaches assemble of panel of training compounds typically deployed in screens for DILI or genotoxicity pipelines and attempt to correlate biological *in vitro* data alongside physicochemical structure data such as those derived from Qualitative Structure Active Relation (QSAR) models. For example in the context of hepatoxicity, AstraZeneca introduced a Bayesian statistical model for the prediction of hepatoxicity using a suite of *in vitro* systems which included 3D HepG2/C3A spheroids, alongside models for mitochondrial toxicity, informing the filtration of potential hazardous NCEs with improvement over using *in vitro* assays alone (Williams et al., 2020); a similar Bayesian approach was undertaken by Pfizer (Aleo et al., 2020) using a panel of compounds assembled from the FDA Liver Tox Knowledge Database (LTKB) and correlated Chen's Rule of Two approach alongside *in vitro* toxicity data, successfully identifying over 80 % the most severe DILI compound classes. Advanced learning modalities are also being deployed for analysing datasets associated with genotoxic or carcinogenic endpoints, for identification of aneugen liabilities and gamma-H2AX assays to acquire data that were inputted into a deep-learning model (Wilson et al., 2021). Using a Bayesian statistical model, it was found that accuracy was captured at 95 % with a high Matthews correlation coefficient versus undertaking the assays alone, reducing overall

analysis time (Wilson et al., 2021). A similar method was applied by the US National Toxicology Programme for the use in carcinogenicity testing termed *DeepCarc*, which improved predictivity versus standardised QSAR models and in vitro datasets by more than 30 % (Li et al., 2021b). Future research should therefore look to assess for the convergence of *in vitro spheroid* datasets and computational modelling approaches, which could be funnelled into a single predictive tool for use in toxicology, potentially limiting or eradicating the need for *in vivo* rodent models entirely.

1.12. Conclusions

Despite advances in 3D cell culture models, the most probable position that such models could occupy under current guidelines is within the nonclinical safety evaluation space for the safety assessment of novel chemical entities, e.g., pharmaceuticals for human use. However, such bodies as the FDA define fundamental questions that need to be addressed in order to pitch these models for regulatory use concerning human toxicity prediction studies, more than current models used, e.g., target organ toxicity and predictive biomarkers, pharmacokinetic – pharmacodynamic (PKPD) and dose finding (Wang et al., 2021). There is still, therefore, a need to understand the 'valued-added' of such approaches in the regulatory context and a deeper understanding as to the potential of 3D cell culture models and their role in both preclinical and regulatory safety testing

1.13. Thesis motivations and aims

There were several overarching aims of this thesis presented which were all centred around the use and deployment of the HepG2/C3A cell line in a range of *in vitro* assays for assessing potential toxicological endpoints, and to further characterise the HepG2/C3A spheroid by

extracellular flux analysis transcriptomic approaches. Therefore, the specific goals of this thesis were to:

i. Undertake a critical assessment of the requirements needed to develop a simple HepG2/C3A spheroid model and deploy it in a series of proof-of-concept studies (**Chapter 2**)
ii. Implement a HepG2/C3A spheroid model in a battery of *in* vitro assays to assess the genotoxic potential of chemical carcinogens (**Chapter 3**)
iii. Develop a robust methodology for the measurement of cellular-mitochondrial respiration in single spheroids of varying sizes and cell lineage (**Chapter 4**)
iv. Evaluate the longevity of HepG2/C3A spheroids through a series of approaches and their applicability to repeat-dose assays to assess genotoxic and hepatotoxic potential of chemicals (**Chapter 5**)
v. Undertake a transcriptomic comparison on HepG2/C3A cells across a continuum from monolayers to spheroids cultured for up to 28 days by use of paired-end RNA-seq (**Chapter 6**)

1.13.1. Thesis overview

Chapter 2 describes a study that critically assesses the use of agarose hydrogels to form cell-repellent microwell plates for the cultivation of spheroids. Given the generally accepted paradigm that culturing hepatic cells in three-dimensions improves their potential hepatic phenotype we subjected HepG2/C3A spheroids to phenotypic assays to assess hepatotoxic and genotoxic endpoints. It was hypothesised that (1) HepG2/C3A would form better spheroids compared to the parental HepG2 cells and (2) that HepG2/C3A spheroids would

be more sensitive to three common hepatotoxicants and two genotoxicants in terms of their phenotypic response, compared to monolayers of cells employed in the same assays.

Chapter 3 presents a study in which the generation of HepG2/C3A spheroids is further optimised and subsequent spheroids and monolayers are used to assess the potential DNA damage induced on exposure to compounds requiring xenobiotic metabolism to toxic intermediates. We hypothesised that (1) HepG2/C3A spheroids could be cultured long-term but would continue to proliferate in both size and cell number but with maintained viability; (2) the basal mRNA expression of key hepatic genes such as those encoding ADME genes, would be significantly enhanced in those spheroids versus monolayers, and further induced on exposure to pro-genotoxicants and (3) sensitivity to pro-genotoxicants would therefore be enhanced in 3D spheroids.

In Chapter 4, in order to assess the impact of spheroids we wanted to understand the impact of cell number and spheroid size in terms of mitochondrial respiratory metabolic analyses of a single spheroid and how these might be used in subsequent chapters to assess metabolism over a time continuum. It was hypothesised that (1) mitochondrial respiration would change in spheroids as a function of total spheroid cell number and size; (2) cellular respiration could be measured in single 3D spheroids of varying size and cell number and (3) cellular metabolism could be distinguished between different carcinoma cell types and this would have important implications for measuring different cellular phenotype of subsequent HepG2/C3A spheroids in the future.

Chapter 5 details a series of studies undertaken in HepG2/C3A spheroids cultivated over a time continuum up to 28 days or assessed the impact of time in terms of exposure modalities. It was hypothesised that (1) viability of spheroids would be maintained at high-enough levels over 28 days to perform phenotypic assays, but overall spheroid vitality would begin to decline at later time points in-line with literature observations; (2) markers of endogenous metabolism such as albumin production and mitochondrial respiration would change in favour of a more hepatic phenotype away from malignant monolayer cell types and (3) repeatedly-exposed HepG2/C3A spheroids would be more sensitive in screens for hepatotoxicity and genotoxicity versus acute dose in Chapter 3.

Finally, in **Chapter 6**, genome-wide RNA-seq transcriptomics is performed on HepG2/C3A monolayers and spheroids grown for 7, 14, 21 or 28 days under standard tissue culture conditions. Our final hypothesis was that (1) HepG2/C3A models would all diverge across a time continuum and that spheroids would be clearly distinguished from monolayer cells in terms of differential gene expression analysis and (2) advanced gene ontology pathway analyses would reveal systematic changes in HepG2/C3A spheroids in favour of a hepatic phenotype, away from its hepatocellular carcinoma origins

1.14. References

Ahn, J., Ahn, J. H., Yoon, S., Nam, Y. S., Son, M. Y. and Oh, J. H. (2019) 'Human three-dimensional in vitro model of hepatic zonation to predict zonal hepatotoxicity', *J Biol Eng,* 13, pp. 22.

Aithal, G. P. (2004) 'Diclofenac-induced liver injury: a paradigm of idiosyncratic drug toxicity', *Expert Opin Drug Saf,* 3(6), pp. 519-23.

Aleo, M. D., Shah, F., Allen, S., Barton, H. A., Costales, C., Lazzaro, S., Leung, L., Nilson, A., Obach, R. S., Rodrigues, A. D. and Will, Y. (2020) 'Moving beyond Binary Predictions of Human Drug-Induced Liver Injury (DILI) toward Contrasting Relative Risk Potential', *Chem Res Toxicol,* 33(1), pp. 223-238.

Allied Market Research (2020) *3D Cell Culture Market Overview* Available at: https://www.alliedmarketresearch.com/3d-cell-cultures-market (Accessed: 15th February 2021 2021).

Aninat, C., Piton, A., Glaise, D., Le Charpentier, T., Langouët, S., Morel, F., Guguen-Guillouzo, C. and Guillouzo, A. (2006) 'Expression of cytochromes P450, conjugating enzymes and nuclear receptors in human hepatoma HepaRG cells', *Drug metabolism and disposition,* 34(1), pp. 75-83.

Anklam, E., Bahl, M. I., Ball, R., Beger, R. D., Cohen, J., Fitzpatrick, S., Girard, P., Halamoda-Kenzaoui, B., Hinton, D., Hirose, A., Hoeveler, A., Honma, M., Hugas, M., Ishida, S., Kass, G. E., Kojima, H., Krefting, I., Liachenko, S., Liu, Y., Masters, S., Marx, U., McCarthy, T., Mercer, T., Patri, A., Pelaez, C., Pirmohamed, M., Platz, S., Ribeiro, A. J., Rodricks, J. V., Rusyn, I., Salek, R. M., Schoonjans, R., Silva, P., Svendsen, C. N., Sumner, S., Sung, K., Tagle, D., Tong, L., Tong, W., Eijnden-van-Raaij, J. V. D., Vary, N., Wang, T., Waterton, J., Wang, M., Wen, H., Wishart, D., Yuan, Y. and Slikker, W., Jr. (2021) 'Emerging technologies and their impact on regulatory science', *Exp Biol Med (Maywood)*, pp. 15353702211052280.

Arima, Y., Nishigori, C., Takeuchi, T., Oka, S., Morimoto, K., Utani, A. and Miyachi, Y. (2006) '4-Nitroquinoline 1-Oxide Forms 8-Hydroxydeoxyguanosine in Human Fibroblasts through Reactive Oxygen Species', *Toxicological Sciences,* 91(2), pp. 382-392.

Arzumanian, V. A., Kiseleva, O. I. and Poverennaya, E. V. (2021) 'The Curious Case of the HepG2 Cell Line: 40 Years of Expertise', *International Journal of Molecular Sciences,* 22(23).

Augustyniak, J., Bertero, A., Coccini, T., Baderna, D., Buzanska, L. and Caloni, F. (2019) 'Organoids are promising tools for species-specific in vitro toxicological studies', *Journal of Applied Toxicology,* 39(12), pp. 1610-1622.

Balaphas, A., Meyer, J., Perozzo, R., Fontana, P., Berndt, S., Turzi, A., Morel, P., Scapozza, L., Sadoul, K., Gonelle-Gispert, C. and Buhler, L. (2019) 'Interactions between platelets and liver sinusoidal endothelial cells promote hepatic stellate cells to drive liver regeneration', *British Journal of Surgery,* 106, pp. 8-9.

Banales, J.M., Huebert, R.C., Karlsen, T., Strazzabosco, M., LaRusso, N.F and Gores, G.J. (2019) 'Cholangiocyte Pathobiology', *Nature Reviews Gastroenterology & Hepatology*, 16(5), pp. 269-81.

Basharat, A., Rollison, H. E., Williams, D. P. and Ivanov, D. P. (2020) 'HepG2 (C3A) spheroids show higher sensitivity compared to HepaRG spheroids for drug-induced liver injury (DILI)', *Toxicol Appl Pharmacol,* 408, pp. 115279.

Baze, A., Parmentier, C., Hendriks, D. F. G., Hurrell, T., Heyd, B., Bachellier, P., Schuster, C., Ingelman-Sundberg, M. and Richert, L. (2018) 'Three-Dimensional Spheroid Primary Human Hepatocytes in Monoculture and Coculture with Nonparenchymal Cells', *Tissue Engineering Part C-Methods,* 24(9), pp. 534-545.

Beggs, K. M., Fullerton, A. M., Miyakawa, K., Ganey, P. E. and Roth, R. A. (2014) 'Molecular mechanisms of hepatocellular apoptosis induced by trovafloxacin-tumor necrosis factor-alpha interaction', *Toxicological sciences : an official journal of the Society of Toxicology,* 137(1), pp. 91-101.

Beken, S., Kasper, P. and van der Laan, J. W. (2016) 'Regulatory Acceptance of Alternative Methods in the Development and Approval of Pharmaceuticals', *Adv Exp Med Biol,* 856, pp. 33-64.

Bell, C. C., Chouhan, B., Andersson, L. C., Andersson, H., Dear, J. W., Williams, D. P. and Soderberg, M. (2020) 'Functionality of primary hepatic non-parenchymal cells in a 3D spheroid model and contribution to acetaminophen hepatotoxicity', *Arch Toxicol,* 94(4), pp. 1251-1263.

Bell, C. C., Dankers, A. C. A., Lauschke, V. M., Sison-Young, R., Jenkins, R. and Rowe, C. (2018a) 'Comparison of hepatic 2D sandwich cultures and 3D spheroids for long-term toxicity applications: a multicenter study', *Toxicol Sci,* 162, pp. 655-66.

Bell, C. C., Dankers, A. C. A., Lauschke, V. M., Sison-Young, R., Jenkins, R., Rowe, C., Goldring, C. E., Park, K., Regan, S. L., Walker, T., Schofield, C., Baze, A., Foster, A. J., Williams, D. P., van de Ven, A. W. M., Jacobs, F., Houdt, J. V., Lahteenmaki, T., Snoeys, J., Juhila, S., Richert, L. and Ingelman-Sundberg, M. (2018b) 'Comparison of Hepatic 2D Sandwich Cultures and 3D Spheroids for Long-term Toxicity Applications: A Multicenter Study', *Toxicol Sci,* 162(2), pp. 655-666.

Bell, C. C., Hendriks, D. F., Moro, S. M., Ellis, E., Walsh, J., Renblom, A., Fredriksson Puigvert, L., Dankers, A. C., Jacobs, F., Snoeys, J., Sison-Young, R. L., Jenkins, R. E., Nordling, A., Mkrtchian, S., Park, B. K., Kitteringham, N. R., Goldring, C. E., Lauschke, V. M. and Ingelman-Sundberg, M. (2016) 'Characterization of primary human hepatocyte spheroids as a model system for drug-induced liver injury, liver function and disease', *Sci Rep,* 6, pp. 25187.

Bell, C. C., Lauschke, V. M., Vorrink, S. U., Palmgren, H., Duffin, R., Andersson, T. B. and Ingelman-Sundberg, M. (2017) 'Transcriptional, Functional, and Mechanistic Comparisons of Stem Cell-Derived Hepatocytes, HepaRG Cells, and Three-Dimensional Human Hepatocyte Spheroids as Predictive In Vitro Systems for Drug-Induced Liver Injury', *Drug Metab Dispos,* 45(4), pp. 419-429.

Benedetti, A., Di Sario, A., Marucci, L., Svegliati-Baroni, G., Schteingart, C.D., Ton-Nu, H.T and Hofmann, A.F. (1997) 'Carrier-Mediated Transport of Conjugated Bile Acids across the Basolateral Membrane of Biliary Epithelial Cells' *The American Journal of Physiology*, 272 (6), pp. 1416-1424.

Benkerroum, N. (2020) 'Chronic and Acute Toxicities of Aflatoxins: Mechanisms of Action', *Int J Environ Res Public Health,* 17(2).

Biazi, B. I., Zanetti, T. A., Marques, L. A., Baranoski, A., Coatti, G. C. and Mantovani, M. S. (2020) 'mRNAs biomarker related to the control of proliferation and cell death in HepG2/C3A spheroid and monolayer cultures treated with piperlongumine', *Applied Cancer Research,* 40(1), pp. 2.

BioIVT (2021) *Human SPHEROID CERTIFIED HEPATOCYTES*. Available at: https://bioivt.com/human-spheroid-certified-hepatocytes (Accessed: 01 June 2021 01 June 2021).

Bjornsson, E. S. (2017) 'Hepatotoxicity of statins and other lipid-lowering agents', *Liver Int,* 37(2), pp. 173-178.

Boehme, K., Dietz, Y., Hewitt, P. and Mueller, S. O. (2010) 'Activation of P53 in HepG2 cells as surrogate to detect mutagens and promutagens in vitro', *Toxicol Lett,* 198(2), pp. 272-81.

Boess, F., Kamber, M., Romer, S., Gasser, R., Muller, D., Albertini, S. and Suter, L. (2003) 'Gene expression in two hepatic cell lines, cultured primary hepatocytes, and liver slices compared to the in vivo liver gene expression in rats: possible implications for toxicogenomics use of in vitro systems', *Toxicol Sci,* 73(2), pp. 386-402.

Bolder, U., Trang, N.V., Hagey, L.R., Schteingart, C.D., Cerre, C., Elferink, R.P and Hofmann, A.F. (1999) 'Sulindac Is Excreted into Bile by a Canalicular Bile Salt Pump and Undergoes a Cholehepatic Circulation in Rats' *Gastroenterology*, 117(4), pp.962-71.

Boon, R., Kumar, M., Tricot, T., Elia, I., Ordovas, L., Jacobs, F., One, J., De Smedt, J., Eelen, G., Bird, M., Roelandt, P., Doglioni, G., Vriens, K., Rossi, M., Vazquez, M. A., Vanwelden, T., Chesnais, F., El Taghdouini, A., Najimi, M., Sokal, E., Cassiman, D., Snoeys, J., Monshouwer, M., Hu, W. S., Lange, C., Carmeliet, P., Fendt, S. M. and Verfaillie, C. M. (2020) 'Amino acid levels determine metabolism and CYP450 function of hepatocytes and hepatoma cell lines', *Nat Commun,* 11(1), pp. 1393.

Bouwens, L., Baekeland, M., Dezanger, R. and Wisse, E. (1986) 'Quantitation, Tissue Distribution and Proliferation Kinetics of Kupffer Cells in Normal Rat-Liver', *Hepatology,* 6(4), pp. 718-722.

Boyer, J. L. (2013) 'Bile formation and secretion', *Compr Physiol,* 3(3), pp. 1035-78.

Bradshaw, P. R., Athersuch, T. J., Stachulski, A. V. and Wilson, I. D. (2020) 'Acyl glucuronide reactivity in perspective', *Drug Discov Today,* 25(9), pp. 1639-1650.

Bradshaw, P. R., Wilson, I. D., Gill, R. U., Butler, P. J., Dilworth, C. and Athersuch, T. J. (2018) 'Metabolic Hydrolysis of Aromatic Amides in Selected Rat, Minipig, and Human In Vitro Systems', *Scientific Reports,* 8(1), pp. 2405.

Brunell, D., Sagher, D., Kesaraju, S., Brot, N. and Weissbach, H. (2011) 'Studies on the metabolism and biological activity of the epimers of sulindac', *Drug Metab Dispos,* 39(6), pp. 1014-21.

Busche, M., Tomilova, O., Schutte, J., Werner, S., Beer, M., Groll, N., Hagmeyer, B., Pawlak, M., Jones, P. D., Schmees, C., Becker, H., Schnabel, J., Gall, K., Hemmler, R., Matz-Soja, M., Damm, G., Beuck, S., Klaassen, T., Moer, J., Ullrich, A., Runge, D., Schenke-Layland, K., Gebhardt, R. and Stelzle, M. (2020) 'HepaChip-MP - a twenty-four chamber microplate for a continuously perfused liver coculture model', *Lab Chip,* 20(16), pp. 2911-2926.

Cai, P., Zheng, H., She, J., Feng, N., Zou, H. and Gu, J. (2020) 'Molecular mechanism of aflatoxin-induced hepatocellular carcinoma derived from a bioinformatics analysis'.

Caipa Garcia, A. L., Arlt, V. M. and Phillips, D. H. (2021) 'Organoids for toxicology and genetic toxicology: applications with drugs and prospects for environmental carcinogenesis', *Mutagenesis*.

Calitz, C., Hamman, J. H., Fey, S. J., Viljoen, A. M., Gouws, C. and Wrzesinski, K. (2019) 'A sub-chronic Xysmalobium undulatum hepatotoxicity investigation in HepG2/C3A spheroid cultures compared to an in vivo model', *J Ethnopharmacol,* 239, pp. 111897.

Caparrotta, T. M., Antoine, D. J. and Dear, J. W. (2018) 'Are some people at increased risk of paracetamol-induced liver injury? A critical review of the literature', *Eur J Clin Pharmacol,* 74(2), pp. 147-160.

Carlsson, J. and Yuhas, J. M. (1984) 'Liquid-Overlay Culture of Cellular Spheroids', *Recent Results in Cancer Research,* 95, pp. 1-23.

Chao, C., Ngo, L. P. and Engelward, B. P. (2020) 'SpheroidChip: Patterned Agarose Microwell Compartments Harboring HepG2 Spheroids are Compatible with Genotoxicity Testing', *ACS Biomaterials Science & Engineering,* 6(4), pp. 2427-2439.

Chatterjee, S., Richert, L., Augustijns, P. and Annaert, P. (2014) 'Hepatocyte-based in vitro model for assessment of drug-induced cholestasis', *Toxicol Appl Pharmacol,* 274(1), pp. 124-36.

Chen, M., Borlak, J. and Tong, W. (2013) 'High lipophilicity and high daily dose of oral medications are associated with significant risk for drug-induced liver injury', *Hepatology,* 58(1), pp. 388-96.

Conway, G. E., Shah, U.-K., Llewellyn, S., Cervena, T., Evans, S. J., Al Ali, A. S., Jenkins, G. J., Clift, M. J. D. and Doak, S. H. (2020) 'Adaptation of the in vitro micronucleus assay for genotoxicity testing using 3D liver models supporting longer-term exposure durations', *Mutagenesis,* 35(4), pp. 319-330.

Corning Life Sciences Inc (2018) *3D Primary Human Hepatocytes (PHH) Spheroids Demonstrate Increased Sensitivity to Drug-induced Liver Injury in Comparison to 2D PHH Monolayer Culture*. Available at: https://www.corning.com/catalog/cls/documents/application-notes/CLS-AN-514.pdf (Accessed: 01 June 2021.

Costa, E. C., Gaspar, V. M., Coutinho, P. and Correia, I. J. (2014) 'Optimization of Liquid Overlay Technique to Formulate Heterogenic 3D Co-Cultures Models', *Biotechnology and Bioengineering,* 111(8), pp. 1672-1685.

Dai, Y., Rashba-Step, J. and Cederbaum, A. I. (1993) 'Stable expression of human cytochrome P4502E1 in HepG2 cells: Characterization of catalytic activities and production of reactive oxygen intermediates', *Biochemistry,* 32, pp. 6928-37.

Daly, A. K., Aithal, G. P., Leathart, J. B., Swainsbury, R. A., Dang, T. S. and Day, C. P. (2007) 'Genetic susceptibility to diclofenac-induced hepatotoxicity: contribution of UGT2B7, CYP2C8, and ABCC2 genotypes', *Gastroenterology,* 132(1), pp. 272-81.

Darnell, M., Schreiter, T., Zeilinger, K., Urbaniak, T., Soderdahl, T., Rossberg, I., Dillner, B., Berg, A. L., Gerlach, J. C. and Andersson, T. B. (2011) 'Cytochrome P450-dependent metabolism in HepaRG cells cultured in a dynamic three-dimensional bioreactor', *Drug Metab Dispos,* 39(7), pp. 1131-8.

Daston, G., Knight, D. J., Schwarz, M., Gocht, T., Thomas, R. S., Mahony, C. and Whelan, M. (2015) 'SEURAT: Safety Evaluation Ultimately Replacing Animal Testing--recommendations for future research in the field of predictive toxicology', *Arch Toxicol,* 89(1), pp. 15-23.

Davis, C. D., Schut, H. A., Adamson, R. H., Thorgeirsson, U. P., Thorgeirsson, S. S. and Snyderwine, E. G. (1993) 'Mutagenic activation of IQ, PhIP, and MeIQx by hepatic microsomes from rat, monkey and man: low mutagenic activation of MeIQx in cynomolgus monkeys in vitro reflects low DNA adduct levels in vivo', *Carcinogenesis,* 14(1), pp. 61-65.

DeLeve, L. D. (2013) 'Liver sinusoidal endothelial cells and liver regeneration', *Journal of Clinical Investigation,* 123(5), pp. 1861-1866.

DiMasi, J. A., Grabowski, H. G. and Hansen, R. W. (2016) 'Innovation in the pharmaceutical industry: New estimates of R&D costs', *J Health Econ,* 47, pp. 20-33.

Dixon, L. J., Barnes, M., Tang, H., Pritchard, M. T. and Nagy, L. E. (2013) 'Kupffer cells in the liver', *Comprehensive Physiology,* 3(2), pp. 785-797.

Dohnal, V., Wu, Q. and Kuca, K. (2014) 'Metabolism of aflatoxins: key enzymes and interindividual as well as interspecies differences', *Arch Toxicol,* 88(9), pp. 1635-44.

Donato, M. T., Lahoz, A., Castell, J. V. and Gomez-Lechon, M. J. (2008) 'Cell lines: a tool for in vitro drug metabolism studies', *Curr Drug Metab,* 9(1), pp. 1-11.

Dorst, N., Oberringer, M., Grasser, U., Pohlemann, T. and Metzger, W. (2014) 'Analysis of cellular composition of co-culture spheroids', *Ann Anat,* 196(5), pp. 303-11.

Dragovic, S., Vermeulen, N. P., Gerets, H. H., Hewitt, P. G., Ingelman-Sundberg, M., Park, B. K., Juhila, S., Snoeys, J. and Weaver, R. J. (2016) 'Evidence-based selection of training compounds for use in the mechanism-based integrated prediction of drug-induced liver injury in man', *Arch Toxicol,* 90(12), pp. 2979-3003.

Elje, E., Hesler, M., Runden-Pran, E., Mann, P., Mariussen, E., Wagner, S., Dusinska, M. and Kohl, Y. (2019a) 'The comet assay applied to HepG2 liver spheroids', *Mutat Res Genet Toxicol Environ Mutagen,* 845, pp. 403033.

Elje, E., Hesler, M., Rundén-Pran, E., Mann, P., Mariussen, E., Wagner, S., Dusinska, M. and Kohl, Y. (2019b) 'The comet assay applied to HepG2 liver spheroids', *Mutation Research/Genetic Toxicology and Environmental Mutagenesis*.

Ellero, A. A., van den Bout, I., Vlok, M., Cromarty, A. D. and Hurrell, T. (2021) 'Continual proteomic divergence of HepG2 cells as a consequence of long-term spheroid culture', *Sci Rep,* 11(1), pp. 10917.

Enlo-Scott, Z., Evans, M., Coltman, N. J., Schroeder, N., Thomas, J., Keene, W. and Schulz-Utermoehl, T. (2017) *Assessment of the in vivo disposition of Cinchophen in rat and potential mechanisms of drug-induced liver injury*. DMDG Open Meeting 2017: Sygnature Disocvery Limited [Scientific Poster]. Available at: https://www.sygnaturediscovery.com/wp-content/uploads/2018/02/Invivo-Cinchophen-Poster-PRESS.pdf.

European Medicines Agency (2010) *Reflection paper on non-clinical evaluation of drug- induced liver injury (DILI)*: Committee for Medicinal Products for Human Use (CHMP). Available at: https://www.ema.europa.eu/en/documents/scientific-guideline/reflection-paper-non-clinical-evaluation-drug-induced-liver-injury-dili_en.pdf (Accessed: 01 June 2021.

Faber, K. N., Muller, M. and Jansen, P. L. M. (2003) 'Drug transport proteins in the liver', *Advanced Drug Delivery Reviews,* 55(1), pp. 107-124.

Farzaneh, Z., Abbasalizadeh, S., Asghari-Vostikolaee, M. H., Alikhani, M., Cabral, J. M. S. and Baharvand, H. (2020) 'Dissolved oxygen concentration regulates human hepatic organoid formation from pluripotent stem cells in a fully controlled bioreactor', *Biotechnol Bioeng,* 117(12), pp. 3739-3756.

Fernandez-Moure, J. S. (2016) 'Lost in Translation: The Gap in Scientific Advancements and Clinical Application', *Front Bioeng Biotechnol,* 4, pp. 43.

Fey, S. J., Korzeniowska, B. and Wrzesinski, K. (2020) 'Response to and recovery from treatment in human liver-mimetic clinostat spheroids: a model for assessing repeated-dose drug toxicity', *Toxicol Res (Camb),* 9(4), pp. 379-389.

Fischer, I., Milton, C. and Wallace, H. (2020) 'Toxicity testing is evolving!', *Toxicol Res (Camb),* 9(2), pp. 67-80.

Foti, R. S. and Dalvie, D. K. (2016) 'Cytochrome P450 and Non-Cytochrome P450 Oxidative Metabolism: Contributions to the Pharmacokinetics, Safety, and Efficacy of Xenobiotics', *Drug Metab Dispos,* 44(8), pp. 1229-45.

Friedman, S. L. and Roll, F. J. (1987) 'Isolation and Culture of Hepatic Lipocytes, Kupffer Cells, and Sinusoidal Endothelial-Cells by Density Gradient Centrifugation with Stractan', *Analytical Biochemistry,* 161(1), pp. 207-218.

Fu, D., Mitra, K., Sengupta, P., Jarnik, M., Lippincott-Schwartz, J. and Arias, I. M. (2013) 'Coordinated elevation of mitochondrial oxidative phosphorylation and autophagy help drive hepatocyte polarization', *Proc Natl Acad Sci U S A,* 110(18), pp. 7288-93.

Funk, C., Ponelle, C., Scheuermann, G. and Pantze, M. (2001) 'Cholestatic Potential of Troglitazone as a Possible Factor Contributing to Troglitazone-Induced Hepatotoxicity: In Vivo and in Vitro Interaction at the Canalicular Bile Salt Export Pump (Bsep) in the Rat', *Molecular Pharmacology,* 59(3), pp. 627-635.

Gaskell, H., Sharma, P., Colley, H. E., Murdoch, C., Williams, D. P. and Webb, S. D. (2016) 'Characterization of a functional C3A liver spheroid model', *Toxicology research,* 5(4), pp. 1053-1065.

Gebhardt, R. (1992) 'Metabolic Zonation of the Liver - Regulation and Implications for Liver-Function', *Pharmacology & Therapeutics,* 53(3), pp. 275-354.

Gerlach, J. C., Mutig, K., Sauer, I. M., Schrade, P., Efimova, E., Mieder, T., Naumann, G., Grunwald, A., Pless, G., Mas, A., Bachmann, S., Neuhaus, P. and Zeilinger, K. (2003) 'Use of primary human liver cells originating from discarded grafts in a bioreactor for liver support therapy and the prospects of culturing adult liver stem cells in bioreactors: a morphologic study', *Transplantation,* 76(5), pp. 781-6.

Giustarini, G., Huppelschoten, S., Barra, M., Oppelt, A., Wagenaar, L., Weaver, R. J., Bol-Schoenmakers, M., Smit, J. J., van de Water, B., Klingmuller, U. and Pieters, R. H. H. (2020) 'The hepatotoxic fluoroquinolone trovafloxacin disturbs TNF- and LPS-induced p65 nuclear translocation in vivo and in vitro', *Toxicol Appl Pharmacol,* 391, pp. 114915.

Giustarini, G., Vrisekoop, N., Kruijssen, L., Wagenaar, L., van Staveren, S., van Roest, M., Bleumink, R., Bol-Schoenmakers, M., Weaver, R. J., Koenderman, L., Smit, J. and Pieters, R. (2019) 'Trovafloxacin-Induced Liver Injury: Lack in Regulation of Inflammation by Inhibition of Nucleotide Release and Neutrophil Movement', *Toxicol Sci,* 167(2), pp. 385-396.

Goldman, I. S., Winkler, M. L., Raper, S. E., Barker, M. E., Keung, E., Goldberg, H. I. and Boyer, T. D. (1985) 'Increased hepatic density and phospholipidosis due to amiodarone', *AJR Am J Roentgenol,* 144(3), pp. 541-6.

Grand View Research (2021) *3D Cell Culture Market Size and Share Report, 2021 - 2028* Available at: https://www.grandviewresearch.com/industry-analysis/3d-cell-culture-market/methodology (Accessed: 15 February 2021.

Granitzny, A., Knebel, J., Müller, M., Braun, A., Steinberg, P., Dasenbrock, C. and Hansen, T. (2017) 'Evaluation of a human in vitro hepatocyte-NPC co-culture model for the prediction of idiosyncratic drug-induced liver injury: A pilot study', *Toxicology reports,* 4, pp. 89-103.

Greenblatt, H. K. and Greenblatt, D. J. (2014) 'Liver injury associated with ketoconazole: review of the published evidence', *J Clin Pharmacol,* 54(12), pp. 1321-9.

Guillouzo, A., Corlu, A., Aninat, C., Glaise, D., Morel, F. and Guguen-Guillouzo, C. (2007) 'The human hepatoma HepaRG cells: a highly differentiated model for studies of liver metabolism and toxicity of xenobiotics', *Chem Biol Interact,* 168(1), pp. 66-73.

Guo, L., Dial, S., Shi, L., Branham, W., Liu, J., Fang, J. L., Green, B., Deng, H., Kaput, J. and Ning, B. (2011) 'Similarities and differences in the expression of drug-metabolizing enzymes between human hepatic cell lines and primary human hepatocytes', *Drug Metab Dispos,* 39(3), pp. 528-38.

Guo, X., Seo, J. E., Li, X. and Mei, N. (2020) 'Genetic toxicity assessment using liver cell models: past, present, and future', *J Toxicol Environ Health B Crit Rev,* 23(1), pp. 27-50.

Gupta, R., Schrooders, Y., Hauser, D., van Herwijnen, M., Albrecht, W., Ter Braak, B., Brecklinghaus, T., Castell, J. V., Elenschneider, L., Escher, S., Guye, P., Hengstler, J. G., Ghallab, A., Hansen, T., Leist, M., Maclennan, R., Moritz, W., Tolosa, L., Tricot, T., Verfaillie, C., Walker, P., van de Water, B., Kleinjans, J. and Caiment, F. (2021) 'Comparing in vitro human liver models to in vivo human liver using RNA-Seq', *Arch Toxicol,* 95(2), pp. 573-589.

Hafiz, E. O. A., Bulutoglu, B., Mansy, S. S., Chen, Y., Abu-Taleb, H., Soliman, S. A. M., El-Hindawi, A. A. F., Yarmush, M. L. and Uygun, B. E. (2021) 'Development of liver microtissues with functional biliary ductular network', *Biotechnol Bioeng,* 118(1), pp. 17-29.

Hardonniere, K., Saunier, E., Lemarie, A., Fernier, M., Gallais, I., Helies-Toussaint, C., Mograbi, B., Antonio, S., Benit, P., Rustin, P., Janin, M., Habarou, F., Ottolenghi, C., Lavault, M. T., Benelli, C., Sergent, O., Huc, L., Bortoli, S. and Lagadic-Gossmann, D. (2016) 'The environmental carcinogen benzo[a]pyrene induces a Warburg-like metabolic reprogramming dependent on NHE1 and associated with cell survival', *Sci Rep,* 6, pp. 30776.

Hartwig, A., Arand, M., Epe, B., Guth, S., Jahnke, G., Lampen, A., Martus, H. J., Monien, B., Rietjens, I., Schmitz-Spanke, S., Schriever-Schwemmer, G., Steinberg, P. and Eisenbrand, G. (2020) 'Mode of action-based risk assessment of genotoxic carcinogens', *Arch Toxicol,* 94(6), pp. 1787-1877.

Hashizume, T., Yoshitomi, S., Asahi, S., Matsumura, S., Chatani, F. and Oda, H. (2009) 'In vitro micronucleus test in HepG2 transformants expressing a series of human cytochrome P450 isoforms with chemicals requiring metabolic activation', *Mutat Res,* 677(1-2), pp. 1-7.

Hashizume, T., Yoshitomi, S., Asahi, S., Uematsu, R., Matsumura, S., Chatani, F. and Oda, H. (2010) 'Advantages of human hepatocyte-derived transformants expressing a series of human cytochrome p450 isoforms for genotoxicity examination', *Toxicol Sci,* 116(2), pp. 488-97.

Hautekeete, M. L. and Geerts, A. (1997) 'The hepatic stellate (Ito) cell: Its role in human liver disease', *Virchows Archiv,* 430(3), pp. 195-207.

Hay, D. C., Fletcher, J., Payne, C., Terrace, J. D., Gallagher, R. C., Snoeys, J., Black, J. R., Wojtacha, D., Samuel, K., Hannoun, Z., Pryde, A., Filippi, C., Currie, I. S., Forbes, S. J., Ross, J. A., Newsome, P. N. and Iredale, J. P. (2008a) 'Highly efficient differentiation of hESCs to functional hepatic endoderm requires ActivinA and Wnt3a signaling', *Proc Natl Acad Sci U S A,* 105(34), pp. 12301-6.

Hay, D. C., Fletcher, J., Payne, C., Terrace, J. D., Gallagher, R. C. J. and Snoeys, J. (2008b) 'Highly efficient differentiation of hESCs to functional hepatic endoderm requires activin A **and Wnt3a signaling**', *Proc Natl Acad Sci USA,* 105, pp. 12301-6.

Hendriks, D. F. G., Puigvert, L. F., Messner, S., Mortiz, W. and Ingelman-Sundberg, M. (2016) 'Hepatic 3D spheroid models for the detection and study of compounds with cholestatic liability', *Scientific Reports,* 6.

Hendriks, D. F. G., Vorrink, S. U., Smutny, T., Sim, S. C., Nordling, A., Ullah, S., Kumondai, M., Jones, B. C., Johansson, I., Andersson, T. B., Lauschke, V. M. and Ingelman-Sundberg, M. (2020a) 'Clinically Relevant Cytochrome P450 3A4 Induction Mechanisms and Drug Screening in Three-Dimensional Spheroid Cultures of Primary Human Hepatocytes', *Clin Pharmacol Ther*.

Hendriks, D. F. G., Vorrink, S. U., Smutny, T., Sim, S. C., Nordling, Å., Ullah, S., Kumondai, M., Jones, B. C., Johansson, I., Andersson, T. B., Lauschke, V. M. and Ingelman-Sundberg, M. (2020b) 'Clinically Relevant Cytochrome P450 3A4 Induction Mechanisms and Drug Screening in Three-Dimensional Spheroid Cultures of Primary Human Hepatocytes', *Clinical Pharmacology & Therapeutics,* 108(4), pp. 844-855.

Herzog, N., Hansen, M., Miethbauer, S., Schmidtke, K. U., Anderer, U., Lupp, A., Sperling, S., Seehofer, D., Damm, G., Scheibner, K. and Kupper, J. H. (2016) 'Primary-like human hepatocytes genetically engineered to obtain proliferation competence display hepatic differentiation characteristics in monolayer and organotypical spheroid cultures', *Cell Biol Int,* 40(3), pp. 341-53.

Hinson, J. A., Roberts, D. W. and James, L. P. (2010) 'Mechanisms of acetaminophen-induced liver necrosis', *Handb Exp Pharmacol,* (196), pp. 369-405.

Huang, S., Howington, M. B., Dobry, C. J., Evans, C. R. and Leiser, S. F. (2021) 'Flavin-Containing Monooxygenases Are Conserved Regulators of Stress Resistance and Metabolism', *Frontiers in Cell and Developmental Biology,* 9(151).

Huang, Y. S., Chern, H. D., Su, W. J., Wu, J. C., Chang, S. C. and Chiang, C. H. (2003) 'Cytochrome P450 2E1 genotype and the susceptibility to antituberculosis drug-induced hepatitis', *Hepatology,* 37, pp. 924-30.

Huch, M., Dorrell, C., Boj, S. F., van Es, J. H., Li, V. S., van de Wetering, M., Sato, T., Hamer, K., Sasaki, N., Finegold, M. J., Haft, A., Vries, R. G., Grompe, M. and Clevers, H. (2013) 'In vitro expansion of single Lgr5+ liver stem cells induced by Wnt-driven regeneration', *Nature,* 494(7436), pp. 247-50.

Huch, M., Gehart, H., van Boxtel, R., Hamer, K., Blokzijl, F., Verstegen, M. M., Ellis, E., van Wenum, M., Fuchs, S. A., de Ligt, J., van de Wetering, M., Sasaki, N., Boers, S. J., Kemperman, H., de Jonge, J., Ijzermans, J. N., Nieuwenhuis, E. E., Hoekstra, R., Strom, S., Vries, R. R., van der Laan, L. J., Cuppen, E. and Clevers, H. (2015) 'Long-term culture of genome-stable bipotent stem cells from adult human liver', *Cell,* 160(1-2), pp. 299-312.

Hurrell, T., Lilley, K. S. and Cromarty, A. D. (2019) 'Proteomic responses of HepG2 cell monolayers and 3D spheroids to selected hepatotoxins', *Toxicology Letters,* 300, pp. 40-50.

Ingber, D. E. (2020) 'Is it Time for Reviewer 3 to Request Human Organ Chip Experiments Instead of Animal Validation Studies?', *Adv Sci (Weinh),* 7(22), pp. 2002030.

Ingelman-Sundberg, M. and Lauschke, V. M. (2021) '3D human liver spheroids for translational pharmacology and toxicology', *Basic & Clinical Pharmacology & Toxicology*.

Iyer, V. V., Yang, H., Ierapetritou, M. G. and Roth, C. M. (2010) 'Effects of glucose and insulin on HepG2-C3A cell metabolism', *Biotechnol Bioeng,* 107(2), pp. 347-56.

Jang, M., Kleber, A., Ruckelshausen, T., Betzholz, R. and Manz, A. (2019) 'Differentiation of the human liver progenitor cell line (HepaRG) on a microfluidic-based biochip', *J Tissue Eng Regen Med,* 13(3), pp. 482-494.

Jang, M., Neuzil, P., Volk, T., Manz, A. and Kleber, A. (2015) 'On-chip three-dimensional cell culture in phaseguides improves hepatocyte functions in vitro'.

Jia, Z., Cheng, Y., Jiang, X., Zhang, C., Wang, G., Xu, J., Li, Y., Peng, Q. and Gao, Y. (2020) '3D Culture System for Liver Tissue Mimicking Hepatic Plates for Improvement of Human Hepatocyte (C3A) Function and Polarity', *BioMed Research International,* 2020, pp. 6354183.

Ju, C., Reilly, T., Bourdi, M., Radonovich, M., Brady, J., George, J. and Pohl, L. (2003) 'Protective role of Kupffer cells in acetaminophen-induced hepatic injury in mice.', *Toxicological Sciences,* 72, pp. 197-197.

Jung, H. J., Jang, H.-J. and Kwon, T.-H. (2021) 'Aquaporins implicated in the cell proliferation and the signaling pathways of cell stemness', *Biochimie,* 188, pp. 52-60.

Jung, H. R., Kang, H. M., Ryu, J. W., Kim, D. S., Noh, K. H., Kim, E. S., Lee, H. J., Chung, K. S., Cho, H. S., Kim, N. S., Im, D. S., Lim, J. H. and Jung, C. R. (2017) 'Cell Spheroids with Enhanced Aggressiveness to Mimic Human Liver Cancer In Vitro and In Vivo', *Sci Rep,* 7(1), pp. 10499.

Jungermann, K. and Kietzmann, T. (1997) 'Role of oxygen in the zonation of carbohydrate metabolism and gene expression in liver', *Kidney Int,* 51(2), pp. 402-12.

Kamiyama, Y., Matsubara, T., Yoshinari, K., Nagata, K., Kamimura, H. and Yamazoe, Y. (2007) 'Role of human hepatocyte nuclear factor 4alpha in the expression of drug-metabolizing enzymes and transporters in human hepatocytes assessed by use of small interfering RNA', *Drug Metab Pharmacokinet,* 22(4), pp. 287-98.

Kanebratt, K. P. and Andersson, T. B. (2008) 'Evaluation of HepaRG cells as an in vitro model for human drug metabolism studies', *Drug Metab Dispos,* 36(7), pp. 1444-52.

Kanebratt, K. P., Janefeldt, A., Vilén, L., Vildhede, A., Samuelsson, K., Milton, L., Björkbom, A., Persson, M., Leandersson, C. and Andersson, T. B. (2021a) 'Primary human hepatocyte spheroid model as a 3D in vitro platform for metabolism studies', *Journal of Pharmaceutical Sciences,* 110(1), pp. 422-431.

Kanebratt, K. P., Janefeldt, A., Vilén, L., Vildhede, A., Samuelsson, K., Milton, L., Björkbom, A., Persson, M., Leandersson, C., Andersson, T. B. and Hilgendorf, C. (2021b) 'Primary Human Hepatocyte Spheroid Model as a 3D In Vitro Platform for Metabolism Studies', *Journal of Pharmaceutical Sciences,* 110(1), pp. 422-431.

Kelly, J. H. (1994) *Permanent human hepatocyte cell line and its use in a liver assist device (LAD).* [Online]. Available at: https://patents.google.com/patent/US5290684A/en#patentCitations.

Kermanizadeh, A., Brown, D. M., Moritz, W. and Stone, V. (2019) 'The importance of inter-individual Kupffer cell variability in the governance of hepatic toxicity in a 3D primary human liver microtissue model', *Sci Rep,* 9(1), pp. 7295.

Khan, S., Mandal, R. K., Elasbali, A. M., Dar, S. A., Jawed, A. and Wahid, M. (2019) 'Pharmacogenetic association between NAT2 gene polymorphisms and isoniazid induced hepatotoxicity: trial sequence meta-analysis as evidence', *Biosci Rep,* 39, pp. 20180845.

Kiang, T. K., Ho, P. C., Anari, M. R., Tong, V., Abbott, F. S. and Chang, T. K. (2006) 'Contribution of CYP2C9, CYP2A6, and CYP2B6 to valproic acid metabolism in hepatic microsomes from individuals with the CYP2C9*1/*1 genotype', *Toxicol Sci,* 94(2), pp. 261-71.

Kim, J. H., Choi, W. G., Lee, S. and Lee, H. S. (2017) 'Revisiting the Metabolism and Bioactivation of Ketoconazole in Human and Mouse Using Liquid Chromatography-Mass Spectrometry-Based Metabolomics', *Int J Mol Sci,* 18(3).

Kirkland, D., Kasper, P., Martus, H.-J., Müller, L., van Benthem, J., Madia, F. and Corvi, R. (2016) 'Updated recommended lists of genotoxic and non-genotoxic chemicals for assessment of the performance of new or improved genotoxicity tests', *Mutation Research/Genetic Toxicology and Environmental Mutagenesis,* 795, pp. 7-30.

Kirkland, D., Pfuhler, S., Tweats, D., Aardema, M., Corvi, R., Darroudi, F., Elhajouji, A., Glatt, H., Hastwell, P., Hayashi, M., Kasper, P., Kirchner, S., Lynch, A., Marzin, D., Maurici, D., Meunier, J.-R., Müller, L., Nohynek, G., Parry, J., Parry, E., Thybaud, V., Tice, R., van Benthem, J., Vanparys, P. and White, P. (2007) 'How to reduce false positive results when undertaking in vitro genotoxicity testing and thus avoid unnecessary follow-up animal tests: Report of an ECVAM Workshop', *Mutation Research/Genetic Toxicology and Environmental Mutagenesis,* 628(1), pp. 31-55.

Kmiec, Z. (2001) 'Cooperation of liver cells in health and disease', *Adv Anat Embryol Cell Biol,* 161, pp. III-XIII, 1-151.

Knowles, B. B., Howe, C. C. and Aden, D. P. (1980) 'Human hepatocellular carcinoma cell lines secrete the major plasma proteins and hepatitis B surface antigen', *Science,* 209(4455), pp. 497-9.

Kolios, G., Valatas, V. and Kouroumalis, E. (2006) 'Role of Kupffer cells in the pathogenesis of liver disease', *World Journal of Gastroenterology,* 12(46), pp. 7413-7420.

Kozyra, M., Johansson, I., Nordling, A., Ullah, S., Lauschke, V. M. and Ingelman-Sundberg, M. (2018a) 'Human hepatic 3D spheroids as a model for steatosis and insulin resistance', *Sci Rep,* 8(1), pp. 14297.

Kozyra, M., Johansson, I., Nordling, Å., Ullah, S., Lauschke, V. M. and Ingelman-Sundberg, M. (2018b) 'Human hepatic 3D spheroids as a model for steatosis and insulin resistance', *Scientific Reports,* 8(1), pp. 14297.

Krasniqi, V., Dimovski, A., Domjanovic, I. K., Bilic, I. and Bozina, N. (2016) 'How polymorphisms of the cytochrome P450 genes affect ibuprofen and diclofenac metabolism and toxicity', *Arh Hig Rada Toksikol,* 67(1), pp. 1-8.

Krewski, D., Andersen, M. E., Tyshenko, M. G., Krishnan, K., Hartung, T., Boekelheide, K., Wambaugh, J. F., Jones, D., Whelan, M., Thomas, R., Yauk, C., Barton-Maclaren, T. and Cote, I. (2020) 'Toxicity testing in the 21st century: progress in the past decade and future perspectives', *Archives of Toxicology,* 94(1), pp. 1-58.

Kuna, L., Bozic, I., Kizivat, T., Bojanic, K., Mrso, M., Kralj, E., Smolic, R., Wu, G. Y. and Smolic, M. (2018) 'Models of Drug Induced Liver Injury (DILI) - Current Issues and Future Perspectives', *Curr Drug Metab,* 19(10), pp. 830-838.

Kyffin, J. A., Cox, C. R., Leedale, J., Colley, H. E., Murdoch, C., Mistry, P., Webb, S. D. and Sharma, P. (2019) 'Preparation of Primary Rat Hepatocyte Spheroids Utilizing the Liquid-Overlay Technique', *Curr Protoc Toxicol,* 81(1), pp. e87.

Lalor, P. F., Shields, P., Grant, A. J. and Adams, D. H. (2002) 'Recruitment of lymphocytes to the human liver', *Immunology and Cell Biology,* 80(1), pp. 52-64.

Lancaster, M. A. and Huch, M. (2019) 'Disease modelling in human organoids', *Dis Model Mech,* 12(7), pp. 039347.

Laskin, D. L. (1990) 'Nonparenchymal Cells and Hepatotoxicity', *Seminars in Liver Disease,* 10(4), pp. 293-304.

Lassila, T., Hokkanen, J., Aatsinki, S. M., Mattila, S., Turpeinen, M. and Tolonen, A. (2015) 'Toxicity of Carboxylic Acid-Containing Drugs: The Role of Acyl Migration and CoA Conjugation Investigated', *Chem Res Toxicol,* 28(12), pp. 2292-303.

Lauer, B., Tuschl, G., Kling, M. and Mueller, S. O. (2009) 'Species-specific toxicity of diclofenac and troglitazone in primary human and rat hepatocytes', *Chem Biol Interact,* 179(1), pp. 17-24.

Lazarska, K. E., Dekker, S. J., Vermeulen, N. P. E. and Commandeur, J. N. M. (2018) 'Effect of UGT2B7*2 and CYP2C8*4 polymorphisms on diclofenac metabolism', *Toxicol Lett,* 284, pp. 70-8.

Lee, S. W., Jung, D. J. and Jeong, G. S. (2020) 'Gaining New Biological and Therapeutic Applications into the Liver with 3D In Vitro Liver Models', *Tissue Eng Regen Med*.

Leite, S., Martins, N. M., Dorta, D. J., Curti, C., Uyemura, S. A. and Cardozo dos Santos, A. (2006) 'Mitochondrial uncoupling by the sulindac metabolite, sulindac sulfide', *Basic & clinical pharmacology & toxicology,* 99(4), pp. 294-299.

Lerche-Langrand, C. and Toutain, H. J. (2000) 'Precision-cut liver slices: characteristics and use for in vitro pharmaco-toxicology', *Toxicology,* 153(1-3), pp. 221-253.

Leroy, K., Silva Costa, C. J., Pieters, A., Dos Santos Rodrigues, B., Van Campenhout, R., Cooreman, A., Tabernilla, A., Cogliati, B. and Vinken, M. (2021) 'Expression and Functionality of Connexin-Based Channels in Human Liver Cancer Cell Lines', *Int J Mol Sci,* 22(22).

Li, D., Knox, B., Gong, B., Chen, S., Guo, L., Liu, Z., Tong, W. and Ning, B. (2021a) 'Identification of Translational microRNA Biomarker Candidates for Ketoconazole-Induced Liver Injury Using Next-Generation Sequencing', *Toxicol Sci,* 179(1), pp. 31-43.

Li, F., Cao, L., Parikh, S. and Zuo, R. (2020) 'Three-Dimensional Spheroids With Primary Human Liver Cells and Differential Roles of Kupffer Cells in Drug-Induced Liver Injury', *J Pharm Sci,* 109(6), pp. 1912-1923.

Li, T., Tong, W., Roberts, R., Liu, Z. and Thakkar, S. (2021b) 'DeepCarc: Deep Learning-Powered Carcinogenicity Prediction Using Model-Level Representation', *Front Artif Intell,* 4, pp. 757780.

Lin, J., Schyschka, L., Muhl-Benninghaus, R., Neumann, J., Hao, L., Nussler, N., Dooley, S., Liu, L., Stockle, U., Nussler, A. K. and Ehnert, S. (2012) 'Comparative analysis of phase I and II enzyme activities in 5 hepatic cell lines identifies Huh-7 and HCC-T cells with the highest potential to study drug metabolism', *Arch Toxicol,* 86(1), pp. 87-95.

Linton, J. D. and Xu, W. (2020) 'Understanding and Managing the Biotechnology Valley of Death', *Trends Biotechnol*.

Liu, Z., Kelly, R., Fang, H., Ding, D. and Tong, W. (2011) 'Comparative analysis of predictive models for nongenotoxic hepatocarcinogenicity using both toxicogenomics and quantitative structure-activity relationships', *Chem Res Toxicol,* 24(7), pp. 1062-70.

Loi, C. M., Alvey, C. W., Vassos, A. B., Randinitis, E. J., Sedman, A. J. and Koup, J. R. (1999) 'Steady-state pharmacokinetics and dose proportionality of troglitazone and its metabolites', *J Clin Pharmacol,* 39(9), pp. 920-6.

Lou, Y.-H., Wang, J.-S., Dong, G., Guo, P.-P., Wei, D.-D., Xie, S.-S., Yang, M.-H. and Kong, L.-Y. (2015) 'The acute hepatotoxicity of tacrine explained by 1H NMR based metabolomic profiling', *Toxicology Research,* 4(6), pp. 1465-1478.

Lucena, M. I., Andrade, R. J., Rodrigo, L., Salmeron, J., Alvarez, A., Lopez-Garrido, M. J., Camargo, R. and Alcantara, R. (2000) 'Trovafloxacin-induced acute hepatitis', *Clin Infect Dis,* 30(2), pp. 400-1.

Madden, S., Woolf, T. F., Pool, W. F. and Park, B. K. (1993) 'An investigation into the formation of stable, protein-reactive and cytotoxic metabolites from tacrine in vitro', *Biochemical Pharmacology,* 46(1), pp. 13-20.

Mandon, M., Huet, S., Dubreil, E., Fessard, V. and Le Hegarat, L. (2019) 'Three-dimensional HepaRG spheroids as a liver model to study human genotoxicity in vitro with the single cell gel electrophoresis assay', *Sci Rep,* 9(1), pp. 10548.

Masyuk, A. I. and LaRusso, N. F. (2006) 'Aquaporins in the hepatobiliary system', *Hepatology,* 43(2 Suppl 1), pp. S75-81.

Mavri-Damelin, D., Damelin, L. H., Eaton, S., Rees, M., Selden, C. and Hodgson, H. J. (2008) 'Cells for bioartificial liver devices: the human hepatoma-derived cell line C3A produces urea but does not detoxify ammonia', *Biotechnol Bioeng,* 99(3), pp. 644-51.

Mavri-Damelin, D., Eaton, S., Damelin, L. H., Rees, M., Hodgson, H. J. and Selden, C. (2007) 'Ornithine transcarbamylase and arginase I deficiency are responsible for diminished urea cycle function in the human hepatoblastoma cell line HepG2', *Int J Biochem Cell Biol,* 39(3), pp. 555-64.

McGill, M. R. and Jaeschke, H. (2013) 'Metabolism and disposition of acetaminophen: recent advances in relation to hepatotoxicity and diagnosis', *Pharm Res,* 30(9), pp. 2174-87.

Means, J. C., Olsen, P. D. and Schoffers, E. (2003) 'Development of an isotope dilution liquid chromatography/tandem mass spectrometry detection method for DNA adducts of selected aromatic amines', *Journal of the American Society for Mass Spectrometry,* 14(9), pp. 1057-1066.

Meseguer, E. S., Elizalde, M. U., Borobia, A. M. and Ramirez, E. (2021) 'Valproic Acid-Induced Liver Injury: A Case-Control Study from a Prospective Pharmacovigilance Program in a Tertiary Hospital', *J Clin Med,* 10(6).

Messner, S., Fredriksson, L., Lauschke, V. M., Roessger, K., Escher, C., Bober, M., Kelm, J. M., Ingelman-Sundberg, M. and Moritz, W. (2018) 'Transcriptomic, Proteomic, and Functional Long-Term Characterization of Multicellular Three-Dimensional Human Liver Microtissues', *Appl In Vitro Toxicol,* 4(1), pp. 1-12.

Metushi, I., Uetrecht, J. and Phillips, E. (2016) 'Mechanism of isoniazid-induced hepatotoxicity: then and now', *Br J Clin Pharmacol,* 81, pp. 1030-6.

Metushi, I. G., Nakagawa, T. and Uetrecht, J. (2012) 'Direct oxidation and covalent binding of isoniazid to rodent liver and human hepatic microsomes: humans are more like mice than rats', *Chemical research in toxicology,* 25(11), pp. 2567-2576.

Miao, Z. H., Rao, V. A., Agama, K., Antony, S., Kohn, K. W. and Pommier, Y. (2006) '4-nitroquinoline-1-oxide induces the formation of cellular topoisomerase I-DNA cleavage complexes', *Cancer Res,* 66(13), pp. 6540-5.

Minerali, E., Foil, D. H., Zorn, K. M., Lane, T. R. and Ekins, S. (2020) 'Comparing Machine Learning Algorithms for Predicting Drug-Induced Liver Injury (DILI)', *Mol Pharm,* 17(7), pp. 2628-2637.

Mitsugi, R., Sumida, K., Fujie, Y., Tukey, R. H., Itoh, T. and Fujiwara, R. (2016) 'Acyl-glucuronide as a Possible Cause of Trovafloxacin-Induced Liver Toxicity: Induction of Chemokine (C-X-C Motif) Ligand 2 by Trovafloxacin Acyl-glucuronide', *Biological & pharmaceutical bulletin,* 39(10), pp. 1604-1610.

Moller, P., Wallin, H., Vogel, U., Autrup, H., Risom, L., Hald, M. T., Daneshvar, B., Dragsted, L. O., Poulsen, H. E. and Loft, S. (2002) 'Mutagenicity of 2-amino-3-methylimidazo[4,5-f]quinoline in colon and liver of Big Blue rats: role of DNA adducts, strand breaks, DNA repair and oxidative stress', *Carcinogenesis,* 23(8), pp. 1379-85.

Muckel, E., Frandsen, H. and Glatt, H. R. (2002) 'Heterologous expression of human N-acetyltransferases 1 and 2 and sulfotransferase 1A1 in Salmonella typhimurium for mutagenicity testing of heterocyclic amines', *Food and Chemical Toxicology,* 40(8), pp. 1063-1068.

Mufti, N. A., Bleckwenn, N. A., Babish, J. G. and Shuler, M. L. (1995) 'Possible involvement of the Ah receptor in the induction of cytochrome P-450IA1 under conditions of hydrodynamic shear in microcarrier-attached hepatoma cell lines', *Biochem Biophys Res Commun,* 208(1), pp. 144-52.

Mun, S. J., Ryu, J.-S., Lee, M.-O., Son, Y. S., Oh, S. J., Cho, H.-S., Son, M.-Y., Kim, D.-S., Kim, S. J., Yoo, H. J., Lee, H.-J., Kim, J., Jung, C.-R., Chung, K.-S. and Son, M. J. (2019) 'Generation of expandable human pluripotent stem cell-derived hepatocyte-like liver organoids', *Journal of Hepatology,* 71(5), pp. 970-985.

Nelson, L. J., Morgan, K., Treskes, P., Samuel, K., Henderson, C. J., LeBled, C., Homer, N., Grant, M. H., Hayes, P. C. and Plevris, J. N. (2017) 'Human Hepatic HepaRG Cells Maintain an Organotypic Phenotype with High Intrinsic CYP450 Activity/Metabolism and Significantly Outperform Standard HepG2/C3A Cells for Pharmaceutical and Therapeutic Applications', *Basic & clinical pharmacology & toxicology,* 120(1), pp. 30-37.

Neuman, M. G., Shear, N. H., Jacobson-Brown, P. M., Katz, G. G., Neilson, H. K., Malkiewicz, I. M., Cameron, R. G. and Abbott, F. (2001) 'CYP2E1-mediated modulation of valproic acid-induced hepatocytotoxicity', *Clin Biochem,* 34(3), pp. 211-8.

Newsome, P. N., Bathgate, A. J., Henderson, N. C., MacGilchrist, A. J., Plevris, J. N., Masterton, G., Garden, O. J., Lee, A., Hayes, P. C. and Simpson, K. J. (2001) 'Referral patterns and social deprivation in paracetamol-induced liver injury in Scotland', *The Lancet,* 358(9293), pp. 1612-1613.

Nicoletti, P., Devarbhavi, H., Goel, A., Venkatesan, R., Eapen, C. E., Grove, J. I., Zafer, S., Bjornsson, E., Lucena, M. I., Andrade, R. J., Pirmohamed, M., Wadelius, M., Larrey, D., Maitland-van der Zee, A. H., Ibanez, L., Watkins, P. B., Daly, A. K. and Aithal, G. P. (2021) 'Genetic Risk Factors in Drug-Induced Liver Injury Due to Isoniazid-Containing Antituberculosis Drug Regimens', *Clin Pharmacol Ther,* 109(4), pp. 1125-1135.

Nishikawa, T., Tanaka, Y., Nishikawa, M., Ogino, Y., Kusamori, K., Mizuno, N., Mizukami, Y., Shimizu, K., Konishi, S., Takahashi, Y. and Takakura, Y. (2017) 'Optimization of Albumin Secretion and Metabolic Activity of Cytochrome P450 1A1 of Human Hepatoblastoma HepG2 Cells in Multicellular Spheroids by Controlling Spheroid Size', *Biol Pharm Bull,* 40(3), pp. 334-338.

OECD (2017) *Overview on genetic toxicology test guidelines and updates performed in 2014-2015*. Series on Testing and Assessment. Report number 238. Paris: Organization for Economic Cooperation and Development (Accessed: 29 June 2020 2020).

Ogimura, E., Sekine, S. and Horie, T. (2011) 'Bile salt export pump inhibitors are associated with bile acid-dependent drug-induced toxicity in sandwich-cultured hepatocytes', *Biochem Biophys Res Commun,* 416(3-4), pp. 313-7.

Oliva-Vilarnau, N., Vorrink, S. U., Ingelman-Sundberg, M. and Lauschke, V. M. (2020) 'A 3D Cell Culture Model Identifies Wnt/β-Catenin Mediated Inhibition of p53 as a Critical Step during Human Hepatocyte Regeneration', *Advanced Science,* 7(15), pp. 2000248.

Ott, L. M., Ramachandran, K. and Stehno-Bittel, L. (2017) 'An automated multiplexed hepatotoxicity and CYP induction assay using HepaRG cells in 2D and 3D', *SLAS Discov Adv Life Sci R D,* 22, pp. 614-25.

Parasuraman, S. (2011) 'Toxicological screening', *J Pharmacol Pharmacother,* 2(2), pp. 74-9.

Park, E., Kim, H. K., Jee, J., Hahn, S., Jeong, S. and Yoo, J. (2019) 'Development of organoid-based drug metabolism model', *Toxicology and applied pharmacology,* 385, pp. 114790.

Park, S.-Y., Lee, S.-M., Ye, S.-K., Yoon, S.-H., Chung, M.-H. and Choi, J. (2006) 'Benzo[a]pyrene-induced DNA damage and p53 modulation in human hepatoma HepG2 cells for the identification of potential biomarkers for PAH monitoring and risk assessment', *Toxicology Letters,* 167(1), pp. 27-33.

Pauli-Magnus, C and Meir, P.J. (2006) 'Hepatobiliary Transporters and Drug-Induced Cholestasis', *Hepatology*, 44(4), pp.778-87.

Peklak-Scott, C., Townsend, A. J. and Morrow, C. S. (2005) 'Dynamics of Glutathione Conjugation and Conjugate Efflux in Detoxification of the Carcinogen, 4-Nitroquinoline 1-Oxide: Contributions of Glutathione, GlutathioneS-Transferase, and MRP1†', *Biochemistry,* 44(11), pp. 4426-4433.

Peng, W. C., Logan, C. Y., Fish, M., Anbarchian, T., Aguisanda, F., Alvarez-Varela, A., Wu, P., Jin, Y., Zhu, J., Li, B., Grompe, M., Wang, B. and Nusse, R. (2018) 'Inflammatory Cytokine TNFalpha Promotes the Long-Term Expansion of Primary Hepatocytes in 3D Culture', *Cell,* 175(6), pp. 1607-1619 e15.

Petreus, T., Cadogan, E., Hughes, G., Smith, A., Pilla Reddy, V., Lau, A., O'Connor, M. J., Critchlow, S., Ashford, M. and Oplustil O'Connor, L. (2021) 'Tumour-on-chip microfluidic platform for assessment of drug pharmacokinetics and treatment response', *Commun Biol,* 4(1), pp. 1001.

Pfuhler, S., van Benthem, J., Curren, R., Doak, S. H., Dusinska, M., Hayashi, M., Heflich, R. H., Kidd, D., Kirkland, D., Luan, Y., Ouedraogo, G., Reisinger, K., Sofuni, T., van Acker, F., Yang, Y. and Corvi, R. (2020) 'Use of in vitro 3D tissue models in genotoxicity testing: Strategic fit, validation status and way forward. Report of the working group from the 7(th) International Workshop on Genotoxicity Testing (IWGT)', *Mutat Res,* 850-851, pp. 503135.

Pimpin, L., Cortez-Pinto, H., Negro, F., Corbould, E., Lazarus, J. V., Webber, L. and Sheron, N. (2018) 'Burden of liver disease in Europe: Epidemiology and analysis of risk factors to identify prevention policies', *Journal of Hepatology,* 69(3), pp. 718-735.

Pluta, K. D., Samluk, A., Wencel, A., Zakrzewska, K. E., Gora, M., Burzynska, B., Ciezkowska, M., Motyl, J. and Pijanowska, D. G. (2020) 'Genetically modified C3A cells with restored urea cycle for improved bioartificial liver', *Biocybernetics and Biomedical Engineering,* 40(1), pp. 378-387.

Poisson, J., Lemoinne, S., Boulanger, C., Durand, F., Moreau, R., Valla, D. and Rautou, P. E. (2017) 'Liver sinusoidal endothelial cells: Physiology and role in liver diseases', *Journal of Hepatology,* 66(1), pp. 212-227.

Ponsoda, X., Bort, R., Jover, R., Gomez-Lechon, M. J. and Castell, J. V. (1995) 'Molecular mechanism of diclofenac hepatotoxicity: Association of cell injury with oxidative metabolism and decrease in ATP levels', *Toxicol In Vitro,* 9(4), pp. 439-44.

Pourahmad, J., Eskandari, M. R., Kaghazi, A., Shaki, F., Shahraki, J. and Fard, J. K. (2012) 'A new approach on valproic acid induced hepatotoxicity: involvement of lysosomal membrane leakiness and cellular proteolysis', *Toxicol In Vitro,* 26(4), pp. 545-51.

Prior, N., Inacio, P. and Huch, M. (2019) 'Liver organoids: from basic research to therapeutic applications', *Gut,* 68(12), pp. 2228-2237.

Proctor, W. R., Foster, A. J., Vogt, J., Summers, C., Middleton, B., Pilling, M. A., Shienson, D., Kijanska, M., Strobel, S., Kelm, J. M., Morgan, P., Messner, S. and Williams, D. (2017) 'Utility of spherical human liver microtissues for prediction of clinical drug-induced liver injury', *Arch Toxicol,* 91(8), pp. 2849-2863.

Rabinowitz, M. A. (1930) 'ATROPHY OF THE LIVER DUE TO CINCHOPHEN PREPARATIONS', *JAMA,* 95(17), pp. 1228-1233.

Ramachandran, A. and Jaeschke, H. (2018) 'Acetaminophen Toxicity: Novel Insights Into Mechanisms and Future Perspectives', *Gene Expr,* 18(1), pp. 19-30.

Ramachandran, S. D., Schirmer, K., Munst, B., Heinz, S., Ghafoory, S., Wolfl, S., Simon-Keller, K., Marx, A., Oie, C. I., Ebert, M. P., Walles, H., Braspenning, J. and Breitkopf-Heinlein, K. (2015) 'In Vitro Generation of Functional Liver Organoid-Like Structures Using Adult Human Cells', *PLoS One,* 10(10), pp. e0139345.

Ramaiahgari, S., Waidyanatha, S., Dixon, D., DeVito, M., Paules, R. and Ferguson, S. (2017) 'From the cover: three-dimensional (3D) HepaRG spheroid model with physiologically relevant xenobiotic metabolism competence and hepatocyte functionality for liver toxicity screening', *Toxicol Sci,* 159, pp. 124-36.

Ramaiahgari, S. C., den Braver, M. W., Herpers, B., Terpstra, V., Commandeur, J. N., van de Water, B. and Price, L. S. (2014) 'A 3D in vitro model of differentiated HepG2 cell spheroids with improved liver-like properties for repeated dose high-throughput toxicity studies', *Arch Toxicol,* 88(5), pp. 1083-95.

Rashidi, H., Alhaque, S., Szkolnicka, D., Flint, O. and Hay, D. C. (2016) 'Fluid shear stress modulation of hepatocyte-like cell function', *Arch Toxicol,* 90(7), pp. 1757-61.

Reder-Hilz, B., Ullrich, M., Ringel, M., Hewitt, N., Utesch, D., Oesch, F. and Hengstler, J. G. (2004) 'Metabolism of propafenone and verapamil by cryopreserved human, rat, mouse and dog hepatocytes: comparison with metabolism in vivo', *Naunyn Schmiedebergs Arch Pharmacol,* 369(4), pp. 408-17.

Reichle, H. S. (1929) 'TOXIC CIRRHOSIS OF LIVER DUE TO CINCHOPHEN', *JAMA Internal Medicine,* 44(2), pp. 281-288.

Rendic, S. and Guengerich, F. P. (2012) 'Contributions of human enzymes in carcinogen metabolism', *Chem Res Toxicol,* 25(7), pp. 1316-83.

Riede, J., Wollmann, B. M., Molden, E. and Ingelman-Sundberg, M. (2021) 'Primary Human Hepatocyte Spheroids as an In Vitro Tool for Investigating Drug Compounds with Low Hepatic Clearance', *Drug Metabolism and Disposition,* 49(7), pp. 501.

Rodrigues, A. S., Duarte Silva, I., Caria, M. H., Laires, A., Chaveca, T., Glatt, H. R. and Rueff, J. (1994) 'Genotoxicity assessment of aromatic amines and amides in genetically engineered V79 cells', *Mutation Research/Genetic Toxicology,* 341(2), pp. 93-100.

Rodriguez, G. (1999) 'A cohort study on the risk of acute liver injury among users of ketoconazole and other antifungal drugs', *British journal of clinical pharmacology,* 48(6), pp. 847-852.

Rose, S., Cuvellier, M., Ezan, F., Carteret, J., Bruyère, A., Legagneux, V., Nesslany, F., Baffet, G. and Langouët, S. (2021) 'DMSO-free highly differentiated HepaRG spheroids for chronic toxicity, liver functions and genotoxicity studies', *Archives of Toxicology*.

Rowe, C., Shaeri, M., Large, E., Cornforth, T., Robinson, A., Kostrzewski, T., Sison-Young, R., Goldring, C., Park, K. and Hughes, D. (2018) 'Perfused human hepatocyte microtissues identify reactive metabolite-forming and mitochondria-perturbing hepatotoxins', *Toxicol In Vitro,* 46, pp. 29-38.

Rushing, B. R. and Selim, M. I. (2019) 'Aflatoxin B1: A review on metabolism, toxicity, occurrence in food, occupational exposure, and detoxification methods', *Food Chem Toxicol,* 124, pp. 81-100.

Russell, D. W. (2009) 'Fifty years of advances in bile acid synthesis and metabolism', *J Lipid Res,* 50 Suppl, pp. S120-5.

Sainz, B., Jr., TenCate, V. and Uprichard, S. L. (2009) 'Three-dimensional Huh7 cell culture system for the study of Hepatitis C virus infection', *Virol J,* 6, pp. 103.

Sampaziotis, F., de Brito, M. C., Madrigal, P., Bertero, A., Saeb-Parsy, K., Soares, F. A. C., Schrumpf, E., Melum, E., Karlsen, T. H., Bradley, J. A., Gelson, W. T., Davies, S., Baker, A., Kaser, A., Alexander, G. J., Hannan, N. R. F. and Vallier, L. (2015) 'Cholangiocytes derived from human induced pluripotent stem cells for disease modeling and drug validation', *Nat Biotechnol,* 33(8), pp. 845-852.

Sarkar, U., Ravindra, K. C., Large, E., Young, C. L., Rivera-Burgos, D., Yu, J., Cirit, M., Hughes, D. J., Wishnok, J. S., Lauffenburger, D. A., Griffith, L. G. and Tannenbaum, S. R. (2017) 'Integrated Assessment of Diclofenac Biotransformation, Pharmacokinetics, and Omics-Based Toxicity in a Three-Dimensional Human Liver-Immunocompetent Coculture System', *Drug Metab Dispos,* 45(7), pp. 855-866.

Schinkel, A. H. and Jonker, J. W. (2003) 'Mammalian drug efflux transporters of the ATP binding cassette (ABC) family: an overview', *Advanced Drug Delivery Reviews,* 55(1), pp. 3-29.

Schofield, C. A., Walker, T. M., Taylor, M. A., Patel, M., Vlachou, D. F., Macina, J. M., Vidgeon-Hart, M. P., Williams, A., McGill, P. J., Newman, C. F. and Sakatis, M. Z. (2021) 'Evaluation of a Three-Dimensional Primary Human Hepatocyte Spheroid Model: Adoption and Industrialization for the Enhanced Detection of Drug-Induced Liver Injury', *Chem Res Toxicol*.

Schults, M. A., Sanen, K., Godschalk, R. W., Theys, J., van Schooten, F. J. and Chiu, R. K. (2014) 'Hypoxia diminishes the detoxification of the environmental mutagen benzo[a]pyrene', *Mutagenesis,* 29(6), pp. 481-487.

Schwarz, D., Kisselev, P., Cascorbi, I., Schunck, W. H. and Roots, I. (2001) 'Differential metabolism of benzo[a]pyrene and benzo[a]pyrene-7,8-dihydrodiol by human CYP1A1 variants', *Carcinogenesis,* 22(3), pp. 453-9.

Shah, U. K., Mallia, J. O., Singh, N., Chapman, K. E., Doak, S. H. and Jenkins, G. J. S. (2018a) 'Reprint of: A three-dimensional in vitro HepG2 cells liver spheroid model for genotoxicity studies', *Mutat Res Genet Toxicol Environ Mutagen,* 834, pp. 35-41.

Shah, U. K., Mallia, J. O., Singh, N., Chapman, K. E., Doak, S. H. and Jenkins, G. J. S. (2018b) 'A three-dimensional in vitro HepG2 cells liver spheroid model for genotoxicity studies', *Mutat Res Genet Toxicol Environ Mutagen,* 825, pp. 51-58.

Shetty, S., Lalor, P. F. and Adams, D. H. (2018) 'Liver sinusoidal endothelial cells - gatekeepers of hepatic immunity', *Nat Rev Gastroenterol Hepatol,* 15(9), pp. 555-567.

Shin, D. S., Seo, H., Yang, J. Y., Joo, J., Im, S. H., Kim, S. S., Kim, S. K. and Bae, M. A. (2018) 'Quantitative Evaluation of Cytochrome P450 3A4 Inhibition and Hepatotoxicity in HepaRG 3-D Spheroids', *Int J Toxicol,* 37(5), pp. 393-403.

Shvartsman, I., Dvir, T., Harel-Adar, T. and Cohen, S. (2009) 'Perfusion cell seeding and cultivation induce the assembly of thick and functional hepatocellular tissue-like construct', *Tissue Eng Part A,* 15(4), pp. 751-60.

Smith, M. T. (2003) 'Mechanisms of troglitazone hepatotoxicity', *Chem Res Toxicol,* 16(6), pp. 679-87.

Snyderwine, E. G., Schut, H. A., Adamson, R. H., Thorgeirsson, U. P. and Thorgeirsson, S. S. (1992) 'Metabolic activation and genotoxicity of heterocyclic arylamines', *Cancer research,* 52(7 Supplement), pp. 2099s-2102s.

Soares, J. B., Pimentel-Nunes, P., Roncon-Albuquerque, R. and Leite-Moreira, A. (2010) 'The role of lipopolysaccharide/toll-like receptor 4 signaling in chronic liver diseases', *Hepatology International,* 4(4), pp. 659-672.

Sommer, S., Buraczewska, I. and Kruszewski, M. (2020) 'Micronucleus Assay: The State of Art, and Future Directions', *Int J Mol Sci,* 21(4).

Stampar, M., Sedighi Frandsen, H., Rogowska-Wrzesinska, A., Wrzesinski, K., Filipic, M. and Zegura, B. (2020) 'Hepatocellular carcinoma (HepG2/C3A) cell-based 3D model for genotoxicity testing of chemicals', *Sci Total Environ*, pp. 143255.

Stampar, M., Tomc, J., Filipic, M. and Zegura, B. (2019) 'Development of in vitro 3D cell model from hepatocellular carcinoma (HepG2) cell line and its application for genotoxicity testing', *Arch Toxicol,* 93(11), pp. 3321-3333.

Štampar, M., Žabkar, S., Filipič, M. and Žegura, B. (2021) 'HepG2 spheroids as a biosensor-like cell-based system for (geno) toxicity assessment', *Chemosphere*, pp. 132805.

Su, Y., Chen, Z., Yan, L., Lian, F., You, J., Wang, X. and Tang, N. (2018) 'Optimizing combination of liver-enriched transcription factors and nuclear receptors simultaneously favors ammonia and drug metabolism in liver cells', *Exp Cell Res,* 362(2), pp. 504-514.

Sykora, P., Witt, K. L., Revanna, P., Smith-Roe, S. L., Dismukes, J., Lloyd, D. G., Engelward, B. P. and Sobol, R. W. (2018) 'Next generation high throughput DNA damage detection platform for genotoxic compound screening', *Sci Rep,* 8(1), pp. 2771.

Takahashi, Y., Hori, Y., Yamamoto, T., Urashima, T., Ohara, Y. and Tanaka, H. (2015) '3D spheroid cultures improve the metabolic gene expression profiles of HepaRG cells', *Bioscience reports,* 35(3), pp. e00208.

Takebe, T., Sekine, K., Enomura, M., Koike, H., Kimura, M. and Ogaeri, T. (2013) 'Vascularized and functional human liver from an iPSC-derived organ bud transplant', *Nature,* 499, pp. 481-4.

Takebe, T., Sekine, K., Kimura, M., Yoshizawa, E., Ayano, S. and Koido, M. (2017) 'Massive and reproducible production of liver buds entirely from human pluripotent stem cells', *Cell Rep,* 21, pp. 2661-70.

Tarazi, E. M., Harter, J. G., Zimmerman, H. J., Ishak, K. G. and Eaton, R. A. (1993) 'Sulindac-associated hepatic injury: analysis of 91 cases reported to the Food and Drug Administration', *Gastroenterology,* 104(2), pp. 569-574.

Tascher, G., Burban, A., Camus, S., Plumel, M., Chanon, S., Le Guevel, R., Shevchenko, V., Van Dorsselaer, A., Lefai, E., Guguen-Guillouzo, C. and Bertile, F. (2019) 'In-Depth Proteome Analysis Highlights HepaRG Cells as a Versatile Cell System Surrogate for Primary Human Hepatocytes', *Cells,* 8(2).

Terashima, J., Goto, S., Hattori, H., Hoshi, S., Ushirokawa, M., Kudo, K., Habano, W. and Ozawa, S. (2015a) 'CYP1A1 and CYP1A2 expression levels are differentially regulated in three-dimensional spheroids of liver cancer cells compared to two-dimensional monolayer cultures', *Drug Metabolism and Pharmacokinetics,* 30(6), pp. 434-440.

Terashima, J., Goto, S., Hattori, H., Hoshi, S., Ushirokawa, M., Kudo, K., Habano, W. and Ozawa, S. (2015b) 'CYP1A1 and CYP1A2 expression levels are differentially regulated in three-dimensional spheroids of liver cancer cells compared to two-dimensional monolayer cultures', *Drug Metab Pharmacokinet,* 30(6), pp. 434-40.

Thakkar, S., Chen, M., Fang, H., Liu, Z., Roberts, R. and Tong, W. (2018) 'The Liver Toxicity Knowledge Base (LKTB) and drug-induced liver injury (DILI) classification for assessment of human liver injury', *Expert Rev Gastroenterol Hepatol,* 12(1), pp. 31-38.

Thakkar, S., Li, T., Liu, Z., Wu, L., Roberts, R. and Tong, W. (2020) 'Drug-induced liver injury severity and toxicity (DILIst): binary classification of 1279 drugs by human hepatotoxicity', *Drug Discovery Today,* 25(1), pp. 201-208.

Thermo Fisher Scientific (2021) *Primary Human Hepatoctye 3D Spheroids for Studying Hepatic Function and Drug Toxicity*. Available at: https://assets.thermofisher.com/TFS-Assets/BID/posters/human-hepatoctye-3d-spheroids-hepatic-function-drug-toxicity-poster.pdf (Accessed: 01 June 2021.

Thybaud, V., Lorge, E., Levy, D. D., van Benthem, J., Douglas, G. R., Marchetti, F., Moore, M. M. and Schoeny, R. (2017) 'Main issues addressed in the 2014-2015 revisions to the OECD Genetic Toxicology Test Guidelines', *Environ Mol Mutagen,* 58(5), pp. 284-295.

Tracy, T. S., Korzekwa, K. R., Gonzalez, F. J. and Wainer, I. W. (1999) 'Cytochrome P450 isoforms involved in metabolism of the enantiomers of verapamil and norverapamil', *Br J Clin Pharmacol,* 47(5), pp. 545-52.

Trefts, E., Gannon, M. and Wasserman, D. H. (2017) 'The liver', *Current Biology,* 27(21), pp. R1147-R1151.

Tsamandouras, N., Kostrzewski, T., Stokes, C. L., Griffith, L. G., Hughes, D. J. and Cirit, M. (2017) 'Quantitative Assessment of Population Variability in Hepatic Drug Metabolism Using a Perfused Three-Dimensional Human Liver Microphysiological System', *J Pharmacol Exp Ther,* 360(1), pp. 95-105.

Tsuchida, T. and Friedman, S. L. (2017) 'Mechanisms of hepatic stellate cell activation', *Nature Reviews Gastroenterology & Hepatology,* 14(7), pp. 397-411.

Tuschl, G., Hrach, J., Walter, Y., Hewitt, P. G. and Mueller, S. O. (2009) 'Serum-free collagen sandwich cultures of adult rat hepatocytes maintain liver-like properties long term: a valuable model for in vitro toxicity and drug-drug interaction studies', *Chem Biol Interact,* 181(1), pp. 124-37.

van Wenum, M., Adam, A. A., Hakvoort, T. B., Hendriks, E. J., Shevchenko, V., van Gulik, T. M., Chamuleau, R. A. and Hoekstra, R. (2016) 'Selecting Cells for Bioartificial Liver Devices and the Importance of a 3D Culture Environment: A Functional Comparison between the HepaRG and C3A Cell Lines', *Int J Biol Sci,* 12(8), pp. 964-78.

Visentin, M., Lenggenhager, D., Gai, Z and Kullak-Ublick, G.A. 'Drug-Induced Bile Duct Injury', *Biochimica et Biophysica Acta (BBA) - Molecular Basis of Disease*, 1864(4), pp.1498–1506.

Vorrink, S. U., Ullah, S., Schmidt, S. F., Nandania, J. T., Velagapudi, V., Beck, O., Ingelman-Sundberg, M. and Lauschke, V. M. (2017) 'Endogenous and xenobiotic metabolic stability of primary human hepatocytes in long-term 3D spheroid cultures revealed by a combination of targeted and untargeted metabolomics', *Faseb Journal,* 31(6), pp. 2696-2708.

Walles, M., Brown, A. P., Zimmerlin, A. and End, P. (2020) 'New Perspectives on Drug-Induced Liver Injury Risk Assessment of Acyl Glucuronides', *Chem Res Toxicol,* 33(7), pp. 1551-1560.

Wang, H., Brown, P. C., Chow, E. C. Y., Ewart, L., Ferguson, S. S., Fitzpatrick, S., Freedman, B. S., Guo, G. L., Hedrich, W., Heyward, S., Hickman, J., Isoherranen, N., Li, A. P., Liu, Q., Mumenthaler, S. M., Polli, J., Proctor, W. R., Ribeiro, A., Wang, J. Y., Wange, R. L. and Huang, S. M. (2021) '3D cell culture models: Drug pharmacokinetics, safety assessment, and regulatory consideration', *Clin Transl Sci,* 14(5), pp. 1659-1680.

Wang, P., Pradhan, K., Zhong, X. B. and Ma, X. (2016) 'Isoniazid metabolism and hepatotoxicity', *Acta Pharm Sin B,* 6(5), pp. 384-392.

Wang, Z., Luo, X., Anene-Nzelu, C., Yu, Y., Hong, X., Singh, N. H., Xia, L., Liu, S. and Yu, H. (2015) 'HepaRG culture in tethered spheroids as an in vitro three-dimensional model for drug safety screening', *Journal of Applied Toxicology,* 35(8), pp. 909-917.

Wang, Z. Y., Li, W. J., Li, Q. G., Jing, H. S., Yuan, T. J., Fu, G. B., Tang, D., Zhang, H. D., Yan, H. X. and Zhai, B. (2019) 'A DMSO-free hepatocyte maturation medium accelerates hepatic differentiation of HepaRG cells in vitro', *Biomed Pharmacother,* 116, pp. 109010.

Weaver, R. J., Blomme, E. A., Chadwick, A. E., Copple, I. M., Gerets, H. H. J., Goldring, C. E., Guillouzo, A., Hewitt, P. G., Ingelman-Sundberg, M., Jensen, K. G., Juhila, S., Klingmuller, U., Labbe, G., Liguori, M. J., Lovatt, C. A., Morgan, P., Naisbitt, D. J., Pieters, R. H. H., Snoeys, J., van de Water, B., Williams, D. P. and Park, B. K. (2020) 'Managing the challenge of drug-induced liver injury: a roadmap for the development and deployment of preclinical predictive models', *Nat Rev Drug Discov,* 19(2), pp. 131-148.

Weisburger, J. H. and Weisburger, E. K. (1973) 'Biochemical Formation and Pharmacological, Toxicological and Pathological Properties of Hydroxylamines and Hydroxamic Acids', *Pharmacological Reviews,* 25(1), pp. 1-66.

Wencel, A., Ciezkowska, M., Wisniewska, M., Zakrzewska, K. E., Pijanowska, D. G. and Pluta, K. D. (2021) 'Effects of genetically modified human skin fibroblasts, stably overexpressing hepatocyte growth factor, on hepatic functions of cocultured C3A cells', *Biotechnol Bioeng,* 118(1), pp. 72-81.

Westerink, W. M. and Schoonen, W. G. (2007) 'Phase II enzyme levels in HepG2 cells and cryopreserved primary human hepatocytes and their induction in HepG2 cells', *Toxicol In Vitro,* 21(8), pp. 1592-602.

Wheeler, M. D. (2003) 'Endotoxin and Kupffer cell activation in alcoholic liver disease', *Alcohol Research & Health,* 27(4), pp. 300-306.

Wilkening (2003) 'Comparison of primary human hepatocytes'.

Williams, D. P., Lazic, S. E., Foster, A. J., Semenova, E. and Morgan, P. (2020) 'Predicting Drug-Induced Liver Injury with Bayesian Machine Learning', *Chem Res Toxicol,* 33(1), pp. 239-248.

Wilson, A., Grabowski, P., Elloway, J., Ling, S., Stott, J. and Doherty, A. (2021) 'Transforming early pharmaceutical assessment of genotoxicity: applying statistical learning to a high throughput, multi end point in vitro micronucleus assay', *Sci Rep,* 11(1), pp. 2535.

Wrzesinski, K., Magnone, M. C., Hansen, L. V., Kruse, M. E., Bergauer, T., Bobadilla, M., Gubler, M., Mizrahi, J., Zhang, K., Andreasen, C. M., Joensen, K. E., Andersen, S. M., Olesen, J. B., Schaffalitzky de Muckadell, O. B. and Fey, S. J. (2013) 'HepG2/C3A 3D spheroids exhibit stable physiological functionality for at least 24 days after recovering from trypsinisation', *Toxicology Research,* 2(3), pp. 163-172.

Wu, I. U., Tsai, J. H. and Ho, C. M. (2021) 'Fatal acute-on-chronic liver failure in amiodarone-related steatohepatitis: a case report', *BMC Gastroenterol,* 21(1), pp. 50.

Xie, Y., Yao, J., Jin, W., Ren, L. and Li, X. (2021) 'Induction and Maturation of Hepatocyte-Like Cells In Vitro: Focus on Technological Advances and Challenges', *Front Cell Dev Biol,* 9, pp. 765980.

Yang, K., Guo, C., Woodhead, J. L., St Claire, R. L., 3rd, Watkins, P. B., Siler, S. Q., Howell, B. A. and Brouwer, K. L. R. (2016) 'Sandwich-Cultured Hepatocytes as a Tool to Study Drug Disposition and Drug-Induced Liver Injury', *J Pharm Sci,* 105(2), pp. 443-459.

Yang, S., Hwang, S. J., Park, J. Y., Chung, E. K. and Lee, J. I. (2019) 'Association of genetic polymorphisms of CYP2E1, NAT2, GST and SLCO1B1 with the risk of anti-tuberculosis drug-induced liver injury: a systematic review and meta-analysis', *BMJ Open,* 9, pp. 027940.

Yokobori, K., Azuma, I., Chiba, K., Akita, H., Furihata, T. and Kobayashi, K. (2019) 'Indirect activation of constitutive androstane receptor in three-dimensionally cultured HepG2 cells', *Biochem Pharmacol,* 168, pp. 26-37.

Yokobori, K., Kobayashi, K., Azuma, I., Akita, H. and Chiba, K. (2017) 'Intracellular localization of pregnane X receptor in HepG2 cells cultured by the hanging drop method', *Drug Metab Pharmacokinet,* 32, pp. 265-72.

Yu, K., Geng, X., Chen, M., Zhang, J., Wang, B., Ilic, K. and Tong, W. (2014) 'High daily dose and being a substrate of cytochrome P450 enzymes are two important predictors of drug-induced liver injury', *Drug Metab Dispos,* 42(4), pp. 744-50.

Zeigerer, A., Wuttke, A., Marsico, G., Seifert, S., Kalaidzidis, Y. and Zerial, M. (2017) 'Functional properties of hepatocytes in vitro are correlated with cell polarity maintenance', *Exp Cell Res,* 350(1), pp. 242-252.

Zhang, C., Zhang, Q., Li, J., Yu, L., Li, F., Li, W., Li, Y., Peng, H., Zhao, J., Carmichael, P. L., Wang, Y., Peng, S. and Guo, J. (2020) 'Integration of in vitro data from three dimensionally cultured HepaRG cells and physiologically based pharmacokinetic modeling for assessment of acetaminophen hepatotoxicity', *Regul Toxicol Pharmacol,* 114, pp. 104661.

Zhou, Z., Xu, M. J. and Gao, B. (2016) 'Hepatocytes: a key cell type for innate immunity', *Cell Mol Immunol,* 13(3), pp. 301-15.

Zientek, M., Miller, H., Smith, D., Dunklee, M. B., Heinle, L., Thurston, A., Lee, C., Hyland, R., Fahmi, O. and Burdette, D. (2008) 'Development of an in vitro drug–drug interaction assay to simultaneously monitor five cytochrome P450 isoforms and performance assessment using drug library compounds', *Journal of Pharmacological and Toxicological Methods,* 58(3), pp. 206-214.

Zou, W., Devi, S. S., Sparkenbaugh, E., Younis, H. S., Roth, R. A. and Ganey, P. E. (2009) 'Hepatotoxic interaction of sulindac with lipopolysaccharide: role of the hemostatic system', *Toxicol Sci,* 108(1), pp. 184-93.

Chapter 2. DEVELOPMENT OF A HEPG2/C3A HEPATIC SPHEROID MODEL FOR TOXICITY STUDIES

2.1. Introduction

The use of advanced *in vitro* cell models is becoming more widely adopted for investigating disease pathology, drug efficacy, safety and toxicity. Such models are now routinely used in the pharmaceutical industry and in academic knowledge transfer (Elliott and Yuan, 2011, Langhans, 2018, Zanoni et al., 2016) . The ability to capture native tissue biology within an *in vitro* system is of fundamental importance to several biological research fields including cancer biology, toxicology and drug discovery, and tissue engineering and regeneration. To undertake such study, methods are required that allow advanced *in vitro* models composed of a diverse range of cells which are typically adherent, and form tightly controlled three dimensional structures, e.g., spheroid cell cultures. Despite growth in the literature for the use of such models in toxicity testing pipelines there remains a lack of coherent protocols and studies demonstrating the re-producibility of such datasets or characterisation of model properties. The agarose liquid-overlay technique is highly regarded as a versatile method for the production of cellular spheroids through promotion of inter-cellular attachment, cellular aggregation and repellence from forming monolayers (Costa et al., 2014). Agarose is a marine-derived biopolymer, formed by thermally linking a series of agarose chains through hydrogen bonding to form a hydrogel that can be engineered for tuneable poration and stiffness (Morita et al., 2013, Narayanan et al., 2006). As an inert biological substance that is commonplace to most research laboratories, several studies have reported on the use of agarose hydrogels in the formation of three dimensional, and advanced *in vitro* cellular models. By exploiting the physical chemical properties of agarose, hydrogels can be formed under tissue culture conditions that promote cellular repellence, forcing single cell populations to aggregate into singular structures that can be studied in the context of

microtissues (Costa et al., 2014). Compared to other methods such as commercially available tissue culture plates, scaffold techniques or those involving matrices, initial review suggests this method is easy to implement, highly cost effective ($\leq$ 1 £GBP per plate) and capable of generating reproducible spheroids. However, although the formation of the agarose hydrogel is relatively simple whereby agarose powder is dispersed in an aqueous buffer, heated to gelation, and then set into a mould of some kind, the process of forming an agarose hydrogel that is cell-repellent, promoting spheroid formation has not been extensively evaluated.

Recent research has emerged demonstrating the use of *in vitro* spheroids for modelling toxicity, and their comparison to cells in 2D monolayers and many of the phenotypes found in the liver *in vivo* are lost or at the very least, repressed in 2D monolayers of cells, but seemingly maintained in 3D spheroid models. Some of the models reported include those in hepatoma cell lines, principally HepG2/C3A cells (Fey and Wrzesinski, 2012, Wrzesinski et al., 2013, Gaskell et al., 2016); HepaRG (Wang et al., 2015, Ramaiahgari et al., 2017); primary human hepatocytes (Hendriks et al., 2016b, Leite et al., 2016, Vorrink et al., 2017b, Baze et al., 2018, Kozyra et al., 2018); and hepatic organoids (Leite et al., 2016, Coll et al., 2018). Given this obvious utility, the aim of this chapter is to therefore see if a monoculture HepG2/C3A spheroid could be recapitulated using literature guidance using the liquid overlay technique and subject them to phenotypic assays that assesses their sensitivity to hepatotoxicants, as well as small molecule pro-mutagens commonly employed in genotoxicity test batteries.

2.2. Materials and methods

2.2.1. Chemicals and reagents

All tissue culture reagents were form Gibco, Paisley, UK. All chemicals were from Merck Life Sciences unless stated otherwise. All cell culture reagents were purchased from Gibco, Paisley, Scotland, UK. The following compounds were used for ADME(T) studies in HepG2/C3A spheroids, as compounds requiring metabolic biotransformation by CYP450 enzymes to reactive intermediates: acetaminophen (APAP), Diclofenac (DCF) and trovafloxacin (TRV) compounds were from Cayman Chemicals, MI, USA; Cinchophen was from Merck-Sigma. CellTiter-Glo luminescent cell viability assay was from Promega, Southampton, UK. QuantiT PicoGreen dsDNA kit from was Thermofisher, Loughborough, UK.

2.2.2. Cell culture

Hepatocellular carcinoma clonal derivative cells (HepG2/C3A) cells, a derivative of HepG2, were chosen due to their optimal contact growth inhibition properties and therefore well-reported use in 3D culture. HepG2/C3A (ATCC, #CRL-10741) and HepG2 (ATCC, #HB-8065) cells were sourced from the American Tissue Culture Collection and cultured in Dulbecco's Modified Eagles Medium (DMEM) containing low (1 g/L) glucose and 2 mM L-glutamine, supplemented with 10 % (v/v) foetal bovine serum (FBS) 100 Units/mL penicillin and 100 μg/mL streptomycin. Cells were cultured under standardised procedures, passaged to a maximum of 25 times with regular mycoplasma testing performed by PCR.

2.2.3. Preparation of cell-repellent microplates by use of the agarose liquid-overlay technique (LOT)

A series of different agaroses were prepared at 1.5 % (w/v) in serum-free DMEM to assess cell-repellent properties. Agaroses were dissolved at 0.5, 3 or optimised at 1.5 % (w/v) in serum free DMEM, and sterilised by autoclaving at 121 ^{o}C for 1 h. The agarose solution was maintained at 85 ^{o}C to prevent premature gelling using a hotplate water-bath setup and 100 μL transferred to appropriate wells within a 96-well flat bottom microplate (Greiner Bio-One, Kremünster, Austria), using an electronic multichannel pipettor; the LOT plates were left to gel at room temperature within the tissue culture cabinet for 30-60 mins or were hermetically sealed and placed at 4 ^{o}C before use. Cells were seeded at 1000 cells in 100 μL of complete DMEM into the inner wells, the outer wells were filled with an equivalent volume of DMEM as an evaporation barrier; plates were centrifuged and then left at room temperature for 15-30 mins allow cells to settle, before centrifugation at 1500 rpm for 5 minutes to form a loose aggregate. The spheroid microplates were then left to form spheroids over 3 – 5 days at 37 ^{o}C, 5 % CO_2 and sampled for subsequent analysis at day 7. Phase contrast microscopy was used throughout the spheroid culture period to monitor spheroid morphology and growth using an inverted microscope with 4 X objective (Nikon Instruments, UK) , fitted with a digital camera head (Canon); all images were exported to FIJI image J for analysis (Schindelin et al., 2012)

2.2.3.1. Determination of the free movement of small molecules across agarose-cell repellent surfaces

A permeability experiment was established using methods presented by Hsu et al. (2018), using transwell inserts and a 48-well microplate to establish a transfer system. To simulate the LOT cell-repellent surface, 100 μL of optimised agarose (1.5 % w/v) was used to coat the insert, termed 'upper [donor] compartment' and left to gel. After gelling, 100 μL of phenol red-free medium was loaded into both the upper and lower [acceptor] compartments. Fluorescein sodium salt was used to monitor permeability transport by loading the upper compartments with 600 μM. Over 24 hours, samples were collected, transferred to black walled microplates and fluorescence measured. The stokes radius of fluorescein was assumed to be 5 x 10^{-10} m (Mustafa et al., 1993, Chenyakin et al., 2017, Hsu et al., 2018). The permeability coefficient of the 1.5 % (w/v) agarose hydrogel used to generate HepG2/C3A spheroids was determined as 1.44 x 10^{-8} m/s.

2.2.3.2. Agarose gel as a slow-release mechanism to induce cytotoxicity in HepG2/C3A spheroids

To further demonstrate free-movement of small molecules between the agarose cell-repellent membrane and cell culture chamber, 4-nitroquinoline-1-oxide was used as a well-known DNA damaging agent to induce toxicity in HepG2/C3A spheroids. At concentrations of 0 – 30 μM, the small molecule was suspended in liquid agarose and allowed to set to form LOT plates. Pre-formed 7-day old spheroids were seeded onto the dosed-agarose gels and left to incubate over 72 h, with phase contrast images collected every 24 h. After 72 h, the

ATP content of spheroids exposed to the dosed-agarose hydrogels was compared against those exposed to vehicle-dosed hydrogels as previously described.

2.2.4. Histological examination of HepG2/C3A spheroids

Individual spheroids were removed from culture plates using wide orifice pipette tips and washed 3x in Dulbecco's PBS (DPBS). A series of small 'boat' vessels were made using foil, spheroids transferred, and residual medium removed. Foil vessels were gently filled with optimal cutting compound (Tissue-Tek O.C.T ®, Sakura Finetek Europe B.V, Netherlands) and flash-frozen in liquid nitrogen. O.C.T-embedded spheroids were adhered to the stock-head of a cryostat held at -10 ^{o}C (OTF5000, Bright Instruments Ltd, Luton, UK), carefully sectioned at 5 μm intervals and transferred to charged poly-D-lysine-coated microscopy slides. Slides were stained with freshly made Haematoxylin and Eosin (pfm medical Ltd, Poynton, UK) to stain nuclei and cytoplasmic and extracellular matrices, and optically cleared in a series of xylene and alcohol baths of 1 minute each. Slides were sealed using DPX mounting medium (CellPath Ltd, Powys, UK) and a coverslip placed on top. Brightfield images were collected using inverted microscope (Zeiss).

2.2.5. Basic immunofluorescence analysis of HepG2/C3A spheroid cultures

Spheroid culture media was removed and the spheroids were washed in PBS 3x times at room temperature. Spheroids were fixed by suspension in paraformaldehyde solution in PBS (PFA, 4 % wt/vol) either in microcentrifuge tubes or in U-bottomed plates (Greiner Bio-One), for 16 – 24 h at 4 ^{o}C. For immunofluorescent staining, spheroids were removed from PFA solution and washed in PBS and incubated overnight at 4 ^{o}C in a permeabilisation buffer of

Triton X-100 (0.5 % v/v) in Tris-Buffered Saline with Tween 20 (0.05 % v/v). Hoescht 33342 was used as a nuclear DNA stain (1:5000, 2 μg/mL) and Phalloidin-FITC was to stain filamentous actin skeletons (1:500,1 μg/mL). Spheroids were placed into 35 mm glass bottomed tissue culture dishes (MatTek, Ashland, MA, USA) and sealed with hydromount histological mounting medium (National diagnostics, Atlanta, GA, USA), and a cover slip. Spheroid images were acquired using a Nikon A1R laser scanning confocal microscope using a 40X oil objective. Spheroid images were acquired using the Nikon Elements software and processed as Z-stacks using FIJI-Image J.

2.2.6. Initial use of the comet assay to assess the DNA damage response capacity in HepG2/C3A spheroids

HepG2 C3A cells in monolayers and 7-day old spheroids were exposed to 4-nitroquinoline 1-oxide (9.5 μg/mL, 50 μM, 4-NQO), a known mutagen or benzo[a]pyrene (12.5 μg/mL, 50 μM, B[a]P), a pro-mutagen requiring metabolic activation via Cytochromes P450 1A1/1B1; cells were subjected to non-lethal exposure for 2h. DNA strand breaks were quantified by use of the alkaline Comet single gel electrophoresis assay, according to Perotti et al. (2015) with some modifications. After exposure, monolayers or spheroids were trypsinised over 15 minutes order to generate a single cell suspension, centrifuged (300 g, 5 mins) and rinsed in PBS. Cell pellets were suspended at approximately 1 x 10^4 cells in 90 μL, 0.7 % (v/v) pre-warmed low melting point agarose (LMA) and embedded onto normal melting agarose (NMA) coated microscope slides, 1 % (v/v). After the agarose had set, a further layer of LMA was used with a cover slip to seal the slides. To induce cell lysis, slides were incubated overnight at 4 ^{o}C in 2.5 M NaCl, 10 mM Na_2EDTA, 10 mM Tris-HCl, 1 % (v/v) Triton-X100 and

10 % DMSO. Electrophoresis was performed at 0 ^{o}C (20 V cm^{-1}, 300 mA) for 20 minutes in 1 mM Na_2EDTA, 300 mM NaOH (pH > 10), in a black electrophoretic chamber. After electrophoresis, slides were neutralised in 2 mL of 0.4 M Tris-HCl, fixed in 70 % (v/v) ethanol at – 20 ^{o}C and dried at room temperature for a minimum of 4 h. DNA was stained with 75 μL SYBR™ Gold Nucleic Acid Stain (1:1000, Invitrogen, UK) and cells were visualised at 20 X magnification under an Axiovert 10 epifluorescence microscope (Carl Zeiss Ltd, Cambridge, UK), equipped with a 515-560 nm excitation and 450-490 nm emission filter, and a 590 nm barrier filter. Images were acquired using a mounted digital camera head (Marlin, Allied Vision Technologies GMBH, Stadtroda, Germany) and slides were scored blindly by counting a minimum of 100 cells across experimental replicates (50 per slide), using the Comet Assay IV imaging system (Instem, Stone, Staffordshire, UK). Median percentage DNA in tail was chosen as the measure parameter of DNA damage as has been previously reported to exhibit less inter-assay variability (Olive and Durand, 2005).

2.2.7. Cytotoxicity assays

HepG2/C3A cells in monolayer or spheroids were exposed to hepatotoxins at various concentrations within the culture medium. Compounds were titrated in dimethyl sulphoxide (DMSO) and exposed to cells in tissue culture medium; the maximum final concentration of DMSO used was 0.5 % v/v. At the end of the exposure period, cellular viability was assessed using the CellTiter-Glo kit (Promega, UK) , according to the manufacturer's instructions but with some minor modifications: tissue culture plates were removed from incubation and equilibrated to room temperature for 15 mins; 50 μL of the incubation media was removed and replaced with the CellTiter-Glo lysis reagent; the assay plates were then incubated for 20

minutes at room temperature and placed aboard a rotating plate shaker at 400 rpm to induce cell lysis. For data acquisition, 50 μL of the final reaction volume from each well was transferred to flat bottom white microplates (Greiner Bio-One); luminescence was read across the plate using a Tecan F200 Infinite Pro multimode plate reader (Tecan, Männedorf, Switzerland). Data was collected in triplicate and experiments performed three times. Data was expressed as the percentage viability of treated spheroids or monolayer cells compared to a vehicle control. Z' primes statistical formula was applied to confirm assay robustness (Zhang et al., 1999).

2.2.8. Statistics and data analysis

All data were analysed either in RStudio (Version 1.0.153, RStudio Inc, Boston, MA, USA) or GraphPad Prism (Version 8, GraphPad Software, San Diego, CA, USA). Normality testing was performed on all relevant data sets using the Saphiro-Wilk method and analysed using either a one- or two-way ANOVA; Kruskal-Wallis non-parametric testing was alternatively performed. Significance was denoted as: $**** p < 0.0001, *** p < 0.001, ** p < 0.01, * p < 0.05.$ Image analysis was conducted using FIJI ImageJ (Schindelin et al., 2012). All figures were drawn and arranged using the Inkscape open-source graphics editor (Free Software Foundation Inc, Boston, MA, USA).

2.3. Results

2.3.1. Optimisation of the liquid overlay technique to form cell-repellent microplate surfaces

To identify the best method for producing single HepG2/C3A spheroids, HepG2/C3A cells were seeded into microplates coated with various agarose types, storage conditions and commercially sourced plates from Greiner Bio-One and PrimeSurface Biomedical, Inc, and the formation of spheroids monitored. Figure 2.1 shows HepG2/C3A at day 7 of cultivation on a range of LOT matrices. Low-gelling agarose coated microplates at 1.5 % (w/v) were unable to form HepG2/C3A spheroids however hydration at 4 ^{o}C for 14 days appeared to form a number micropores throughout the agarose surface that formed microcosms into which cells were able to settle and form aggregates; forced pipetting did not dislodge the spheroid bodies suggesting they were physically growing on the inert surface. High gelling agarose set *in situ* or over 14 days at 4 ^{o}C, formed suboptimal spheroids. Spheroid formation within the commercial plate #1 ultra-low attachment plate from Greiner-Bio one formed spheroids most equivalent to those in optimised normal gelling agarose microplates whereas the other 2 commercial plates produced inadequate spheroids. Cells clearly aggregated together but they appeared to allow excess cellular proliferation resulting in the loss of spheroid structure and sphericity suggesting poor repellence from microplate coating (commercial plate #3 from Primesurface Biomedical); whereas commercial plate #2, from Greiner BioOne was unable to cultivate singular spheroids but rather a series of miniaturised spheroids, albeit well-formed with clearly defined outer membrane; most likely this is a result of the plate's flat-bottomed structure whereas most spheroid microplates are U-bottomed, enhancing the aggregation of cells suspended towards the centre of the centre .

Normal gelling/melting agarose (NMA) was found to be optimum for forming HepG2/C3A spheroids at 1.5 % (w/v) in serum-free DMEM forming spheroids with a maintained spherical structure with tight periphery indicating the disposition of extracellular matrices aiding the compaction of HepG2/C3A cells into uniform homogenous spheroids, compared to the same agarose suspended by either 3 or 0.5 % (w/v). Hydration and hermetic sealing of plates at 4 ^{o}C did not aid in the formation of spheroids suggesting deterioration of the agarose layers over time.

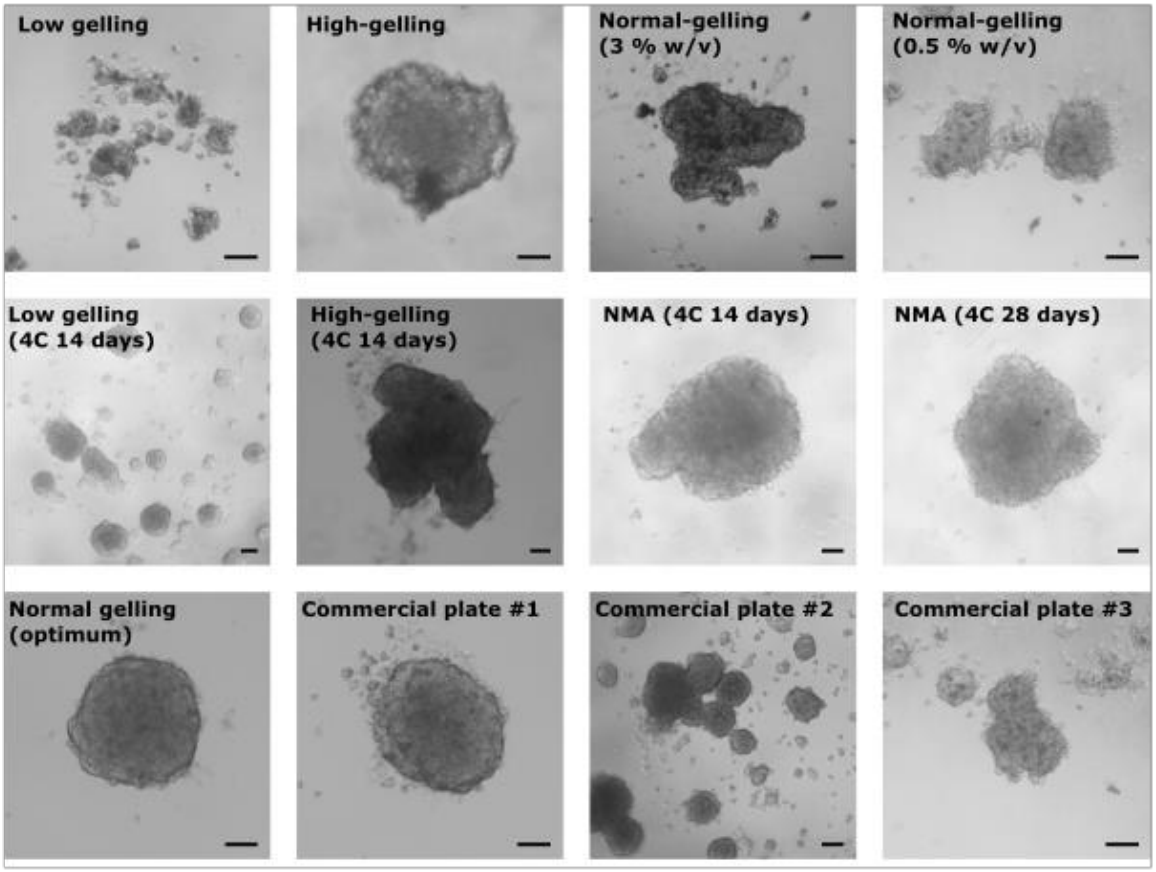

Figure 2.1. Overview of the approaches used to generate HepG2/C3A spheroids. *A range of agaroses were used to perform the liquid overlay technique (LOT) or commercially available spheroid microplates were sourced to form cell-repellent wells into which cell suspensions were seeded. LOT microplates were prepared in serum-free, phenol red- free tissue culture medium and allowed to set in situ or were hermetically sealed and stored at 4 ^{o}C before use.*

Commercial plate #1 (ULA) and #2 (Flat) were from Greiner BioOne; plate #3 was from PrimeSurface Biomedical Inc. Scale bars= 100 μm.

2.3.2. HepG2/C3A cells generate better spheroids than the HepG2 parental cell line

HepG2 parental cells or HepG2/C3A were seeded into agarose coated plates according to the optimised LOT at 1 x 10^3 cells/well and left to form spheroids as previously described. Previous evidence from the literature suggests that HepG2/C3A cells can form better spheroids that are maintained for a longer period versus the HepG2 parent which was assessed here (Fey et al., 2020, Gaskell et al., 2016, Wrzesinski and Fey, 2013). After 7 days in culture HepG2/C3A spheroids formed round spheroids with maintained membrane around the circumference whereas the parent cell line was less well formed (Figure **2.2**A) with evidence of cells migrating around the spheroid circumference. Spheroid structure was maintained between day 7 and 14 in HepG2/C3A spheroids with an approximate 14 % increase in diameter to 463 μm (Figure **2.2**B) on average whereas HepG2 cells continued to proliferate, yielding a spheroid of greater than 640 μm. Overall, HepG2/C3A spheroids appeared more compact compared to parent HepG2 spheroids, indicating uncontrolled over-proliferation with cells that seemingly looked as though they were becoming detached from the main spheroid body. In addition, using the ferret diameter of planimetric image data, relative circularity of spheroids was calculated where 1.0 represents a 'perfect circle', where the relative circularity of HepG2/C3A spheroids was greater than HepG2 spheroids at day 7 with a greater condensed membrane throughout the periphery, but equivalent at day 14.

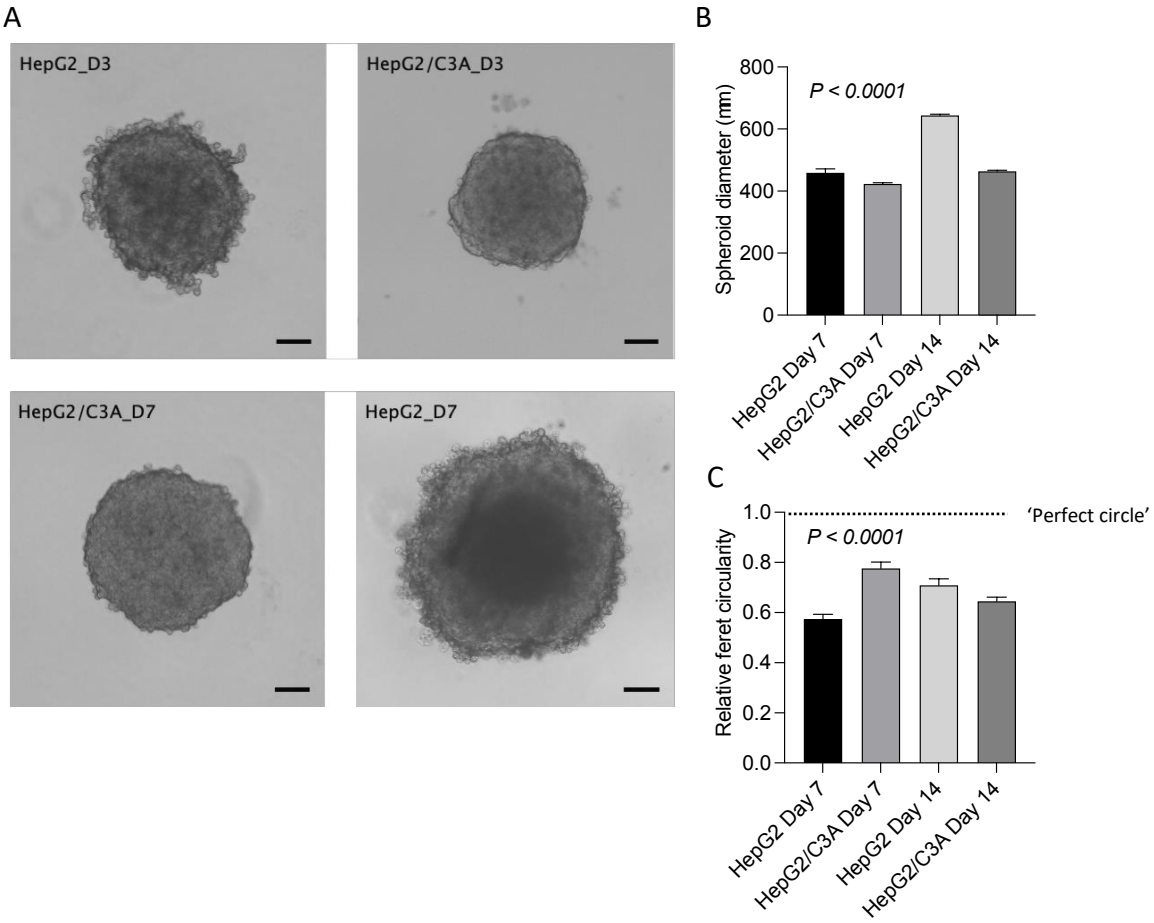

Figure 2.2.HepG2/C3A cells outperform parental HepG2 cells for the formation of cellular spheroids *(A) representative phase contrast images collected at day 7 and day 14 of growth and (B) planimetric data collected from images reporting spheroid diameter and (C) relative circularity of spheroids using minimum and maximum Feret parameters where a value of 1.0 is a perfect circle. Data is of mean n=12 spheroids from 4 separate experiments, P values were obtained one-way ANOVA, error bars are SEM. Scale bar = 100 μm.*

2.3.3. Permeability of LOT agarose surfaces to the transportation of small molecules

The dynamic free movement of fluorescein was measured from above and below LOT surfaces formed from normal-gelling agarose at 1.5 % (w/v), (Figure 2.3A - B) The initial lag-phase of fluorescein permeation across the agarose layer was 0-6 hours. There was linear permeation of the fluorescein solute between 6 and 12 hours whereby a dynamic equilibrium was reached between the apical and basal compartments to the agarose

hydrogel. Fluorescein permeation continued before reaching a mean steady state concentration of 0.32 M and 0.26 M in the lower and upper compartments respectively, demonstrating free movement of permeate across the agarose membrane and an equilibrium in small molecule distribution between the two compartments.

To further investigate transfer of small molecules from agarose to the aqueous phase 4-NQO was suspended in LOT gels at 0 – 30 μM and allowed to set. Previously formed spheroids were then transferred into those wells (Figure 2.3C). HepG2/C3A seeded onto vehicle-dosed agarose gels remained viable and maintained a clearly defined circumference throughout the culture period of 72 h, exemplifying the inertness of the LOT agarose layer (Figure 2.3D). After 24 h, evidence of cytotoxicity could only be seen as evidenced by light ruffling at the outer spheroid edges and some evidence of cellular detachment from the main spheroid body in wells containing 30 μM in the agarose. Cellular condensation across the spheroid body occurred after 48 h at concentrations of 10-30 μM in the agarose gels and a reduction in overall spheroid diameter. The most significant effects could be seen after 72 h of incubation (Figure 2.3D); at 3 μM 4-NQO in agarose, there was 40 % reduction in spheroid viability, which was further reduced to 10 and 5 % spheroid viability at 10 and 30 μM, respectively, further indicating a free movement of small-molecules across the hydrogel layer and the induction of cytotoxicity in HepG2/C3A spheroids.

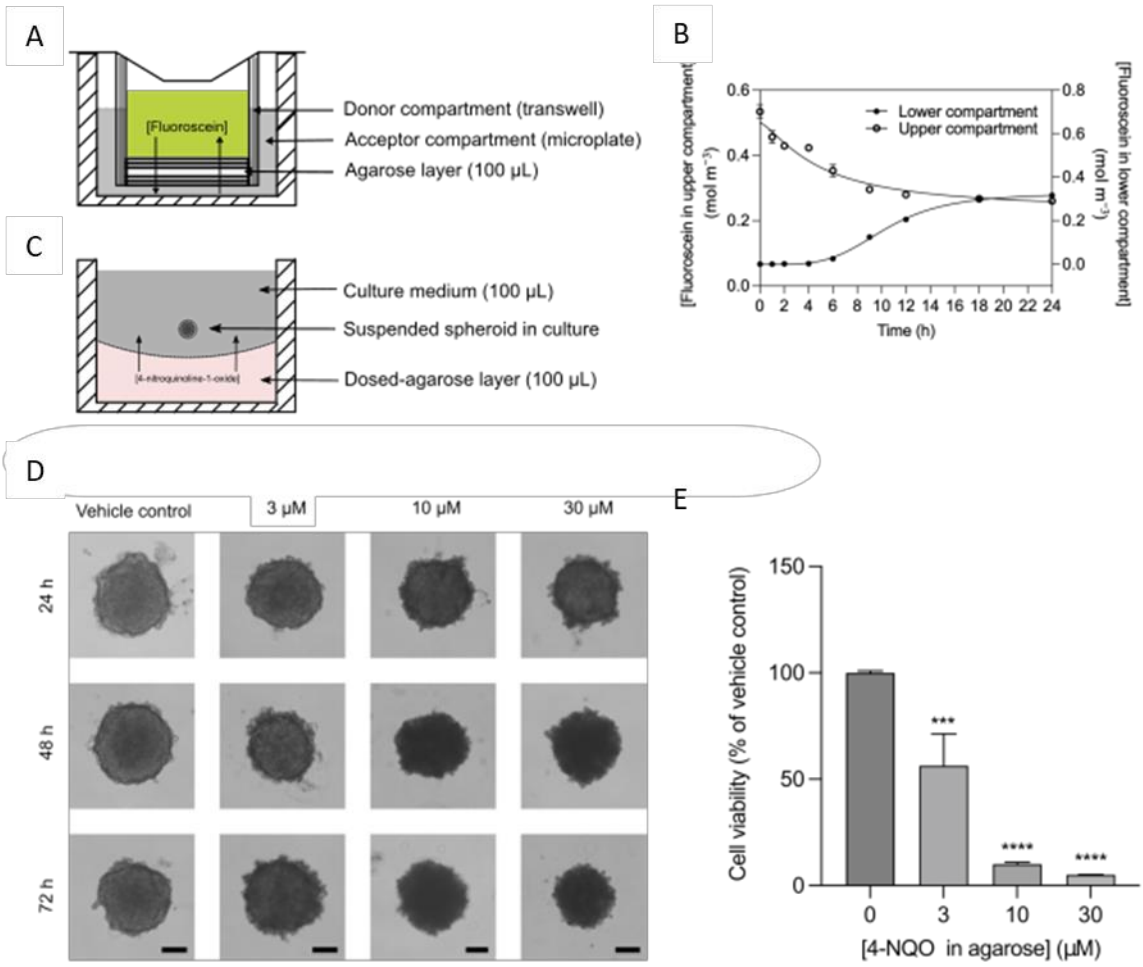

Figure 2.3. Permeation of small molecules across agarose cell-repellent surfaces*. Permeation parameters through the agarose hydrogel layers were established using a transwell-insert membrane coated with 1.5 % (w/v) agarose (A) and fluorescein sodium salt used as the studied permeate kinetically over 24 h (B). 4-nitro-quinoline-1-oxide was suspended into agarose gels and ready-formed spheroids placed on top (C), and the induction of cytotoxicity in HepG2/C3A spheroids monitored over 72 h by phase-contrast microscopy (D and by ctotoxicty assay (E). Data is of n=12 spheroids from 4 separate experiments, error bars = SEM. P values were obtained one-way ANOVA compared to control: *** p < 0.001 and **** p < 0.0001; image scale bars = 100 µm.*

2.3.4. Initial assessment of spheroid structure by confocal microscopy and histology

To further examine spheroidal structure, HepG2/C3A spheroids formed with the optimised agarose LOT plates at day-7 were fixed using PFA and stained to observe the localisation of nuclei (Hoescht, blue, Figure 2.4A) and filamentous actin as a secondary structure

(Phalloidin, green, Figure 2.4B); spheroids were observed by confocal microscopy. Cell nuclei were evenly distributed throughout the HepG2/C3A spheroids, however sphericity was lost around the periphery of the membrane suggesting impairment to spheroid structure between removal from growth plate and embedding for imaging, compared to pre-fixed phase contrast images. Z- Stacked maximum intensity projection images of spheroids revealed filamentous actin expression between cell nuclei, suggesting hepatocyte polarisation, and showed the early signs of a network formation throughout the spheroid structure, in which individual green foci appeared interconnected at points throughout the images. H&E staining revealed poorly maintained spheroid structures (Figure 2.4D) with ill-defined morphology in non-fixed spheroids however this was improved when spheroids were fixed in PFA (Figure 2.4E). Where evident, H&E-stained nuclei were evenly distributed throughout the structures but spheroid membrane ruffling, and protrusions could be seen at the periphery with evidence of extracellular matrix deposition could be seen between compact cells throughout the HepG2/C3A spheroid. These observations were greatly improved in **Chapter 3, Figure 3** by the use of optimised techniques to ensure adequate fixation of spheroids, and permeabilisation steps to ensure optical clearance of molecular probes, thus aiding a greater penetration of light into the spheroid bodies and hence greater resolution of acquired spheroid images.

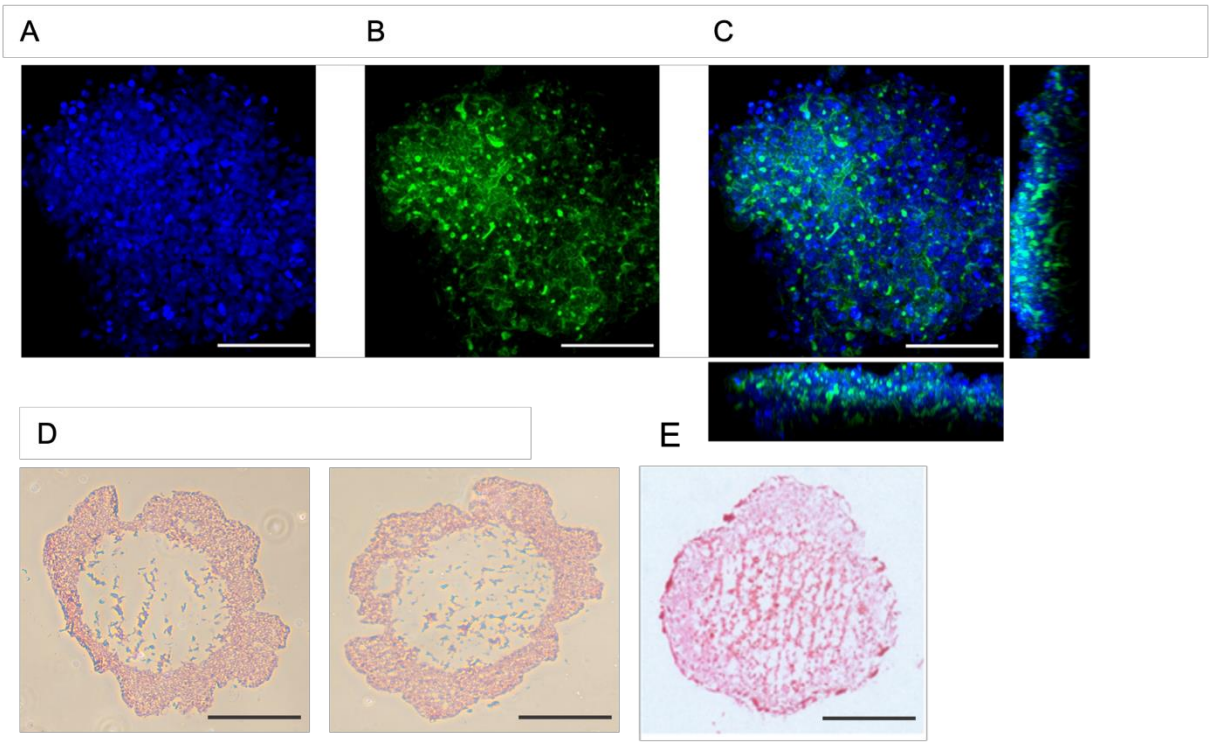

Figure 2.4. Spheroid structure examination by fluorescence microscopy and histology using non-optimised approaches . *HepG2/C3A spheroids were cultured for 7 days using the agarose LOT method and analysed by immunofluorescent imaging or cryo-sectioning to analyse internal structure. Spheroids were imaged using a Nikon A1R confocal microscope at 20X magnification Hoescht (blue, A) for nuclear staining and phalloidin (green, B) for filamentous actin. (C) Composite image of two channels as a maximum Z-stack projection along the x and y-axis. Scale bar is 100 μm. (D) Non-fixed spheroids sectioned using a cryostat microtome at 5 μm sections. (E) Spheroid that was pre-fixed with PFA prior to sectioning using cryostat microtome in order to maintain structure.*

2.3.5. Initial use of HepG2 C3A spheroids to study genotoxic response

A long-term aim of the thesis was to develop a 3D model that could be used for repeat dose genotoxicity studies which is introduced and discussed in **Chapter 5**. Presented here are initial experiments optimising the comet assay technique in 3D cultures of HepG2/C3A. The initial comet assay technique presented here used a standardised technique that had previously been implemented in our laboratory in basic cell culture models (2D cells) and had not been especially optimised for use with 3D cell culture models. However, a novel use

of an optimised comet assay technique is presented in **Chapter 3** for use in a higher-throughput scenario using the mini-gel approach, with optimised approaches to ensure minimal background damage is carried across into the subsequent datasets. There was more background DNA damage found in spheroids compared to 2D monolayers of cells (Figure 2.5B); median tail intensity was found to be 10.6 % in spheroids versus 0.09 % in 2D (Figure 2.5A). There was limited difference between DNA damage induced by 4-NQO in either model which was found to be 84.2 % in 2D monolayers compared to 73.8 % in spheroids however B[a]P was only found to show activity in the spheroids causing very limited DNA damage in the 2D monolayer cells with median % DNA damage of 0.139 in 2D cells but increased to 47.4 % in spheroids. There was some early evidence of hedgehog comets (Figure 2.5B) in the vehicle-treated spheroids suggesting an induction of apoptosis, by incurred by the disaggregation process whereas this was absent in monolayers.

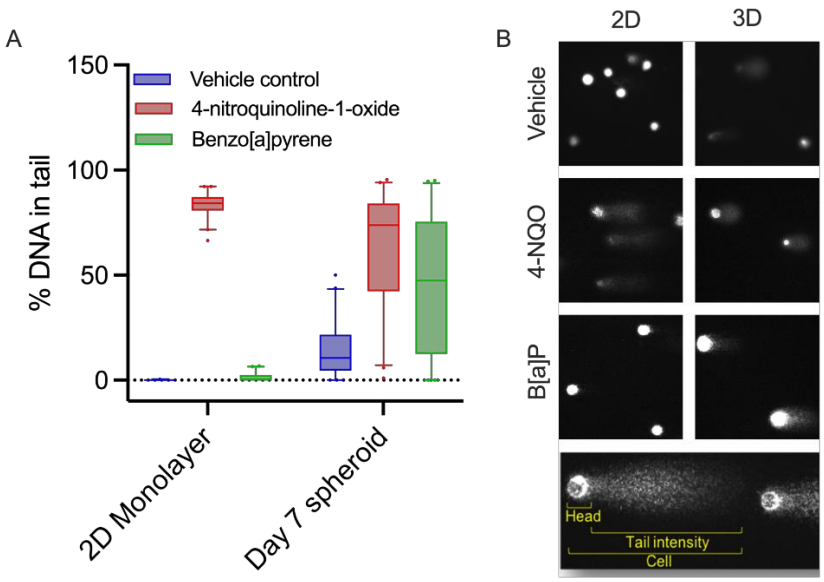

Figure 2.5. HepG2/C3A spheroids show sensitivity to genotoxic carcinogens in the Comet assay. *HepG2 C3A cells in 2D or 7-day old spheroids were exposed to a DMSO vehicle control (0.5 %, Left), the mutagen 4-nitroquinoline-1-oxide (centre) or the pro-mutagen benzo[a]pyrene (Right), for 24 h. The comet assay was used to analyse the % of DNA translocated from the nucleus of cells as an indicator of DNA damage. (A) Box plots show the*

median with whiskers presenting the 2.5 – 97.5 percentile. (B) exemplar images from comet assay. Data is from 200 blindly-scored comets across two duplicate slides per experiment (n=2) but not statistically compared due to limited independent biological replicates.

2.3.6. Screening of human hepatotoxic compounds against HepG2/C3A spheroid models

To compare the sensitivity of spheroid models to hepatotoxins, cell viability was measured using intracellular ATP content as an endpoint assay (**Figure** 2.6). In the first model, HepG2/C3A cells and 7-day old spheroids were treated with four hepatotoxic compounds titrated in DMSO (maximum 0.5 % DMSO), these were: acetaminophen diclofenac, trovafloxacin or cinchophen. For the spheroids, I implemented a 24 h incubation regime was at day 2 as originally proposed by Hendriks et al. (2016b) and Gaskell et al. (2016). For comparison, 2D monolayer cultures were given an acute dose (24 h) as is typical for these assay types, and in HepG2/C3A cells which over-proliferate and become over-confluent when cultured beyond 24 h, resulting in a loss of cellular viability. There was a dose-dependent reduction in cellular viability when HepG2/C3A spheroids were treated with acetaminophen and trovafloxacin, wherein 3D cultures were more sensitive to these compounds by comparison to 2D monolayers of cells. The IC_{50} value for acetaminophen in C3A spheroids was 4805 μM ± 716.2, and ≥ 10,000 μM in 2D monolayers (Figure 2.6A). Trovafloxacin only reduced cellular viability to approximately 21 % at ≥ 250 μM in C3A spheroids, whereas viability was only reduced to 75 % at ≥ 250 μM in 2D (Figure 2.6C). Diclofenac did not decrease cell viability in either model at the doses tested; however, spheroids appeared sensitised at the highest concentration (400 μM) in the spheroid model versus 2D monolayer of cells (Figure 2.6B). Cinchophen treatment did not successfully yield

an IC_{50} value however spheroids appeared sensitised at highest dose (1000 μM) versus 2D monolayer.

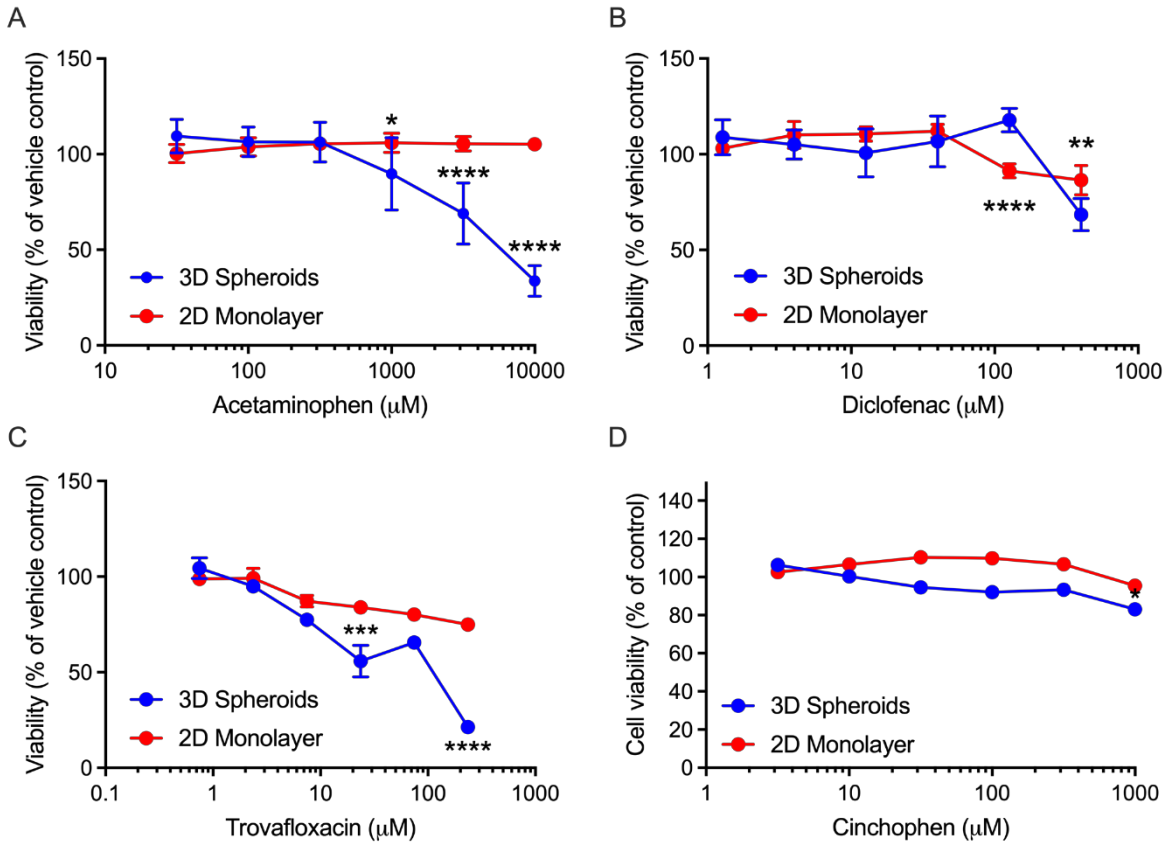

Figure 2.6. HepG2/C3A spheroids show increased sensitivity to selected hepatotoxins versus 2D monolayers of cells. *HepG2 C3A cells were seeded as monolayers or cultured as spheroids for 7-days; monolayers were treated acutely for 24 h or spheroids were subjected to a repeat-dosing regimen over 96 h. Models were treated with (A) acetaminophen; (B) diclofenac; (C)| trovafloxacin or (D) cinchophen. Data shown is cell viability expressed as a percentage of DMSO untreated control; values are the mean ±SEM (n=3, duplicates); * p < 0.05, ** p < 0.01, *** p < 0.001 and **** p < 0.0001.*

2.4. Discussion

The LOT agarose technique is easily implementable within most standard tissue culture laboratories and does not carry the economic burden associated with commercially sourced alternatives, for example, between 5 and 15 agarose-coated plates can be generated within the same costings as a single commercially sourced plate, depending on the provider. Despite the fact that one of the first reported uses of HepG2/C3A (Gaskell et al., 2016) and primary rat hepatocyte spheroids (Kyffin et al., 2019b) was in LOT microplates there are limited studies describing such approaches, in-full; in particular the contribution that the agarose-gel makes to the overall cell culture environment. It was therefore necessary to investigate and further optimise this technique for our own purposes, particularly as it forms the principal mechanism for generating the datasets throughout this thesis. Contrary to methods published for the development of a primary rat hepatocyte spheroid model (Kyffin et al., 2019a), hermitic sealing and refrigeration at 4 ^{o}C to hydrate and stabilise agarose hydrogels did nothing to promote the optimum formation of HepG2/C3A spheroids. Moreover, refrigeration of agarose gels typically resulted in gel deterioration and sub-optimal surfaces onto which cells typically adhered rather than forming floating aggregates. The preferred method generated here was far easier and quicker to implement and involved the use of a standard normal-gelling agarose that was dispensed into microwell plates and used on the same day to form homogenous HepG2/C3A spheroids within 5-days of initial seeding, in line with other studies (Dorst et al., 2014, Herzog et al., 2016).

One of the concerns of the model developed for these studies was that hydrogel poration would create a partition within the culture wells, allowing the cell-repellent agarose layers to

perform as a molecular sink to small molecules such as nutrients required for cell culture medium and to potential assayed chemicals, resulting in poor tissue culture conditions as well as potentially reducing exposure of spheroids to test compounds in future studies, an area that has not been fully addressed by the literature to date. By use of fluorescein as monitorable small molecule, and 4-NQO for the induction of cytotoxicity in spheroids, agarose gels do allow for the dynamic-flux of small molecules, as would be expected. Fluorescein and 4-NQO have molecular weights of 332.31 and 190.16 Da and LogP partition coefficient of 2.64 and 1.1, respectively, and hence represent physicochemical properties within the range of most small molecule chemicals used throughout this thesis. Interestingly, fluorescein was found in equilibrium in the transwell membrane experiment after 24 h under standard culture conditions, suggesting free movement of the molecule across the agarose and equal partition between both gel and aqueous compartments. The pore mesh size and gel stiffness of agarose are commensurate with the concentration of agarose in solution, with the predicted pore size of a 1.5 % agarose in the range of 200 – 800 nm (Narayanan et al., 2006). This of course easily allows to the free-flow of small molecule chemicals but may retard those of a larger size, i.e., proteins. Given that the agarose-gels and cell culture medium occupy a similar volume (~ 100 μL) this would therefore suggest that the initial starting concentration of any molecule in cell culture medium would in effect be halved - we do not believe this has been considered elsewhere and the same would be true when working with other hydrogels in similar applications, e.g., Matrigel approaches (Molina-Jimenez et al., 2012). Similarly, the gradual decline of spheroid health over 72 h suggests that 4-NQO can be gradually eluted from agarose-gels into cell culture medium, and presumably in reverse; this therefore highlights the importance of suspending agarose in

inert material such as cell culture medium. Such approaches may serve utility for the controlled delivery of such small molecules in cell culture experiments (Khodadadi Yazdi et al., 2020). Because of these factors, in all future chapters the concentration of small molecule used is reported as the initial concentration in the cell culture medium. Future studies should include where possible analytical confirmation of the actual test concentration in media throughout the experiment, but this was beyond the scope of this thesis.

By histological staining for connective tissue and fluorescent probing for actin structures, a complex of interconnected network of structures surrounding HepG2/C3A cells was observed. Gap-junction proteins and extracellular matrices are critical for the polarisation of hepatocytes in the liver. Indeed, similar observations have been identified in other hepatocytes models, including the expression of drug transporter proteins and bile canaliculi (Wang et al., 2015, Gaskell et al., 2016, Hendriks et al., 2016b, Ramaiahgari et al., 2017, Vorrink et al., 2017b, Baze et al., 2018). HepG2/C3A spheroid structures were poorly maintained. It appears that the spheroid structures may have been damaged during flash-freezing in liquid nitrogen or under the cryostat knife which rather than cutting through the structures, scored and thus stretched the spheroid (Dorst et al., 2014). In **Chapter 3** and **Chapter 5** it is demonstrated that this can be remedied by fixation in PFA to maintain the spheroid structure, however over-fixation of spheroids with PFA may not be appropriate in all cases; for example the induction of the gamma-H2AX DNA damage marker is known to be heavily cross-linked by PFA thus requiring extensively optimised parameters for its detection (Muslimovic et al., 2008) . By both confocal microscopy and sectioning, it is evident that

fixation and the careful transfer of spheroids is paramount to the maintenance of spheroid structure. Elsewhere, other authors have reported the use of a sucrose gradient to both maintain the spheroid volume and as a cryoprotectant (Bell et al., 2016b, Torizal et al., 2019). It is likely that the preferred method moving forward in subsequent chapters for the sectioning of HepG2/C3A spheroids would be by paraffin-embedding which has been shown to preserve spheroid structure during sectioning, and allow histological retrieval of antigens for further examination within the geometry of spheroid body (Vorrink et al., 2017a, Leite et al., 2016).

The potential utility of HepG2/C3A has been demonstrated in these proof-of-concept studies to recapitulate data published form the literature, we implemented day-7 spheroids into assays for the detection of genotoxicants and hepatotoxicants and assessed their sensitivity of detection. Genotoxicity screening was performed by use of the comet assay single-cell electrophoreses method (Perotti et al., 2015) by crudely disaggregating HepG2/C3A spheroids using trypsin-EDTA; prior to the submission of this thesis this was the first time this has been attempted in this HepG2/C3A 3D model and has revealed novel data that is further expanded in **Chapter 3**. Datasets collected from spheroids were more variable than 2D cultures most likely, this is due to the length of time required (minimum of 15 mins) to disaggregate HepG2/C3A spheroids into a single cell suspension using the enzyme trypsin-EDTA. Seemingly loss of viability associated with trypsin-EDTA was not assessed by (Stampar et al., 2019, Shah et al., 2018b) in a HepG2 spheroid model for genotoxicity; however other authors report the use of alternative dissociation reagents to promote cellular viability in disaggregated cells such as Accutase or TrypLE (Kim et al., 2015, Mandon et al., 2019, Wang

et al., 2019). Such approaches to spheroid disaggregation approaches could therefore ultimately enhance cellular recovery rate and viability, thus reducing background noise in the comet assay applied to spheroids as seen in **Chapter 3, Figure 3.9**. Data after 24 h exposure showed that spheroids exposed to B[a]P were more sensitive to DNA damage than monolayers of cells. B[a]P - a pro-mutagen, requires biotransformation principally via CYP1A1 and 1A2 isoforms to form the bioactive diol epoxide (BDPE), which intercalates covalently with DNA (Park et al., 2006). Shah et al. (2018a) report the successful use of B[a]P for inducing genotoxicity in a HepG2 spheroid model measured by micronucleus detection, within similar concentrations to those tested in our model, and also indicate the enhanced expression of CYP1A1 and 1A2 enzymes In contrast, there was limited difference between monolayers and spheroids treated with 4-NQO- a mutagen that binds directly to DNA, forming lesions not corrected by nucleotide excision repair pathways (Arima et al., 2006), as would be expected for this mutagen not requiring biotransformation. Indeed, one aspect not tested here was the effects of the genotoxicants in terms of general cytotoxicity to the models such as to avoid apoptosis-induce DNA damage acquired from cytotoxic mechanisms versus DNA damage response; it is likely that 50 μM 4-NQO for example, may subsequently be too high and a lower concentration required to differentiate between the two mechanisms (Arima et al., 2006). Further development and optimisation of our model for assessment of genotoxicity and cytotoxicity is presented in **Chapter 3**.

Four compounds with reported mechanism of action relating to hepatotoxicity is the generation of a reactive metabolite were also screened in HepG2/C3A spheroids. These were: acetaminophen, APAP (Davidson and Eastham, 1966, Hinson et al., 2010, McGill and

Jaeschke, 2013); diclofenac, DCF (Bort et al., 1999a, Bort et al., 1999b, Boelsterli, 2003); and trovafloxacin, TRV (Lucena et al., 2000, Beggs et al., 2014, Mitsugi et al., 2016). Cinchophen (CINCH) was a fourth compound reputed to be the first compound associated with drug-induced hepatotoxicity for which very little information exists in the literature (Lucena et al., 2000, Beggs et al., 2014, Mitsugi et al., 2016). In the presented HepG2/C3A model, only APAP and TRV had greater toxicity in spheroids versus a 2D monolayer but at significantly high concentrations (10 mM in the case of APAP). APAP cytotoxicity in hepatic spheroids could be due to enhanced expression of xenobiotic transforming enzymes in the 3D model, particularly CYP2E1 in the generation of the quinone-imine metabolite of APAP. However, in **Chapter 4 (Figure 4.1)** although overall transcriptional activation of drug metabolising genes in spheroids is observed, CYP2E1 is not transcriptionally enhanced.

Regarding drug induced hepatotoxicity, one of the key drivers for the induction of toxicity is typically associated with drug metabolism and metabolic activation. Several researchers in this area are now developing *in vitro* models that allow for repeat dosing strategies which we have also tried to address in **Chapter 5**, for low metabolic turnover compounds (Gu et al., 2018, Novik et al., 2017, Ramaiahgari et al., 2014, Holmgren et al., 2014). Importantly, the concentrations used here are within the reported maximum plasma concentration (Cmax) for these compounds, and hence are clinically relevant; however, this did not account for the potential of plasma protein-binding between the serum proteins within the cell culture medium which was maintained at 10 % throughout, for example Sison-Young et al. (2017) determined predictive hepatotoxicity in hepatic models by a ratio of IC50/Cmax > 20. Bell et al. (2016a), and Richert et al. (2016) implemented 4, and 28-day dosing regimens in primary

human hepatocyte spheroids, allowing them to successfully demonstrate drug metabolism and hepatotoxicity profiles seen *in vivo*.

Other researchers have also managed to yield datasets with increased sensitivity, though in repeat-dosed HepG2 and HepG2/C3A spheroids (Ramaiahgari et al., 2014, Gaskell et al., 2016), and PHHs (Hendriks et al., 2016a) but not achievable by (Fey and Wrzesinski, 2012) which only implemented acute dosing in a HepG2/C3A model but nevertheless demonstrated superior sensitivity of their 3D models by comparison to monolayers of the same cell type. Our data and observations are markedly like those presented but warrant further review as our model did not successfully identify all compounds tested as was expected; we expect this to be as a result of the dosing regimen, incubation time and age of spheroids used, for example, the induction of xenobiotic metabolism enzymes for metabolic transformation of compounds to reactive intermediate, e.g., NAPQI in the case of APAP (Zhang et al., 2020, Vinken and Hengstler, 2018) and glucuronide-conjugates (UGT2B7) in the case of DCF (Lazarska et al., 2018). Although the cytotoxicity of TRV was enhanced in spheroids it is likely that the lack of sensitivity could be because of there only being one cell-type present (hepatocyte-like cells).

Similarly, in **Chapter 3, Figure 3.5** the basal mRNA expression of selected UGT enzymes is increased basally in spheroids, and further induced by key small molecule substrates however this does not necessarily confirm their functional activity. Likewise evidence for enhanced expression of GSH-encoding genes is also not seen in HepG2/C3A thus detoxification of the APAP-NAPQI metabolite is unlikely to explain gene expression. Little is

known about cinchophen however given that it is a small molecule NSAID then hydroxylation followed by acyl - glucuronidation or glycine conjugation, would be expected for its metabolism, evidently not achieved in this model presented and would require empirical evaluation, as seen previously (Enlo-Scott et al., 2017).

2.5. Conclusion

The data presented in this chapter has shown the validity of the LOT technique for generation of 3D-cultures of HepG2/C3A cells and the superiority of this cell line to the parent HepG2 cell line. It has also begun to explore the utility our model as an *in* vitro system to study different modes of hepatotoxicity including genotoxicity. Subsequent chapters of the thesis further develop this culture model as a widely applicable tool for *in vitro* hepatoxicity studies. Results presented in **Chapter 3** describe its full utility for genotoxicity assessment and includes a targeted qPCR analysis of transcriptional changes related to drug metabolism and stress response (Coltman et al., 2021a). Results presented in **Chapter 4** describes optimised approaches to measure mitochondrial metabolism in single 3D spheroid models (Coltman et al., 2021b), and used to calculate metabolic differences between 2D and 3D HepG2/C3A cultures over time in **Chapter 5**. Finally, results presented in **Chapter 6** present data from an RNA sequencing experiment comparing in detail the dynamic changes in the global transcriptome of HepG2/C3A 3D cultures over time compared to 2D cell cultures (Coltman et al., 2021c [manuscript in preparation]).

2.6. References

Arima, Y., Nishigori, C., Takeuchi, T., Oka, S., Morimoto, K., Utani, A. and Miyachi, Y. (2006) '4-Nitroquinoline 1-Oxide Forms 8-Hydroxydeoxyguanosine in Human Fibroblasts through Reactive Oxygen Species', *Toxicological Sciences,* 91(2), pp. 382-392.

Baze, A., Parmentier, C., Hendriks, D. F. G., Hurrell, T., Heyd, B., Bachellier, P., Schuster, C., Ingelman-Sundberg, M. and Richert, L. (2018) 'Three-Dimensional Spheroid Primary Human Hepatocytes in Monoculture and Coculture with Nonparenchymal Cells', *Tissue Engineering Part C-Methods,* 24(9), pp. 534-545.

Beggs, K. M., Fullerton, A. M., Miyakawa, K., Ganey, P. E. and Roth, R. A. (2014) 'Molecular mechanisms of hepatocellular apoptosis induced by trovafloxacin-tumor necrosis factor-alpha interaction', *Toxicological sciences : an official journal of the Society of Toxicology,* 137(1), pp. 91-101.

Bell, C. C., Hendriks, D. F., Moro, S. M., Ellis, E., Walsh, J., Renblom, A., Fredriksson Puigvert, L., Dankers, A. C., Jacobs, F., Snoeys, J., Sison-Young, R. L., Jenkins, R. E., Nordling, A., Mkrtchian, S., Park, B. K., Kitteringham, N. R., Goldring, C. E., Lauschke, V. M. and Ingelman-Sundberg, M. (2016a) 'Characterization of primary human hepatocyte spheroids as a model system for drug-induced liver injury, liver function and disease', *Sci Rep,* 6, pp. 25187.

Bell, C. C., Hendriks, D. F. G., Moro, S. M. L., Ellis, E., Walsh, J. and Renblom, A. (2016b) 'Characterization of primary human hepatocyte spheroids as a model system for drug-induced liver injury, liver function and disease', *Sci Rep,* 6, pp. 25187.

Boelsterli, U. A. (2003) 'Diclofenac-induced liver injury: a paradigm of idiosyncratic drug toxicity', *Toxicol Appl Pharmacol,* 192(3), pp. 307-22.

Bort, R., Mace, K., Boobis, A., Gomez-Lechon, M. J., Pfeifer, A. and Castell, J. (1999a) 'Hepatic metabolism of diclofenac: role of human CYP in the minor oxidative pathways', *Biochem Pharmacol,* 58(5), pp. 787-96.

Bort, R., Ponsoda, X., Jover, R., Gomez-Lechon, M. J. and Castell, J. V. (1999b) 'Diclofenac toxicity to hepatocytes: a role for drug metabolism in cell toxicity', *J Pharmacol Exp Ther,* 288(1), pp. 65-72.

Chenyakin, Y., Ullmann, D. A., Evoy, E., Renbaum-Wolff, L., Kamal, S. and Bertram, A. K. (2017) 'Diffusion coefficients of organic molecules in sucrose–water solutions and comparison with Stokes–Einstein predictions', *Atmospheric Chemistry and Physics,* 17(3), pp. 2423-2435.

Coll, M., Perea, L., Boon, R., Leite, S. B., Vallverdu, J., Mannaerts, I., Smout, A., El Taghdouini, A., Blaya, D., Rodrigo-Torres, D., Graupera, I., Aguilar-Bravo, B., Chesne, C., Najimi, M., Sokal, E., Lozano, J. J., van Grunsven, L. A., Verfaillie, C. M. and Sancho-Bru, P. (2018) 'Generation of Hepatic Stellate Cells from Human Pluripotent Stem Cells Enables In Vitro Modeling of Liver Fibrosis', *Cell Stem Cell,* 23(1), pp. 101-113 e7.

Coltman, N. J., Coke, B. A., Chatzi, K., Shepherd, E. L., Lalor, P. F., Schulz-Utermoehl, T. and Hodges, N. J. (2021a) 'Application of HepG2/C3A liver spheroids as a model system for genotoxicity studies', *Toxicol Lett,* 345, pp. 34-45.

Coltman, N. J., Rochford, G., Hodges, N. J., Ali-Boucetta, H. and Barlow, J. P. (2021b) 'Optimised protocols to expore mitochondrial energy metabolism in spheorids using Agilent Seahorse Extracellular Flux Analysis', *Journal of Visualized Experiments,* n/a(e63346).

Costa, E. C., Gaspar, V. M., Coutinho, P. and Correia, I. J. (2014) 'Optimization of Liquid Overlay Technique to Formulate Heterogenic 3D Co-Cultures Models', *Biotechnology and Bioengineering,* 111(8), pp. 1672-1685.

Davidson, D. G. and Eastham, W. N. (1966) 'Acute liver necrosis following overdose of paracetamol', *Br Med J,* 2(5512), pp. 497-9.

Dorst, N., Oberringer, M., Grasser, U., Pohlemann, T. and Metzger, W. (2014) 'Analysis of cellular composition of co-culture spheroids', *Ann Anat,* 196(5), pp. 303-11.

Elliott, N. T. and Yuan, F. (2011) 'A review of three-dimensional in vitro tissue models for drug discovery and transport studies', *J Pharm Sci,* 100(1), pp. 59-74.

Enlo-Scott, Z., Evans, M., Coltman, N. J., Schroeder, N., Thomas, J., Keene, W. and Schulz-Utermoehl, T. (2017) *Assessment of the in vivo disposition of Cinchophen in rat and potential mechanisms of drug-induced liver injury*. DMDG Open Meeting 2017: Sygnature Disocvery Limited [Scientific Poster]. Available at: https://www.sygnaturediscovery.com/wp-content/uploads/2018/02/Invivo-Cinchophen-Poster-PRESS.pdf.

Fey, S. J., Korzeniowska, B. and Wrzesinski, K. (2020) 'Response to and recovery from treatment in human liver-mimetic clinostat spheroids: a model for assessing repeated-dose drug toxicity', *Toxicol Res (Camb),* 9(4), pp. 379-389.

Fey, S. J. and Wrzesinski, K. (2012) 'Determination of drug toxicity using 3D spheroids constructed from an immortal human hepatocyte cell line', *Toxicol Sci,* 127(2), pp. 403-11.

Gaskell, H., Sharma, P., Colley, H. E., Murdoch, C., Williams, D. P. and Webb, S. D. (2016) 'Characterization of a functional C3A liver spheroid model', *Toxicology research,* 5(4), pp. 1053-1065.

Gu, X., Albrecht, W., Edlund, K., Kappenberg, F., Rahnenfuhrer, J., Leist, M., Moritz, W., Godoy, P., Cadenas, C., Marchan, R., Brecklinghaus, T., Pardo, L. T., Castell, J. V., Gardner, I., Han, B., Hengstler, J. G. and Stoeber, R. (2018) 'Relevance of the incubation period in cytotoxicity testing with primary human hepatocytes', *Arch Toxicol,* 92(12), pp. 3505-3515.

Hendriks, D. F. G., Fredriksson Puigvert, L., Messner, S., Mortiz, W. and Ingelman-Sundberg, M. (2016a) 'Hepatic 3D spheroid models for the detection and study of compounds with cholestatic liability', *Sci Rep,* 6, pp. 35434.

Hendriks, D. F. G., Puigvert, L. F., Messner, S., Mortiz, W. and Ingelman-Sundberg, M. (2016b) 'Hepatic 3D spheroid models for the detection and study of compounds with cholestatic liability', *Scientific Reports,* 6.

Hinson, J. A., Roberts, D. W. and James, L. P. (2010) 'Mechanisms of acetaminophen-induced liver necrosis', *Handb Exp Pharmacol,* (196), pp. 369-405.

Holmgren, G., Sjogren, A. K., Barragan, I., Sabirsh, A., Sartipy, P., Synnergren, J., Bjorquist, P., Ingelman-Sundberg, M., Andersson, T. B. and Edsbagge, J. (2014) 'Long-term chronic toxicity testing using human pluripotent stem cell-derived hepatocytes', *Drug Metab Dispos,* 42(9), pp. 1401-6.

Hsu, H.-H., Kracht, J.-K., Harder, L. E., Rudnik, K., Lindner, G., Schimek, K., Marx, U. and Pörtner, R. (2018) 'A Method for Determination and Simulation of Permeability and Diffusion in a 3D Tissue Model in a Membrane Insert System for Multi-well Plates', *Journal of Visualized Experiments,* (132).

Khodadadi Yazdi, M., Taghizadeh, A., Taghizadeh, M., Stadler, F. J., Farokhi, M., Mottaghitalab, F., Zarrintaj, P., Ramsey, J. D., Seidi, F., Saeb, M. R. and Mozafari, M. (2020) 'Agarose-based biomaterials for advanced drug delivery', *J Control Release,* 326, pp. 523-543.

Kim, J. H., Jang, Y. J., An, S. Y., Son, J., Lee, J., Lee, G., Park, J. Y., Park, H. J., Hwang, D. Y., Kim, J. H. and Han, J. (2015) 'Enhanced Metabolizing Activity of Human ES Cell-Derived Hepatocytes Using a 3D Culture System with Repeated Exposures to Xenobiotics', *Toxicol Sci,* 147(1), pp. 190-206.

Kozyra, M., Johansson, I., Nordling, A., Ullah, S., Lauschke, V. M. and Ingelman-Sundberg, M. (2018) 'Human hepatic 3D spheroids as a model for steatosis and insulin resistance', *Sci Rep,* 8(1), pp. 14297.

Kyffin, J. A., Cox, C. R., Leedale, J., Colley, H. E., Murdoch, C., Mistry, P., Webb, S. D. and Sharma, P. (2019a) 'Preparation of Primary Rat Hepatocyte Spheroids Utilizing the Liquid-Overlay Technique', *Curr Protoc Toxicol,* 81(1), pp. e87.

Kyffin, J. A., Sharma, P., Leedale, J., Colley, H. E., Murdoch, C., Harding, A. L., Mistry, P. and Webb, S. D. (2019b) 'Characterisation of a functional rat hepatocyte spheroid model', *Toxicology in Vitro,* 55, pp. 160-172.

Langhans, S. A. (2018) 'Three-Dimensional in Vitro Cell Culture Models in Drug Discovery and Drug Repositioning', *Front Pharmacol,* 9, pp. 6.

Lazarska, K. E., Dekker, S. J., Vermeulen, N. P. E. and Commandeur, J. N. M. (2018) 'Effect of UGT2B7*2 and CYP2C8*4 polymorphisms on diclofenac metabolism', *Toxicol Lett,* 284, pp. 70-8.

Leite, S. B., Roosens, T., El Taghdouini, A., Mannaerts, I., Smout, A. J., Najimi, M., Sokal, E., Noor, F., Chesne, C. and van Grunsven, L. A. (2016) 'Novel human hepatic organoid model enables testing of drug-induced liver fibrosis in vitro', *Biomaterials,* 78, pp. 1-10.

Lucena, M. I., Andrade, R. J., Rodrigo, L., Salmeron, J., Alvarez, A., Lopez-Garrido, M. J., Camargo, R. and Alcantara, R. (2000) 'Trovafloxacin-induced acute hepatitis', *Clin Infect Dis,* 30(2), pp. 400-1.

Mandon, M., Huet, S., Dubreil, E., Fessard, V. and Le Hégarat, L. (2019) 'Three-dimensional HepaRG spheroids as a liver model to study human genotoxicity in vitro with the single cell gel electrophoresis assay', *Sci Rep,* 9, pp. 10548.

McGill, M. R. and Jaeschke, H. (2013) 'Metabolism and disposition of acetaminophen: recent advances in relation to hepatotoxicity and diagnosis', *Pharm Res,* 30(9), pp. 2174-87.

Mitsugi, R., Sumida, K., Fujie, Y., Tukey, R. H., Itoh, T. and Fujiwara, R. (2016) 'Acyl-glucuronide as a Possible Cause of Trovafloxacin-Induced Liver Toxicity: Induction of Chemokine (C-X-C Motif) Ligand 2 by Trovafloxacin Acyl-glucuronide', *Biological & pharmaceutical bulletin,* 39(10), pp. 1604-1610.

Molina-Jimenez, F., Benedicto, I., Dao Thi, V. L., Gondar, V., Lavillette, D., Marin, J. J., Briz, O., Moreno-Otero, R., Aldabe, R., Baumert, T. F., Cosset, F. L., Lopez-Cabrera, M. and Majano, P. L. (2012) 'Matrigel-embedded 3D culture of Huh-7 cells as a hepatocyte-like polarized system to study hepatitis C virus cycle', *Virology,* 425(1), pp. 31-9.

Morita, T., Narita, T., Mukai, S.-a., Yanagisawa, M. and Tokita, M. (2013) 'Phase behaviors of agarose gel', *AIP Advances,* 3(4).

Muslimovic, A., Ismail, I. H., Gao, Y. and Hammarsten, O. (2008) 'An optimized method for measurement of gamma-H2AX in blood mononuclear and cultured cells', *Nat Protoc,* 3(7), pp. 1187-93.

Mustafa, M. B., Tipton, D. L., Barkley, M. D., Russo, P. S. and Blum, F. D. (1993) 'Dye diffusion in isotropic and liquid-crystalline aqueous (hydroxypropyl)cellulose', *Macromolecules,* 26(2), pp. 370-378.

Narayanan, J., Xiong, J.-Y. and Liu, X.-Y. (2006) 'Determination of agarose gel pore size: Absorbance measurements vis a vis other techniques', *Journal of Physics: Conference Series,* 28, pp. 83-86.

Novik, E. I., Dwyer, J., Morelli, J. K., Parekh, A., Cho, C., Pludwinski, E., Shrirao, A., Freedman, R. M., MacDonald, J. S. and Jayyosi, Z. (2017) 'Long-enduring primary hepatocyte-based co-cultures improve prediction of hepatotoxicity', *Toxicol Appl Pharmacol,* 336, pp. 20-30.

Olive, P. L. and Durand, R. E. (2005) 'Heterogeneity in DNA damage using the comet assay', *Cytometry Part A,* 66a(1), pp. 1-8.

Park, S.-Y., Lee, S.-M., Ye, S.-K., Yoon, S.-H., Chung, M.-H. and Choi, J. (2006) 'Benzo[a]pyrene-induced DNA damage and p53 modulation in human hepatoma HepG2 cells for the identification of potential biomarkers for PAH monitoring and risk assessment', *Toxicology Letters,* 167(1), pp. 27-33.

Perotti, A., Rossi, V., Mutti, A. and Buschini, A. (2015) 'Methy-sens Comet assay and DNMTs transcriptional analysis as a combined approach in epigenotoxicology', *Biomarkers,* 20(1), pp. 64-70.

Ramaiahgari, S. C., den Braver, M. W., Herpers, B., Terpstra, V., Commandeur, J. N., van de Water, B. and Price, L. S. (2014) 'A 3D in vitro model of differentiated HepG2 cell spheroids with improved liver-like properties for repeated dose high-throughput toxicity studies', *Arch Toxicol,* 88(5), pp. 1083-95.

Ramaiahgari, S. C., Waidyanatha, S., Dixon, D., DeVito, M. J., Paules, R. S. and Ferguson, S. S. (2017) 'From the Cover: Three-Dimensional (3D) HepaRG Spheroid Model With Physiologically Relevant Xenobiotic Metabolism Competence and Hepatocyte Functionality for Liver Toxicity Screening', *Toxicological sciences : an official journal of the Society of Toxicology,* 159(1), pp. 124-136.

Richert, L., Baze, A., Parmentier, C., Gerets, H. H. J., Sison-Young, R., Dorau, M., Lovatt, C., Czich, A., Goldring, C., Park, B. K., Juhila, S., Foster, A. J. and Williams, D. P. (2016) 'Cytotoxicity evaluation using cryopreserved primary human hepatocytes in various culture formats', *Toxicol Lett,* 258, pp. 207-215.

Schindelin, J., Arganda-Carreras, I., Frise, E., Kaynig, V., Longair, M., Pietzsch, T., Preibisch, S., Rueden, C., Saalfeld, S., Schmid, B., Tinevez, J.-Y., White, D. J., Hartenstein, V., Eliceiri, K., Tomancak, P. and Cardona, A. (2012) 'Fiji: an open-source platform for biological-image analysis', *Nature Methods,* 9, pp. 676.

Shah, U.-K., Mallia, J. d. O., Singh, N., Chapman, K. E., Doak, S. H. and Jenkins, G. J. S. (2018a) 'A three-dimensional in vitro HepG2 cells liver spheroid model for genotoxicity studies', *Mutation Research/Genetic Toxicology and Environmental Mutagenesis,* 825, pp. 51-58.

Shah, U. K., Mallia, J. O., Singh, N., Chapman, K. E., Doak, S. H. and Jenkins, G. J. S. (2018b) 'Reprint of: A three-dimensional in vitro HepG2 cells liver spheroid model for genotoxicity studies', *Mutat Res Genet Toxicol Environ Mutagen,* 834, pp. 35-41.

Sison-Young, R. L., Lauschke, V. M., Johann, E., Alexandre, E., Antherieu, S., Aerts, H., Gerets, H. H. J., Labbe, G., Hoet, D., Dorau, M., Schofield, C. A., Lovatt, C. A., Holder, J. C., Stahl, S. H., Richert, L., Kitteringham, N. R., Jones, R. P., Elmasry, M., Weaver, R. J., Hewitt, P. G., Ingelman-Sundberg, M., Goldring, C. E. and Park, B. K. (2017) 'A multicenter assessment of single-cell models aligned to standard measures of cell health for prediction of acute hepatotoxicity', *Arch Toxicol,* 91(3), pp. 1385-1400.

Stampar, M., Tomc, J., Filipic, M. and Zegura, B. (2019) 'Development of in vitro 3D cell model from hepatocellular carcinoma (HepG2) cell line and its application for genotoxicity testing', *Arch Toxicol,* 93(11), pp. 3321-3333.

Torizal, F. G., Kimura, K., Horiguchi, I. and Sakai, Y. (2019) 'Size-dependent hepatic differentiation of human induced pluripotent stem cells spheroid in suspension culture', *Regen Ther,* 12, pp. 66-73.

Vinken, M. and Hengstler, J. G. (2018) 'Characterization of hepatocyte-based in vitro systems for reliable toxicity testing', *Arch Toxicol,* 92(10), pp. 2981-2986.

Vorrink, S. U., Ullah, S., Schmidt, S., Nandania, J., Velagapudi, V., Beck, O., Ingelman-Sundberg, M. and Lauschke, V. M. (2017a) 'Endogenous and xenobiotic metabolic stability of primary human hepatocytes in long-term 3D spheroid cultures revealed by a combination of targeted and untargeted metabolomics', *FASEB J,* 31(6), pp. 2696-2708.

Vorrink, S. U., Ullah, S., Schmidt, S. F., Nandania, J. T., Velagapudi, V., Beck, O., Ingelman-Sundberg, M. and Lauschke, V. M. (2017b) 'Endogenous and xenobiotic metabolic stability of primary human hepatocytes in long-term 3D spheroid cultures revealed by a combination of targeted and untargeted metabolomics', *Faseb Journal,* 31(6), pp. 2696-2708.

Wang, Z., Li, W., Jing, H., Ding, M., Fu, G., Yuan, T., Huang, W., Dai, M., Tang, D., Zeng, M., Chen, Y., Zhang, H., Zhu, X., Peng, Y., Li, Q., Yu, W. F., Yan, H. X. and Zhai, B. (2019) 'Generation of hepatic spheroids using human hepatocyte-derived liver progenitor-like cells for hepatotoxicity screening', *Theranostics,* 9(22), pp. 6690-6705.

Wang, Z., Luo, X., Anene-Nzelu, C., Yu, Y., Hong, X., Singh, N. H., Xia, L., Liu, S. and Yu, H. (2015) 'HepaRG culture in tethered spheroids as an in vitro three-dimensional model for drug safety screening', *Journal of Applied Toxicology,* 35(8), pp. 909-917.

Wrzesinski, K. and Fey, S. J. (2013) 'After trypsinisation, 3D spheroids of C3A hepatocytes need 18 days to re-establish similar levels of key physiological functions to those seen in the liver', *Toxicol. Res.,* 2(2), pp. 123-135.

Wrzesinski, K., Magnone, M. C., Hansen, L. V., Kruse, M. E., Bergauer, T., Bobadilla, M., Gubler, M., Mizrahi, J., Zhang, K., Andreasen, C. M., Joensen, K. E., Andersen, S. M., Olesen, J. B., Schaffalitzky de Muckadell, O. B. and Fey, S. J. (2013) 'HepG2/C3A 3D spheroids exhibit

stable physiological functionality for at least 24 days after recovering from trypsinisation', *Toxicology Research,* 2(3), pp. 163-172.

Zanoni, M., Piccinini, F., Arienti, C., Zamagni, A., Santi, S., Polico, R., Bevilacqua, A. and Tesei, A. (2016) '3D tumor spheroid models for in vitro therapeutic screening: a systematic approach to enhance the biological relevance of data obtained', *Sci Rep,* 6, pp. 19103.

Zhang, C., Zhang, Q., Li, J., Yu, L., Li, F., Li, W., Li, Y., Peng, H., Zhao, J., Carmichael, P. L., Wang, Y., Peng, S. and Guo, J. (2020) 'Integration of in vitro data from three dimensionally cultured HepaRG cells and physiologically based pharmacokinetic modeling for assessment of acetaminophen hepatotoxicity', *Regul Toxicol Pharmacol,* 114, pp. 104661.

Zhang, J. H., Chung, T. D. and Oldenburg, K. R. (1999) 'A Simple Statistical Parameter for Use in Evaluation and Validation of High Throughput Screening Assays', *J Biomol Screen,* 4(2), pp. 67-73.

Chapter 3. APPLICATION OF HEPG2/C3A LIVER SPHEROIDS AS A MODEL SYSTEM FOR GENOTOXICITY STUDIES

Declaration The data presented in this chapter has been published in Toxicology Letters (Coltman *et* al, 2021, DOI: 10.1016/j.toxlet.2021.04.004) and reproduced here *in verbatim* including supplementary documents.

An unpublished addendum to this chapter is appended as section 3.7 and contains datasets derived after the time of publication.

Author declarations

N.J.C conducted all experimental design, data collection and analyses described. B. A. Coke and K. Chatzi contributed to the development of methods described for the comet assay in this research. Throughout this research, N.J.C was supported by E.L. Shepherd, P.F. Lalor and N.J. Hodges.

Acknowledgements and funding sources

N.J.C was supported by a BBSRC MIBTP CASE studentship award (BB/M01116X/1, 1940003). This paper presents independent research supported by the NIHR Birmingham Biomedical Research Centre at the University Hospitals Birmingham NHS Foundation Trust and the University of Birmingham. The views expressed are those of the author(s) and not necessarily those of the NHS, the NIHR or the Department of Health and Social Care.

3.1. Abstract

HepG2 cells continue to be a valuable tool in early drug discovery and pharmaceutical development. In the current study we develop a 3D in vitro liver model, using HepG2/C3A cells that is predictive of human genotoxic exposure. HepG2/C3A cells cultured for 7-days in agarose-coated microplates formed spheroids which were uniform in shape and had well defined outer perimeters and no evidence of a hypoxic core. Quantitative real-time-PCR analysis showed statistically significant transcriptional upregulation of xenobiotic metabolising genes (*CYP1A1, CYP1A2, UG1A1, UGT1A3, UGT1A6, EPHX,NAT2*) and genes linked to liver function (*ALB, CAR*) in 3D cultures. In response to three model pro-genotoxicants: benzo[a]pyrene, amino-1-methyl-6-phenylimidazo[4,5-b]pyridine (PhIP) and 2-amino-anthracene (2-AA), we observed further transcriptional upregulation of xenobiotic metabolising genes (*CYP1A1, CYP1A2, NAT1/2, SULT1A2, UGT1A1, UGT1A3*) compared to untreated spheroids. Consistent with this, spheroids were more sensitive than 2D monolayers to compound induced single- and double-stranded DNA-damage as assessed by the comet assay and γ-H2AX phosphorylation respectively. In contrast, levels of DNA-damage induced by the direct acting mutagen 4-nitroquinoline N-oxide (4NQO) was the same in spheroids and monolayers. In support of the enhanced genotoxic response in spheroids we also observed transcriptional upregulation of genes relating to DNA-damage and cellular stress response (e.g., *GADD45A* and *CDKN1A*) in spheroids. In conclusion, HepG2/C3A 3D spheroids are a sensitive model for in vitro genotoxicity assessment with potential applications in early-stage drug development.

3.2. Introduction

HepG2 cells are a frequently used model for genotoxic assessment of chemicals (Guo et al., 2020, Mišík et al., 2019) and one of the first cell lines used in the comet assay and for studying mutagen-induction of micronuclei (Knasmüller et al., 1998). Primary human hepatocytes (PHHs) are used in toxicology studies (Vinken and Hengstler, 2018) because of their metabolic competency and normal hepatocyte phenotype (Hewitt et al., 2007, Fraczek et al., 2013, Vinken and Hengstler, 2018). Unlike HepG2 cells, PHHs lack proliferative capacity (Zhang et al., 2018) and rapidly dedifferentiate limiting their application for long term studies. Similarly, HepaRG cells are a proliferative hepatoma cell line that express phase I (Anthérieu et al., 2010) and phase II enzymes including uridine 5'-diphospho-glucuronosyltransferases (*UGTs*) and sulfotransferases (*SULT*s) (Aninat et al., 2006). HepaRG also express nuclear receptors such as the aryl hydrocarbon (*AhR*), constitutive androstane (*CAR*), pregnane X receptors (*PXR*) and drug transporter proteins (Aninat et al., 2006).

Despite the clear utility of PHH and HepaRG cells, the low cost of HepG2 cells makes them an attractive tool for the development of high throughput, physiologically relevant models of liver function. This is exemplified by the generation of transgenic HepG2 lines expressing drug metabolising genes for use in genetic toxicology (Hashizume et al., 2009, Hashizume et al., 2010) and hepatotoxicity studies (Xuan et al., 2016, Gómez-Lechón et al., 2017). Another approach to increase physiological relevance of hepatocyte models is the development of three-dimensional (3D) culture models. The use of advanced *in vitro* cell models including spheroids, microtissues, organoids and organ-on-a-chip technology, is becoming more widely adopted for investigating disease pathology, drug efficacy, safety and toxicity. Such

models are now being routinely used for a number of applications (Elliott and Yuan, 2011, Zanoni et al., 2016, Langhans, 2018) however, their potential for integration into genetic toxicology risk assessment requires further investigation (Pfuhler et al., 2020). Both PHHs and HepaRG cells have being used in genotoxicity studies (Seo et al., 2020, Mandon et al., 2019); however, their sensitivity and specificity compared to traditional hepatoma cell lines such as HepG2 is still been assessed (Guillouzo and Guguen-Guillouzo, 2008, Guo et al., 2020).

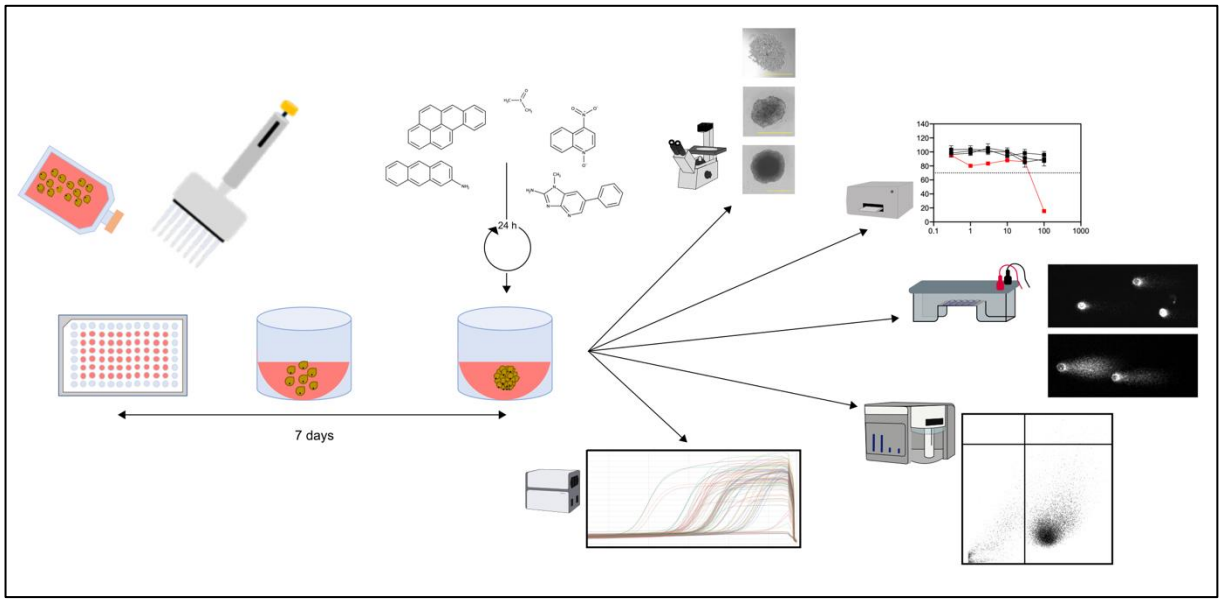

Figure 3.1. Graphical abstract for the utility of HepG2/C3A spheroids in genotoxicity studies

In the current study, we present the use of 3D-spheroids of the HepG2/C3A cell line, a clonal derivative of HepG2 with favoured phenotypic characteristics, as sensitive model system for use in genotoxicity studies. We demonstrate that, compared to 2D-monolayer cultures, HepG2/C3A 3D-spheroids are more sensitive to model genotoxic compounds requiring

metabolic activation. Consistent with this, expression levels of a panel of phase I and phase II drug metabolising genes were enhanced in spheroids compared to 2D-cultures. In conclusion, spheroid cultures of HepG2/C3A cells are a low cost and useful model for *in vitro* genotoxicity assessment and may serve a potential role in the pre-clinical and regulatory testing of novel chemical entities and pharmaceuticals.

3.3. Materials and methods

3.3.1. Chemicals and reagents

Dulbecco's Modified Eagles Medium (DMEM), foetal bovine serum (FBS), phosphate buffered saline (PBS), penicillin-streptomycin and TrypLExpress were purchased from Gibco (Paisley, Scotland, UK). Genotoxicants used in this study were purchased from Merck Life Sciences (Dorset, UK): Benzo[a]pyrene (B[a]P, CAS: 50-32-8), 2-Aminoanthracene (2-AA, 613-13-8) and 4-nitroquinoline *N*-oxide (4-NQO, CAS: 56-57-5) or Cayman Chemical Company Michigan, USA): Amino-1-methyl-6-phenylimidazo[4,5-b]pyridine (PhIP, CAS:105650-23-5). Normal melting point agarose (NMPA, #A9539), low melting point agarose (LMPA, #A9414), dimethylsulphoxide (DMSO) and Hoescht 33342 were also from Merck Life sciences. CellTiter-Glo luminescent cell viability assay was from Promega (Southampton, UK). SYBR Gold nucleic acid gel stain, Prolong gold antifade mountant, propidium iodide and goat anti-mouse FITC antibody were all purchase from Life Technologies (Warrington, UK). Phalloidin – 565 was from Biotium (CA, USA). Anti-gamma H2AX (phosphor s139) antibody was from Abcam (ab11174, Cambridge, UK). RNeasy Mini and RNAse-Free DNA kits were obtained from Qiagen (Manchester, UK) while High Capacity cDNA Reverse Transcription and

PowerUp SYBR Green Master mix kits were purchased from Applied Biosystems (Warrington, UK).

3.3.2. Cell culture

Hepatocellular carcinoma cells (HepG2/C3A) cells, a clonal derivative of HepG2, were sourced from the American Tissue Culture Collection (ATCC, #CRL-10741) and were cultured in DMEM containing low glucose (1g/L), L-glutamine (3.9 mM) and sodium-pyruvate (1 mM), supplemented with FBS (10 % v/v) and penicillin-streptomycin (100 Units/mL, 100 μg/mL). Cells were maintained at 37 ^{o}C, 5 % CO_2 and sub-cultured regularly to maintain viability to a maximum of 25 passages. Cells cultures were routinely screened for *Mycoplasma sp.* using the EZ-PCR Mycoplasma test Kit (Biological Industries, Beit Haemek, Israel).

Spheroids were propagated using cell-repellent microplates created using an agarose liquid overlay technique (LOT) adapted from Gaskell et al. (2016) . Cells were seeded into pre-warmed LOT plates at 1000 cells/well in complete cell culture medium with the outer wells filled with PBS as an evaporation barrier. Cells were left to settle at room temperature and then subjected to centrifugation at 300 g for 15 minutes to form loose aggregates. The loose aggregates were transferred to the incubator and left to form spheroids for a minimum of 3 days. For all biochemical experiments, spheroids were grown to an age of 7-days, a time point that we show produces well-formed spheroids without a hypoxic core before being exposed to test compounds for 24 hours before processing for downstream biochemical assays.

3.3.3. Spheroid growth monitoring and planimetry

Spheroids were monitored throughout the culture period using an Eclipse TS100 phase-contrast microscope (Nikon, Surrey, UK) equipped with a 4X objective, and photomicrographs captured using a digital camera head (Cannon, Uxbridge, UK). Planimetry was analysed using the FIJI open source image analysis software (Schindelin et al., 2012) and a dedicated plugin for obtaining size and circularity parameters (Ivanov et al., 2017). Growth was also determined by quantification of cell number, and viability using the trypan blue exclusion method. Spheroids were washed with PBS and disaggregated with TrypLE Express at 50 μL/spheroid for approximately 30 mins at 37 ^{o}C. Cells were resuspended by aspiration in complete DMEM and counted by haemocytometer.

3.3.4. Cell viability analysis

Monolayers or 7-day old spheroids were dosed with either a DMSO vehicle control (0.3 %), a Triton X-100 positive control (0.1 %) or model compounds and exposed for 24, 48 or 72 h. Culture medium was removed and replaced with an equal volume of the CellTiter-Glo viability reagent followed by incubation for 1 hour on an orbital shaker. Equal volumes of the developed reagent were transferred into white-walled microplates (Greiner Bio-One) and luminescence quantified using a Tecan F200 Infinite Pro multimode plate reader (Tecan, Männedorf, Switzerland). Data was subjected to the *Z'* prime statistic for analysis of assay robustness between positive and negative cytotoxicity controls (Zhang et al., 1999) and results expressed as percentage viability compared to vehicle control.

3.3.5. Comet assay

A mini-gel approach (six 20 μL mini gels in a 3 x 2 array) adapted from Shaposhnikov et al. (2010), Shaposhnikov and Collins (2017) was used by mounting cells dissociated from cultured monolayers or spheroids. One slide was prepared for each compound or vehicle treatment, 2 replicate gels per condition, and left to set for 5 minutes at 4 ^{o}C. Next, slides were incubated overnight at 4 ^{o}C in 2.5 M NaCl, 10 mM Na_2EDTA, 10 mM Tris-HCl, 1 % (v/v) Triton-X100 and 10 % DMSO. DNA unwinding was performed by electrophoretic migration at 4 ^{o}C (20 V cm^{-1}, 300 mA) for 20 minutes in 1 mM Na_2EDTA, 300 mM NaOH (pH > 10), in a black electrophoretic chamber. Slides were neutralised in 2 mL of 0.4 M Tris-HCl, fixed in 70 % (v/v) ethanol at -20 ^{o}C and dried at room temperature for a minimum of 4 h. DNA was stained with SYBR Gold (1:1000, v/v in dH_2O) and cells visualised at 20X magnification under an Axiovert 10 epifluorescence microscope (Carl Zeiss Ltd, Cambridge, UK), using 450-490 nm excitation and 515-560 nm emission filters. Images were acquired using a mounted digital camera head (Marlin, Allied Vision Technologies GMBH, Stadtroda, Germany) and slides scored blindly by counting a minimum of 100 cells across 2 experimental replicates using the Comet Assay IV imaging system (Instem, Stone, Staffordshire, UK). A minimum of 300 comets were scored per treatment across a minimum of 4 independent experiments. Median percentage DNA in tail was chosen as the measure parameter of DNA damage as it exhibits less inter-assay variability (Olive and Durand, 2005).

3.3.6. Detection of γ-H2Ax foci by flow cytometry

Single cell suspensions were prepared at approximately 450,000 cells/mL by enzymatic dissociation of cell monolayers or spheroids, as previously described, pelleted at 120 g for 5

min and fixed in ice-cold ethanol (70 %) overnight at 4 ^{o}C. Fixed cells were centrifuged and permeabilised in 0.25 % Triton X-100 in PBS (w/v) for 5 min before blocking in 2 % bovine serum albumin in PBS (w/v) for 30 min at RT. The blocking solution was removed by centrifugation and the cells exposed to the primary anti-gamma H2AX antibody in blocking solution (1:500, v/v) for 1 h at RT and the cells washed before resuspension in the goat anti-mouse FITC antibody (1:200, v/v) for 1 h in the dark at RT. After removal and washing, cells were counterstained with propidium iodide solution in PBS (10μg/mL) supplemented with RNase (50 μg/mL). The Attune NxT flow cytometer (Life Technologies, Carlsbad, CA, USA) was used to detect fluorescent foci formation of γH2AX-FITC positive cells in the FL-1 channel (EX_{488} – $EM_{530/30}$ nm) and propidium iodide-positive cells in the FL-2 channel (EX_{561} – $EM_{620/15}$ nm). Flow cytometric analysis was performed using FlowJo Software, version 10.6.2 for Mac (Ashland, Oregan, USA). Initial gating was performed on fluorescent controls (Primary only, secondary only or no staining control) to define double negative fractions. Within the double negative fraction of cells, both debris and non-debris was gated by comparison of forward (FSC) and Side Scatter (SSC) events and doublet discrimination performed by comparison of Width and Height within those groups. Finally, classification of cell populations was made within the non-debris cluster using gating to first define PI+VE cells (FSC vs PI) and a second gated population to define γH2AX-FITC positive cells and the geometric mean statistic recorded for each experimental comparison within the assay.

3.3.7. Isolation of cellular RNA and cDNA synthesis

Cellular RNA extraction (60 pooled spheroids or 450, 000 cells) was performed using the RNeasy Mini Kit according to manufacturer's instructions, suspended in RNase-free water and stored at – 80 ^{o}C for further use. RNA purity and concentration were determined using a NanoDrop™ 8000 Spectrophotometer (Thermo Scientific). Total extracted RNA (500 ng) was reverse transcribed using the High-Capacity cDNA Reverse Transcription kit, including an RNase inhibitor according to the manufacturer's instructions. A no-enzyme and no-template control was also prepared.

3.3.8. Gene expression profiling

Gene expression analysis was performed by quantitative real-time PCR (qRT-PCR) with primers designed using the opensource Primer-BLAST tool (Ye et al., 2012). Primers were obtained from Merck Life Sciences (Table 3.1. Primer sequences for gene expression analysis by qPCR. qPCR was performed on a Roche Lightcycler RT-PCR instrument (Roche Diagnostics Gmbh, Mannheim, Germany) using PowerUp SYBR Green PCR master mix. Primer efficiency was determined by preparing serial dilutions of control template DNA and the Pfaffl method (Pfaffl, 2001) was used for calculation of relative quantification, normalised to the geometric mean of *18S RNA*, *ACTB* and *GAPDH* internal control reference genes.

3.3.9. Spheroid histology

Seven-day old spheroids were washed three times in PBS and fixed in 4 % buffered paraformaldehyde at 4 ^{o}C overnight. Next, spheroids were embedded using an agarose array mould-maker as described by Ivanov and Grabowska (2017). Embedded spheroids were

loaded into histological cassettes, suspended in formalin and subjected to automated tissue processing (Intelsint Srl, Turnin, Italy). Paraffin blocks containing the arrays, were sectioned a 5 μm and transferred onto poly lysine-coated slides. Slides were stained with freshly made Haematoxylin, Eosin or Van Gieson's staining solutions (Pfm medical, Poynton, UK) and brightfield images acquired.

3.3.10. Immunohistochemical analysis

For immunofluorescence imaging, fixed spheroids were washed in PBS and permeabilised overnight at 4 ^{o}C in PBS containing Tween 20 (0.5 %, v/v) and Triton X-100 (0.2 %, v/v). Spheroids were incubated for 2 h at 4 ^{o}C in permeabilization buffer supplemented with 3 % bovine serum albumin (BSA, w/v). Fluorescence microscopy was used for the immunohistochemical detection of nuclear DNA (Hoescht 33342, 1:5000, v/v), filamentous actin (Phalloidin-565, 1:500, v/v). Spheroids were mounted onto glass slides using Prolong Gold antifade mountant and imaged using a confocal microscope (Nikon A1R). A series of images were acquired across the Z-plane of the spheroid and processed using the opensource image processing software, FIJI-Image J.

3.3.11. Statistical analyses

Statistical analysis was conducted using GraphPad Prism version 8.00, (GraphPad Software, La Jolla, California, USA). Two-way ANOVA with Sidak's correction for multiple comparisons was used to compare HepG2/C3A spheroids to monolayer controls. For quantitative PCR analysis, raw *P* values were acquired from comparisons between control and treatment groups by Student's t-test and corrected for multiple testing using the Benjamini-Hochberg

correction. Pearson correlation coefficient analyses and heatmaps were prepared using the open source statistical analysis software, R (R Core Team, 2019) using the Tidyverse (Wickham et al., 2019) collection of packages. All data is represented as mean $\pm$ standard error unless stated otherwise.

Table 3.1. Primer sequences for gene expression analysis by qPCR.

Gene	Gene name	Forward primer	Reverse primer
18S	18S RNA	GTAACCCGTTGAACCCCATT	CCATCCAATCGGTAGTAGCG
ACTB	b - actin	ACTCTTCCAGCCTTCCTTCC	GTTGGCGTACAGGTCTTTGC
AHR	aryl hydrocarbon receptor	ATCCATACCGAAGACCGAGC	GACCAGTGGCTTCTTCAATTCC
ALB	albumin	AAAGCATGGGCAGTAGCTCG	GCATTCCGTGTGGACTTTGG
ARNT	aryl hydrocarbon receptor nuclear translocator	CTACTGCCAACCCCGAAATG	CCGCTTAATAGCCCTCTGGA
BRACA2	breast cancer type 2 susceptibility gene	GTTTCCACACCTGTCTCAGC	GGTGGAGGTAAAGGCAGTCT
BSEP	bile salt export pump	TGAGTAAGATTCAGCATGGGC	AAGAGCTTGATTTCCCTGGC
CAR	constitutive androstane receptor	CACAAAACTTCCTCTGCGGG	GTAACTCCAGGTCGGTCAGG
CASP3	caspase 3	GCCTCTTCCCCCATTCTCAT	CTTCCATGTATGATCTTTGGTTCC
CDK2	cyclin dependant kinase 2	CATCTTTGCTGAGATGGTGACT	ACTTGGCTTGTAATCAGGCAT
CDK7	cyclin dependant kinase 7	CTCGGGCAAAGCGTTATGAG	CTCTGGCCTTGTAAACGGTG
CDKN1A	cyclin-dependent kinase inhibitor 1	GCCGAAGTCAGTTCCTTGTG	CATGGGTTCTGACGGACATC
CPS1	carbamoyl phosphate synthetase I	CGCAAGGAGCCATTGTTTGG	TGATTCTGCCCTCTGTTGGC
CYP1A1	cytochromes P450 1A1	CGACACTCTTCCTTCGTCCC	ACCCATAGCTTCTGGTCATGG
CYP1A2	cytochromes P450 1A2	GAGGTTCCTGTGGTTCCTGC	GACTGTGTCAAATCCTGCTCC
E2F1	E2F transcription factor 1	CTTCGTAGCATTGCAGACCC	TATGGTGGCAGAGTCAGTGG
EPHX	epoxide hydrolase	GTTTCGGGAGGTTTCTTGGC	ATTCAGAGCAGAGCCTACGG
ERCC4	excision repair cross-complementing rodent repair deficiency, complementation 4	GGCCAAGGTTCCATGTAGCA	TCAAGCGATGGGTTATGGCA
GADD45A	growth Arrest and DNA Damage Inducible Alpha	CACTGTCGGGGTGTACGAAG	CCTGGATCAGGGTGAAGTGG
GAPDH	glyceraldehyde 3-phosphate dehydrogenase	CACTAGGCGCTCACTGTTCT	GCCCAATACGAC CAAATCCGT
GSTM1	glutathione s-transferase mu-1	TGGACTTTCCCAATCTGCCC	ATCTTCTCCTCTTCTGTCTCCC
HIF1A	hypoxia inducing factor 1	GACAAGCCACCTGAGGAGAG	ACGCGGAGAAGAGAAGGAAA
HUS1	checkpoint protein HUS1	GACTTGGTGTAGTAGCCAGAA	CGGGGTGAACACACTGAAAT
MDM2	mouse double minute 2 homolog	CGAGCTTGGCTGCTTCTG	GTACGCACTAATCCGGGGAG
MGST1	microsomal glutathione s-transferase -1	TAGAACGTGTACGCAGAGCC	GTGGTAGATCCGTGCTCCG
MKI67	antigen KI67	ACTCCAAAGAAGCCTGTGGG	AGTTGTTGAGCACTCTGTAGGG
MRP2	multidrug resistance-associated protein 2	AGCCATAGAGCTGGCCC	AACCAGGAGCCATGTGCC
NAT1	N-acetyltransferase 1	AATACAGCACTGGCATGATTCAC	GGAAGATACAAGGCACCTGAGG
NAT2	N-acetyltransferase 2	GGCCAAAGGGATCATGGACA	CTTCTCAAAGGGAACAGCCCG
NFKB1	nuclear factor kappa B	CTTAGGAGGGAGAGCCCAC	CTTCTGCCATTCTGAAGCCG
NQO1	NAD(P)H dehydrogenase [quinone] 1	GGACTGCACCAGAGCCAT	TCCTTTCTTCTTCAAAGCCG
NRF2	nuclear factor erythroid 2-related factor 2	ACCAAAACCACCCTGAAAGC	AGGCCAAGTAGTGTGTCTCC
PXR	pregnane X receptor	ACTTCAGTGGGAATCTCGGC	CCTCTTGGACTGCTTGGTGG
RBBP8	retinoblastoma-binding protein 8	CTCAGAAAGTGCTCGCTTCC	TCTGCAGAGTTAGGGCTTCC
SERTAD1	SERTA domain-containing protein 1	GCCGTTTCCTGATTGGTTGT	AGACCCTTGCTCAGCATCTT
SULT1A1	sulfotransferase 1A1	AAGGTGGTCTATGTTGCCCG	GATCCGTAGGACACTTCTCCG
SULT1A2	sulfotransferase 1A2	CAAAGGATGTGGCGGTTTCC	CCCATAGGACACTTCTCCAGC
TP53	tumour protein 53	GTGACACGCTTCCCTGGATT	ACAGTCAGAGCCAACCTCAG
TP63	tumour protein 63	GCTTATCAACCCTCAGCAGC	ACAATGCTGCAATCTGTGGG
TP73	tumour protein 73	GACGGAATTCACCACCATCC	CCTCATCAGCTTTTCGGTCG
UGT1A1	UDP -glucuronosyltransferase 1A1	CAAAACGATCTGCTTGGTCAC	TCCAGCTCCCTTAGTCTCCA
UGT1A3	UDP -glucuronosyltransferase 1A3	ACCCGACCATCGAATCTTGC	GCATGGGTGATAAAGGCACG
UGT1A6	UDP -glucuronosyltransferase 1A6	ACTTGTCTCAGGAATTTGAAGCC	AGATTCGATGGTCGGGTTCC

3.4. Results

3.4.1. Formation and characterisation of spheroids

Cells were seeded at 250 – 2000 cells per well and monitored for 28 days (Figure 3.2). Cells formed a loose aggregate at day 0, which condensed over the subsequent 3 days developing to spheroids of uniform shape after 5 days. Cells seeded at 1000 cells/well, formed spheroids with a diameter and surface area (Figure 3.3) that increased over the culture period. The diameter of spheroids was found to increase from 260 μm ± 5.4 (day 3) to 556 μm ± 9.5 (day 10). Cell number strongly correlated with surface area (Figure 3.3) increasing up to around 14 days and reaching a plateau for the rest of the culture period. The maximum number of cells was reached at approximately 21– 25 days at which point cell number plateaued indicating a halt in cellular proliferation; cellular doubling times were approximately every 48 h up to 7 days of culture, extending to greater than 100 hours after 21 days. Cell viability was maintained above 90 % throughout the cultivation period. Using this data, we chose to culture spheroids seeded at 1000 cells/well for 7 days before beginning exposure experiments where it was found this time point yielded spheroids that remained uniform in structure across a 96-microwell plate (Figure 3.3) and were of a size that allowed ease of handling in downstream experiments.

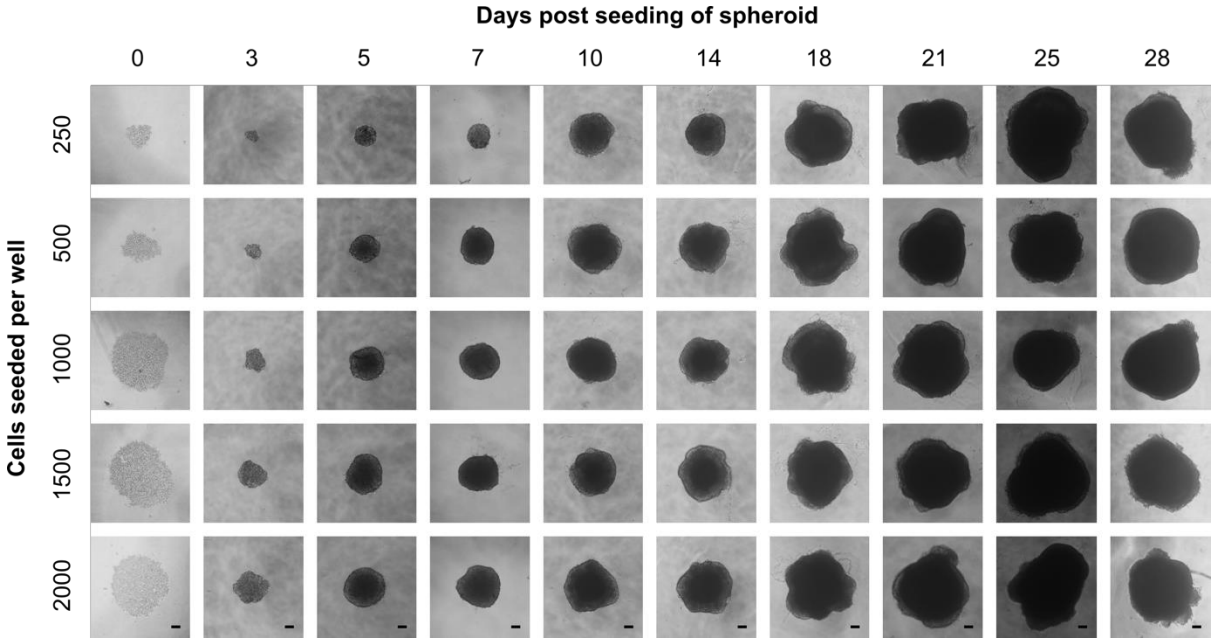

Figure 3.2. HepG2/C3A spheroid formation and planimetry is influenced by initial seeding density and culture period. *HepG2/C3A cells were seeded into agarose-coated 96 well plates at 250, 500, 1000, 1500 and 2000 cells/well and left to form spheroids (3D). Phase-contrast photomicrographs were acquired at random of spheroids from point of seeding to 28 days. Scale bar = 100 µm.*

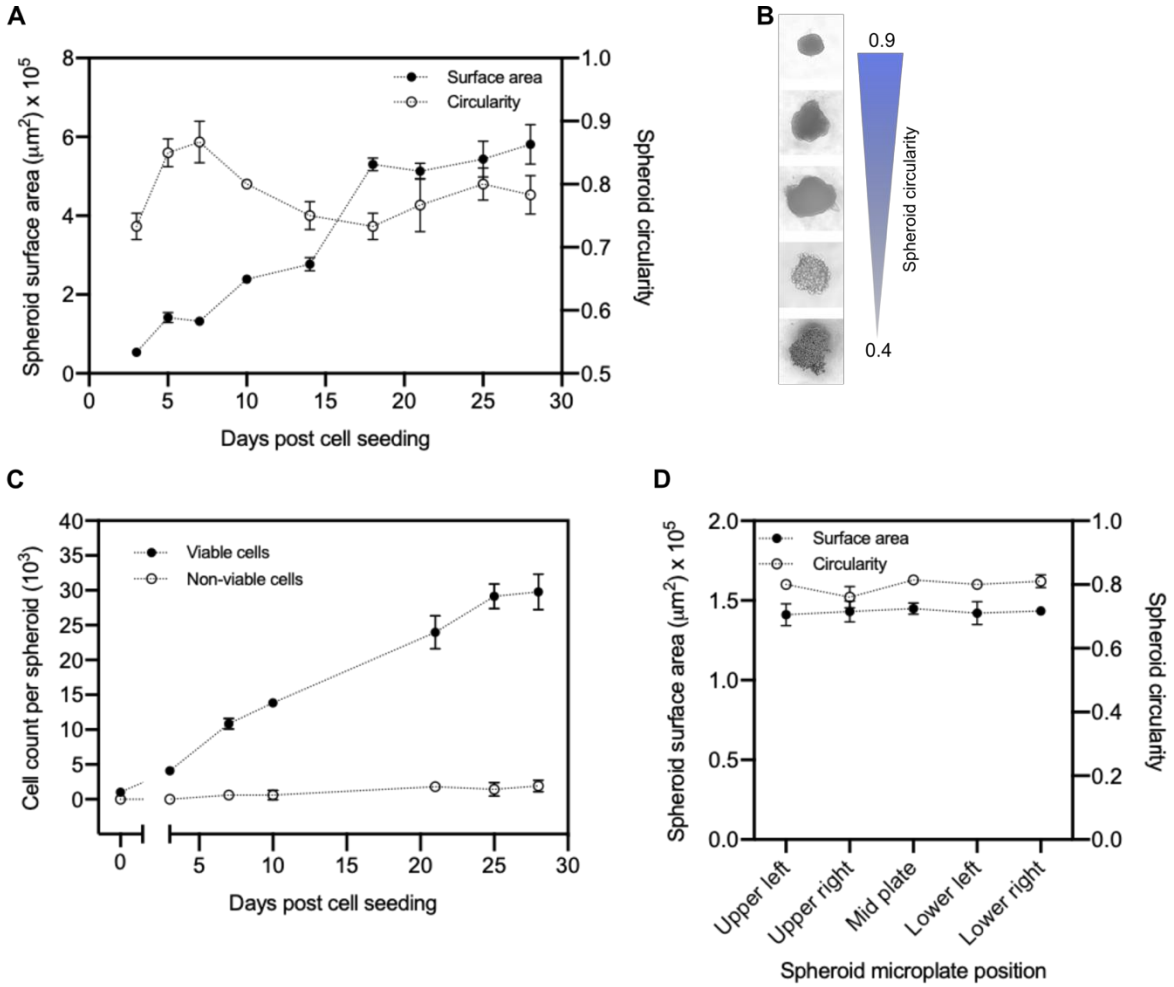

Figure 3.3. HepG2/C3A cells seeded at 1000 cells/per well remain as viable spheroids for up to 28 days post seeding. *Spheroid growth (surface area) and circularity were recorded over time (days) (A), spheroid circularity scoring guide (B), spheroid viability was determined by the trypan-blue exclusion assay (C), spheroids grown for 7 days plates were monitored for their size and circularity in agarose-coated microwell plates (D). Data represented as mean ± standard error (minimum n=3 with replicates).*

3.4.2. Internal structure of HepG2/C3A spheroids

To assess internal structure and morphology, 7-day old spheroids were analysed by immunofluorescence microscopy and histology, revealing cell nuclei that were evenly distributed throughout the HepG2/C3A spheroid structure (Figure **3.4**A). Z-plane projection photomicrographs demonstrated filamentous actin expression between cell nuclei in which filaments appeared interconnected at points throughout the images. Paraffin-embedded sections of HepG2/C3A spheroids stained with either H&E or Van Gieson's solution for visualisation of connective tissues and extracellular matrices, revealed spheroidal structures with well-defined morphology (Figure **3.4**B). HepG2/C3A spheroids had clearly defined outer perimeters. H&E-stained nuclei were evenly distributed throughout the structures with no evidence of either apoptosis (condensed nuclei) or necrosis (cloudy cytoplasm or membrane damage).

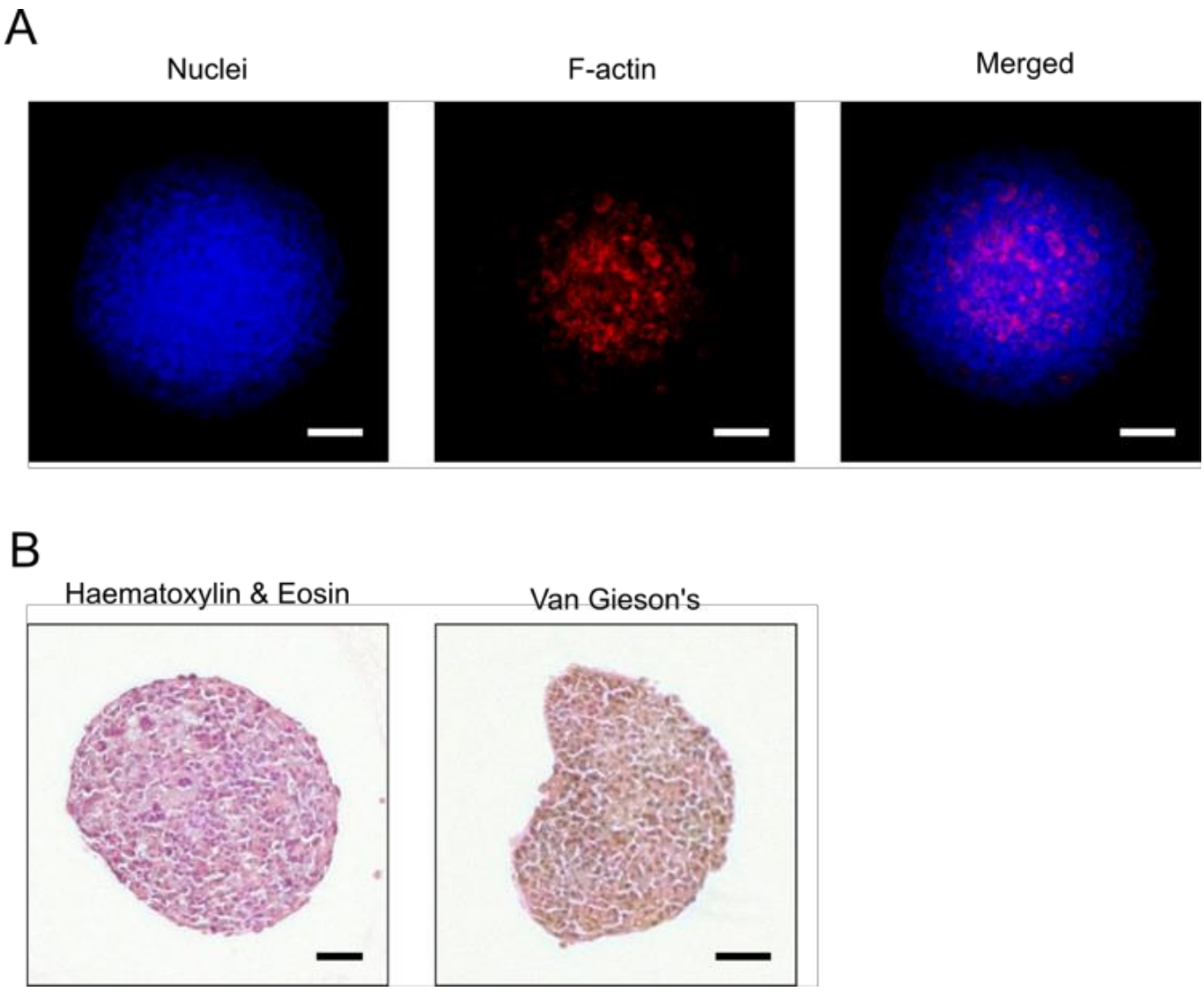

Figure 3.4. HepG2/C3A cells cultured in liquid-overlay plates over 7-days form spheroids with intact structure and maintained morphology throughout spheroid volume*. (A) HepG2/C3A spheroids were subjected to immunofluorescent staining with phalloidin for filamentous actin and counterstained with Hoescht 33358 for cell nuclei. (B) Histological examination of spheroids stained with H&E (cytoplasmic and nuclei) and Van Gieson's (connective tissue). Scale bars = 100 μm.*

3.4.3. Basal mRNA expression of genes relating to xenobiotic metabolism and liver function

Compared to 2D cultures, HepG2/C3A spheroids grown for 7-days showed transcriptional upregulation of genes considered markers of liver function *in vivo* (Figure 3.5). Specifically, albumin (*ALB*) was significantly upregulated by 3-fold compared to 2D monolayer cultures,

and carbamoyl phosphate synthetase 1 (*CPS1*), an enzyme forming the first critical step of the urea cycle which was upregulated by more than 2.4-fold.

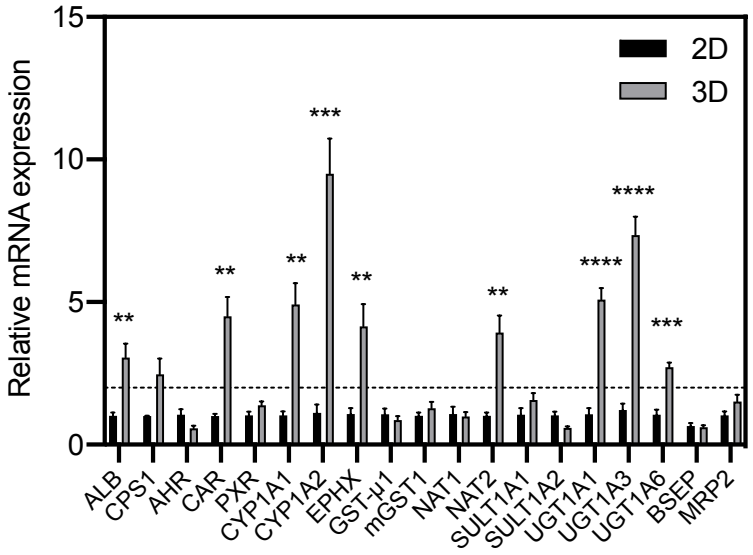

Figure 3.5. Basal mRNA expression of selected genes related to liver function and hepatic xenobiotic metabolism between HepG2/C3A cells cultured in monolayers (2D) or spheroids (3D). *Upregulated and downregulated genes were determined by a ≥1.5-fold increase or ≤ 0.5-fold decrease in mRNA expression, respectively. Data shown as mean of 4 independent samples (n=4). Statistical significance determined by student's t test (P < 0.05) with Benjamini-Hochberg correction for multiple testing:* ** p < 0.01 ***, p < 0.001 and **** p < 0.0001.

Furthermore, albumin synthesis continued to be upregulated in spheroids for up to 28 days in culture (Figure 3.6). The nuclear receptor, *CAR,* was upregulated 4-fold in spheroids but there was no upregulation of either *AHR* or *PXR* nuclear receptors. Genes encoding phase I enzymes *CYP1A1* and *EPHX* were upregulated by more than 4-fold whilst *CYP1A2* was upregulated by more than 9.5-fold. Expression of phase II conjugative enzymes *UGT1A1*, *1A3* and *1A6* were all greater in spheroids at 5, 7.3 and 2.7-fold increase compared to monolayers, whist *NAT2* was also upregulated by 3.9-fold. In contrast, there was no

upregulation of expression of *NAT1*, *SULT1A1*, *SULT1A2*, *GSTm1* or *GSTμ1* in spheroids compared to 2D-cultures.

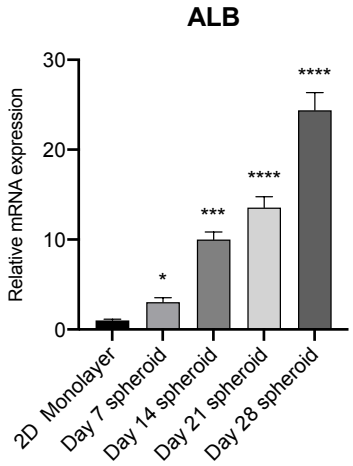

Figure 3.6. mRNA expression of albumin in HepG2/C3A spheroid models over time. *HepG2/C3A cells were cultured in monolayers (2D) or spheroids (3D) for 7 – 28 days and targeted for mRNA expression of albumin (ALB) by use of qPCR. Data shown as mean of 4 independent samples (n=4). Statistical significance denoted as: ****, P<0.0001; ***, P<0.001; *, P<0.05.*

3.4.4. Effects of exposure to genotoxic agents on cellular viability

Quantification of intracellular ATP-levels showed that the direct acting mutagen (4-NQO) induced cytotoxicity in a concentration-dependent manner and was equipotent in monolayer and spheroid cultures where viability was reduced to approximately 70 % at 30 µM and further reduced to 13 and 16 %, respectively at 100 µM (Figure 3.7A). For the three pro-genotoxicants tested (B[a]P, PhIP and 2-AA), concentrations between 0.3 and 100 µM did not reduce viability to below that of the vehicle control in either spheroid or monolayer

cultures over 24 h (Figure 3.7B – D). As assessed by phase contrast microscopy, spheroids exposed to B[a]P, PhIP and 2-AA maintained their morphology after 24 h exposure to model compounds at all three concentrations investigated when compared to control, with minimal shrinkage or disruption to the outer periphery of spheroid structure (Figure 3.8). In contrast and in agreement with ATP measurements, in spheroids exposed to 30 μM 4-NQO, there was evidence of morphological change such as ruffling to the outer spheroid edges. Based on this cytotoxicity data, non-toxic concentrations of 3, 10 and 30 μM were selected to assess compound-induced genotoxicity.

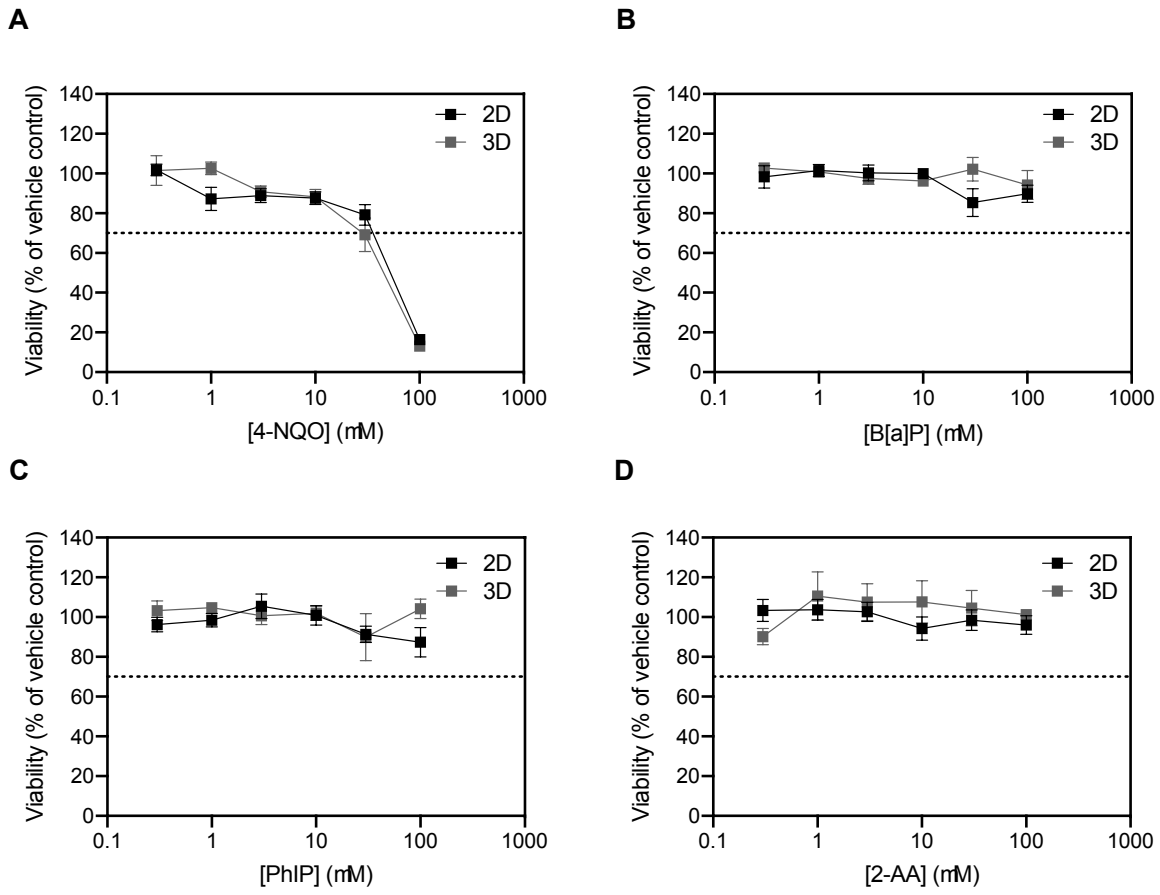

Figure 3.7. Viability assessment of HepG2/C3A models exposure to genotoxicants. *HepG2/C3A cells as monolayers (2D) and spheroids (3D) were exposed over 24 h to 4-NQO (A), B[a]P (B), PhiP (C) or 2-AA (D) titrated in DMSO. Viability was determined by luminescent ATP assay by comparing treated models to DMSO vehicle control. Dotted line represents 70 % viability threshold, data presented as the mean ± standard error (n=4, in duplicate) and compared by two-way ANOVA with Sidak's correction for multiple comparisons (P < 0.05).*

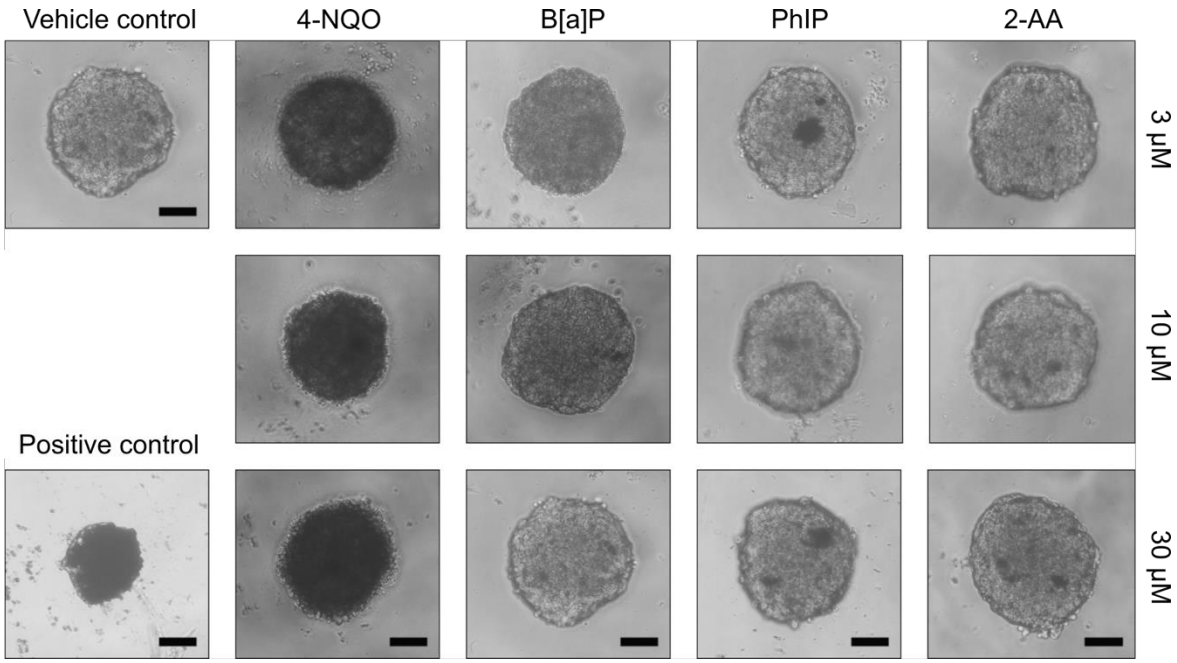

Figure 3.8. Maintenance of three-dimensional structure in exposed spheroids. *Phase-contrast photomicrographs with 7-day old spheroids exposed to control agents or genotoxic chemicals at titrated concentrations over 24 h. Scale bar = 100 µm.*

3.4.5. Induction of single stranded DNA breaks is enhanced in treated spheroid cultures compared to 2D monolayers

In both the 2D and 3D untreated control samples no statistically significant differences were found in the levels of single strand breaks between 2D (4.8 $\pm$ 1.5 %) and 3D (5.5 $\pm$ 0.7 %) culture models ($P > 0.05$). The direct-acting mutagen, 4-NQO, induced DNA-strand breaks in a concentration-dependent manner with no statistically significant difference between the response in spheroid- and 2D-culture models (Figure 3.9A). In contrast, B[a]P, PhIP and 2-AA induced statistically significant increases in levels of DNA strand breaks in a concentration-dependent manner in spheroids but not 2D-monolayers (Figure 3.9B – D). In spheroid models exposed to B[a]P levels of DNA strand breaks were 12.4 $\pm$ 1.9 %, 23.2 $\pm$ 4.4 % and 33.

8 ± 0.7 % following treatment with 3, 10 and 30 μM concentrations respectively. In spheroid models exposed to PhIP levels of DNA strand breaks were 9.4 ± 1.0 %, 11.6 ± 1.4 % and 15.8 ± 1.9 % following treatment with 3, 10 and 30 μM concentrations respectively. Finally, in spheroid models exposed to 2-AA levels of DNA strand breaks were 12.1 ± 0.8 %, 15.7 ± 1.3 % and 17.4 ± 4.6 % following treatment with 3, 10 and 30 μM concentrations respectively.

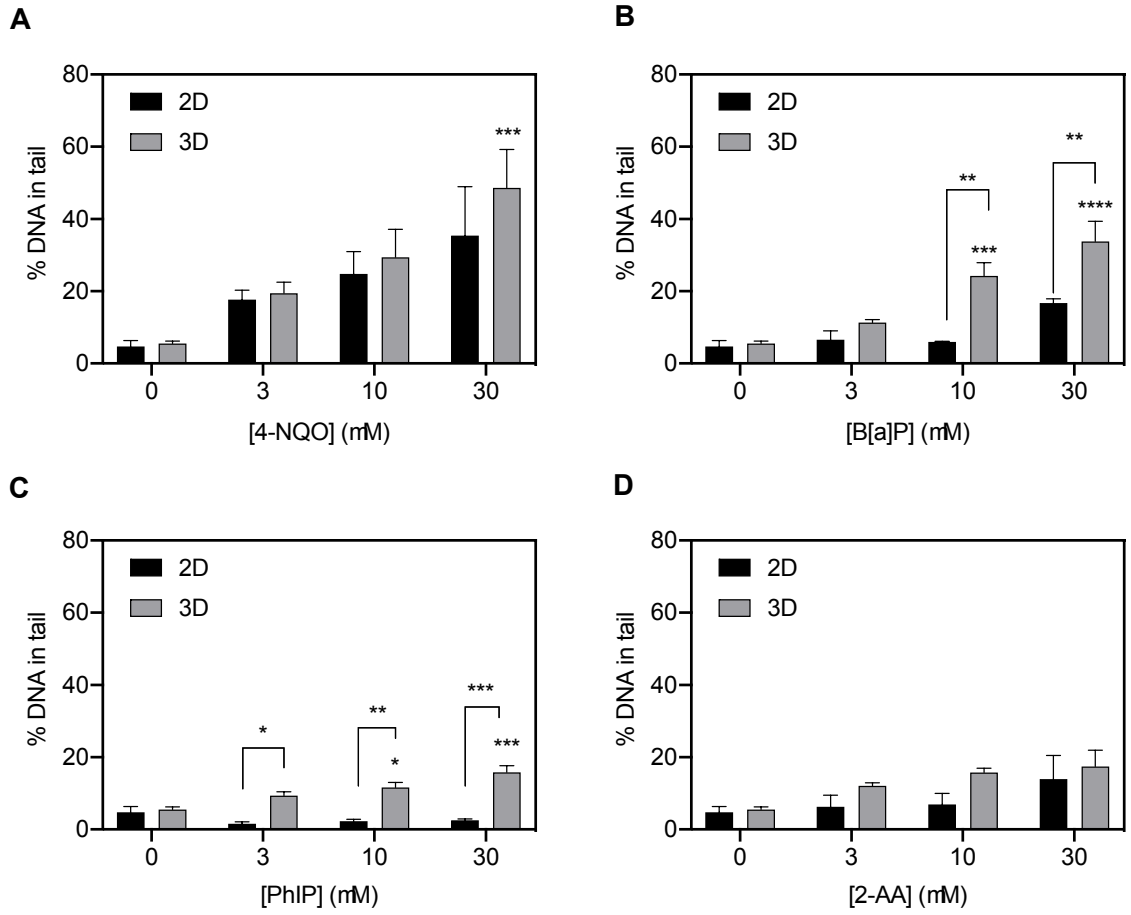

Figure 3.9. DNA damage induction as measured by the comet assay. *HepG2/C3A monolayers (2D) or 7-day old spheroids (3D) were exposed to direct-acting genotoxicants 4-NQO (A) or pro-genotoxicants B[a]P (B), PhIP (C) or 2-AA (D) for 24 h or a DMSO vehicle control. The comet assay was used to assess and measure DNA damage in the selected models by quantifying DNA tail intensity %. One-hundred nuclei were scored per experimental unit, in at least 3 independent experiments and collected as median values; 5 experiments were performed in the vehicle control group. Data is presented as the mean of*

*experimental median values ± standard error. Statistical significance denoted as: ****, P<0.00001; ***, P<0.0001; **, P<0.001; *, P<0.05.*

In order to assess whether spheroid age had any effect on sensitivity to genotoxicants, 10-day old spheroids were also analysed (Figure 3.10). There was no difference in the level of background DNA damage in spheroids at 7 day (5.6 ± 0.7 %) or 10 day (5.7 ± 0.9 %). Furthermore, there was no significant difference in DNA damage in 10-day old spheroids exposed to 4-NQO, B[a]P or 2-AA. In contrast, there was a greater response of 10-day old spheroids treated with PhIP (30 μM, $P < 0.05$) but this was not seen at lower concentrations.

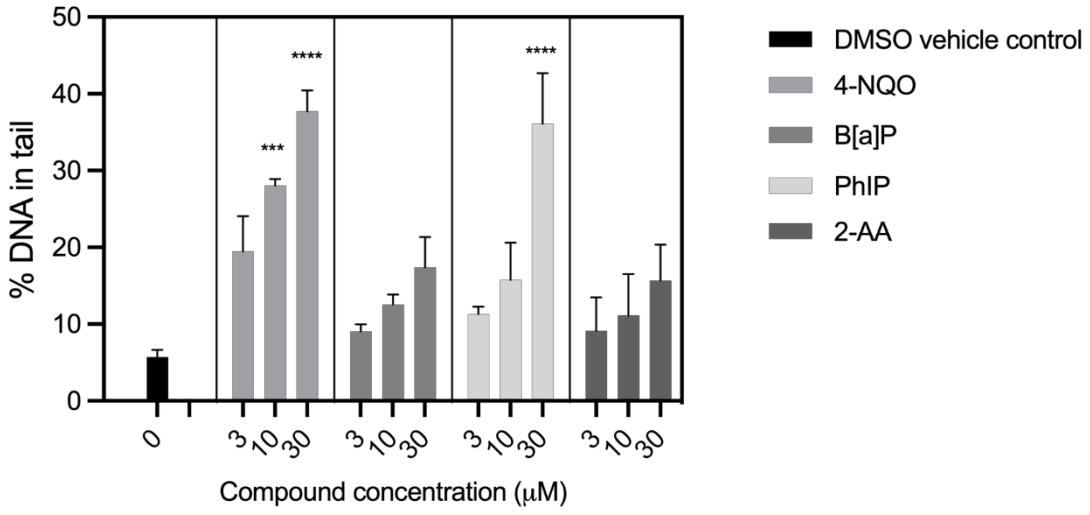

***Figure 3.10. Comet assay performed in 10-day old spheroids**. One-hundred nuclei were scored per experimental unit and collected as median values. Data is presented as the mean of experimental median values ± standard error. Statistical significance was determined by comparisons between compound concentrations and vehicle control: ****, P<0.00001; ***, P<0.0001; **, P<0.001; *, P<0.05; ns, P>0.05.*

3.4.6. Induction of γH2AX-phosphorylation by genotoxicants

4-NQO caused a concentration-dependent increase in numbers of double stranded breaks in both monolayers and spheroids cultures (Figure 3.11A). B[a]P induced DSB in both 2D- and spheroid- cultures, the overall response was smaller in 2D-cultures. In both 2D- and spheroid-cultures there was evidence for a plateau in the response at concentrations greater than 3 and 10 μM respectively (Figure 3.11B). Both PhIP and 2-AA also induced double-stranded DNA breaks (Figure 3.11C and D). In both cases the response was significantly enhanced in spheroid cultures. Interestingly there was evidence of a plateau in response in spheroid cultures at PhIP concentrations greater than 3 μM where there was a 2.2 and 1.8 - fold increase compared to untreated controls. In contrast, in 2D-cultures PhIP (0–30 μM) had no statistically significant effect on levels of DNA double-strand breaks. Similarly, a maximal response was reached in spheroids treated with 2-AA, where γH2AX phosphorylation was increased 2.0, 1.8 and 1.9 – fold at 3, 10 and 30 μM versus control. In 2D-cultures treated with 2-AA there was a statistically significant increase in levels of γH2AX phosphorylation, but the response was less pronounced than observed in 3D-cultures with a maximal response observed at 30 μM.

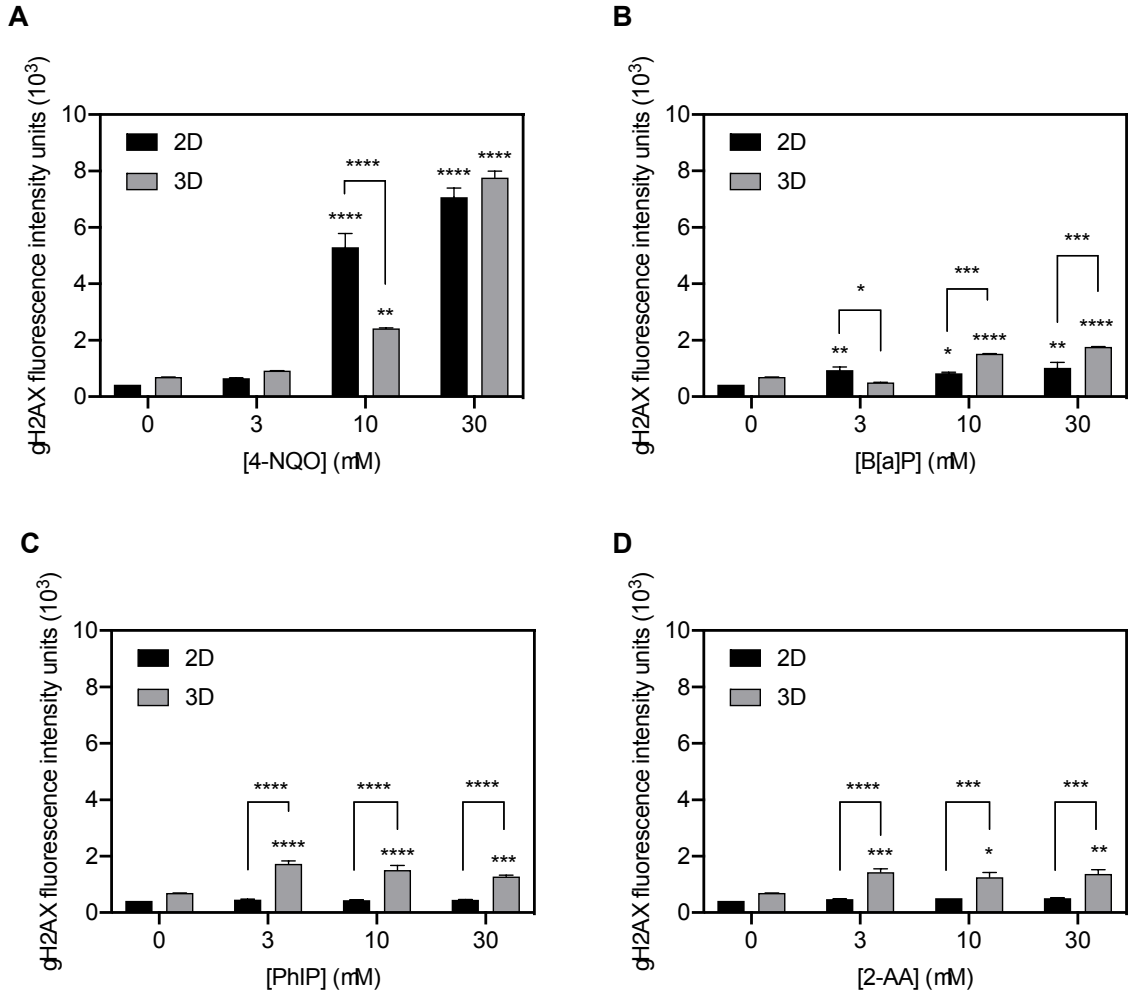

Figure 3.11. DNA damage measured by flow cytometric quantification of γH2Ax – positive cells. *The geometric mean of fluorescence intensity was collected for γ-H2AX-FITC immunostained HepG2/C3A cells from monolayers or spheroids treated with 4-NQO (A), B[a]P (B), PhIP (C) or 2-AA (D). Data presented is the mean ± standard error. Statistical significance denoted as: ****, P<0.00001; ***, P<0.0001; **, P<0.001; *, P<0.05.*

In both spheroids and monolayers there was a strong correlation between the measured number of positive γH2AX foci and the percentage of DNA found in comet tail (Figure 3.12), ($P < 0.05$, as determined by Pearson's correlation coefficient), where R values were found to be 0.80 and 0.78, in monolayers and spheroids respectively.

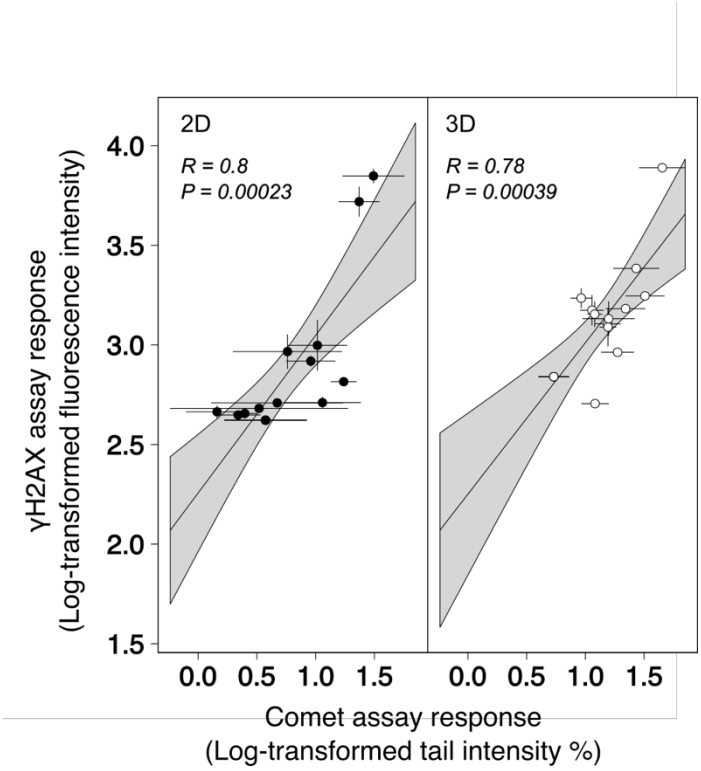

Figure 3.12. Correlation between the alkaline comet assay and γH2AX-phosphorylation. *DNA damage measurement by flow cytometry or by the comet assay in monolayers and spheroids of HepG2/C3A cells were compared by Pearson's correlation coefficient (black line, $p < 0.05$) was calculated for log-transformed data extracted from the comet assay or the flow cytometric analysis of γ-H2AX positive cells. Data is the mean ± standard error; confidence intervals are mapped by grey contouring.*

3.4.7. Transcriptional analysis of xenobiotic metabolism genes

HepG2/C3A spheroids were exposed to test compounds or a vehicle control and expression of a panel of genes encoding xenobiotic metabolism targets quantified using real-time qPCR. Raw data expressed as fold change is presented in Table 3.2. Overall mRNA expression for the selected gene targets were elevated in treated HepG2/C3A spheroids compared to the vehicle control (**Figure 3.13**A). *AHR* and its nuclear translocator *ARNT,* were significantly upregulated by more than 1.5-fold in spheroids exposed to 4-NQO and B[a]P over 24 hours.

CAR was also upregulated in 4-NQO, PhIP and 2-AA-treated spheroids but upregulation was not statistically significant in B[a]P exposed spheroids. Expression of the pregnane X nuclear receptor (*PXR*) did not change with either 4-NQO or B[a]P exposure but was significantly downregulated in PhIP and 2-AA treated spheroids compared to vehicle control treated spheroids. Exposure to 4-NQO and PhIP significantly induced expression of phase I enzyme genes *CYP1A1* and *1A2* by more than 5-fold and 2-fold, respectively. B[a]P induced the expression of *CYP1A1* by 29-fold and *1A2* by greater than 48-fold, compared to control spheroids. *CYP1A2* was downregulated in spheroids treated with 2-AA. Both 4-NQO and B[a]P induced the expression of epoxide hydrolase (*EPHX*) by 2.4- and 1.85-fold, respectively.

Genes encoding phase II enzymes were also induced following the treatment of spheroids. *NAT1/NAT2*, *SULT1A2* and *UGT* glucuronidase enzymes *1A1/1A3/1A6* were all significantly upregulated in spheroids treated with 4-NQO by more than 2-fold. In spheroids treated with B[a]P, *UGT1A6* was upregulated by more than 6.5-fold and *UGT1A3/1A1* by 3.4 and 2.7-fold. *NAT1* (3-fold), *NAT2* (2.3-fold) and *SULT1A2* (2.8-fold) were also significantly induced by B[a]P. PhIP induced the expression of *SULT1A2* (2.1-fold) and *UGT1A1* (1.72-fold) but not *UGT1A3* or *1A6*. *SULT1A2* was upregulated in 2-AA – treated spheroids (2.1-fold) but *SULT1A1* and *UGT1A3* were both downregulated to 0.4- and 0.3- of control levels. Genes encoding glutathione S transferase enzymes were not significantly induced in any of treated models however *GSTM1* was marginally downregulated in PhIP-treated spheroids.

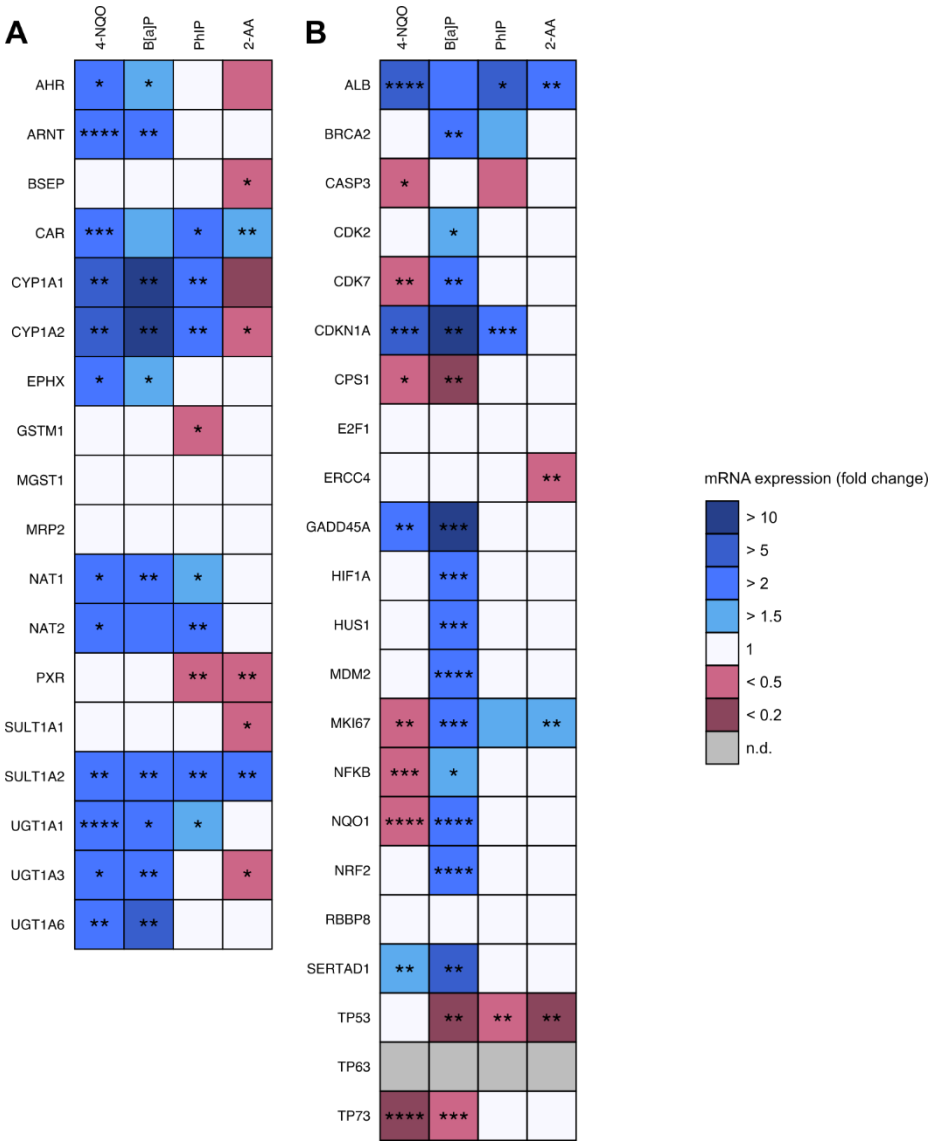

Figure 3.13. Expression of genes relating to xenobiotic metabolism (A) or cellular stress and DNA damage response pathways (B) in HepG2/C3A spheroids exposed to genotoxicants over 24 h. *A heatmap was constructed from qPCR fold-change gene expression data compared between treated and control spheroids. Upregulated and downregulated genes were determined by a ≥1.5-fold increase or ≤0.5-fold decrease in mRNA expression, respectively. Data shown as mean of 4 independent samples (n=4). Abbreviation: n.d., not detected. Statistical significance determined by student's t test (P < 0.05).*

3.4.8. Transcriptional analysis of genes relating to cellular stress and DNA damage response pathways

The expression of selected genes relating to liver function, cellular stress and DNA damage response were also compared between control and genotoxicant treated spheroids (**Figure 3.13**B). Raw data expressed as fold change is presented in Table 3.2. Interestingly, *ALB* was upregulated by all four genotoxic compounds whilst *CPS1* was downregulated on exposure to both 4-NQO (0.2 of control value) and B[a]P (0.1 of control). The expression of *MKI67*, a marker for cellular proliferation was significantly upregulated by 2.3-fold with B[a]P and 1.5-fold with 2-AA. PhIP marginally upregulated *MKI67* but expression was downregulated in 4-NQO-treated spheroids by 0.4 of control. *GADD45A* was significantly upregulated in 4-NQO-treated spheroids by 2.6-fold., *CDKN1A* was also induced by 4-NQO and PhIP by greater than 2-fold and 10-fold, respectively. B[a]P exposure significantly upregulated the expression of several genes relating to DNA damage and repair, specifically: *BRCA2 (3-fold)*; cyclin dependent kinases *CDK2 (1.7-fold), CDK7 (2.2-fold)* and *CDKN1A (45.8-fold)*; *GADD45A (15-fold)*, *HUS1 (2.5-fold)*, *MDM2 (2.9-fold)* and *SERTAD1 (9.3-fold)*. Intriguingly, B[a]P was the only genotoxicant to induce the significant expression of hypoxia inducing factor, *HIF1A, NFKB, NQO1* and *NRF2*, relating to inflammatory and oxidative stress pathways. Tumour suppressor gene *TP53* was downregulated on exposure to B[a]P (0.1 control), PhIP (0.3 of control) and 2-AA (0.1 of control) but not by 4-NQO. *TP73* was significantly downregulated in 4-NQO (0.17 of control) and B[a]P (0.36 of control) treated spheroids whereas *TP63* expression could not be detected in any of the treated samples.

Table 3.2.Fold-change expression of genes by real-time qPCR

	4-NQO			B[a]P			PhIP			2-AA		
Gene	Fold change	*P* value	*q* value	Fold change	*P* value	*q* value	Fold change	*P* value	*q* value	Fold change	*P* value	*q* value
genes associated with xenobiotic metabolism												
AHR	2.18	0.00	0.01	1.78	0.02	0.03	0.71	0.23	0.29	0.93	0.64	0.69
ARNT	4.57	<0.0001	<0.0001	3.00	0.01	0.02	0.83	0.18	0.25	1.01	0.98	0.98
BSEP	0.64	0.47	0.60	0.71	0.39	0.47	0.64	0.69	0.69	0.28	0.03	0.06
CAR	3.89	0.00	0.00	1.56	0.11	0.17	2.96	0.02	0.03	1.67	0.01	0.03
CYP1A1	7.84	0.00	0.00	48.71	0.00	0.01	2.98	0.01	0.02	1.32	0.32	0.01
CYP1A2	5.45	0.00	0.00	29.35	0.00	0.01	2.60	0.00	0.02	1.65	0.03	0.01
EPHX	2.40	0.00	0.01	1.85	0.02	0.04	0.80	0.34	0.38	0.73	0.29	0.41
GST-µ1	0.73	0.12	0.16	1.20	0.62	0.66	0.43	0.01	0.03	0.60	0.07	0.11
mGST1	1.11	0.81	0.86	0.66	0.15	0.21	0.82	0.42	0.45	0.64	0.15	0.22
MRP2	1.01	0.91	0.91	0.83	0.59	0.66	0.77	0.17	0.25	0.80	0.37	0.47
NAT1	2.62	0.01	0.01	3.01	0.01	0.01	1.52	0.03	0.05	0.90	0.57	0.64
NAT2	3.61	0.01	0.01	2.31	0.08	0.14	3.09	0.00	0.02	1.17	0.65	0.69
PXR	0.96	0.64	0.72	0.77	0.25	0.32	0.45	0.00	0.02	0.28	0.00	0.01
SULT1A1	1.19	0.50	0.60	1.14	0.66	0.66	0.49	0.02	0.03	0.45	0.01	0.04
SULT1A2	2.75	0.00	0.00	2.84	0.00	0.01	2.11	0.00	0.02	2.11	0.00	0.01
UGT1A1	2.44	<0.0001	0.00	2.70	0.00	0.01	1.72	0.02	0.03	0.55	0.05	0.10
UGT1A3	2.03	0.00	0.01	3.47	0.00	0.01	0.66	0.15	0.25	0.36	0.00	0.01
UGT1A6	2.45	0.00	0.00	6.56	0.01	0.01	0.79	0.28	0.34	0.53	0.02	0.05
genes associated with cellular and genotoxic stress												

ALB	4.99	<0.0001	0.00	2.80	0.05	0.05	5.24	0.05	0.16	2.74	0.01	0.01
BRCA2	0.57	0.00	0.01	3.15	0.00	0.00	1.60	0.19	0.40	1.42	0.00	0.01
CAS3	0.33	0.01	0.02	1.05	0.01	0.02	0.47	0.56	0.68	0.54	0.91	0.50
CDK2	0.55	0.01	0.02	1.70	0.04	0.04	0.93	0.81	0.90	0.65	0.00	0.01
CDK7	0.46	0.00	0.00	2.18	0.01	0.01	1.01	0.99	0.99	1.10	0.34	0.24
CDKN1A	5.37	0.00	0.00	45.89	0.00	0.00	2.07	0.00	0.01	1.29	0.19	0.17
CPS1	0.20	0.01	0.02	0.11	0.01	0.01	0.72	0.25	0.43	0.60	0.10	0.10
E2F1	0.51	0.00	0.01	0.69	0.03	0.03	1.02	0.96	0.99	0.65	0.01	0.01
ERCC4	0.74	0.12	0.14	0.50	0.01	0.01	0.68	0.06	0.19	0.49	0.01	0.01
GADD45A	2.60	0.00	0.00	15.00	0.00	0.00	0.83	0.37	0.57	0.97	0.72	0.43
HIF1A	0.94	0.58	0.60	3.95	0.00	0.00	0.83	0.38	0.57	0.85	0.24	0.19
HUS1	0.76	0.06	0.07	2.48	0.00	0.00	1.15	0.45	0.61	1.28	0.01	0.02
MKI67	0.49	0.00	0.00	2.36	0.00	0.00	1.70	0.01	0.04	1.52	0.00	0.01
MDM2	0.72	0.01	0.01	2.90	0.00	0.00	0.90	0.58	0.68	0.88	0.11	0.11
NFKB	0.35	0.00	0.00	1.61	0.01	0.02	0.72	0.02	0.07	0.97	0.68	0.43
NQO1	0.21	<0.0001	<0.0001	3.71	0.00	0.00	0.55	0.00	0.03	0.92	0.20	0.17
NRF2	0.60	0.00	0.01	3.09	0.00	0.00	0.75	0.17	0.40	0.69	0.01	0.01
RBBP8	1.04	0.76	0.76	1.15	0.22	0.22	1.26	0.46	0.61	0.99	0.83	0.48
SERTAD1	1.59	0.00	0.00	9.32	0.00	0.00	0.76	0.17	0.40	0.95	0.63	0.43
TP53	0.89	0.53	0.58	0.17	0.00	0.00	0.38	0.01	0.04	0.15	0.00	0.01
TP63	n.d.	-	-	n.d.	-	-	n.d.	-	-	n.d.	-	-
TP73	0.17	<0.0001	<0.0001	0.36	0.00	0.00	0.79	0.24	0.43	0.75	0.01	0.01

3.5. Discussion

In the current study we adapted and optimised the agarose liquid overlay technique (Carlsson and Yuhas, 1984, Costa et al., 2014, Gaskell et al., 2016, Kyffin et al., 2019c) as a method for the culture of HepG2/C3A spheroids. HepG2/C3A cells display contact inhibition and are less proliferative than the parent HepG2 line, emulating the growth characteristics of primary hepatocytes. This feature makes them more physiologically relevant and less prone to overgrowth and more suitable for 3D cell culture (Gaskell et al., 2016). In addition, HepG2/C3A cells have been shown to display enhanced albumin synthesis and urea production compared to HepG2 cells (Wrzesinski et al., 2013, Pluta et al., 2020), suggestive of a more hepatocyte-like phenotype (Sussman et al., 1992, van Wenum et al., 2016). Consistent with this, in the current study, both albumin and carbamoyl phosphate synthetase 1, an enzyme forming the first critical step of the urea cycle were upregulated in 3D-HepG2/C3A spheroids. Extended culture of spheroids not achievable in 2D monolayers improves their utility as *in vitro* models, particularly for chronic exposure studies not possible in 2D models. Ramaiahgari et al. (2014) have cultured HepG2 spheroids over 28 days for repeat dose toxicity studies and Conway et al. (2020) have demonstrated that HepG2 spheroids can detect genotoxic response following chronic treatment with aflatoxin B1. Similarly, the C3A HepG2 clone has been successfully used over 21 days as a model for sub-chronic, repeat-dose toxicity testing (Calitz et al., 2019), Fey and Wrzesinski (2012). However, it is recognised that there is a narrow window for the use of spheroid models as *in vitro* liver function models as opposed to a model of liver cancer (Gaskell et al., 2016, Leedale et al., 2019) with the size of spheroids known to be critical especially in relation to the formation of a hypoxic core (Däster et al., 2017, Eilenberger et al., 2019).

In the current study spheroids were approximately 300 μm in diameter. There was no evidence of a hypoxic core and displayed a normal phenotype consistent with the previous data (Daster *et al* 2017). Furthermore, there was no evidence of transcriptional activation of *HIFa* which is also consistent with a lack of a hypoxic core. We also report that markers of hepatocyte differentiation e.g. albumin and CPS (urea synthesis) are transcriptional upregulated in 7-day old spheroids compared to 2D-cultures with albumin synthesis maintained for up to 28 days in culture. Together, these data are strongly indicative of a "normal" hepatocyte phenotype rather than a tumour model and that our model is a valid platform for investigating normal liver function.

Previous studies have reported enhanced metabolic competency of HepG2 cells cultured as spheroids, including enhanced expression of phase I and II genes (Elje et al., 2020, Hurrell et al., 2019, Elje et al., 2019, Luckert et al., 2017, Ramaiahgari et al., 2014) and nuclear receptors including *AhR (Luckert et al., 2017, Shah et al., 2018, Terashima et al., 2015a)*. In contrast, the expression of phase I and II genes in HepG2/C3A 3D-culture is less well understood. In the current study, transcriptional activation of many but not all phase I and II genes investigated was observed in untreated HepG2/C3A spheroids. Of the genes studied, *CYP1A1*, *CYP1A2*, *EPHX*, *NAT2*, *UGT1A1*, *UGT1A3* and *UGT1A6* were significantly transcriptionally upregulated. In contrast, *GSTm1*, *GSTμ1*, *SULT1A1* and *SULT1A2* expression was not upregulated. The reason for this is unclear but suggests differential transcriptional regulation of these genes.

Expression was further enhanced following exposure to genotoxins most notably, 4-NQO and B[a]P. Consistent with our data, Shah et al. (2018) report induction of *CYP1A2* and *1A1* genes and enhanced enzymatic activity on exposure to B[a]P and PhIP in HepG2 spheroids. Stampar et al. (2019) also reported induction of *CYP1A1*, *1A2* and *3A4* in untreated spheroids that was enhanced by B[a]P and PhIP. Both of these studies used high concentrations of test compounds, Here we report Induction by concentrations as low as 3 μM in HepG2/C3A spheroids, showing a more sensitive responsive to these agents. Also induced by B[a]P were *AHR* and *ARNT*, suggesting a co-ordinated transcriptional response to B[a]P in our spheroid culture model. Similarly in the current study, PhIP caused a statistically significant increase in the expression of *CYP1A1* and *CYP1A2*. *N*-hydroxylated metabolites of PhIP are metabolised by *NAT* and *SULT* to reactive esters (Muckel et al., 2002, Rendic and Guengerich, 2012). *NAT1/2, UGT1A1* and *SULT1A2* were also all upregulated, a finding that correlates with increased genotoxicity of PhIP in spheroids. In 2-AA treated spheroids there was no evidence of transcriptional upregulation of any of the phase I enzymes studied. Lack of P450 induction may account for the reduced sensitivity of spheroids to 2-AA in our study.

In the current study, consistent with the induction of phase I and II metabolism genes, induction of DNA-damage by pro-genotoxins was enhanced in spheroid cultures and this was comparable to previous data using HepG2 (Stampar et al., 2019) and HepaRG spheroids Mandon et al. (2019). Interestingly, PhIP was relatively inactive as previously reported by (Wilkening et al., 2003) and (Stampar et al., 2019). In further support of enhanced sensitivity of spheroids to genotoxins, Shah at al. (2018) reported that induction of micronuclei was enhanced in HepG2 spheroid models. Recently, Stampar et al. (2020) demonstrated that

HepG2/C3A spheroids were sensitive to genotoxicity induced by chronic low level exposure to B[a]P and PhiP further demonstrating the utility of HePG2/C3A spheroids as a sensitive *in vitro* model for genotoxicity testing. Similarly, Mandon et al. (2019) showed that HepaRG cells cultured as spheroids were 10-times more sensitive to 2-AAF than 2D-cultures further emphasising the advantage of spheroid culture models. In a recent study, HepG2/C3A were found to be more sensitive than HepaRG when screening for cytotoxicity in compounds associated with drug induced liver injury (DILI) (Basharat et al., 2020). The authors found that spheroid models of C3A and HepaRG cells shared similar specificity in the prediction of over 100 chemically diverse compounds but C3A were on average 10 % more sensitive versus the equivalent HepRG model thus indicating C3A HepG2 clone cell line as a highly suitable model for use in *in vitro* genotoxicity studies.

Induction of markers of DNA damage and cell cycle arrest have also been reported by Stampar et al. (2019) in HepG2 spheroids exposed to B[a]P, AFB1 and etoposide. In the current study we also report transcriptional changes related to DNA-damage response and cell cycle arrest in HepG2/C3A spheroids but at lower concentrations than previously reported demonstrating the enhanced sensitivity of our HepG2/C3A model to these compounds. Cellular oxidative stress induced by compounds like B[a]P is also known to induce DNA damage. In support of this, B[a]P was found to induce the transcription of ROS-protective genes *NRF2* and *NQO1*. Interestingly Hypoxia inducible factor 1 (*HIF1A*) was also significantly induced by B[a]P treatment. Previous studies have linked B[a]P to metabolic reprogramming of cells and altered redox status via a Warburg-like effect dependent on

HIF1A activation (Hardonniere et al., 2016). But to the best of our knowledge this is the first time this biological effect has been observed in an *in vitro* 3D-culture model of hepatocytes.

3.6. Conclusion

We have developed a low-cost method for 3D-culture of HepG2/C3A cells that shows enhanced expression of drug metabolism genes and inducibility at concentrations lower than previously reported for other 3D-hepatocyte culture models. We also demonstrate increased sensitivity to genotoxicity induced by model pro-genotoxins compared to 2D cultures and comparable with previous studies in 3D-cultures. Our data suggests that HepG2/C3A spheroids are a powerful model for genotoxicity assessment with a number of advantages compared to existing models, including PHHs and HepaRG cells. For example, in addition to their sensitivity they are easy to culture, lack the batch variability associated with primary cell cultures and are economically appealing. Although regulatory toxicology still relies on studies conducted *in vivo*; it is becoming increasingly clear that advanced 3D-culture models can play an important role in genotoxicity assessment and help contribute to a reduction in the number of animals used in scientific research.

3.7. References

Aninat, C., Piton, A., Glaise, D., Le Charpentier, T., Langouet, S., Morel, F., Guguen-Guillouzo, C. and Guillouzo, A. (2006) 'Expression of cytochromes P450, conjugating enzymes and nuclear receptors in human hepatoma HepaRG cells', *Drug Metab Dispos,* 34(1), pp. 75-83.

Anthérieu, S., Chesné, C., Li, R., Camus, S., Lahoz, A., Picazo, L., Turpeinen, M., Tolonen, A., Uusitalo, J., Guguen-Guillouzo, C. and Guillouzo, A. (2010) 'Stable Expression, Activity, and Inducibility of Cytochromes P450 in Differentiated HepaRG Cells', *Drug Metabolism and Disposition,* 38(3), pp. 516.

Basharat, A., Rollison, H. E., Williams, D. P. and Ivanov, D. P. (2020) 'HepG2 (C3A) spheroids show higher sensitivity compared to HepaRG spheroids for drug-induced liver injury (DILI)', *Toxicol Appl Pharmacol,* 408, pp. 115279.

Bell, C. C., Chouhan, B., Andersson, L. C., Andersson, H., Dear, J. W., Williams, D. P. and Soderberg, M. (2020) 'Functionality of primary hepatic non-parenchymal cells in a 3D spheroid model and contribution to acetaminophen hepatotoxicity', *Arch Toxicol,* 94(4), pp. 1251-1263.

Calitz, C., Hamman, J. H., Fey, S. J., Viljoen, A. M., Gouws, C. and Wrzesinski, K. (2019) 'A sub-chronic Xysmalobium undulatum hepatotoxicity investigation in HepG2/C3A spheroid cultures compared to an in vivo model', *J Ethnopharmacol,* 239, pp. 111897.

Carlsson, J. and Yuhas, J. M. (1984) 'Liquid-Overlay Culture of Cellular Spheroids', *Recent Results in Cancer Research,* 95, pp. 1-23.

Cipriano, M., Correia, J. C., Camoes, S. P., Oliveira, N. G., Cruz, P., Cruz, H., Castro, M., Ruas, J. L., Santos, J. M. and Miranda, J. P. (2017) 'The role of epigenetic modifiers in extended cultures of functional hepatocyte-like cells derived from human neonatal mesenchymal stem cells', *Arch Toxicol,* 91(6), pp. 2469-2489.

Conway, G. E., Shah, U.-K., Llewellyn, S., Cervena, T., Evans, S. J., Al Ali, A. S., Jenkins, G. J., Clift, M. J. D. and Doak, S. H. (2020) 'Adaptation of the in vitro micronucleus assay for genotoxicity testing using 3D liver models supporting longer-term exposure durations', *Mutagenesis,* 35(4), pp. 319-330.

Costa, E. C., Gaspar, V. M., Coutinho, P. and Correia, I. J. (2014) 'Optimization of Liquid Overlay Technique to Formulate Heterogenic 3D Co-Cultures Models', *Biotechnology and Bioengineering,* 111(8), pp. 1672-1685.

Däster, S., Amatruda, N., Calabrese, D., Ivanek, R., Turrini, E., Droeser, R. A., Zajac, P., Fimognari, C., Spagnoli, G. C., Iezzi, G., Mele, V. and Muraro, M. G. (2017) 'Induction of hypoxia and necrosis in multicellular tumor spheroids is associated with resistance to chemotherapy treatment', *Oncotarget,* 8(1), pp. 1725-1736.

Donato, M. T., Gomez-Lechon, M. J. and Castell, J. V. (1993) 'A microassay for measuring cytochrome P450IA1 and P450IIB1 activities in intact human and rat hepatocytes cultured on 96-well plates', *Anal Biochem,* 213(1), pp. 29-33.

Donato, M. T., Jimenez, N., Castell, J. V. and Gomez-Lechon, M. J. (2004) 'Fluorescence-based assays for screening nine cytochrome P450 (P450) activities in intact cells expressing individual human P450 enzymes', *Drug Metab Dispos,* 32(7), pp. 699-706.

Eilenberger, C., Rothbauer, M., Ehmoser, E. K., Ertl, P. and Kupcu, S. (2019) 'Effect of Spheroidal Age on Sorafenib Diffusivity and Toxicity in a 3D HepG2 Spheroid Model', *Sci Rep,* 9(1), pp. 4863.

Elje, E., Hesler, M., Rundén-Pran, E., Mann, P., Mariussen, E., Wagner, S., Dusinska, M. and Kohl, Y. (2019) 'The comet assay applied to HepG2 liver spheroids', *Mutation Research/Genetic Toxicology and Environmental Mutagenesis*.

Elje, E., Mariussen, E., Moriones, O. H., Bastus, N. G., Puntes, V., Kohl, Y., Dusinska, M. and Runden-Pran, E. (2020) 'Hepato(Geno)Toxicity Assessment of Nanoparticles in a HepG2 Liver Spheroid Model', *Nanomaterials (Basel),* 10(3).

Elliott, N. T. and Yuan, F. (2011) 'A review of three-dimensional in vitro tissue models for drug discovery and transport studies', *J Pharm Sci,* 100(1), pp. 59-74.

Feng, W. Y., Wen, J. and Stauber, K. (2018) 'In vitro Drug Metabolism Investigation of 7-Ethoxycoumarin in Human, Monkey, Dog and Rat Hepatocytes by High Resolution LC-MS/MS', *Drug Metab Lett,* 12(1), pp. 33-53.

Fey, S. J. and Wrzesinski, K. (2012) 'Determination of drug toxicity using 3D spheroids constructed from an immortal human hepatocyte cell line', *Toxicol Sci,* 127(2), pp. 403-11.

Fraczek, J., Bolleyn, J., Vanhaecke, T., Rogiers, V. and Vinken, M. (2013) 'Primary hepatocyte cultures for pharmaco-toxicological studies: at the busy crossroad of various anti-dedifferentiation strategies', *Arch Toxicol,* 87(4), pp. 577-610.

Gaskell, H., Sharma, P., Colley, H. E., Murdoch, C., Williams, D. P. and Webb, S. D. (2016) 'Characterization of a functional C3A liver spheroid model', *Toxicology research,* 5(4), pp. 1053-1065.

Gómez-Lechón, M. J., Tolosa, L. and Donato, M. T. (2017) 'Upgrading HepG2 cells with adenoviral vectors that encode drug-metabolizing enzymes: application for drug hepatotoxicity testing', *Expert Opinion on Drug Metabolism & Toxicology,* 13(2), pp. 137-148.

Guillouzo, A. and Guguen-Guillouzo, C. (2008) 'Evolving concepts in liver tissue modeling and implications for in vitro toxicology', *Expert Opinion on Drug Metabolism & Toxicology,* 4(10), pp. 1279-1294.

Guo, X., Seo, J. E., Li, X. and Mei, N. (2020) 'Genetic toxicity assessment using liver cell models: past, present, and future', *J Toxicol Environ Health B Crit Rev,* 23(1), pp. 27-50.

Hardonniere, K., Saunier, E., Lemarie, A., Fernier, M., Gallais, I., Helies-Toussaint, C., Mograbi, B., Antonio, S., Benit, P., Rustin, P., Janin, M., Habarou, F., Ottolenghi, C., Lavault, M. T., Benelli, C., Sergent, O., Huc, L., Bortoli, S. and Lagadic-Gossmann, D. (2016) 'The

environmental carcinogen benzo[a]pyrene induces a Warburg-like metabolic reprogramming dependent on NHE1 and associated with cell survival', *Sci Rep,* 6, pp. 30776.

Hashizume, T., Yoshitomi, S., Asahi, S., Matsumura, S., Chatani, F. and Oda, H. (2009) 'In vitro micronucleus test in HepG2 transformants expressing a series of human cytochrome P450 isoforms with chemicals requiring metabolic activation', *Mutat Res,* 677(1-2), pp. 1-7.

Hashizume, T., Yoshitomi, S., Asahi, S., Uematsu, R., Matsumura, S., Chatani, F. and Oda, H. (2010) 'Advantages of human hepatocyte-derived transformants expressing a series of human cytochrome p450 isoforms for genotoxicity examination', *Toxicol Sci,* 116(2), pp. 488-97.

Hendriks, D. F. G., Vorrink, S. U., Smutny, T., Sim, S. C., Nordling, Å., Ullah, S., Kumondai, M., Jones, B. C., Johansson, I., Andersson, T. B., Lauschke, V. M. and Ingelman-Sundberg, M. (2020) 'Clinically Relevant Cytochrome P450 3A4 Induction Mechanisms and Drug Screening in Three-Dimensional Spheroid Cultures of Primary Human Hepatocytes', *Clinical Pharmacology & Therapeutics,* 108(4), pp. 844-855.

Hewitt, N. J., Lechon, M. J., Houston, J. B., Hallifax, D., Brown, H. S., Maurel, P., Kenna, J. G., Gustavsson, L., Lohmann, C., Skonberg, C., Guillouzo, A., Tuschl, G., Li, A. P., LeCluyse, E., Groothuis, G. M. and Hengstler, J. G. (2007) 'Primary hepatocytes: current understanding of the regulation of metabolic enzymes and transporter proteins, and pharmaceutical practice for the use of hepatocytes in metabolism, enzyme induction, transporter, clearance, and hepatotoxicity studies', *Drug Metab Rev,* 39(1), pp. 159-234.

Hurrell, T., Lilley, K. S. and Cromarty, A. D. (2019) 'Proteomic responses of HepG2 cell monolayers and 3D spheroids to selected hepatotoxins', *Toxicology Letters,* 300, pp. 40-50.

Ivanov, D. P. and Grabowska, A. M. (2017) 'Spheroid arrays for high-throughput single-cell analysis of spatial patterns and biomarker expression in 3D', *Scientific Reports,* 7.

Ivanov, D. P., Grabowska, A. M. and Garnett, M. C. (2017) 'High-Throughput Spheroid Screens Using Volume, Resazurin Reduction, and Acid Phosphatase Activity', *Cell Viability Assays: Methods and Protocols,* 1601, pp. 43-59.

Kamiyama, Y., Matsubara, T., Yoshinari, K., Nagata, K., Kamimura, H. and Yamazoe, Y. (2007) 'Role of human hepatocyte nuclear factor 4alpha in the expression of drug-metabolizing enzymes and transporters in human hepatocytes assessed by use of small interfering RNA', *Drug Metab Pharmacokinet,* 22(4), pp. 287-98.

Knasmüller, S., Parzefall, W., Sanyal, R., Ecker, S., Schwab, C., Uhl, M., Mersch-Sundermann, V., Williamson, G., Hietsch, G., Langer, T., Darroudi, F. and Natarajan, A. T. (1998) 'Use of metabolically competent human hepatoma cells for the detection of mutagens and antimutagens', *Mutation Research/Fundamental and Molecular Mechanisms of Mutagenesis,* 402(1), pp. 185-202.

Kyffin, J. A., Cox, C. R., Leedale, J., Colley, H. E., Murdoch, C., Mistry, P., Webb, S. D. and Sharma, P. (2019a) 'Preparation of Primary Rat Hepatocyte Spheroids Utilizing the Liquid-Overlay Technique', *Curr Protoc Toxicol,* 81(1), pp. e87.

Kyffin, J. A., Sharma, P., Leedale, J., Colley, H. E., Murdoch, C., Harding, A. L., Mistry, P. and Webb, S. D. (2019b) 'Characterisation of a functional rat hepatocyte spheroid model', *Toxicology in Vitro,* 55, pp. 160-172.

Kyffin, J. A., Sharma, P., Leedale, J., Colley, H. E., Murdoch, C., Harding, A. L., Mistry, P. and Webb, S. D. (2019c) 'Characterisation of a functional rat hepatocyte spheroid model', *Toxicol In Vitro,* 55, pp. 160-172.

Lake, B. G., Evans, J. G., Lewis, D. F. V. and Price, R. J. (1994) 'Comparison of the hepatic effects of coumarin, 3,4-Dimethylcoumarin, dihydrocoumarin and 6-methylcoumarin in the rat', *Food and Chemical Toxicology,* 32(8), pp. 743-751.

Lake, B. G., Gray, T. J. B., Evans, J. G., Lewis, D. F. V., Beamand, J. A. and Hue, K. L. (1989) 'Studies on the mechanism of coumarin-induced toxicity in rat hepatocytes: Comparison with dihydrocoumarin and other coumarin metabolites', *Toxicology and Applied Pharmacology,* 97(2), pp. 311-323.

Langhans, S. A. (2018) 'Three-Dimensional in Vitro Cell Culture Models in Drug Discovery and Drug Repositioning', *Front Pharmacol,* 9, pp. 6.

Larigot, L., Juricek, L., Dairou, J. and Coumoul, X. (2018) 'AhR signaling pathways and regulatory functions', *Biochim Open,* 7, pp. 1-9.

Leedale, J., Colley, H. E., Gaskell, H., Williams, D. P., Bearon, R. N., Chadwick, A. E., Murdoch, C. and Webb, S. D. (2019) 'In silico-guided optimisation of oxygen gradients in hepatic spheroids', *Computational Toxicology,* 12.

Lima, K. G., Krause, G. C., da Silva, E. F. G., Xavier, L. L., Martins, L. A. M., Alice, L. M., da Luz, L. B., Gassen, R. B., Filippi-Chiela, E. C., Haute, G. V., Garcia, M. C. R., Funchal, G. A., Pedrazza, L., Reghelin, C. K. and de Oliveira, J. R. (2018) 'Octyl gallate reduces ATP levels and Ki67 expression leading HepG2 cells to cell cycle arrest and mitochondria-mediated apoptosis', *Toxicol In Vitro,* 48, pp. 11-25.

Lucendo-Villarin, B., Meseguer-Ripolles, J., Drew, J., Fischer, L., Ma, W. S. E., Flint, O., Simpson, K., Machesky, L., Mountford, J. and Hay, D. (2020) 'Development of a cost effective automated platform to produce human liver spheroids for basic and applied research', *Biofabrication*.

Luckert, C., Schulz, C., Lehmann, N., Thomas, M., Hofmann, U., Hammad, S., Hengstler, J. G., Braeuning, A., Lampen, A. and Hessel, S. (2017) 'Comparative analysis of 3D culture methods on human HepG2 cells', *Archives of Toxicology,* 91(1), pp. 393-406.

Mandon, M., Huet, S., Dubreil, E., Fessard, V. and Le Hegarat, L. (2019) 'Three-dimensional HepaRG spheroids as a liver model to study human genotoxicity in vitro with the single cell gel electrophoresis assay', *Sci Rep,* 9(1), pp. 10548.

Mišík, M., Nersesyan, A., Ropek, N., Huber, W. W., Haslinger, E. and Knasmueller, S. (2019) 'Use of human derived liver cells for the detection of genotoxins in comet assays', *Mutation Research/Genetic Toxicology and Environmental Mutagenesis,* 845, pp. 402995.

Muckel, E., Frandsen, H. and Glatt, H. R. (2002) 'Heterologous expression of human N-acetyltransferases 1 and 2 and sulfotransferase 1A1 in Salmonella typhimurium for mutagenicity testing of heterocyclic amines', *Food and Chemical Toxicology,* 40(8), pp. 1063-1068.

Nelson, L. J., Morgan, K., Treskes, P., Samuel, K., Henderson, C. J., LeBled, C., Homer, N., Grant, M. H., Hayes, P. C. and Plevris, J. N. (2017) 'Human Hepatic HepaRG Cells Maintain an Organotypic Phenotype with High Intrinsic CYP450 Activity/Metabolism and Significantly Outperform Standard HepG2/C3A Cells for Pharmaceutical and Therapeutic Applications', *Basic & clinical pharmacology & toxicology,* 120(1), pp. 30-37.

Nishikawa, T., Tanaka, Y., Nishikawa, M., Ogino, Y., Kusamori, K., Mizuno, N., Mizukami, Y., Shimizu, K., Konishi, S., Takahashi, Y. and Takakura, Y. (2017) 'Optimization of Albumin Secretion and Metabolic Activity of Cytochrome P450 1A1 of Human Hepatoblastoma HepG2 Cells in Multicellular Spheroids by Controlling Spheroid Size', *Biol Pharm Bull,* 40(3), pp. 334-338.

Olive, P. L. and Durand, R. E. (2005) 'Heterogeneity in DNA damage using the comet assay', *Cytometry Part A,* 66a(1), pp. 1-8.

Ott, L. M., Ramachandran, K. and Stehno-Bittel, L. (2017) 'An automated multiplexed hepatotoxicity and CYP induction assay using HepaRG cells in 2D and 3D', *SLAS Discov Adv Life Sci R D,* 22, pp. 614-25.

Pfaffl, M. W. (2001) 'A new mathematical model for relative quantification in real-time RT-PCR', *Nucleic acids research,* 29(9), pp. e45-e45.

Pfuhler, S., van Benthem, J., Curren, R., Doak, S. H., Dusinska, M., Hayashi, M., Heflich, R. H., Kidd, D., Kirkland, D., Luan, Y., Ouedraogo, G., Reisinger, K., Sofuni, T., van Acker, F., Yang, Y. and Corvi, R. (2020) 'Use of in vitro 3D tissue models in genotoxicity testing: Strategic fit, validation status and way forward. Report of the working group from the 7(th) International Workshop on Genotoxicity Testing (IWGT)', *Mutat Res,* 850-851, pp. 503135.

Pillai, V. C., Strom, S. C., Caritis, S. N. and Venkataramanan, R. (2013) 'A sensitive and specific CYP cocktail assay for the simultaneous assessment of human cytochrome P450 activities in primary cultures of human hepatocytes using LC-MS/MS', *Journal of pharmaceutical and biomedical analysis,* 74, pp. 126-132.

Pluta, K. D., Samluk, A., Wencel, A., Zakrzewska, K. E., Gora, M., Burzynska, B., Ciezkowska, M., Motyl, J. and Pijanowska, D. G. (2020) 'Genetically modified C3A cells with restored urea cycle for improved bioartificial liver', *Biocybernetics and Biomedical Engineering,* 40(1), pp. 378-387.

R Core Team (2019) *R: A language and environment for statistical computing.*: R Foundation for Statistical Computing, Vienna, Austria. Available at: https://www.R-project.org/.

Ramaiahgari, S. C., den Braver, M. W., Herpers, B., Terpstra, V., Commandeur, J. N., van de Water, B. and Price, L. S. (2014) 'A 3D in vitro model of differentiated HepG2 cell spheroids with improved liver-like properties for repeated dose high-throughput toxicity studies', *Arch Toxicol,* 88(5), pp. 1083-95.

Reif, R., Karlsson, J., Günther, G., Beattie, L., Wrangborg, D., Hammad, S., Begher-Tibbe, B., Vartak, A., Melega, S., Kaye, P. M., Hengstler, J. G. and Jirstrand, M. (2015) 'Bile canalicular dynamics in hepatocyte sandwich cultures', *Archives of Toxicology,* 89(10), pp. 1861-1870.

Rendic, S. and Guengerich, F. P. (2012) 'Contributions of human enzymes in carcinogen metabolism', *Chem Res Toxicol,* 25(7), pp. 1316-83.

Schindelin, J., Arganda-Carreras, I., Frise, E., Kaynig, V., Longair, M., Pietzsch, T., Preibisch, S., Rueden, C., Saalfeld, S., Schmid, B., Tinevez, J.-Y., White, D. J., Hartenstein, V., Eliceiri, K., Tomancak, P. and Cardona, A. (2012) 'Fiji: an open-source platform for biological-image analysis', *Nature Methods,* 9, pp. 676.

Schofield, C. A., Walker, T. M., Taylor, M. A., Patel, M., Vlachou, D. F., Macina, J. M., Vidgeon-Hart, M. P., Williams, A., McGill, P. J., Newman, C. F. and Sakatis, M. Z. (2021) 'Evaluation of a Three-Dimensional Primary Human Hepatocyte Spheroid Model: Adoption and Industrialization for the Enhanced Detection of Drug-Induced Liver Injury', *Chem Res Toxicol*.

Seo, J. E., Wu, Q., Bryant, M., Ren, L., Shi, Q., Robison, T. W., Mei, N., Manjanatha, M. G. and Guo, X. (2020) 'Performance of high-throughput CometChip assay using primary human hepatocytes: a comparison of DNA damage responses with in vitro human hepatoma cell lines', *Arch Toxicol,* 94(6), pp. 2207-2224.

Shah, U. K., Mallia, J. O., Singh, N., Chapman, K. E., Doak, S. H. and Jenkins, G. J. S. (2018) 'Reprint of: A three-dimensional in vitro HepG2 cells liver spheroid model for genotoxicity studies', *Mutat Res Genet Toxicol Environ Mutagen,* 834, pp. 35-41.

Shaposhnikov, S., Azqueta, A., Henriksson, S., Meier, S., Gaivao, I., Huskisson, N. H., Smart, A., Brunborg, G., Nilsson, M. and Collins, A. R. (2010) 'Twelve-gel slide format optimised for comet assay and fluorescent in situ hybridisation', *Toxicol Lett,* 195(1), pp. 31-4.

Shaposhnikov, S. and Collins, A. (2017) 'Twelve-Gel Comet Assay Format for Quick Examination of DNA Damage and Repair', *Methods Mol Biol,* 1644, pp. 181-186.

Stampar, M., Sedighi Frandsen, H., Rogowska-Wrzesinska, A., Wrzesinski, K., Filipic, M. and Zegura, B. (2020) 'Hepatocellular carcinoma (HepG2/C3A) cell-based 3D model for genotoxicity testing of chemicals', *Sci Total Environ*, pp. 143255.

Stampar, M., Tomc, J., Filipic, M. and Zegura, B. (2019) 'Development of in vitro 3D cell model from hepatocellular carcinoma (HepG2) cell line and its application for genotoxicity testing', *Arch Toxicol,* 93(11), pp. 3321-3333.

Subramanian, K., Owens, D. J., Raju, R., Firpo, M., O'Brien, T. D., Verfaillie, C. M. and Hu, W. S. (2014) 'Spheroid culture for enhanced differentiation of human embryonic stem cells to hepatocyte-like cells', *Stem Cells Dev,* 23(2), pp. 124-31.

Sussman, N. L., Chong, M. G., Koussayer, T., He, D.-E., Shang, T. A., Whisennand, H. H. and Kelly, J. H. (1992) 'Reversal of fulminant hepatic failure using an extracorporeal liver assist device', *Hepatology,* 16(1), pp. 60-65.

Terashima, J., Goto, S., Hattori, H., Hoshi, S., Ushirokawa, M., Kudo, K., Habano, W. and Ozawa, S. (2015a) 'CYP1A1 and CYP1A2 expression levels are differentially regulated in three-dimensional spheroids of liver cancer cells compared to two-dimensional monolayer cultures', *Drug Metabolism and Pharmacokinetics,* 30(6), pp. 434-440.

Terashima, J., Goto, S., Hattori, H., Hoshi, S., Ushirokawa, M., Kudo, K., Habano, W. and Ozawa, S. (2015b) 'CYP1A1 and CYP1A2 expression levels are differentially regulated in three-dimensional spheroids of liver cancer cells compared to two-dimensional monolayer cultures', *Drug Metab Pharmacokinet,* 30(6), pp. 434-40.

Tomizawa, M., Shinozaki, F., Motoyoshi, Y., Sugiyama, T., Yamamoto, S. and Ishige, N. (2017) 'Hepatocyte selection medium-enriched hepatocellular carcinoma cells are positive for alpha-fetoprotein and CD44', *Oncol Lett,* 14(1), pp. 899-902.

Tostões, R. M., Leite, S. B., Serra, M., Jensen, J., Björquist, P., Carrondo, M. J. T., Brito, C. and Alves, P. M. (2012) 'Human liver cell spheroids in extended perfusion bioreactor culture for repeated-dose drug testing', *Hepatology,* 55(4), pp. 1227-1236.

van Wenum, M., Adam, A. A., Hakvoort, T. B., Hendriks, E. J., Shevchenko, V., van Gulik, T. M., Chamuleau, R. A. and Hoekstra, R. (2016) 'Selecting Cells for Bioartificial Liver Devices and the Importance of a 3D Culture Environment: A Functional Comparison between the HepaRG and C3A Cell Lines', *Int J Biol Sci,* 12(8), pp. 964-78.

Vinken, M. and Hengstler, J. G. (2018) 'Characterization of hepatocyte-based in vitro systems for reliable toxicity testing', *Arch Toxicol,* 92(10), pp. 2981-2986.

Vorrink, S. U., Ullah, S., Schmidt, S., Nandania, J., Velagapudi, V., Beck, O., Ingelman-Sundberg, M. and Lauschke, V. M. (2017) 'Endogenous and xenobiotic metabolic stability of primary human hepatocytes in long-term 3D spheroid cultures revealed by a combination of targeted and untargeted metabolomics', *FASEB J,* 31(6), pp. 2696-2708.

Waxman, D. J. and Chang, T. K. (2006) 'Use of 7-ethoxycoumarin to monitor multiple enzymes in the human CYP1, CYP2, and CYP3 families', *Cytochrome P450 Protocols*: Springer, pp. 153-156.

Westerink, W. M. and Schoonen, W. G. (2007) 'Phase II enzyme levels in HepG2 cells and cryopreserved primary human hepatocytes and their induction in HepG2 cells', *Toxicol In Vitro,* 21(8), pp. 1592-602.

Wickham, H., Averick, M., Bryan, J., Chang, W., McGowan, L., François, R., Grolemund, G., Hayes, A., Henry, L., Hester, J., Kuhn, M., Pedersen, T., Miller, E., Bache, S., Müller, K., Ooms, J., Robinson, D., Seidel, D., Spinu, V., Takahashi, K., Vaughan, D., Wilke, C., Woo, K. and Yutani, H. (2019) 'Welcome to the Tidyverse', *Journal of Open Source Software,* 4(43).

Wilkening, S., Stahl, F. and Bader, A. (2003) 'Comparison of primary human hepatocytes and hepatoma cell line Hepg2 with regard to their biotransformation properties', *Drug Metab Dispos,* 31(8), pp. 1035-42.

Wrzesinski, K., Magnone, M. C., Hansen, L. V., Kruse, M. E., Bergauer, T., Bobadilla, M., Gubler, M., Mizrahi, J., Zhang, K., Andreasen, C. M., Joensen, K. E., Andersen, S. M., Olesen, J. B., Schaffalitzky de Muckadell, O. B. and Fey, S. J. (2013) 'HepG2/C3A 3D spheroids exhibit stable physiological functionality for at least 24 days after recovering from trypsinisation', *Toxicology Research,* 2(3), pp. 163-172.

Xuan, J., Chen, S., Ning, B., Tolleson, W. H. and Guo, L. (2016) 'Development of HepG2-derived cells expressing cytochrome P450s for assessing metabolism-associated drug-induced liver toxicity', *Chem Biol Interact,* 255, pp. 63-73.

Ye, J., Coulouris, G., Zaretskaya, I., Cutcutache, I., Rozen, S. and Madden, T. L. (2012) 'Primer-BLAST: a tool to design target-specific primers for polymerase chain reaction', *BMC bioinformatics,* 13(1), pp. 134.

Zanoni, M., Piccinini, F., Arienti, C., Zamagni, A., Santi, S., Polico, R., Bevilacqua, A. and Tesei, A. (2016) '3D tumor spheroid models for in vitro therapeutic screening: a systematic approach to enhance the biological relevance of data obtained', *Sci Rep,* 6, pp. 19103.

Zhang, J. H., Chung, T. D. and Oldenburg, K. R. (1999) 'A Simple Statistical Parameter for Use in Evaluation and Validation of High Throughput Screening Assays', *J Biomol Screen,* 4(2), pp. 67-73.

Zhang, K., Zhang, L., Liu, W., Ma, X., Cen, J., Sun, Z., Wang, C., Feng, S., Zhang, Z., Yue, L., Sun, L., Zhu, Z., Chen, X., Feng, A., Wu, J., Jiang, Z., Li, P., Cheng, X., Gao, D., Peng, L. and Hui, L. (2018) 'In Vitro Expansion of Primary Human Hepatocytes with Efficient Liver Repopulation Capacity', *Cell Stem Cell,* 23(6), pp. 806-819 e4.

3.8. Addendum to Chapter 3

Declaration

This data is presented as an addendum to this thesis chapter and has not been published as part of Coltman et al ., 2021, DOI: 10.1016/j.toxlet.2021.04.004. Datasets were generated post-publication but as part of this thesis results chapter.

3.8.1. Materials and methods

All materials and methods as in main chapter

Table 3.3. Additional Primers used for gene expression analysis by qPCR.

Gene symbol	Gene ID	Forward primer	Reverse primer
18S	18S RNA	GTAACCCGTTGAACCCCATT	CCATCCAATCGGTAGTAGCG
ACTB	beta actin	ACTCTTCCAGCCTTCCTTCC	GTTGGCGTACAGGTCTTTGC
GAPDH	glyceraldehyde 3-phosphate dehydrogenase	CACTAGGCGCTCACTGTTCT	GCCCAATACGAC CAAATCCGT
AFP	alpha foetal protein	TTTTGGGACCCGAACTTTCC	CATCCTGCAGACAATCCAGC
ARNT	aryl hydrocarbon receptor nuclear translocator	CTACTGCCAACCCCGAAATG	CCGCTTAATAGCCCTCTGGA
CYP2C19	cytochromes P450 2C19	GCAGCTGACTTACTTGGAGC	TGTATCTCTGGACCTCGTGC
CYP2C9	cytochromes P450 2C9	CAGAGACGACAAGCACAACC	TGTATCTCTGGACCTCGTGC
CYP2D6	cytochromes P450 2D6	CATCACCAACCTGTCATCGG	GCAGGGAGGTGAAGAAGAGG
CYP2E1	cytochromes P450 2E1	AATTGACAGGGTGATTGGGC	AAAATGGTGTCTCGGGTTGC
CYP3A4	cytochromes P450 3A4	CTGGCTATGAAACCACGAGC	TGAGCGTTTCATTCACCACC
HNF1A	hepatocyte nucelar factor 1	CTTGGCTAGTGGGGTTTTGG	CTGGATCAGTGCCTCTTTGC
HNF4A	hepatocyte nucelar factor 4	AAGAATGGTGTGGGAGAGGG	AGCCTCATTACTCTCACCCG
MKI67	antigen KI67	ACTCCAAAGAAGCCTGTGGG	AGTTGTTGAGCACTCTGTAGGG
NQO1	NAD(P)H dehydrogenase [quinone] 1	GGACTGCACCAGAGCCAT	TCCTTTCTTCTTCAAAGCCG
NRF2	nuclear factor erythroid 2-related factor 2	ACCAAAACCACCCTGAAAGC	AGGCCAAGTAGTGTGTCTCC

3.8.1.1. Use of coumarin to as a potential substrate for CYP1A activity in HepG2/C3A spheroids

To measure potential CYP1A activity in spheroids, the approaches by Donato et al. (2004), Wilkening et al. (2003), for the development of fluorogenic CYP450 assays in PHHs and HepG2 cells, were adapted for use with HepG2/C3A spheroids grown for 7 days. In order to assess the quantity of protein and therefore the number of spheroids, required, 10, 15, 20 or 25 spheroids were carefully removed from cell culture after 7-days of growth, pooled and suspended into microplate wells containing 300 μL of incubation buffer (1 mM Na_2HPO_4, 137 mM NaCl, 5 mM KCl, 0.5 mM, $MgCl_2$, 2 mM $CaCl_2$, 1g/L matched glucose, and 10 mM Hepes), which was buffered to pH 7.4. Spheroids were then incubated with titrations of 7-ethoxycoumarin at 0, 10 or 50 μM (0.5 % maximum DMSO vehicle content in incubation buffer) and kinetic readings taken over 120 mins by micro sampling of fluorescent product and measurement 355_{EX} – 450_{EM} nm in black-walled microplates using a plate reader and background correction performed. Data is only representative of two independent experiments (n=2).

3.8.2. Addendum results

3.8.2.1. Expansion of gene sets induced in HepG2/C3A spheroids compared to monolayer cultures

The gene list published in **Chapter 3** was expanded to include other targets related to the development of a hepatic phenotype in HepG2/C3A spheroids (Figure 3.14). Related to hepatic maturation, hepatic nuclear factor 4 alpha (*HNF4A*) was significantly upregulated in spheroids by more than 2.3-fold, but not *HNF1A*. Expression of another marker of hepatic

differentiation, alpha-1-fetoprotein (*AFP*) was increased more than 4.9-fold in HepG2/C3A spheroids but not the cellular proliferation marker (*MKI67*) - Figure 3.14A. Five further genes which form the major suite of CYP450 enzymes responsible for the majority of prescribed xenobiotics were screened for relative mRNA expression (Figure 3.14B). CYP isoforms *2C19* and *2E1* were not induced however, *CYP2D6* had favourable expression in spheroids by more than 1.83-fold indicating enrichment. Strikingly, both *CYP2C9* and *CYP3A4* had upregulated expression in the spheroid equivalent to more than 30.8- and 10.8-fold, respectively compared to monolayers. Strangely however, in line with a lack of expression of the aryl hydrocarbon receptor (*AhR)*, its nuclear translocator (*ARNT*) was not significantly expressed in spheroids, similarly, linked genes nuclear factor erythroid 2-related factor (*NRF2*) and NAD(P)H dehydrogenase [quinone] 1 (*NQO1*), related to the xenobiotic response element pathway as mediators of the oxidative stress response, were also not induced in spheroids.

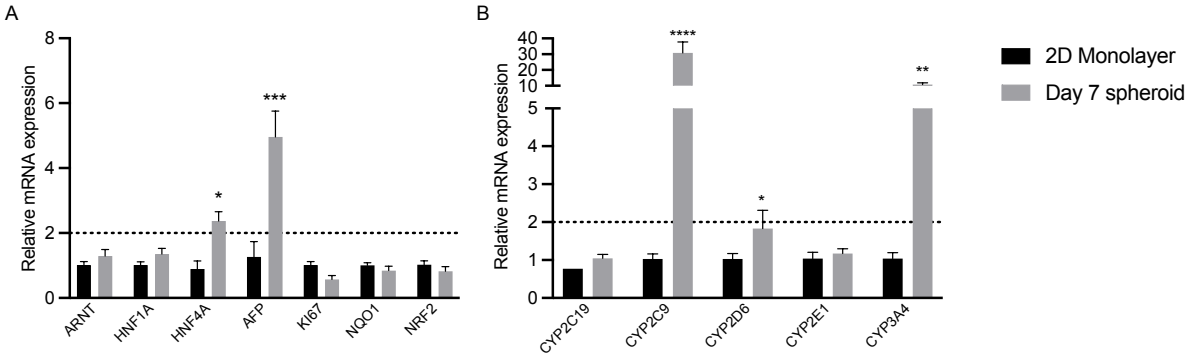

Figure 3.14. Expression of selected genes in HepG2/C3A spheroids related to hepatocyte differentiation and xenobiotic metabolism*. Markers of hepatic differentiation (A) and major CYP450 isoforms responsible for xenobiotic metabolism (B) were between HepG2/C3A cells cultured in monolayers (2D) or spheroids (3D) grown for 7 days by qPCR. Upregulated and downregulated genes were determined by a ≥1.5-fold increase or ≤0.5-fold decrease in mRNA expression, respectively. Data shown as mean of 4 independent samples (n=4). Statistical significance determined by student's t test with Benjamini-Hochberg correction for multiple testing: ****, P<0.00001; ***, P<0.0001; **, P<0.001; *, P<0.05; ns, P>0.05.*

3.8.2.2. Development of an assay to study CYP1A-mediated O-deethylation of 7-ethoxycoumarin

In the published **Chapter 3**, we revealed that both *CYP1A1* and *CYP1A2* genes were basally upregulated in HeG2/C3A spheroids, and further induced in those exposed to genotoxicants. We therefore sought to develop an assay capable of measuring this response as the protein level. 7-ethoxycoumarin (7-EC) is a non-fluorescent substrate for the CYP1A family of xenobiotic metabolism enzymes which is deeethylated to 7-hydroxycoumarin, allowing for fluorescence shift to be measured by fluorimetry over time in pooled spheroids (**Figure 3.15**). Incubation with the vehicle control did not increase the arbitrary fluorescence signal in any of the spheroid conditions, however incubation with even 10 μM of coumarin was sufficient to yield an arbitrary signal within 15 minutes of incubation with linearised reaction rate. A pool of 10 spheroids was enough to raise the reaction output above background control where fluorescence intensity continued to increase over 45-60 mins before plateauing, suggesting a kinetic yield of fluorescent metabolite and complete enzymatic saturation. On average the number of fluorescence units increased with the number of incubated spheroids. This was also the case in spheroids incubated with 50 μM of the substrate however 5-fold increase in substrate concentration only yielded and additional 29 % of total assay output. Intriguingly, in a pool of 10 spheroids, the arbitrary signal began to decline after approximately 75 minutes of reaction time, perhaps suggesting further conversion to a non-fluorescent chemical moiety or non-stabilised signal but this was not seen elsewhere.

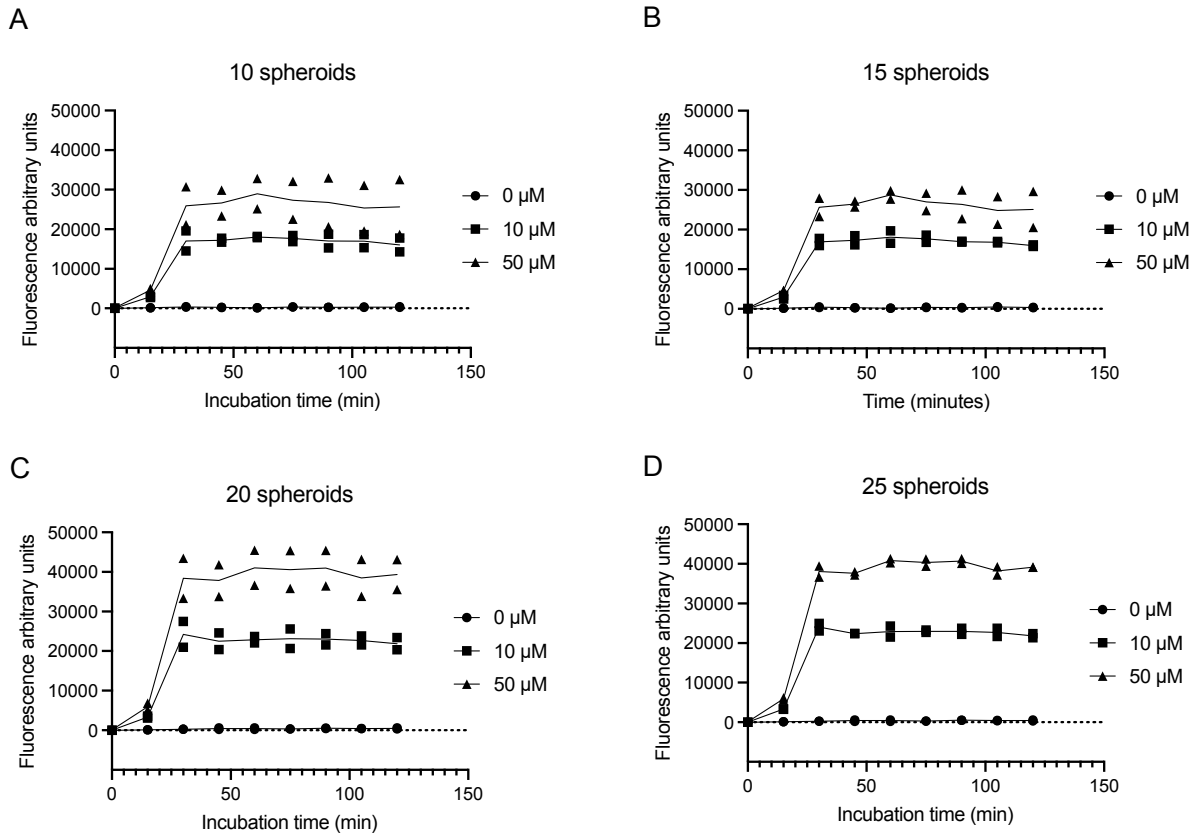

Figure 3.15. Time course of an arbitrary fluorescent signal suggested from the 7-hydroxycouamrin metabolite from 7-EC, in pooled HepG2/C3A spheroids. *Pooled spheroids were incubated in a reaction buffer containing 0, 10 or 50 μM coumarin for up to 120 mins and the generated signal measured fluorometrically. Data corresponds to n=2 per concentration, with both replicates shown.*

3.8.3. Addendum discussion

Chapters 2 and 3 have shown that culture of HepG2/C3A cells as spheroids appears to slow the proliferation rate of cells over time, compared against monolayers over a total of 28 days in culture, as evidenced by an initial increase in spheroid size before reaching a plateau around 2-3 weeks of cultivation (**Chapter 3, Figure 3.1**). Unlike the HepG2 parental cell line that are extensively proliferative in monolayer form, often forming quasi-spheroids or

cellular aggregates at full confluency, the HepG2/C3A clone does have an initial exponential phase of cellular replication which slows over time as cell cluster together, in such a way as to promote the notion of 'contact inhibition'. In the development study (**Chapter 2**) it was found that HepG2/C3A did indeed form more promising spheroids versus HepG2 parent resulting in more-compact spheroids with a smaller diameter compared to HepG2 spheroids which appeared to continue to proliferate. Surprisingly, a common marker of cellular proliferation (*MKI67*) was not found to be differentially expressed between HepG2/C3A monolayers and spheroids. Lima et al. (2018) showed that treatment of HepG2 cells with the antioxidant octyl gallate markedly reduced cellular ATP synthesis and stalled cell-cycle progression, suppressed Ki67 and pushed cells into apoptosis (Lima et al., 2018), indicating that HepG2 grown as monolayers are highly energetic and reliant on a high-turnover of ATP. In line with this, **Chapter 5** reveals that normalised (dsDNA) cellular ATP content is indeed higher in monolayers versus spheroids grown for 7 – 28 days, suggesting that cells grown in monolayers are still very much within the normal cell-cycle and in a highly metabolic state. In line with this, the doubling time of HepG2/C3A cells transitioning between monolayers and spheroids is rapidly reduced and further reduced across spheroids grown over 28 days, even though spheroid size continues to steadily increase. However, it is not clear at this stage as to how this marker is maintained throughout longer period of HepG2/C3A spheroid culture. Another marker of differentiation, *AFP* was found to be upregulated in spheroids versus monolayers which is typically suppressed in mature hepatocytes (Tomizawa et al., 2017, Cipriano et al., 2017), suggesting that HepG2/C3A spheroids are still on a lineage of maturation by comparison to monolayers, in line with this, we found *ALB* expression continued across spheroids cultured for up to 28 days (**Chapter 3, Coltman et al., 2021**).

Surprisingly, it was also found that *CPS1* as one of the first putative steps of the urea cycle, was upregulated in spheroids though this does not necessarily confer urea cycle function. The exact deduction as to why HepG2/C3A cells grow in this way and achieve greater refined spheroids than their parent cell line remains unclear and evidently warrants further attention, however it would seem likely that proteins functioning as signalling regulators for the cell cycle, growth a proliferation of hepatocellular carcinoma cells are, in some way, differentially expressed in the HepG2/C3A cell line and not HepG2.

HNF4A is considered a master transcriptional regulator of many hepatic systems, particularly those relating to xenobiotic metabolism (Kamiyama et al., 2007), with particular regulation of downstream nuclear receptors *PXR* and *CAR,* whereas *AhR* is typically induced by xenobiotics such as PAHs (Larigot et al., 2018) which would account for its absence at the basal transcriptional level, but induced in spheroids exposed to B[a]P, for example (Chapter 3, Coltman et al., 2021). Many of the ADME genes screened by qPCR in HepG2/C3A had preferential expression compared to related pathways, for example *NAT2* was upregulated but not *NAT1, CYP2C9* was significantly upregulated but not the isoform *2C19,* and likewise there was significant upregulation of UGT-encoding genes and not SULTs. It would therefore seem obvious that divergence away from monolayers of cells promotes pathway-specific events in HepG2/C3A spheroids and an expansion of specific endogenous pools of those enzymes identified, perhaps by epigenetic cues (Cipriano et al., 2017). Regarding these specific enzyme expressions in spheroids, although high mRNA does not always necessarily reflect enzyme protein formed, of course. We therefore attempted to monitor the metabolic conversion of the pro-fluorescent substrate, 7-EC as the major substrate for the

CYP1A family but also a minor substrate for CYP2 and CYP3 families (Waxman and Chang, 2006). Therefore we devised a method using the simple pro-fluorometric substrate, 7-EC, to assess potential CYP450 enzymatic function in 3D spheroids, similarly ethoxyresorufin O-deethylation (EROD) has also been used to measure CYP1A activity in hepatic monolayers of cells and isolated microsomes (Donato et al., 1993) and in spheroids (Subramanian et al., 2014). The rationale behind developing an assay of this kind was due to the inherent ease, flexibility and efficiency with which assay development could take place compared to the gold standard liquid-chromatography mass spectrometry (LC-MS/MS), or even diode-array based HPLC. The CYP1A superfamily of enzymes is responsible for the metabolism of large percentage of pharmaceuticals such as acetaminophen, as well as polycyclic aromatic hydrocarbons (PAH) such as B[a]P. Using a similar approach, Shah et al. (2018) found that metabolic conversions of luciferin-conjugated 6-chloroethyl ether (CYP1A1) and 6-ethyl ether (CYP1A2) activity was enhanced in HepG2 spheroids using these commercially-available luminogenic probes when compared to monolayers, and further induced on exposure to genotoxic compounds; however the induction of CYP1A activity was seemingly lower in HepG2 spheroid compared to HepaRG spheroids (Ott et al., 2017) or spheroids formed from hepatic stem cells (Lucendo-Villarin et al., 2020) using the same technology. One aspect of this study design that was not considered was the potential for 7-EC to be further transformed by glucuronidation of sulphation (Feng et al., 2018). For example in **Chapter 3, Coltman et al., 2021** it was found that basal mRNA expression of the UGT1A family (1A3, 1A1, and 1A6) were significantly higher in HepG2/C3A spheroids versus monolayers, and further induced on exposure to the B[a]P small molecule; UGT and SULT enzymes are also known to be inducible in HepG2 cells (Westerink and Schoonen, 2007) and

pooled HepG2/C3A spheroids (Gaskell et al., 2016, Wrzesinski et al., 2013) which may, in part explain for the reduction in the fluorescence signal after 1h of incubation, though within 1h this would seem unlikely. It may also be conceivable that the substrate was exported from the spheroid after the initial linear increase in signal as part of protective mechanism against cytotoxicity; whilst the main route of metabolism for coumarins is by 7-hydroxylation, the formation of a DNA or protein-reactive epoxide intermediate of the lactone ring may also be possible (Lake et al., 1994, Lake et al., 1989). Indeed, permeability of compounds across the spheroid diameter may also have implicated the results generated from the assay whereby the accumulating fluorescent metabolite was trapped within the spheroid; for example in **Chapter 4** penetration kinetics of the small molecule oligomycin, significantly influenced assay sensitivity when monitoring spheroid metabolism but not in monolayers of HepG2/C3A, which was similarly recapitulated in **Chapter 5** using spheroids of varying diameter. Schofield et al. (2021) found the depletion of 7-EC to be maintained throughout a 14-day PHH spheroid culture period which may suggest a longer incubation time was required to enable steady-state kinetics of 7-EC metabolism. Although they only monitored loss of parent structure thus conjugation to secondary metabolite was not confirmed but viability of PHH was not diminished during that time suggesting that accumulating hydroxy metabolites were exported from the spheroid (Schofield et al., 2021). Similarly, Tostões et al. (2012) also found that the metabolic-turnover of 7-EC was continuous over 48 h in perfused hepatic spheroids which further induced on exposure to rifampicin, for example, suggesting that fluid dynamics may aid in achieving total bioavailability across spheroid structures. A derivative of the pro-fluorescent fluorescein diacetate has been used in a number of hepatic spheroids models to confirm apical

membrane drug transport (Gaskell et al., 2016), (Kyffin et al., 2019a, Reif et al., 2015) as well as enhanced expression of BSEP, however mRNA expression could not be confirmed in the current C3A spheroid (Coltman et al., 2021) and hence its unclear as to how this could impact the data presented. Taken together however, it is suggested that 7-EC may serve as a stable substrate for monitoring CYP1A enzymatic activity in hepatic spheroids. The study presented here was only monitored over 120 mins and hence it's not clear as to whether CYP1A activity and metabolic conversion of 7-EC would continue in HepG2/C3A spheroids beyond this time point. In this study it appeared that as few as 10 HepG2/C3A spheroids at day 7, equating to approximately 7-8 x 10^4 cells, was sufficient to achieve an assay response; similarly Nishikawa et al. (2017) found that EROD activity at 10 μM substrate was enhanced in pooled HepG2 spheroids versus monolayers, equating to 35-9 spheroids [8 x 10^4 total cells] but such guidance is not reported by Shah et al. (2018). Observing common hepatic spheroid culture techniques in the literature, hepatic spheroids are often pooled in order to assess xenobiotic metabolism, even by LC-MS/MS (Hendriks et al., 2020, Bell et al., 2020, Kyffin et al., 2019b, Vorrink et al., 2017). Typically in the order to 5-15 spheroids per reaction, this approach is inherently lower throughout than the preparation of cell monolayers in such experiments. Nevertheless, it has been surmised that HepG2/C3A spheroids appear to biotransform coumarin to its fluorescent metabolite, demonstrative of CYP1A activity in the spheroid model but also potentially CYP2 and CYP3 activity which is in-line with observations made by Gaskell et al. (2016) and (Terashima et al., 2015b). How this compares to 2D monolayers was beyond the scope of studies here and indeed enzymatic activity could be further confirmed by addition of pan-CYP450 inhibitory substrates such as ketoconazole. Notwithstanding these results, the data from the first three chapters of this

thesis suggests that CYP1A activity is indeed evidenced in HepG2/C3A spheroids, however it is acknowledged that the ability to multiplex several substrates for multiple CYP targets would be advantageous (Nelson et al., 2017, Pillai et al., 2013), in such regard, the development of a suitable method by LC-MS/MS is needed which would improve the sensitivity of small-molecule metabolism assays presented here, whilst simultaneously monitoring for loss of parent and gain of metabolites, using control metabolite standards. **Appendix 3** of this thesis describes a work in progress study which due to the impact of Covid-19, is awaiting the acquisition of LC-MS/MS data. This study aims to assess HepG2/C3A CYP450 (1A2, 2C9, 2C19, 2D6 AND 3A4) biotransformation capacity in spheroids cultivated over 28 days and compared to monolayers over several timepoints.

Chapter 4. OPTIMISED PROTOCOLS TO EXPLORE MITOCHONDRIAL ENERGY METABOLISM OF SINGLE 3D MICROTISSUE SPHEROIDS USING EXTRACELLULAR FLUX ANALYSIS

Declaration

The data presented in this chapter has been accepted for publication in Journal of Visualised Experiments (Coltman N.J et al., 2021, DOI: 10.3791/63346) and reproduced here in verbatim including supplementary documents. However, a summary of the materials and methods used in this chapter are provided in their original published form, appended to this thesis as **Appendix 2**.

Author declarations

N.J.C was involved in all facets of this research and conducted all experimental design, data collection and analyses described. J.P Barlow provided a bespoke analysis script and contributed to the analyses of advanced XF datasets. Throughout this research, N.J.C was supported G. Rochford, N.J. Hodges., H. Ali-Boucetta, H , and J. P. Barlow.

Acknowledgements and funding sources

N.J.C was supported by a BBSRC MIBTP CASE studentship award (BB/M01116X/1, 1940003). The authors acknowledge the financial support of a BBSRC CASE Studentship Award [BB/M01116X/1, 1940003].

4.1. Abstract

Three-dimensional (3D) cellular aggregates, termed spheroids have become the forefront of *in vitro* cell culture in recent years. In contrast to culturing cells as two-dimensional single cell monolayers (2D culture), spheroid cell culture promotes, regulates, and supports physiological cellular architecture and characteristics that exist *in vivo*, including expression of extracellular matrix proteins, cell signalling, gene expression, protein production, differentiation, and proliferation. The importance of 3D culture has been recognised in many research fields including oncology, diabetes, stem cell biology and tissue engineering. Over the last decade, improved methods have been developed to produce spheroids and assess their metabolic function and fate. Agilent Seahorse Extracellular Flux (XF) Analysers have been used to explore mitochondrial function in 3D microtissues such as spheroids using either an XF24 islet capture plate or XFe96 spheroid microplate. However distinct protocols, and the optimisation of approaches for probing mitochondrial energy metabolism in spheroids using XF technology have not been defined in detail. In this manuscript we provide detailed protocols of how to probe mitochondrial energy metabolism from 3D spheroids in XFe96 spheroid microplates using the XFe96 XF analyser. Using different cancer cell lines, we highlight that XF technology is capable of distinguishing between cellular respiration in 3D spheroids of not only different size but also different volume, cell number, DNA content and type. The optimal mitochondrial effector compound concentrations of oligomycin, BAM15, rotenone, and antimycin A are used to probe specific parameters of mitochondrial energy metabolism in 3D spheroids. We also discuss methods to normalise XF data obtained from spheroids and address many considerations that should be considered when exploring

spheroid metabolism using XF technology. This protocol will help drive research in advanced *in vitro* spheroid models.

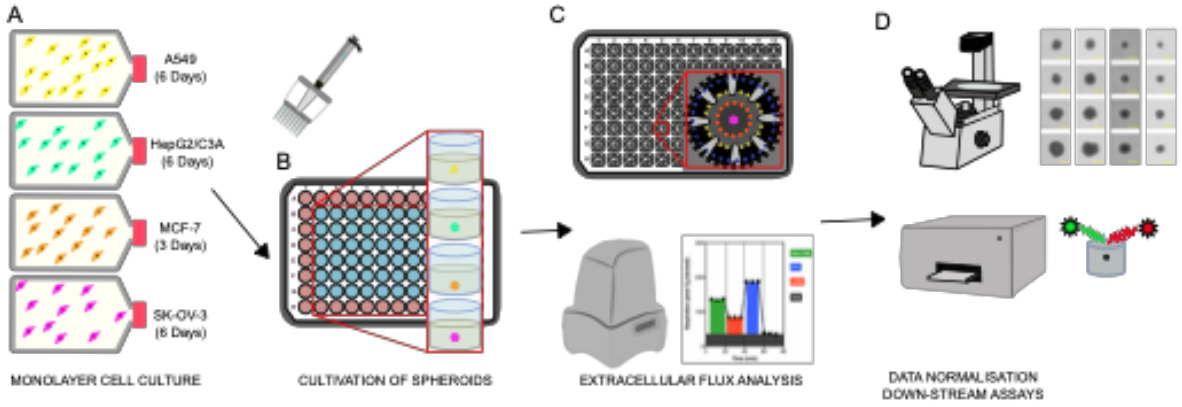

Figure 4.1. Graphical workflow for the generation of cellular spheroids, extracellular flux analysis and downstream assays. *Four cancer cell lines were selectively cultured as monolayers (A), detached from tissue culture flasks, seeded into ultra-low attachment 96-well microplates to form spheroids (B). A549 lung carcinoma, HepG2/C3A liver carcinoma, SK-OV-3 ovarian adenocarcinoma and MCF-7 breast carcinoma cells were seeded at 1 - 8x10^3 cells/well and grown up to 7 days to form single spheroids, and to optimise spheroid seeding density and cultivation time by use of continuous observation and planimetric measurements. Once formed, single spheroids were washed into a serum-free XF medium and carefully seeded into XFe96 spheroid assay microplates, pre-coated with poly-D-lysine (C). Spheroids were subjected to extracellular flux analysis using the XFe96 analyser using several protocols to address: (1) optimum spheroid size for basal mitochondrial respiration response; (2) optimised titration of mitochondrial respiratory inhibitors; (3) optimisation of spheroid placement within microplate wells. (D) Post-XF analyses, phase contrast microscopy and spheroid DNA quantification were used for data normalisation and other downstream in vitro assays.*

4.2. Introduction

Advances of *in vitro* models in biological research have rapidly progressed over the last 20 years. Such models now include organ-on-a-chip modalities, organoids and three-dimensional (3D) microtissue spheroids. All of which have become a common focus to improve the translation between *in vitro* and *in vivo* studies. The use of advanced *in vitro* models, particularly spheroids, spans several research fields including tissue engineering, stem cell research, cancer and disease biology (Correa de Sampaio et al., 2012, Amann et al., 2014, Russell et al., 2017, Zanoni et al., 2016, Song et al., 2018, Courau et al., 2019, Ivanova et al., 2020), and safety testing including genetic toxicology (Mandon et al., 2019, Stampar et al., 2020, Coltman et al., 2021), nano materials toxicology (Tchoryk et al., 2019, Leite et al., 2019, Elje et al., 2020, Conway et al., 2020), drug safety and efficacy testing (Wang et al., 2015, Proctor et al., 2017, Mandon et al., 2019, Basharat et al., 2020, Benning et al., 2020, Mittler et al., 2017).

Normal cell morphology is critical to biological phenotype and activity. Culturing cells into 3D microtissue spheroids allow cells to adopt a morphology, phenotypic function, and architecture, more akin to that *in vivo* which are difficult to capture with classical monolayer cell culture techniques. Both *in vivo* and *in vitro,* cellular function is directly impacted by the cellular microenvironment which is not limited to: cellular communication and programming (e.g., cell-cell junction formations, opportunities to form cell niches); cell exposure to hormones and growth factors in the immediate environments (e.g., cellular cytokine exposure as part of an inflammatory response); composition of physical and chemical matrices (e.g., are cells grown in stiff tissue culture plastic or in an elastic tissue

environment) and most importantly, how cellular metabolism is impacted by nutrition and access to oxygen as well as the processing of metabolic waste products such as lactic acid.

Metabolic flux analysis is a powerful way to examine cellular metabolism within defined *in vitro* systems. Specifically, extracellular flux (XF) technology allows for the analysis of live, real-time changes in cellular bioenergetics of intact cells and tissues. Datasets can be concurrently collected that allow extracellular acidification rate (ECAR) to be calculated as a function of glycolytic flux and oxygen consumption rate (OCR) to determine oxidative phosphorylation and thus mitochondrial function. Given that many intracellular metabolic events occur within the order of seconds to minutes, real-time functional approaches are paramount for understanding real-time changes in cellular metabolic flux in intact cells and tissues *in vitro*. In this manuscript, we provide protocols for cultivating cancer-derived cell lines A549 (lung adenocarcinoma), HepG2/C3A (hepatocellular carcinoma), MCF-7 (breast adenocarcinoma) and SK-OV-3 (ovarian adenocarcinoma) as *in vitro* 3D spheroid models using forced-aggregation approaches. We also (i) describe in detail how to probe mitochondrial energy metabolism of single 3D spheroids using the Agilent XFe96 XF analyser, (ii) highlight ways to optimise XF assays using single 3D spheroids, and (iii) discuss important considerations and limitations of probing 3D spheroid metabolism using this approach.

4.3. Lay summary of materials and methods used in study

Declaration: A summary of methods used in this study is presented below and outlined pictorially in Figure 4.1. This summary is not published. Full methods which are published as part of this protocol are appended to this thesis (**Appendix 3)**, taken in verbatim in their original imperative language.

4.3.1. Cell culture and cultivation of spheroids

A549, MCF-7 and SK-OV-3 cells were cultured in fully supplemented RPMI medium; HepG2/C3A cells were cultured in low-glucose DMEM as previously described. All cell lines were cultured under standard cell culture condition, regularly assessed for mycoplasma contamination, and passaged a maximum of 25 times. An optimised number of cells were seeded into cell-repellent 96-well microplates, briefly centrifuged at 300 x g, and left to form spheroids at 37 ^{o}C, 5 % CO_2. Optimum spheroids of MCF-7 cells were achieved in only 3 days whereas A549, HepG2/C3A and SK-OV-3 were left for 5 days to achieve spheroids with a clearly defined and maintained cellular structure. In addition, spheroid growth and health were continually assessed by phase contrast miscopy and several parameters, e.g., spheroid volume, circularity, were defined for analyses. In addition, to obtain estimations to spheroid cell number and DNA content, and to be able to normalise assay data acquired from extracellular flux analysis, a method was developed and optimised using dsDNA extracted from lysed spheroids by use of the Quant-iT PicroGreen assay Kit (Life technologies, UK). Owing to their ability to form archetypal spheroids with maintained spherical symmetry, MCF-7 spheroids were used as principal models to which HepG2/C3A, A549 and SK-OV-3, were compared throughout the analyses.

4.3.2. Use of XFe96 technology to measure mitochondrial energy flux in 3D spheroids

A series of optimised experiments using the XFe96 extracellular flux technology (Agilent Technologies, Cheadle, UK) was devised to assess mitochondrial energy metabolism in four different carcinoma-derived cell lines of varying cell number and size in a 96-well plate format. The small molecule respiratory inhibitors used were oligomycin, Bam15 and rotenone-antimycin A. Specific XFe96 spheroid microplates were pre-coated with poly-D lysine adhesive and left to equilibrate prior to use. By use of wide orifice pipette tips, spheroids were carefully transferred to the assay microplates and left to adhere. Accordingly, the XFe96 instrumentation was programmed according to a number of different assays established to assess: basal mitochondrial respiration; optimisation of respiratory inhibitor compound titrations to achieve assay response. and the importance of spheroid placement criteria within the assay plates.

4.3.3. Data and statistical analysis

Advanced analysis of XF datasets was performed using a customised analysis script within Microsoft Excel; assay performance was assessed using the Z' primes formula (Zhang et al., 1999), data were normalised to spheroid DNA content and Statistical analysis performed using GraphPad Prism for Mac. Image analysis was performed using the open source FIJI software (Schindelin et al., 2012).

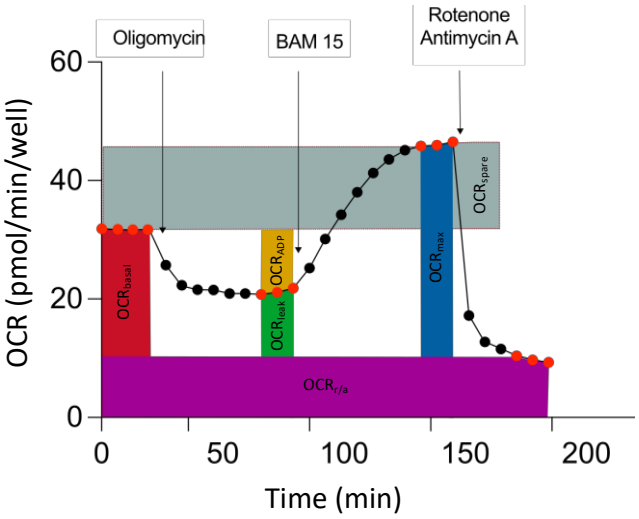

Parameter	Definition	Calculation
OCR_{basal}	Basal mitochondrial respiration is the amount of mitochondrial respiration required to meet the energetic demands of the biological model being measured assuming substrate availability to the cell is not limiting.	$OCR_{basal} = OCR - OCR_{r/a}$
OCR_{ADP}	ADP phosphorylation respiration is the proportion of basal mitochondrial respiration sensitive to oligomycin.	$OCR_{ADP} = OCR_{basal} - (OCR_{omy} - OCR_{r/a})$
OCR_{leak}	Leak respiration is the proportion of basal mitochondrial respiration insensitive to oligomycin.	$OCR_{leak} = OCR_{omy} - OCR_{r/a}$
Coupling efficiency	Coupling efficiency of oxidative phosphorylation is the amount of respiration couple to ATP synthesis, approximated using OCR_{ADP} as a percentage of OCR_{basal}.	$(1- (OCR_{leak}/OCR_{basal})) \times 100$
OCR_{max}	Maximum respiratory capacity is a theoretical maximum rate of mitochondrial respiration that is achieved when phosphorylation control over energy demand is not rate limiting. This is measured by complete uncoupling and thus collapse of the proton gradient using protonophores such as BAM 15, or FCCP.	$OCR_{max} = OCR_{BAM15} - OCR_{r/a}$
OCR_{spare}	Spare respiratory capacity is a metabolic insurance policy of a cell and highlights a theoretical rate of respiration above OCR_{basal} that could be reached for surplus energy demand.	$OCR_{spare} = ((OCR_{max}/OCR_{basal}) -1) \times 100$
$OCR_{r/a}$	Non-mitochondrial respiration is the oxygen consumption remaining in the absence of mitochondrial metabolism, achieved through the complete shutdown of the electron transport chain with inhibitors of respiratory complexes I and III (rotenone–antimycin A).	-

Figure 4.2. Schematic descriptors for parameters derived from extracellular flux data analyses

4.4. Results

4.4.1. Spheroid growth parameters determine baseline mitochondrial respiration

To obtain well-formed, compact spheroids, each cell line was optimized individually for seeding density and duration of cultivation (Figure 4.3). A549, HepG2/C3A, and SK-OV-3 cell lines initially formed loose aggregates that did not progress to round spheroids with clearly defined perimeters until after 7 days in culture. Conversely, MCF-7 cells could form spheroids within 3 days. For all spheroid models, there was clear correlation between original cell seeding density and spheroid volume after the culture period. Spheroid size and morphology were optimized to seeding density. Morphology and circularity began to decline with increased spheroid size in all models. Seeding strategies for cell lines were optimized at 4×10^3 cells/well for A549 and SK-OV-3 cells; HepG2/C3A cells have been previously optimized elsewhere to 1×10^3 cells/well, and MCF-7 cells were used at 4×10^3 cells/well in all assays. At optimized seeding strategies, spheroid volume was between 5.46×10^7 μm^3 (SK-OV-3) and 1.45×10^8 μm^3 (A549) (Figure 4.3B). All spheroid types had linear correlation between original seeding density and spheroid volume where A549 and HepG2/C3A had R^2 values of 0.957 and 0.947, respectively. MCF-7 and SK-OV-3 spheroid volumes were both found to have a greater correlation with original seeding density, R^2=0.977 (Figure 4.3A).

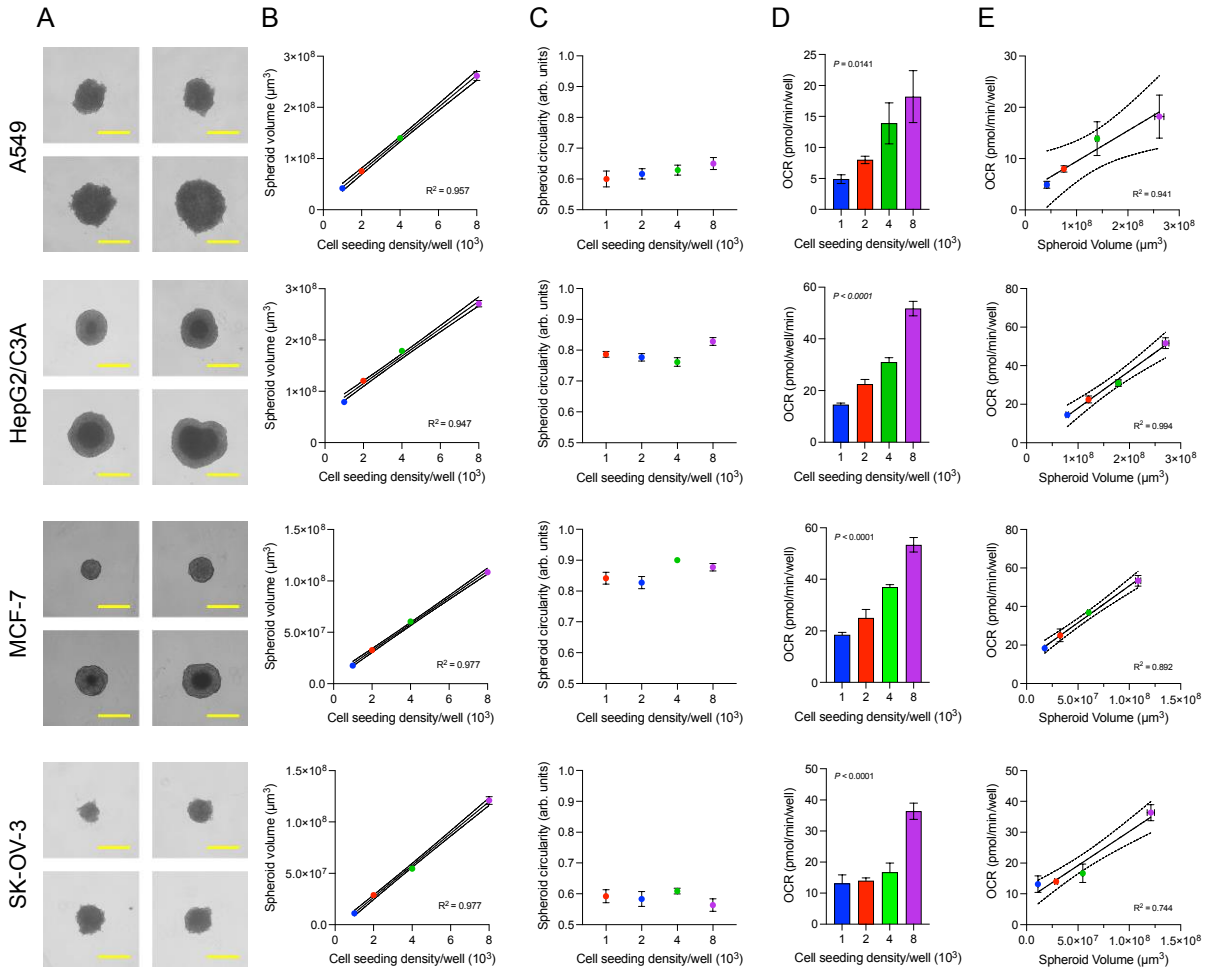

Figure 4.3. Spheroid growth parameters determine baseline mitochondrial respiration. *(A) A549, HepG2/C3A, MCF-7, and SK-OV-3 spheroids were optimized for seeding density and their growth monitored at 1 × 10³, 2 × 10³, 4 × 10³, and 8 × 10³ cells/well in each of the photomicrographs, from upper left to lower right, respectively; scale bars = 500 µm. (B) Spheroid size was calculated using planimetric data from collected photomicrographs and compared using Pearson's correlation statistic; dotted lines represent distribution of 95% confidence interval. (C) Spheroid morphology was compared by calculation of circularity. (D) OCR was measured 5x after which rotenone–antimycin A was added to account for nonmitochondrial respiratory rate using the Agilent Seahorse XFe96 analyzer. OCR_{basal} measured as OCR – $OCR_{r/a}$ was compared between seeding density (D) and spheroid volume (E). Data are averages ± SEM from 5–8 well replicates per spheroid type and cell seeding density. P* values were obtained with one-way ANOVA.

Spheroid circularity was calculated using image planimetry within FIJI analysis software using the long and short spheroid diameters, where perfect spheroid symmetry had circularity =

1.0; deviation from 1.0 indicated a loss of circularity (Figure 4.3C). Circularity was greater in MCF-7 spheroids compared with other models where circularity was maintained between 0.83 and 0.9 at all seeding densities. By comparison, the outer perimeter of SK-OV-3 spheroids was not as clearly defined, and spheroid volume was significantly smaller even after 7 days in culture, yielding spheroids with a maximum circularity of 0.61 at a seeding density of 4×10^3/well. HepG2/C3A cells were also found to form tight, well-formed spheroids with an even morphology across the surface area of all spheroids, with circularity maintained at 0.79 for cells seeded at 1×10^3 cells/well. A549 cells appeared to follow a trend wherein spheroid circularity and morphology were enhanced with seeding density; however, circularity was not greater than 0.63 at the density used in these experiments.

Basal mitochondrial respiration was calculated as OCR measured from spheroids seeded at 1×10^3, 2×10^3, 4×10^3, or 8×10^3 cells/well in ultralow attachment spheroid culture microplates (Figure 4.3D). For all spheroid types, OCR increased with spheroid size and was found to be linearly correlated to spheroid volume with R^2 highest in MCF-7 spheroids at 0.988 and lowest in SK-OV-3 spheroids at 0.744 (Figure 4.3E). The measured OCR was statistically different between all experimental groups. A549 had the lowest OCR, achieving only 18 pmol/min/well at the largest spheroid size (Figure 4.3D). Conversely, MCF-7 spheroids yielded a similar OCR at the smallest spheroid size after only 3 days in culture, reaching a maximum baseline OCR of 53 pmol/min/well for the largest spheroid size (Figure 4.3D). HepG2/C3A yielded OCR data highly consistent with spheroid size and morphology. In HepG2/C3A spheroids seeded from 1×10^3 cells/well, baseline OCR reached an average of 15 pmol/min/well, increasing to a maximum of 52 pmol/min/well in the largest spheroids

(Figure 4.3D). OCR in SK-OV-3 spheroids was only significant between spheroids grown from 4×10^3 cells/well and 8×10^3 cells/well, with limited difference seen in spheroids grown between 1×10^3, 2×10^3, or 4×10^3 cells. Despite size differences, OCR data were highly similar between HepG2/C3A and MCF-7 spheroids at all size points. Relative to spheroid size (μm^3), baseline OCR by MCF-7 spheroids was comparable to that of HepG2/C3A spheroids grown over 7 days from 1,000 cells per well.

4.4.2. Titration of respiratory modulator compounds are an important step for optimizing extracellular flux analysis

The concentration and time course for exposure to respiratory modulators in XF analysis is a critical step in assay optimization. Respiratory modulator compounds—oligomycin, BAM 15, a mixture of rotenone–antimycin A—or a DMSO vehicle control were sequentially injected through the sensor cartridge injection ports into microplate wells containing the MCF-7 spheroids (Figure 4.4).

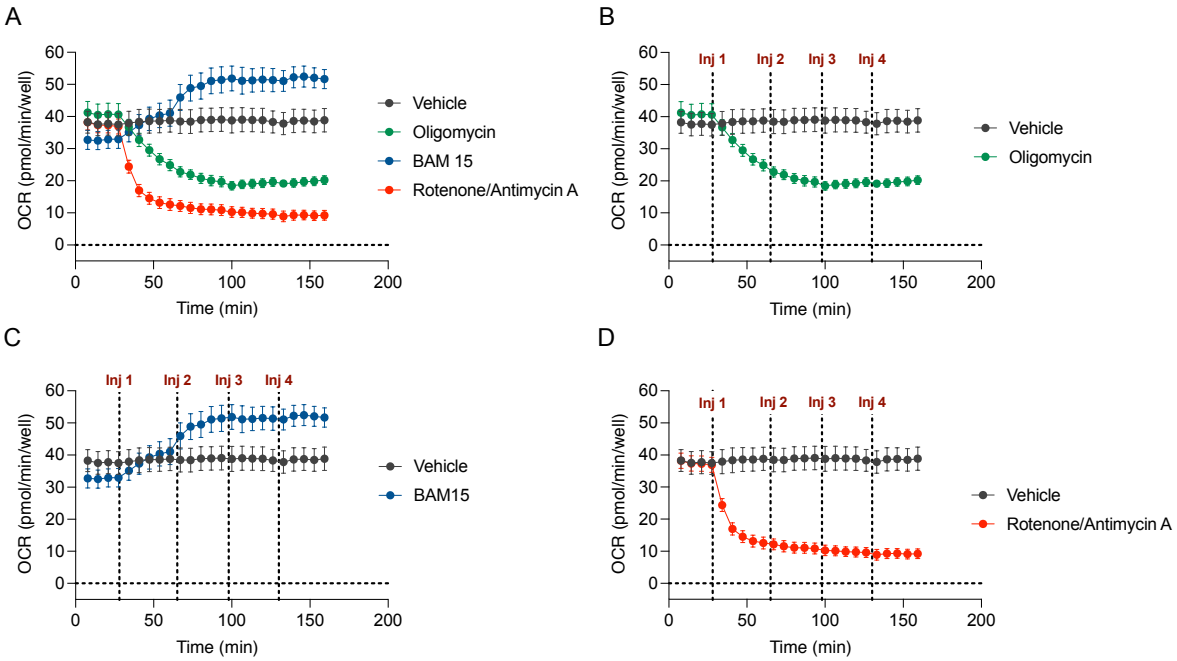

Figure 4.4. Titration of respiratory modulator compounds as an important step for optimizing extracellular flux analysis*. (A) MCF-7 spheroids were seeded at 4 × 10^3 cells/well and cultured over 3 days before being placed in wells of a spheroid assay microplate containing XF RPMI and probed for OCR ± mitochondrial modulators using the XFe96 analyzer. OCR was measured 5x after which titrations of either vehicle control, oligomycin (B), BAM15 (C), or rotenone–antimycin A (D) were added to inhibit mitochondrial ATP synthase, determine maximal respiratory capacity, or establish nonmitochondrial respiratory rate, respectively. The concentration of each mitochondrial modulator was increased over 4 individual titration injection strategies (0.5 µM, 1.5 µM, 3 µM, and 6 µM; units for oligomycin are µg/mL) to determine maximal steady-state OCR in response to optimal compound concentration. OCR was measured for 5 measurement cycles between each injection. Data are averages ± SEM from 5–8 individual well replicates. Abbreviation: OCR = oxygen consumption rate.*

Four measurement cycles were completed to determine the average basal OCR of 30–40 pmol/min/well for all sample groups. For the remainder of the assay duration, respiratory modulators were sequentially added every 5 measurement cycles to achieve final well concentrations of 0.5 µM (0.5 µg/mL oligomycin) after injection 1; 2.0 µM (2 µg/mL

oligomycin) after injection 2; 5 µM (5 µg/mL oligomycin) after injection 3; and finally, a maximum well concentration of 11 µM (11 µg/mL oligomycin) after the fourth sequential addition. MCF-7 spheroids did not respond to the vehicle control throughout the experiment (Figure 4.4A).

Basal OCR immediately changed after the first injection of each respective compound at the lowest concentration of 0.5 µM or 0.5 µg/mL oligomycin (Figure 4.4B). OCR in MCF-7 spheroids was lowered with oligomycin from 41 pmol/min/well to 23 pmol/min/well after 5 measurement cycles following the first injection of 0.5 µg/mL (Figure 4.4B). In response to 0.5 µm BAM 15, OCR was increased from 33 to 41 pmol/min/well before the second injection (Figure 4.4C). Comparatively, the combination of rotenone plus antimycin A lowered OCR from 37 to 13 pmol/min/well before the second injection (Figure 4.4D). Kinetic traces further revealed a steady linear decrease (oligomycin and rotenone–antimycin A) or increase (BAM 15) in OCR. For all compound dosing regimens, a steady-state OCR was achieved within 10–12 complete measurement cycles (60–72 min) at a total well concentration of 2 µM BAM 15, 2 µM rotenone, 2 µM antimycin A, and 2 µg/mL oligomycin (Figure 4.4A). Oxygen consumption rate reached a steady-state plateau at ~19 pmol/min/well (oligomycin), 52 pmol/min/well (BAM 15), and 10 pmol/min/well (rotenone–antimycin A) (Figure 4.4A). Increasing compound concentration of oligomycin, BAM 15, or rotenone plus antimycin A further had no obvious effect on OCR, which remained constant throughout the remainder of the assay. These data demonstrate that both compound concentration and time course of exposure to respiratory modulator compounds should be considered for assay optimization when using 3D spheroids.

4.4.3. Single or sequential injection of mitochondrial respiratory compounds

One of the main benefits of XF technology is the ability to probe mitochondrial function in intact cells and tissues. To examine specific aspects of mitochondrial function in cells and tissues, mitochondrial modulators are added sequentially to wells of the sample microplate through the 4 available injection ports on the sensor cartridge. The typical sequence of modulators used to probe mitochondrial parameters in XF assays are: oligomycin, a protonophore (e.g., FCCP or BAM 15), and a combination of rotenone plus Antimycin A, which are added sequentially to inhibit the mitochondrial ATP synthase, determine maximal respiratory capacity, and correct for nonmitochondrial respiratory rate, respectively. This typical sequence of modulator additions is termed the MitoStress test by the assay technology manufacturer. Given that oligomycin can inhibit uncoupler-stimulated respiration in some cell monolayers (Brand and Nicholls, 2011), we examined this with cancer-derived 3D spheroids by measuring uncoupled-stimulated OCR (OCR_{max}) before (single) and after (sequential) oligomycin injection (Figure 4.5A–D). OCR_{max} was not significantly limited by the addition of oligomycin in spheroids formed from HEPG2/C3A or SK-OV-3 (Figure 4.5E and Figure 4.5G). However, OCR_{max} was significantly lowered in A549 and MCF-7 spheroids following a sequential injection of BAM15 after oligomycin compared to OCR_{max} achieved from a single injection of BAM15 (Figure 4.5F and Figure 4.5H). Unless otherwise known, it is therefore recommended to use separate wells to treat with oligomycin and uncoupler, with a final addition of rotenone and antimycin A when exploring mitochondrial energy metabolism of 3D spheroids. This approach still allows for the

calculation of all mitochondrial parameters as with a typical MitoStress test where compounds are added sequentially.

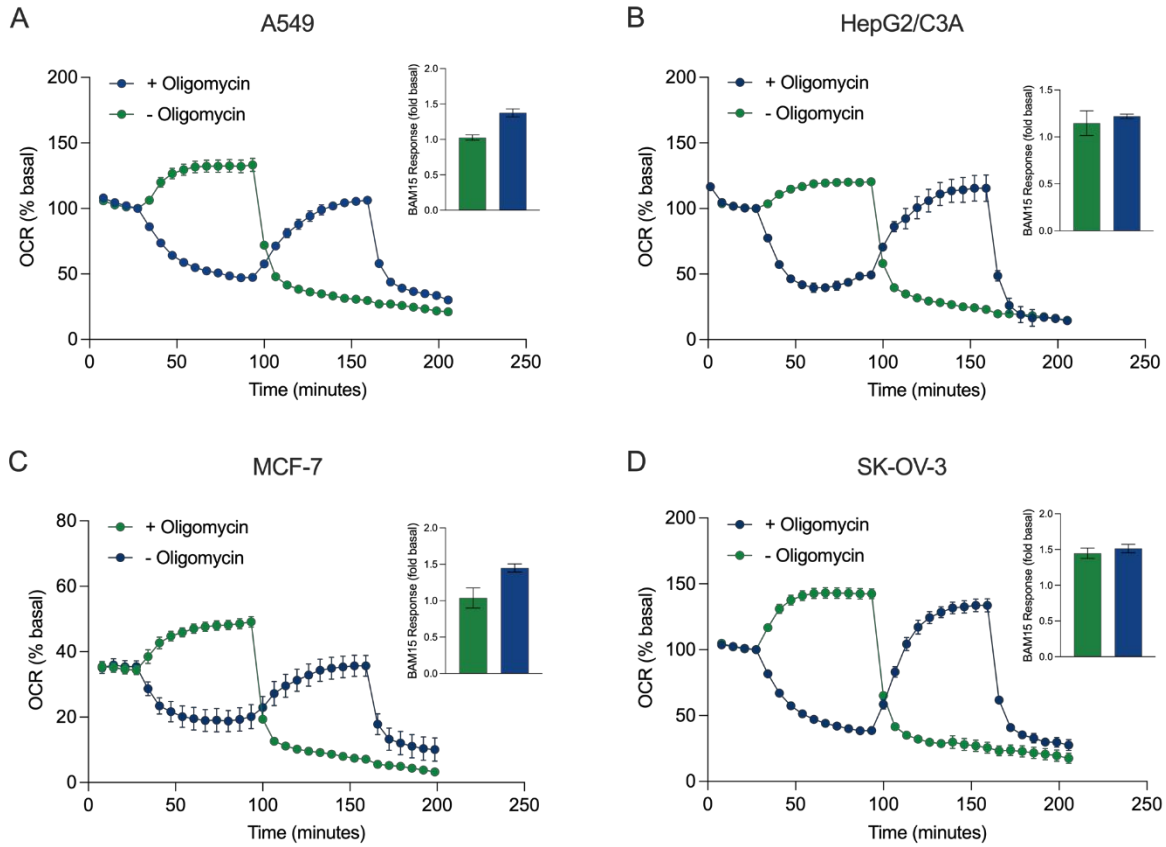

Figure 4.5. Single or sequential injection of mitochondrial respiratory compounds. *Cancer-cell-derived spheroids MCF-7, HEPG2/C3A, SK-OV-3, and A549 were placed into wells of an XFe96 spheroid microplate in XF RPMI and probed for OCR using the Agilent Seahorse XFe96 analyzer. OCR was measured 5x after which 2 µg/mL oligomycin (injection Port A: green trace) or 5 µM BAM15 (injection Port A: blue trace or injection port B: green trace) to inhibit the mitochondrial ATP synthase and determine maximal respiratory capacity, respectively. Kinetic OCR data are expressed as % basal (A–D). Maximal respiratory capacity (OCR_{max}) was calculated as a factor of basal OCR by the equation: $OCR_{max} = OCR_{BAM15} / OCR_{basal}$. OCR_{max} was obtained from OCR averages across measurement cycles 8–10 post BAM 15 injection with (green bars) and without (blue bars) oligomycin. Data are averages ± SEM from 3–8 individual well replicates across the spheroid assay microplate.*

4.4.4. Probing OCR with XF technology to establish mitochondrial energy metabolism of cancer-derived spheroids

*Using optimal cell seeding densities, compound concentrations, injection strategy, and measurement cycle period determined in these optimization experiments (Table 3), we have developed a detailed protocol for accurately probing basal mitochondrial respiration: OCR_{basal} (**Figure 4.6**A), ADP phosphorylation respiration: OCR_{ADP} (**Figure 4.6**B), leak respiration: OCR_{omy} (**Figure 4.6**C), coupling efficiency (**Figure 4.6**D), maximal respiratory capacity: OCR_{max} (**Figure 4.6**E), and spare respiratory capacity: OCR_{spare} (**Figure 4.6**F) using cancer-derived 3D spheroids.*

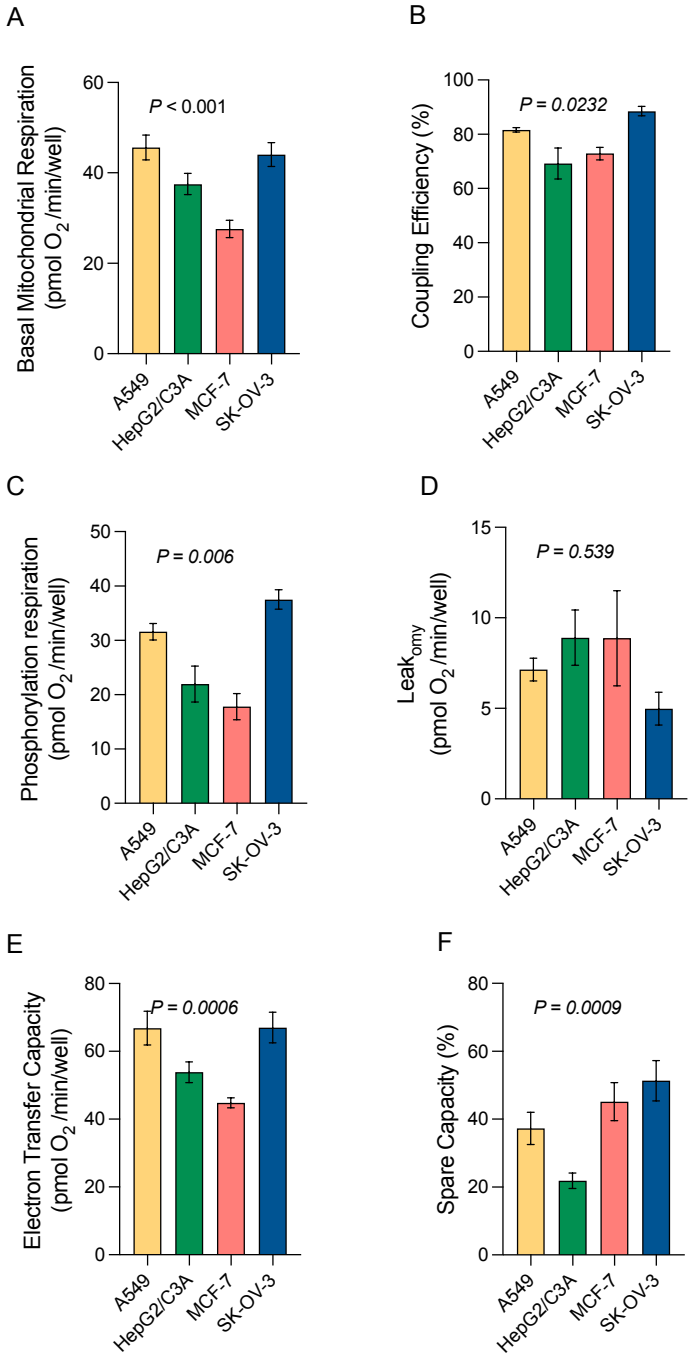

Figure 4.6. Probing OCR with XF technology to establish mitochondrial energy metabolism of cancer-derived spheroids. *Cancer-cell-derived spheroids MCF-7, HEPG2/C3A, SK-OV-3, and A549 were placed in wells of a spheroid assay microplate in XF RPMI and probed for OCR using the Agilent Seahorse XFe96 analyzer. OCR was measured 5x after which 2 µg/mL oligomycin, or 5 µM BAM15, and RA was added to inhibit the mitochondrial ATP synthase, determine maximal respiratory capacity, and calculate non-mitochondrial respiratory rate, respectively. (A) Basal mitochondrial respiration (OCR_{basal}) was calculated as the average of OCR from the 3 measurement cycles before port A injection. (B) Coupling efficiency of*

oxidative phosphorylation was approximated by expressing OCR_{ADP} (OCR_{basal} – OCR_{leak}) as a percentage of OCR_{basal}. (C) ADP phosphorylation respiration (OCR_{ADP}) was measured as oligomycin-sensitive OCR, calculated from the averaged OCR across measurement cycles 11–13 prior to BAM 15 injection. (D) $Leak_{omy}$ respiration (OCR_{leak}) was measured as OCR insensitive to oligomycin, calculated from the mean averaged OCR across measurement cycles 11–13. (E) Maximal respiratory capacity (OCR_{max}) was measured as the average maximum OCR measured following BAM 15 injection. (F) Spare respiratory capacity was calculated by expressing OCR_{spare} (OCR_{max} – OCR_{basal}) as a percentage of OCR_{basal}. OCR after rotenone–antimycin A injection ($OCR_{r/a}$) was subtracted from all rates to correct for nonmitochondrial OCR. Data are averages ± SEM from 3–8 individual well replicates across the XFe96 spheroid plate, P values were obtained by one-way ANOVA.

4.4.5. Placement of spheroids within the spheroid assay microplate dictates basal OCR and mitochondrial modulator effects using XF technology

MCF-7 spheroids grown from 4×10^3 cells/well over 3 days were used as a model to determine optimum transfer, placement, and analysis within spheroid assay microplates. Using dimensions provided for the spheroid microplate from the manufacturer, the well surface was split into three zone-areas for optimum spheroid placement (Figure 4.7A), where zone 1 was highlighted as being the optimal zone at the center of the well. With careful pipetting using wide-orifice pipette tips, spheroids were transferred into the spheroid plates and randomly distributed across the well-surfaces by gravity elution (Figure 4.7B). Where spheroids were carefully transferred using gravity elution, most spheroids could typically be found in zones 1–2 of the microplate, using the recommended transfer techniques from the manufacturer. Where spheroids were forced out of the pipette tip by aspiration, spheroids were often placed beyond these zones and could not be seen using microscopy.

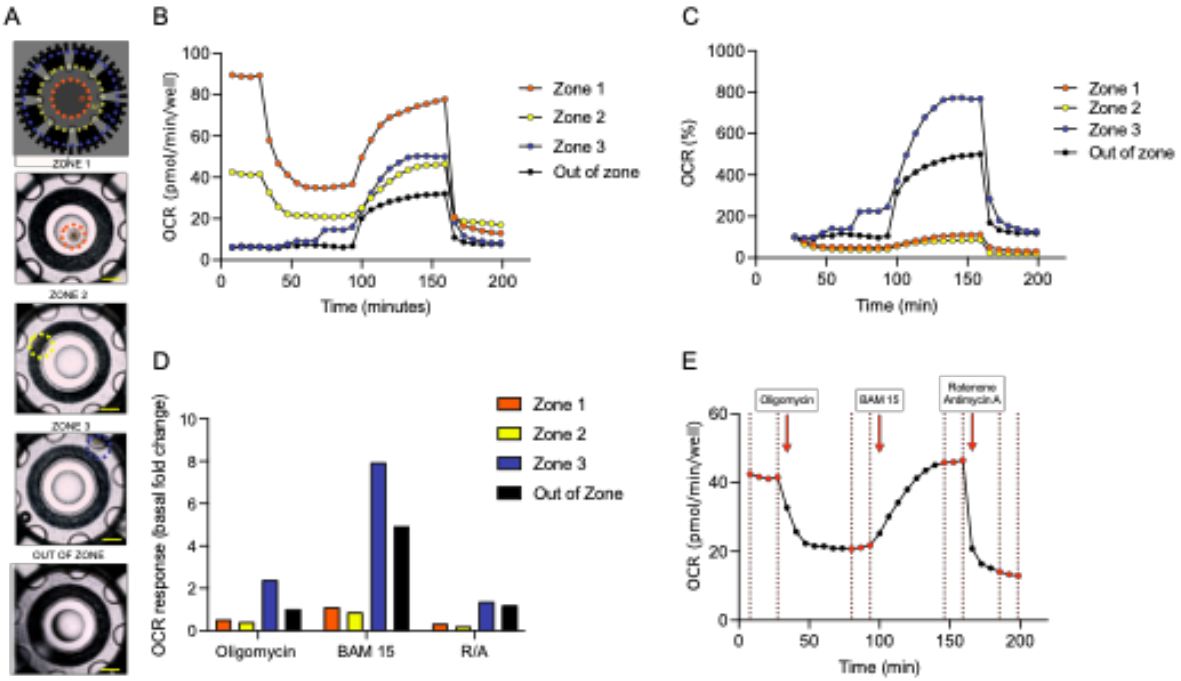

Figure 4.7. Placement of spheroids within the spheroid assay microplate dictates basal OCR and mitochondrial modulator effects using XF technology. *MCF-7 spheroids were seeded at 4 × 10^3 cells/well and cultured over 3 days before being placed into wells of spheroid microplate containing XF RPMI and probed for OCR ± mitochondrial modulators using the Agilent Seahorse XFe96 analyzer. (A) Photomicrographs of spheroid zone positions in spheroid assay microplates after assay duration; scale bar = 500 micrometer and OCR captured from corresponding wells over time expressed as either pmol/min/well (B) or % basal (C). (D) Mitochondrial modulator effects of MCF-7 spheroids placed in different zones within the spheroid assay microplate; data expressed as fold change from basal. (E) Example kinetic trace highlighting which OCR data measurements (red circles) are used to calculate the response of each mitochondrial modulator for data presented in E. Data shown are from individual well responses. Abbreviation: OCR = oxygen consumption rate.*

To compare spheroid placement positions, MCF-7 spheroids were transferred into the spheroid assay microplates in designated zones 1–3 or out of zone (Figure 4.7A). These 4 wells were tracked through a kinetic experiment OCR at baseline and after the addition of oligomycin, BAM 15, or rotenone–antimycin A (Figure 4.7C). OCR was calculated from the mean of three cycle readings before each injection (Figure 4.7B). OCR was measured

kinetically over 200 min in the 4 selected wells (Figure 4.7C) and baseline-corrected (Figure 4.7D). Where spheroids were placed in zone 3 or out of zone, baseline OCR were significantly lower than spheroids placed in zones 1 and 2 (Figure 4.7C). The effect of respiratory compounds oligomycin, BAM15, and rotenone–antimycin A also differed dramatically between spheroids placed in zones 1 and 2 compared with zone 3 and out-of-zone regions. An increase in OCR was seen with oligomycin in spheroids placed in zone 3 or out of zone (Figure 4.7E). Moreover, spheroids placed in zone 3 or out of zone experienced an excessively high response to BAM15 with OCR higher than baseline following rotenone–antimycin A injection (Figure 4.7E). Despite an almost two-fold increase in basal OCR (Figure 4.7C) with spheroids placed in zone 2 versus zone 1, the fold-changes in response to all respiratory compounds were very similar (Figure 4.7E), suggesting that differences in basal OCR between spheroids placed in zones 1 or 2 are unlikely to be the result of placement within the well.

4.4.6. Random selection of wells for background correction to improve the control for temperature gradients across the spheroid assay microplate

The selection criteria for background are of high importance; the use of outermost wells for background correction is not representative of all microplate wells, which may lead to incorrect data assumptions being drawn and erroneous data conclusions due to edge effects across the spheroid microplate. To assess this observation, MCF-7 spheroids were used to compare the assay correction procedures to derive OCR values in response to the addition of a vehicle control, oligomycin, BAM 15, or rotenone–antimycin A (Figure 4.8). All respiratory compounds yielded the expected kinetic OCR profiles for the selected compounds, revealing

an average steady basal respiration rate of 20–30 pmol/min/well (Figure 4.8A). However, where the assay data were analyzed using the outermost wells for background temperature correction (A1, A12, H1, and H12), values revealed for OCR after the addition of respiratory compounds were especially low; OCR yielded negative values for rotenone–antimycin A. In response to these observations, alternative analysis was performed using a series of empty wells, randomly distributed across the spheroid microplate, to use as background temperature correction wells (Figure 4.8B). Where alternative background correction was applied, all relative compound effects on OCR were the same in both analysis sets; however, absolute OCR values increased by approximately 10 pmol/min/well (Figure 4.8). These data highlight the power and importance of background temperature correction on spheroid assay microplates and emphasize the importance of user optimization for XF analysis.

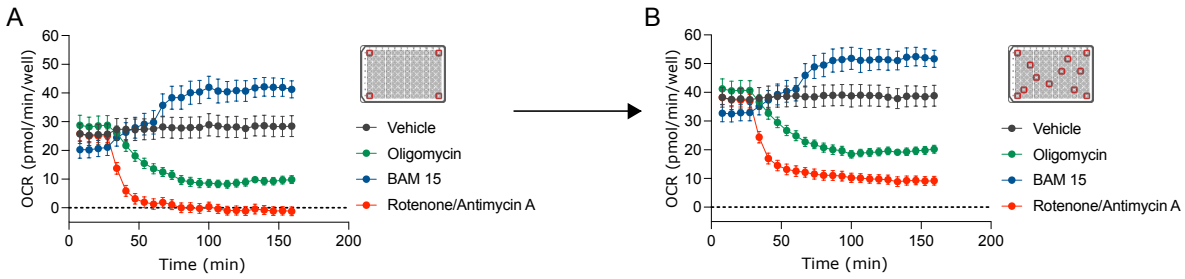

Figure 4.8. Random selection of wells for background correction to improve the control for temperature gradients across the spheroid assay microplate. *OCR data extrapolated from Figure 4.2A using recommended wells for background correction (A) versus randomly assigned wells for background correction (B). Abbreviation: OCR = oxygen consumption rate.*

4.4.7. Normalization of extracellular flux data acquired from cellular spheroids

Unlike cell monolayers, spheroids represent a heterogenous aggregation of cells in a 3D space and therefore require thorough consideration with respect to analysis, particularly when normalizing these data. This paper presents three approaches to normalize XF data acquired from MCF-7 spheroids (**Figure 4.9**). When unnormalized, OCR positively correlates

(R^2 = 0.98) with spheroid size (determined by initial cell seeding density) significantly when compared statistically with Pearson correlation coefficient, *P* = 0.0057 (**Figure 4.9**A). This linear relationship is lowered when OCR is normalized to the initial cell seeding density (R^2 = 0.78) and no longer significantly correlates with spheroid size (*P* = 0.117, **Figure 4.9**B). This is also the case when normalized to spheroid volume (R^2 = 0.77; Pearson correlation coefficient *P* = 0.120,(**Figure 4.9**C) and nuclear dsDNA content (R^2 = 0.58; Pearson correlation coefficient *P*= 0.233, **Figure 4.9**D). These data highlight the importance of normalizing XF data when probing mitochondrial metabolism of spheroids, especially if they are of different size.

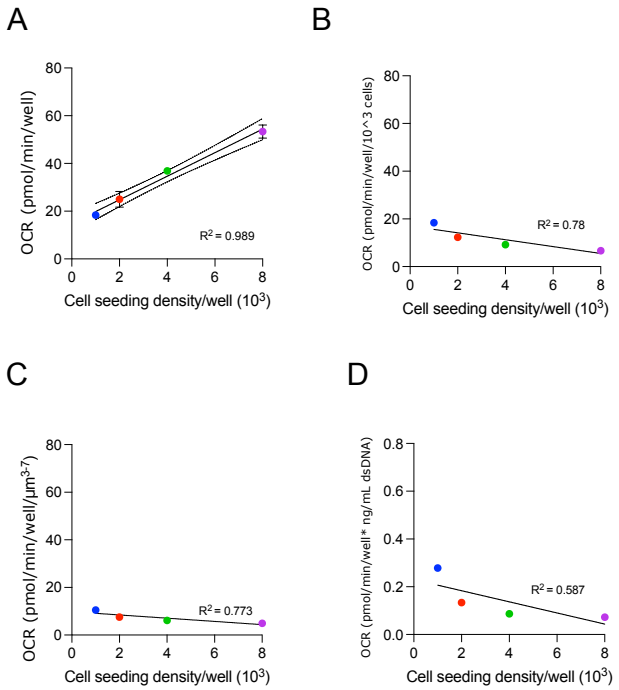

Figure 4.9. Normalization of extracellular flux data acquired from cellular spheroids. *(A) Raw OCR data were obtained from MCF-7 cultured over 3 days and plotted using Pearson's model to obtain a correlation coefficient between spheroid seeding density and OCR; P value set at 0.05. (B) Raw OCR data were normalized against initial spheroid seeding density; (C) MCF-7 spheroid volume obtained from microscopy planimetry; and (D) nuclear ds DNA*

content compared using Pearson's correlation coefficient. Abbreviations: OCR = oxygen consumption rate; ds DNA = double-stranded DNA.

4.5. Discussion

4.5.1. Main findings and outputs

In this manuscript we provide a detailed protocol to probe mitochondrial energy metabolism of single 3D spheroids using a series of cancer-derived cell lines with the XFe96 XF Analyzer. A method is developed and described for the rapid cultivation of A549, HepG2/C3A, MCF7 and SK-OV-3 cellular spheroids using cell-repellent technologies for forced-aggregation. In our protocol we have addressed many considerations of probing spheroid metabolism with XF technology which includes: (1) optimisation of spheroid culture protocols; the handling of spheroids and the transfer of spheroids into specific spheroid assay microplates from the technology manufacturer from their original culturing vessels; (2) the concentration of respiratory compounds to be used, time dependency of compound penetration; (3) injection strategies to be used, and (4) ways to normalise data between experimental groups. All these considerations have been examined in the current manuscript and are discussed in further detail below. Our methods are presented as simplified approaches to generating consistent metabolic oxygen flux data using single 3D spheroids with the XFe96 Flux analyser. Our experimental approach can be used as a starting point and rubric for use in other spheroid models that are easily implemented within a basic laboratory setting.

4.5.2. Considerations

4.5.2.1. Spheroid size and sensitivity of XF technology

To establish reproducible data with XF technology it is essential to characterise and optimise the assay for your specific model. In a basic monolayer of cells, this approach is relatively simple, however when cultivating cells as 3D spheroids this presents additional challenges. Since cellular oxygen consumption rate (OCR) measured by XF technology is proportional to cell density when the cell number in the well is within the sensitivity of the system, it was important to investigate this relationship using single 3D spheroids. By probing OCR by single 3D spheroids cultured from 4 different cancer cell lines seeded at densities of 1, 2, 4 or 8, 000 cells per well, we show that the XFe96 analyser is sensitive enough to pick up changes in the rate of mitochondrial respiration between 3D spheroids grown from different cell seeding densities (Figure 4.3). We show that the optimum range of cell seeding density, and thus spheroid volume for forming 3D spheroids for probing OCR, differs depending on cell type. This is shown by the linear relationship between OCR and seeding density or spheroid volume (Figure 4.3). For A549 and HepG2/C3A cells, the optimal seeding density for OCR sensitivity was between 1,000 and 8,000 cells/well. Whereas for MCF-7 it was between 2-8,000 cells/well and for SK-OV-3 4-8,000 cells/well. These data demonstrate that optimisation of spheroid size is of particular importance when assessing OCR using XF technology.

4.5.2.2. Choice of mitochondrial uncouplers for extracellular flux assays

Proton ionophores such as carbonyl cyanide 4-(trifluoromethoxy) phenylhydrazone (FCCP)(Benz and McLaughlin, 1983), carbonyl cyanide m-chlorophenyl hydrazone (CCCP)(Kasianowicz et al., 1984) or BAM15(Kenwood et al., 2013) are potent small molecule chemicals, capable of disrupting the electrochemical proton gradient across mitochondrial

membranes, inhibiting the production of ATP and ultimately uncoupling mitochondrial respiration (Mitchell, 1961). New small molecules continue to be developed for these purposes , particularly in the therapeutic treatment of metabolic disease (Alexopoulos et al., 2020, Chen et al., 2021, Goedeke and Shulman, 2021); we direct the reader to two excellent reviews (Hill et al., 2012, Demine et al., 2019). Conversely, uncoupling of the oxidative respiration has been linked with undesirable off-target toxicity (Wang et al., 2018). Within *in vitro* cellular assays however, the molecule FCCP is known to depolarise mitochondrial membrane potential but also exerts off target effects such as plasma membrane depolarisation, disrupting NA^+ ion flux (Tretter et al., 1998); interference with cellular protein processing (Connop et al., 1999) and has even been shown to induce cellular senescence (Stöckl et al., 2007). BAM15 was originally introduced as a mitochondrial uncoupler with minimal influence on plasma membranes in 2013 (Kenwood et al., 2013); with protonophoric activity in the micromolar range in whole cells and nanomolar range in isolated mitochondria (Kenwood et al., 2013, Firsov et al., 2021). Given the potency of FCCP on plasma membrane depolarisation, the use of BAM15 in extracellular flux assays is a more reliable protonophore to uncouple respiration in intact whole cells. Although FCCP, and its counterpart, CCCP have been used for over 50 years to assay maximal respiratory capacities and continue to be used widely in XF studies, use of these small molecules often underestimate mitochondrial and cellular metabolic capacity. This is in part linked to why so many publications using XF technology fall into the trap of reporting negative spare respiratory capacities or underestimate true mitochondrial respiratory capacities when FCCP is used. The added potency of FCCP in intact cells and tissues often leads to compromised mitochondrial function and cells can struggle to operate appropriately to sustain a maximum

respiratory capacity across multiple measurement cycles following their addition, even at very low concentrations (Dranka et al., 2010). Therefore, the response of cells to FCCP can be found in many studies to drop off following the initial measurement cycle period. Whilst FCCP have been routinely used for XF analysis, in cases where whole cells or spheroid models are concerned, BAM15 is used preferentially, given that it can maintain a maximum respiratory capacity in fully depolarised mitochondria at concentrations as high as 10 μM^3. Moreover, BAM15 induces effects on extracellular acidification which coincides with that of nutrient oxidation through the hydration of CO2 to form HCO3- and H+ to a greater extent to that of FCCP. In the case of isolated mitochondria and permeabilised cells, any of these uncouplers should perform as well for mitochondrial uncoupling if titrated at the correct concentration.

4.5.2.3. Kinetics of compound penetration and assay cycling

The concentration, penetration and kinetic profile of chemical compounds used to conduct a typical 'MitoStress' test with 3D spheroids using the XF analyser is more complex to address. Given that spheroids present 3D structure, the penetration of molecules across the diameter of the spheroid is an infinitely more complex process than that of cell monolayers; for example, the kinetic penetration and therefore sensitivity to the chemotherapeutic sorafenib, was determined by spheroid age and therefore size in a HepG2 spheroid model (Eilenberger et al., 2019). The ability of small chemical molecules (e.g., drugs, nanoparticles) to reach a biological target is dependent on several underlying factors including the complexity of the system it is required to dynamically penetrate and diffuse through(van den Brand et al., 2018, Niora et al., 2020). This is particularly true for drugs targeting tumour

tissue (Millard et al., 2017). Similarly, to tumour targeting, in the context of a 3D spheroid, size, compactness, and other phenotypic responses such as the expression of drug transporter proteins, can govern the penetration time and concentration of compound required to elicit a biological response. In this protocol, we addressed the issue around penetration time and small molecule concentration in response to the ATP synthase inhibitor oligomycin, the protonophore and mitochondrial uncoupler BAM15 and the combination of the Complex I and Complex III inhibitors rotenone and antimycin A. By probing the OCR of single MCF-7 spheroids exposed to multiple titrations of these common respiratory compounds, we demonstrate that the optimal concentration of each compound required to induce a steady-state respiratory rate falls within a similar range to that of monolayer cells (Figure 4.4). Importantly, and differing from their monolayer counterparts, it is shown that increasing the number of measurement cycles between injections is key to achieving a steady-state OCR in single 3D spheroids. These data highlight the importance of compound penetration and their respective kinetic profiles when exploring mitochondrial respiratory parameters of 3D spheroids using these approaches. Using spheroid optimisation properties, concentrations of compounds and measurement cycle times informed by the data presented in Figure 4.3 - Figure 4.5, we were able to establish a validated 'MitoStress' test for probing specific parameters of mitochondrial oxidative metabolism in a range of cancer-derived 3D spheroids (***Figure 4.6***). Of importance, and like some monolayer cancer cell lines (Ruas et al., 2016), we discovered that maximal respiratory capacity (rate of uncoupled-stimulated respiration) of certain cancer-derived 3D spheroids is inhibited by oligomycin (Figure 4.5). Specifically, 3D spheroids grown from either A549 or MCF-7 cells obtained a significantly lower maximal rate of respiration when uncoupled with BAM15

following oligomycin injection compared to being uncoupled by BAM15 without oligomycin (Figure 4.5F and H). Given that this effect may be present within other 3D spheroid cultures, we suggest that unless a previously validated protocol is employed, maximal respiratory capacity in 3D spheroids should be estimated without oligomycin.

4.5.2.4. Spheroid formation, handling, transfer and movement

Some cell lines are better suited to the formation of spheroids than others and may not form spheroids at all, e.g., MCF-7 ovarian cancer cells have been shown by ourselves and others (Benton et al., 2015, Hirpara et al., 2019) to form highly circular spheroids compared to other cell lines (Figure 4.3). For example, Capan-1 pancreatic cancer cells have been shown to form better spheroids than Panc-1 or BxPC3 (Ware et al., 2016). Similarly, hepatic carcinoma cell lines are known to have variable abilities to form compact spheroids(Song et al., 2017, Song et al., 2018), with an observed change in phenotype such as enhanced drug metabolism, or the production of albumin as is the case for HepG2 versus HepG2/C3A (Wrzesinski et al., 2013, Gaskell et al., 2016, Stampar et al., 2020) or HepaRG spheroids (Basharat et al., 2020, Takahashi et al., 2015, Hendriks et al., 2016). Users should therefore optimise spheroid culturing techniques accordingly and perform titration experiments to pinpoint optimum seeding density and cultivation time course. In addition, the formulation and composition of assay media has been shown to impact spheroid formulation, including the addition of methylcellulose, often added to media to increase matrix viscosity (Leung et al., 2015, Cavo et al., 2020, Ware et al., 2016); optimum cell medium composition should be determined empirically for all cell lines used. The number of medium exchanges throughout spheroid culture is determined by the cell line used but typically, a half-volume medium

exchange every 2-3 days is applicable in most cases to replenish nutrients. We used the forced-aggregate approach to generate 3D spheroids using cell-repellent microplates, from commercially available sources for rapid development and deployment of spheroid models in XF analyses studies. However alternative platforms may be better suited to generate spheroids from other cell types, e.g., hanging-drop or matrix-embedded approaches. In resource-limited laboratories, users may wish to look towards the agarose-liquid overlay technique for formation of cell-repellent microplate surfaces (Carlsson and Yuhas, 1984, Costa et al., 2014) to significantly reduce economic costs of initial spheroid method development steps. The movement of spheroids between culture vessels is a necessary step to perform XF analysis and other downstream assays. Ease of transfer is typically dictated by spheroid size and overall density. We recommend using a P200 or P1000 wide-orifice pipette tip to maintain spheroid integrity, smaller bore pipette tips risk mechanical disruption of the spheroid which can be bought sourced commercially or, with care, made by simply trimming the end of pipette tip to increase the orifice. However, we found that this approach was liable to introduce furring to the plastic around the end of tip which could cause mechanical disruption during handling. The use of a backlight or lightbox is also useful for spheroid handling and observation under a dissection microscope as an essential step to ensure successful transfer of spheroids into the spheroid assay microplate. Moreover, we show that spheroid position within the well of a spheroid assay microplate is of particular importance and directly impacts OCR and compound effect during a typical 'MitoStress' test (Figure 4.7), most likely due to the relationship of the spheroid position and the sensor probe fluorophores.

4.5.2.5. Background correction and temperature control wells

The use of microplate-based assays is a widely used approach in several areas of research; however, their use presents several practical challenges that require addressing. As is true in other experimental approaches, particularly those that use the 96 (or greater) array format, microplate geometry and positioning can influence temperature and gas-exchange gradients across the plate over time, often referred to as 'edge effects'(Lundholt et al., 2003, Zhang et al., 2007). We found the same to be true of the spheroid assay microplate. Under the manufacturer's guidelines and protocols, the outermost corner wells: A1, A12, H1 and H12 are always designated as background correction and temperature control wells for the XFe96 analyser, conversely, with the 24-well array format, A1 and D6 are designated as control wells, alongside two other wells evenly spread across the middle of the plate at B4 and C3. On performing XF spheroid analysis, we found significant deviation in data initially collected using the manufacturer's guidance, despite including the necessary steps to ensure assay pre-equilibration to temperature and CO_2 content, prior to commencing the acquisition of data, often yielding negative values for OCR following the injection of certain respiratory inhibitors (Figure 4.8). We found these observations likely to be due to edge effects across the spheroid assay microplate. In Figure 4.8, we found that redistributing background control wells across the microplate, XF data was adjusted approximately 2-fold. Two most likely reasons are (1): due to evaporation effects at the edge wells resulting in a smaller total volume chamber for the XFe96 probe to sample from, and (2): from inadequate temperature equilibrations between those wells designated for background correction and sample wells, resulting in datasets that either mask or over-inflate OCR. To avoid such outcomes, it is therefore recommended, especially within the context of spheroid analysis,

that users re-distribute wells designated for background correction across the entirety of the spheroid assay microplate and take necessary steps to pre-equilibrate their assay prior to acquiring XF data.

4.5.2.6. Normalisation of data

In addition to providing a detailed protocol for probing mitochondrial energy metabolism of single 3D spheroids with XF technology, we also present possible ways to normalise mitochondrial respiratory rate data obtained with 3D spheroids. Using respiratory rate data obtained with MCF-7 spheroids cultured at different cell seeding densities (Figure 4.3) we present basal mitochondrial respiratory rates from MCF-7 spheroids of increasing size and diameter when normalised to initial cell seeding density, spheroid volume and dsDNA content (**Figure 4.9**). The appropriate normalisation method is paramount for the accurate interpretation of XF datasets, particularly when comparing *in vitro* 3D spheroid models and different cell types. Poor normalisation can lead to erroneous results that simply cannot be compared between datasets. Protein content is not preferred for normalisation of spheroid XF data, since pre-treatments may impact rates of protein synthesis, without significant effect on respiratory rate. Moreover, significant inconsistent amounts of protein can bind to spheroid microplates upon cell lysis, introducing variation of protein content between wells. This may be further complicated in XF analyses using spheroids or non-adherent cells that require biomolecular glues to bind to which may contain protein. Contrary to intracellular protein content, nuclear DNA content is independent of cell type and is proportional to cell number (**Figure 4.9**D) – a more accurate and less time-consuming approach than the disaggregation of spheroids for cell number quantification. Conversely, Yepez et al. (2018),

conducting XF analyses in monolayers of fibroblasts cells, found that normalising XF data to cell number introduced greater dispersion of data than was achieved prior to normalisation. Nuclear DNA content is independent of differentiated state or phenotype and hence is more accurate for the normalisation of spheroid data in XF assays than protein content. DNA content has also been a proven strategy for the analysis of other metabolism-linked datasets (Silva et al., 2013). It is important to note, however, that nuclear DNA content is quantified from all cells present within the spheroid, therefore normalisation to DNA content is not recommended for XF datasets whereby spheroids undergo treatments that may result in significant loss of cell viability. For such datasets, if feasible, normalisation to cell viability is preferred or baseline correct the data to basal respiration.

4.6. Conclusion

The spheroid models generated here, present a range of cancer-types and architecture, that cannot be captured in classical 2D models. These include heterogenous, spatial arrangement of cells in three-dimensions, enhanced cell-cell contacts (e.g., formation of gap junctions and extracellular matrices), and biochemical gradients across spheroid diameter (e.g., pH gradients, oxygen diffusion access to nutrients). Using extracellular flux to study *in vitro* spheroid biology could allow optimum targets for drug therapies to be identified through metabolic perturbation observations. These could be extrapolated from *in vitro* spheroids to *in vivo* tumours and identify pathways that may target spheroid-tumour metabolism, e.g., carbohydrate utilisation during spheroid growth. Therapeutic modalities may be effective in targeting spheroids in early growth phases but prove less effective in the latter phases of spheroid growth as metabolic network complexity matures. To conclude the development of

3D cell culture models and sophisticated analysis technologies for use in biological research will continue to be a dynamic and rapidly changing field with unsurpassed potential. Extracellular flux analysis of *in vitro* cell culture spheroids could be employed as a cutting-edge research method to advance research outcomes that could be extrapolated to better understand human-relevant biology, reduce the use of animal models in research, and enhance patient-centric research.

4.7. References

Alexopoulos, S. J., Chen, S.-Y., Brandon, A. E., Salamoun, J. M., Byrne, F. L., Garcia, C. J., Beretta, M., Olzomer, E. M., Shah, D. P., Philp, A. M., Hargett, S. R., Lawrence, R. T., Lee, B., Sligar, J., Carrive, P., Tucker, S. P., Philp, A., Lackner, C., Turner, N., Cooney, G. J., Santos, W. L. and Hoehn, K. L. (2020) 'Mitochondrial uncoupler BAM15 reverses diet-induced obesity and insulin resistance in mice', *Nature Communications,* 11(1), pp. 2397.

Amann, A., Zwierzina, M., Gamerith, G., Bitsche, M., Huber, J. M., Vogel, G. F., Blumer, M., Koeck, S., Pechriggl, E. J. and Kelm, J. M. (2014) 'Development of an innovative 3D cell culture system to study tumour-stroma interactions in non-small cell lung cancer cells', *PloS one,* 9(3), pp. e92511.

Basharat, A., Rollison, H. E., Williams, D. P. and Ivanov, D. P. (2020) 'HepG2 (C3A) spheroids show higher sensitivity compared to HepaRG spheroids for drug-induced liver injury (DILI)', *Toxicol Appl Pharmacol,* 408, pp. 115279.

Benning, L., Peintner, A., Finkenzeller, G. and Peintner, L. (2020) 'Automated spheroid generation, drug application and efficacy screening using a deep learning classification: a feasibility study', *Sci Rep,* 10(1), pp. 11071.

Benton, G., DeGray, G., Kleinman, H. K., George, J. and Arnaoutova, I. (2015) 'In Vitro Microtumors Provide a Physiologically Predictive Tool for Breast Cancer Therapeutic Screening', *PLOS ONE,* 10(4), pp. e0123312.

Benz, R. and McLaughlin, S. (1983) 'The molecular mechanism of action of the proton ionophore FCCP (carbonylcyanide p-trifluoromethoxyphenylhydrazone)', *Biophysical journal,* 41(3), pp. 381-398.

Brand, M. D. and Nicholls, D. G. (2011) 'Assessing mitochondrial dysfunction in cells', *The Biochemical journal,* 435(2), pp. 297-312.

Carlsson, J. and Yuhas, J. M. (1984) 'Liquid-Overlay Culture of Cellular Spheroids', *Recent Results in Cancer Research,* 95, pp. 1-23.

Cavo, M., Delle Cave, D., D'Amone, E., Gigli, G., Lonardo, E. and del Mercato, L. L. (2020) 'A synergic approach to enhance long-term culture and manipulation of MiaPaCa-2 pancreatic cancer spheroids', *Scientific Reports,* 10(1), pp. 10192.

Chen, S.-Y., Beretta, M., Alexopoulos, S. J., Shah, D. P., Olzomer, E. M., Hargett, S. R., Childress, E. S., Salamoun, J. M., Aleksovska, I., Roseblade, A., Cranfield, C., Rawling, T., Quinlan, K. G. R., Morris, M. J., Tucker, S. P., Santos, W. L. and Hoehn, K. L. (2021) 'Mitochondrial uncoupler SHC517 reverses obesity in mice without affecting food intake', *Metabolism - Clinical and Experimental,* 117.

Coltman, N. J., Coke, B. A., Chatzi, K., Shepherd, E. L., Lalor, P. F., Schulz-Utermoehl, T. and Hodges, N. J. (2021) 'Application of HepG2/C3A liver spheroids as a model system for genotoxicity studies', *Toxicol Lett,* 345, pp. 34-45.

Connop, B. P., Thies, R. L., Beyreuther, K., Ida, N. and Reiner, P. B. (1999) 'Novel effects of FCCP [carbonyl cyanide p-(trifluoromethoxy) phenylhydrazone] on amyloid precursor protein processing', *Journal of neurochemistry,* 72(4), pp. 1457-1465.

Conway, G. E., Shah, U. K., Llewellyn, S., Cervena, T., Evans, S. J., Al Ali, A. S., Jenkins, G. J., Clift, M. J. D. and Doak, S. H. (2020) 'Adaptation of the in vitro micronucleus assay for genotoxicity testing using 3D liver models supporting longer-term exposure durations', *Mutagenesis,* 35(4), pp. 319-330.

Correa de Sampaio, P., Auslaender, D., Krubasik, D., Failla, A. V., Skepper, J. N., Murphy, G. and English, W. R. (2012) 'A heterogeneous in vitro three dimensional model of tumour-stroma interactions regulating sprouting angiogenesis', *PloS one,* 7(2), pp. e30753.

Costa, E. C., Gaspar, V. M., Coutinho, P. and Correia, I. J. (2014) 'Optimization of Liquid Overlay Technique to Formulate Heterogenic 3D Co-Cultures Models', *Biotechnology and Bioengineering,* 111(8), pp. 1672-1685.

Courau, T., Bonnereau, J., Chicoteau, J., Bottois, H., Remark, R., Assante Miranda, L., Toubert, A., Blery, M., Aparicio, T., Allez, M. and Le Bourhis, L. (2019) 'Cocultures of human colorectal tumor spheroids with immune cells reveal the therapeutic potential of MICA/B and NKG2A targeting for cancer treatment', *J Immunother Cancer,* 7(1), pp. 74.

Demine, S., Renard, P. and Arnould, T. (2019) 'Mitochondrial Uncoupling: A Key Controller of Biological Processes in Physiology and Diseases', *Cells,* 8(8), pp. 795.

Dranka, B. P., Hill, B. G. and Darley-Usmar, V. M. (2010) 'Mitochondrial reserve capacity in endothelial cells: The impact of nitric oxide and reactive oxygen species', *Free Radic Biol Med,* 48(7), pp. 905-14.

Eilenberger, C., Rothbauer, M., Ehmoser, E. K., Ertl, P. and Kupcu, S. (2019) 'Effect of Spheroidal Age on Sorafenib Diffusivity and Toxicity in a 3D HepG2 Spheroid Model', *Sci Rep,* 9(1), pp. 4863.

Elje, E., Mariussen, E., Moriones, O. H., Bastus, N. G., Puntes, V., Kohl, Y., Dusinska, M. and Runden-Pran, E. (2020) 'Hepato(Geno)Toxicity Assessment of Nanoparticles in a HepG2 Liver Spheroid Model', *Nanomaterials (Basel),* 10(3).

Firsov, A. M., Popova, L. B., Khailova, L. S., Nazarov, P. A., Kotova, E. A. and Antonenko, Y. N. (2021) 'Protonophoric action of BAM15 on planar bilayers, liposomes, mitochondria, bacteria and neurons', *Bioelectrochemistry,* 137, pp. 107673.

Gaskell, H., Sharma, P., Colley, H. E., Murdoch, C., Williams, D. P. and Webb, S. D. (2016) 'Characterization of a functional C3A liver spheroid model', *Toxicology research,* 5(4), pp. 1053-1065.

Goedeke, L. and Shulman, G. I. (2021) 'Therapeutic potential of mitochondrial uncouplers for the treatment of metabolic associated fatty liver disease and NASH', *Molecular Metabolism,* 46, pp. 101178.

Hendriks, D. F. G., Puigvert, L. F., Messner, S., Mortiz, W. and Ingelman-Sundberg, M. (2016) 'Hepatic 3D spheroid models for the detection and study of compounds with cholestatic liability', *Scientific Reports,* 6.

Hill, B. G., Benavides, G. A., Lancaster, J. R., Jr., Ballinger, S., Dell'Italia, L., Jianhua, Z. and Darley-Usmar, V. M. (2012) 'Integration of cellular bioenergetics with mitochondrial quality control and autophagy', *Biological chemistry,* 393(12), pp. 1485-1512.

Hirpara, J., Eu, J. Q., Tan, J. K. M., Wong, A. L., Clement, M.-V., Kong, L. R., Ohi, N., Tsunoda, T., Qu, J., Goh, B. C. and Pervaiz, S. (2019) 'Metabolic reprogramming of oncogene-addicted cancer cells to OXPHOS as a mechanism of drug resistance', *Redox Biology,* 25, pp. 101076.

Ivanova, E., Kuraguchi, M., Xu, M., Portell, A. J., Taus, L., Diala, I., Lalani, A. S., Choi, J., Chambers, E. S., Li, S., Liu, S., Chen, T., Barbie, T. U., Oxnard, G. R., Haworth, J. J., Wong, K. K., Dahlberg, S. E., Aref, A. A., Barbie, D. A., Bahcall, M., Paweletz, C. P. and Janne, P. A. (2020) 'Use of Ex Vivo Patient-Derived Tumor Organotypic Spheroids to Identify Combination Therapies for HER2 Mutant Non-Small Cell Lung Cancer', *Clin Cancer Res,* 26(10), pp. 2393-2403.

Kasianowicz, J., Benz, R. and McLaughlin, S. (1984) 'The kinetic mechanism by which CCCP (carbonyl cyanide m-chlorophenylhydrazone) transports protons across membranes', *The Journal of membrane biology,* 82(2), pp. 179-190.

Kenwood, B. M., Weaver, J. L., Bajwa, A., Poon, I. K., Byrne, F. L., Murrow, B. A., Calderone, J. A., Huang, L., Divakaruni, A. S., Tomsig, J. L., Okabe, K., Lo, R. H., Cameron Coleman, G., Columbus, L., Yan, Z., Saucerman, J. J., Smith, J. S., Holmes, J. W., Lynch, K. R., Ravichandran, K. S., Uchiyama, S., Santos, W. L., Rogers, G. W., Okusa, M. D., Bayliss, D. A. and Hoehn, K. L. (2013) 'Identification of a novel mitochondrial uncoupler that does not depolarize the plasma membrane', *Molecular metabolism,* 3(2), pp. 114-123.

Leite, P. E. C., Pereira, M. R., Harris, G., Pamies, D., Dos Santos, L. M. G., Granjeiro, J. M., Hogberg, H. T., Hartung, T. and Smirnova, L. (2019) 'Suitability of 3D human brain spheroid models to distinguish toxic effects of gold and poly-lactic acid nanoparticles to assess biocompatibility for brain drug delivery', *Part Fibre Toxicol,* 16(1), pp. 22.

Leung, B. M., Lesher-Perez, S. C., Matsuoka, T., Moraes, C. and Takayama, S. (2015) 'Media additives to promote spheroid circularity and compactness in hanging drop platform', *Biomaterials Science,* 3(2), pp. 336-344.

Lundholt, B. K., Scudder, K. M. and Pagliaro, L. (2003) 'A simple technique for reducing edge effect in cell-based assays', *J Biomol Screen,* 8(5), pp. 566-70.

Mandon, M., Huet, S., Dubreil, E., Fessard, V. and Le Hegarat, L. (2019) 'Three-dimensional HepaRG spheroids as a liver model to study human genotoxicity in vitro with the single cell gel electrophoresis assay', *Sci Rep,* 9(1), pp. 10548.

Millard, M., Yakavets, I., Zorin, V., Kulmukhamedova, A., Marchal, S. and Bezdetnaya, L. (2017) 'Drug delivery to solid tumors: the predictive value of the multicellular tumor spheroid model for nanomedicine screening', *International journal of nanomedicine,* 12, pp. 7993-8007.

Mitchell, P. (1961) 'Coupling of phosphorylation to electron and hydrogen transfer by a chemi-osmotic type of mechanism', *Nature,* 191, pp. 144-8.

Mittler, F., Obeïd, P., Rulina, A. V., Haguet, V., Gidrol, X. and Balakirev, M. Y. (2017) 'High-Content Monitoring of Drug Effects in a 3D Spheroid Model', *Frontiers in Oncology,* 7(293).

Niora, M., Pedersbæk, D., Münter, R., Weywadt, M. F. d. V., Farhangibarooji, Y., Andresen, T. L., Simonsen, J. B. and Jauffred, L. (2020) 'Head-to-Head Comparison of the Penetration Efficiency of Lipid-Based Nanoparticles into Tumor Spheroids', *ACS Omega,* 5(33), pp. 21162-21171.

Proctor, W. R., Foster, A. J., Vogt, J., Summers, C., Middleton, B., Pilling, M. A., Shienson, D., Kijanska, M., Strobel, S., Kelm, J. M., Morgan, P., Messner, S. and Williams, D. (2017) 'Utility

of spherical human liver microtissues for prediction of clinical drug-induced liver injury', *Arch Toxicol,* 91(8), pp. 2849-2863.

Ruas, J. S., Siqueira-Santos, E. S., Amigo, I., Rodrigues-Silva, E., Kowaltowski, A. J. and Castilho, R. F. (2016) 'Underestimation of the Maximal Capacity of the Mitochondrial Electron Transport System in Oligomycin-Treated Cells', *PLoS One,* 11(3), pp. e0150967.

Russell, S., Wojtkowiak, J., Neilson, A. and Gillies, R. J. (2017) 'Metabolic Profiling of healthy and cancerous tissues in 2D and 3D', *Sci Rep,* 7(1), pp. 15285.

Schindelin, J., Arganda-Carreras, I., Frise, E., Kaynig, V., Longair, M., Pietzsch, T., Preibisch, S., Rueden, C., Saalfeld, S., Schmid, B., Tinevez, J.-Y., White, D. J., Hartenstein, V., Eliceiri, K., Tomancak, P. and Cardona, A. (2012) 'Fiji: an open-source platform for biological-image analysis', *Nature Methods,* 9, pp. 676.

Silva, L. P., Lorenzi, P. L., Purwaha, P., Yong, V., Hawke, D. H. and Weinstein, J. N. (2013) 'Measurement of DNA Concentration as a Normalization Strategy for Metabolomic Data from Adherent Cell Lines', *Analytical Chemistry,* 85(20), pp. 9536-9542.

Song, Y., Kim, J.-S., Choi, E. K., Kim, J., Kim, K. M. and Seo, H. R. (2017) 'TGF-β-independent CTGF induction regulates cell adhesion mediated drug resistance by increasing collagen I in HCC', *Oncotarget,* 8(13), pp. 21650-21662.

Song, Y., Kim, J. S., Kim, S. H., Park, Y. K., Yu, E., Kim, K. H., Seo, E. J., Oh, H. B., Lee, H. C., Kim, K. M. and Seo, H. R. (2018) 'Patient-derived multicellular tumor spheroids towards optimized treatment for patients with hepatocellular carcinoma', *J Exp Clin Cancer Res,* 37(1), pp. 109.

Stampar, M., Sedighi Frandsen, H., Rogowska-Wrzesinska, A., Wrzesinski, K., Filipic, M. and Zegura, B. (2020) 'Hepatocellular carcinoma (HepG2/C3A) cell-based 3D model for genotoxicity testing of chemicals', *Sci Total Environ*, pp. 143255.

Stöckl, P., Zankl, C., Hütter, E., Unterluggauer, H., Laun, P., Heeren, G., Bogengruber, E., Herndler-Brandstetter, D., Breitenbach, M. and Jansen-Dürr, P. (2007) 'Partial uncoupling of oxidative phosphorylation induces premature senescence in human fibroblasts and yeast mother cells', *Free Radical Biology and Medicine,* 43(6), pp. 947-958.

Takahashi, Y., Hori, Y., Yamamoto, T., Urashima, T., Ohara, Y. and Tanaka, H. (2015) '3D spheroid cultures improve the metabolic gene expression profiles of HepaRG cells', *Bioscience reports,* 35(3), pp. e00208.

Tchoryk, A., Taresco, V., Argent, R. H., Ashford, M., Gellert, P. R., Stolnik, S., Grabowska, A. and Garnett, M. C. (2019) 'Penetration and Uptake of Nanoparticles in 3D Tumor Spheroids', *Bioconjugate Chemistry,* 30(5), pp. 1371-1384.

Tretter, L., Chinopoulos, C. and Adam-Vizi, V. (1998) 'Plasma membrane depolarization and disturbed Na+ homeostasis induced by the protonophore carbonyl cyanide-p-trifluoromethoxyphenyl-hydrazon in isolated nerve terminals', *Molecular pharmacology,* 53(4), pp. 734-741.

van den Brand, D., Veelken, C., Massuger, L. and Brock, R. (2018) 'Penetration in 3D tumor spheroids and explants: Adding a further dimension to the structure-activity relationship of cell-penetrating peptides', *Biochimica et Biophysica Acta (BBA) - Biomembranes,* 1860(6), pp. 1342-1349.

Wang, J., He, H., Xiang, C., Fan, X.-Y., Yang, L.-Y., Yuan, L., Jiang, F.-L. and Liu, Y. (2018) 'Uncoupling effect of F16 is responsible for its mitochondrial toxicity and anticancer activity', *Toxicological Sciences,* 161(2), pp. 431-442.

Wang, Z., Luo, X., Anene-Nzelu, C., Yu, Y., Hong, X., Singh, N. H., Xia, L., Liu, S. and Yu, H. (2015) 'HepaRG culture in tethered spheroids as an in vitro three-dimensional model for drug safety screening', *Journal of Applied Toxicology,* 35(8), pp. 909-917.

Ware, M. J., Colbert, K., Keshishian, V., Ho, J., Corr, S. J., Curley, S. A. and Godin, B. (2016) 'Generation of Homogenous Three-Dimensional Pancreatic Cancer Cell Spheroids Using an Improved Hanging Drop Technique', *Tissue engineering. Part C, Methods,* 22(4), pp. 312-321.

Wrzesinski, K., Magnone, M. C., Hansen, L. V., Kruse, M. E., Bergauer, T., Bobadilla, M., Gubler, M., Mizrahi, J., Zhang, K., Andreasen, C. M., Joensen, K. E., Andersen, S. M., Olesen, J. B., Schaffalitzky de Muckadell, O. B. and Fey, S. J. (2013) 'HepG2/C3A 3D spheroids exhibit stable physiological functionality for at least 24 days after recovering from trypsinisation', *Toxicology Research,* 2(3), pp. 163-172.

Yepez, V. A., Kremer, L. S., Iuso, A., Gusic, M., Kopajtich, R., Konarikova, E., Nadel, A., Wachutka, L., Prokisch, H. and Gagneur, J. (2018) 'OCR-Stats: Robust estimation and statistical testing of mitochondrial respiration activities using Seahorse XF Analyzer', *PLoS One,* 13(7), pp. e0199938.

Zanoni, M., Piccinini, F., Arienti, C., Zamagni, A., Santi, S., Polico, R., Bevilacqua, A. and Tesei, A. (2016) '3D tumor spheroid models for in vitro therapeutic screening: a systematic approach to enhance the biological relevance of data obtained', *Sci Rep,* 6, pp. 19103.

Zhang, J. H., Chung, T. D. and Oldenburg, K. R. (1999) 'A Simple Statistical Parameter for Use in Evaluation and Validation of High Throughput Screening Assays', *J Biomol Screen,* 4(2), pp. 67-73.

Zhang, X. D., Ferrer, M., Espeseth, A. S., Marine, S. D., Stec, E. M., Crackower, M. A., Holder, D. J., Heyse, J. F. and Strulovici, B. (2007) 'The Use of Strictly Standardized Mean Difference for Hit Selection in Primary RNA Interference High-Throughput Screening Experiments', *Journal of Biomolecular Screening,* 12(4), pp. 497-509.

Chapter 5. CHRONOLOGICAL PROFILING OF HEPG2/C3A SPHEROIDS AND THEIR UTILITY IN REPEAT-DOSE STUDIES

5.1. Introduction

The results presented in **Chapter 2-5** are demonstrative of a collection of methods with the primary focus of utilising HepG2/C3A spheroids as a central paradigm.

It has been starkly apparent that unlike parental HepG2 cells, HepG2/C3A cells do appear to possess a mechanism of contact inhibition which allowed amenability for long term cultivation of spheroids, concordant with previous studies (Wrzesinski et al., 2013, Gaskell et al., 2016, Calitz et al., 2019). However, compared to previous studies, the use of specialised agaroses to produce LOT microwell plates (Kyffin et al., 2019, Gaskell et al., 2016) was unnecessary and that basic molecular biology-grade agarose was sufficient and did not require subjection to long-term gelation by refrigeration. In this way, spheroids were yielded within 3–5 days that were maintained for up to 28 days without the induction of a necrotic spheroid core, related to hypoxia inducing factors. The production, use and cost-effectiveness of HepG2/C3A spheroids is perhaps even easier than initially thought, capable of generating ready-to-use heterogenous spheroids. It has been demonstrated that cellular 3D-HepG2/C3A *in vitro* models are more sensitive at detecting genotoxic and hepatotoxic compounds compared to assays in which cells are cultured in 2D, as well as presenting evidence for sensitivity towards common hepatotoxicants, such as APAP and DCF.

Toxicological pathways such as those related to genotoxicity and hepatotoxicity are diverse covering a multiple pathologies and molecular initiating events (MIEs); though these datasets have only considered toxicological end points, the sensitivity to these mechanisms has been demonstrably enhanced in spheroids. HepG2/C3A spheroid models could serve as a sensitive and useful model for assessing genotoxicity and would be beneficial versus cells in 2D for the generation of reactive metabolites from mutagenic or hepatotoxic compounds

(Coltman et al., 2021a, Basharat et al., 2020, Stampar et al., 2020). Using a small subset of gene targets, we have demonstrated that the basal expression of several ADME genes and hepatic function-related genes such as those encoding the production of albumin or the urea cycle, are upregulated in HepG2/C3A spheroids compared to monolayers, which have since been confirmed in a range of 3D liver models with profound effects (Stampar et al., 2020, Li et al., 2020, Hurrell et al., 2019), although transcriptional upregulation does not necessarily reflect functionally active enzyme-protein formation and hence expanding gene identification sets would be beneficial to understand how other metabolic pathways are affected in cultured spheroids. A final element of this chapter is to understand how endogenous metabolism is changed in the paradigm of HepG2/C3A spheroids by use of respirometry. Mitochondrial metabolism is critical to hepatic function *in vivo* where typical PHHs have high metabolic turnover compared to cell-lines such as HepG2/C3A where enhanced xenobiotic function, and synthesis of hepatic molecules such as albumin and apoliproteins are known to enhance the oxygen consumption rate of hepatocytes (Cho et al., 2007, Gehre et al., 2020). Because HepG2 are known to be able to adapt to breaks in mitochondrial respiration utilising the Crabtree effect via anaerobic metabolism such as glycolysis (Marroquin et al., 2007), it was hypothesised that the gain in hepatic function of HepG2/C3A spheroids was as a result of a switch in metabolism away from those of a malignant phenotype and towards a functional liver phenotype. The intent of this chapter was therefore to further expand the knowledge of the HepG2/C3A spheroid compared to its 2D counterpart to try and ascertain how sensitivity towards hepatotoxicants and pro-genotoxicants was improved.

5.2. Materials and methods

5.2.1. Chemicals and reagents

All cell culture reagents were purchased from Gibco, Paisley, Scotland, UK. The following compounds were used for ADME(T) studies in HepG2/C3A spheroids:

Etoposide, Isoniazid, Midazolam, Valproic acid and Verapamil (Merck Life Sciences, Surrey, UK); Amiodarone (Acros Organics); Bufuralol (Cambridge Bioscience, UK); S-mephenytoin (Apexbio Technology, TX, USA) and Tacrine (Alfa Aesar, Heysham, UK). BAM15 was from TOCRIS Bio-Techne, Abingdon. All other ADME(T) compounds were sourced from Cayman Chemicals, MI, USA. Acquisition of all other reagents are described in **Chapters 2-4** of this thesis.

5.2.2. Cell culture

HepG2/C3A monolayers and spheroids were generated as previously described (**Chapter 3**) under standard tissue culture conditions, using the agarose-liquid overlay technique. After 3 days of initial spheroid formation, half-volume medium exchanges were performed with spheroid cultures every 3 days throughout the culture period up to 28 days, and vitality assessed regularly by use of phase-contrast microscopy. Cells were confirmed mycoplasma - free by PCR.

5.2.3. Monitoring spheroid growth and normalisation using double-stranded DNA

Planimetric analysis of spheroid images was performed as in **Chapter 3, Coltman et al., 2021a**, throughout the spheroid growth period. In addition to planimetry, double-stranded

nuclear DNA (dsDNA) was used to determine the number of cells per spheroid according to an optimised protocol (**Chapter 4, (Coltman et al., 2021b)** by use of the Quant-iT dsDNA kit.

5.2.4. Viability analyses of HepG2/C3A models by annexin-V and propidium iodide labelling

To assess spheroid viability, flow cytometric analysis was used to quantify cellular populations labelled positively for annexin V binding to phosphatidylserine (apoptosis) and propidium iodide (PI, dead cells – late apoptosis or necrosis). Matched experiments were performed in 2D monolayers and spheroids grown for up to 28 days, and compared against a day 7 spheroid treated with etoposide over 12 h at 10 μM as an apoptosis control group. Spheroids or monolayers were washed 3 x in PBS and incubated at 37 ^{o}C with TrypLE Express, with gentle shaking to applied to spheroids to encourage dissociation for approximately 30 mins which was previously optimised to maintain spheroid viability compared to conventional typsin-EDTA. Enzymatic dissociation was quenched with complete DMEM and cellular suspensions were left to recover for 15 mins at 37 ^{o}C, 5 % CO_2. Cells were washed twice in PBS and resuspended at 4.5 x 10^5 cells/100 μL in 1X annexin binding buffer freshly prepared at 140 mM NaCl, 2.5 mM $CaCl_2$ and 10 mM hepes (pH 7.4). Five microlitres of annexin V pacific blue conjugate was added to 100 μL of cell suspension, briefly pulsed by vortexing and incubated for 15 minutes at room temperature protected from light. Propidium iodide was added at 10 μg/mL and a further 400 μL of annexin binding buffer added; cells were briefly vortexed prior to acquisition of data. The Attune NxT flow cytometer (Life Technologies, Carlsbad, CA, USA) was used to detect annexin V – positive cells in the VL-1 channels and propidium iodide (PI)-positive cells in the YL-1 channel (EX_{561} –

$EM_{620\ nm}$) using both stained and non-stained controls. Flow cytometric analysis was performed using FlowJo Software (version 10.6.2 for Mac, Ashland, Oregan, USA). In the first instance, double negative fractions were defined using the polygon function on ungated data set by comparison of annexin V and PI channels. Within the double negative fraction of cells, both debris and non-debris was gated by comparison of forward (FSC) and Side Scatter (SSC) events and doublet discrimination performed by comparison of Width and Height within those groups. Finally, classification of cell populations was made within the non-debris cluster using quadrant gating to define cells as Live (-VE annexin and -VE PI staining), Apoptotic (+VE annexin but -VE PI staining), or cells were defined as Late apoptotic/necrotic (weak or -VE annexin staining but +VE PI staining), group mean comparisons were made between groups throughout the assay.

5.2.5. Histological examination of spheroids

HepG2/C3A spheroids were collected at days 7, 14, 21 or 28 of culture using a wide-orifice pipette tip, transferred to U-bottomed microplates (Greiner Bio-One) and washed 3 x in PBS. To aid visualisation and handling, spheroids were pre-stained with erythrosine B in PBS (0.2 % w/v) for 2 mins and washed 3 x in PBS. Spheroids were then fixed in paraformaldehyde (4 % v/v, Alfa Aesar, Lanashire, UK) for 1 h at 37 ^{o}C and all subsequent steps were performed according to **Coltman et al. (2021a), Chapter 3**.

5.2.6. Albumin measurements in culture medium

Throughout the spheroid culture period, half-volume medium exchanges were performed every 3 days using complete phenol-free DMEM. After the addition of fresh medium, 100 μL

samples were collected after 72 h from both 2D monolayers at approximately 2.5 x 10^4 cells/well, and spheroids at each respective timepoint. Samples were immediately frozen and stored at -80 ^oC for further analyses. Human albumin was quantified in collected medium samples using an enzyme-linked immunosorbent assay (ELISA) according to the manufacturer's instructions (Bethyl Laboratories Inc, Montgomery, TX, USA), against a standard curve of human albumin prepared using half-log titrations between 500 – 0.68 ng/mL and the absorbance of the product measured at 450 nm using a plate reader. Data were normalised to dsDNA content of HepG2/C3A model.

5.2.7. Measurement of intracellular ATP content in HepG2/C3A spheroids and monolayers

To assess intracellular ATP production, HepG2/C3A spheroids at selected timepoints were collected in parallel to the albumin assay, i.e., 3-days post-medium exchange. Spheroids or monolayers were lysed using the CellTiter-GLO ATP assay kit as previously described with additional steps to ensure complete lysis and ATP recovery, according to the Manufacturer's instructions, with rigorous shaking to induce lysis by use of an orbital plate shaker. An ATP standard curve was also prepared from 0 – 10 μM and luminesce recorded using a plate reader. Acquired data were compared to the standard curve to quantify ATP and normalised to the dsDNA content of HepG2/C3A model.

5.2.8. Metabolic profiling of HepG2/C3A monolayers and spheroids by XF24 extracellular flux analysis

To assess the metabolic phenotype exhibited by HepG2/C3A cells cultured as monolayers and as spheroids, we utilised the Agilent Seahorse XF24 technology where XF96 spheroid

microplates impeded this ability. In order to probe for extracellular acidification rate (ECAR) as a function of glycolytic metabolic flux ,and oxygen consumption rate (OCR) to determine oxidative phosphorylation (OXPHOS) and thus mitochondrial respiratory function, adapted from a published protocol for use in pancreatic islets and those direct from the manufacturer (Wikstrom et al., 2012, Agilent Technologies Inc, 2017). In brief, 1 x 10^5 HepG2/C3A cells were seeded into wells of an XF-24 plate as monolayers in complete cell culture media and left to settle overnight. On the day of assay, cell culture medium was replaced by serum and phenol red – free Seahorse assay media (1 g/L glucose, 1mM sodium pyruvate, Hepes buffered, pH 7.4). In parallel, a pool of 15 spheroids representing 1 – 1.2 x 10^5 cells, were washed in the assay medium and transferred into the depression of empty wells and permeable 'islet capture disks' inserted to keep spheroids in-place within the vessel wells. Well volumes were maintained at 500 μL and assay plates incubated for at least 1 h in a CO_2, 37 ^oC incubator. All subsequent experimental parameters were performed as in **Chapter 4, Coltman et al., 2021b** . At the end of the assay, raw data was exported and normalised to double-stranded DNA extracted from the plates using the QuantiT PicoGreen dsDNA kit to account for cell number differences between the HepG2/C3A models.

5.2.9. Metabolic profiling of HepG2/C3A spheroids under prolonged cultivation by XF96 spheroid extracellular flux analysis

The metabolic profiling of HepG2/C3A spheroid models was performed using protocols assembled in **Chapter 4, Coltman et al. (2021b)** using the Agilent Seahorse XFe96 extracellular Flux technology. Spheroids at days 7, 14, 21 and 28 of culture were extracted from culture vessels and washed into Seahorse XF assay medium containing 1 g/L glucose,

2mM L-glutamine and 1mM sodium pyruvate buffered to pH 7.4, and submitted for analysis as previously described.

5.2.10. Repeat-dose hepatotoxicity screening assay in HepG2/C3A monolayers and spheroids

HepG2/C3A cells were seeded into 96-well tissue culture plates at 1 x 10^4 cells/well in complete tissue culture medium and incubated overnight to adhere at 37 ^oC, 5 % CO_2 to form a monolayer, before single-dose exposure to selected compounds over 48 h. A matched experiment was performed over 48 h in day 7 spheroids. In addition, HepG2/C3A spheroids were grown for 7, 14 ,21 or 28 days and used for the assessment compound cytotoxicity in a repeat dose regimen adapted from Basharat et al. (2020) over 5 days. Twelve small molecule compounds were selected with a range of clinical DILI severities and Cmax values from literature sources (Chen et al., 2020, Thakkar et al., 2020), and stocks were prepared in DMSO and stored as frozen aliquots at $^-20$ ^oC. A serial titration curve was made for each respective compound in DMSO and further diluted in cell culture medium before addition to monolayers or spheroids. Titrations were prepared in 100 % DMSO to cover the C_{max} relative to each compound (see Table 5.1) and diluted to 10 % DMSO in complete cell culture medium to achieve a 10X working stock. Serial titrations were then added to monolayers or spheroids at 1X final assay concentration; the highest concentrations tested were 1000 μM for acetaminophen, valproic acid and isoniazid, above which solubility could not be achieved in the 1 % DMSO-cell culture matrix. For the spheroid repeat dose regimen, each spheroid type was dosed on day 1 and re-dosed on day 3 following a half-volume medium exchange to mimic typical liver clearance in vivo; the spheroid study was

terminated at day 5. DMSO concentration was maintained at each titre point, the vehicle control was therefore 1 % DMSO; etoposide was used as a positive cytotoxicity control at 500 μM. To terminate the studies, 50 μL of culture medium was removed and replaced with an equal volume of the CellTiter-Glo 3D viability reagent. To ensure lysis, particularly those of larger diameter, spheroids underwent incubation for 1 - 1.5 h on an orbital shaker at room temperature and observed under the microscope to ensure adequate penetration of the reagent and lysis. Equal volumes of the developed reagent were transferred into white-walled microplates (Greiner Bio-One) and luminescence quantified using a plate reader. To ensure assay robustness, data was subjected to the Z' prime statistic (Zhang et al., 1999) to compare the assay window of response between the positive (etoposide) and negative (DMSO vehicle) cytotoxicity controls.

5.2.11. Repeat dose genotoxicity study in HepG2/C3A spheroids

To mimic human, daily exposure to environmental genotoxicants, we developed a 7-day repeat low-dosing strategy in 7-day old HepG2/C3A spheroids exposed to pro-mutagens benzo[a]pyrene B[a]P, amino-1-methyl-6-phenylimidazo[4,5-b]pyridine (PhIP) and 2-aminoanthracene (2-AA), alongside direct acting mutagen 4-nitroquinoline N-oxide (4NQO). Owing to limited differences seen between the comet assay performed in 7 and 10 day-old spheroids **(Chapter 3, Coltman et al., 2021a)** spheroids were only grown to 7-days, with regular medium interchanges, prior to exposure to genotoxicants for a further 5 days. Every two-days from day 7 – 12, a half culture medium exchange was performed on HepG2/C3A spheroids mimicking typical human liver metabolic clearance. Fresh medium was replaced containing 10-fold lower concentrations of the four respective genotoxicants than described

in previous 24 -48 h spheroid studies (Coltman et al., 2021a, Štampar et al., 2021, Stampar et al., 2020, Conway et al., 2020); at 3, 1 and 0.3 μM or DMSO vehicle control. An ATP spheroid viability assay was run in parallel as previously described in **Chapter 3** to confirm DNA-damage in the absence of cytotoxicity. On day 12 after 5 days of exposure to reduced concentrations of genotoxicants, spheroids were harvested for trypsinisation, and the comet assay performed as previously described (Coltman et al., 2021a). A minimum of 300 comets were scored per treatment across 4 independent experiments using the median percentage DNA in tail as the parameter for statistical analyses.

5.2.12. Statistics and data analysis

All data were analysed either in RStudio (Version 1.0.153, RStudio Inc, Boston, MA, USA) or GraphPad Prism (Version 8, GraphPad Software, San Diego, CA, USA). Normality testing of datasets was performed as required. Significance was denoted as: **** $p < 0.0001$, *** $p < 0.001$, ** $p < 0.01$, * $p < 0.05$. All data is displayed as mean ± SEM unless stated otherwise.

5.3. Results

5.3.1. HepG2/C3A spheroids growth characteristics

To obtain spheroid growth parameters, planimetric and biochemical datasets were collected from a minimum of 16 spheroids taken from 4 individual biological experiments (n=4, 4 technical replicates per experiment), Figure 5.1 . HepG2/C3A cells seeded at 1 x 10^3 cells/well formed uniform spheroids within 5 days of culture and continued to proliferate reaching a growth plateau at approximately 21 days of culture. In keeping with our previous

observations in Chapter 3, spheroid diameter increased from day 7 (477 μm ± 0.14 standard error) to day 14 (547 μm ± 0.012 stand error) and maintained between days 21 and 28 at approximately 700 μm (Figure 5.1C). Spheroids were healthy in appearance with clearly defined peripheral membranes. Using planimetry captured form photomicrographs, spheroid circularity was maintained between days 7 – 21 but declined at day 28 (Figure 5.1D) .An estimate of spheroid cell number was obtained by quantification of dsDNA extracted from spheroids and compared to dsDNA extracted from standard curves of known cell quantity and found to be in the range of 7 – 41 x 10^3 cells/spheroid between day 7 and 28 (Figure 5.1B), respectively, in-line with previous datasets acquired in Chapter 3, Coltman **et al., 2021a**, cell-doubling/replication times were therefore reduced across the spheroid culture period.

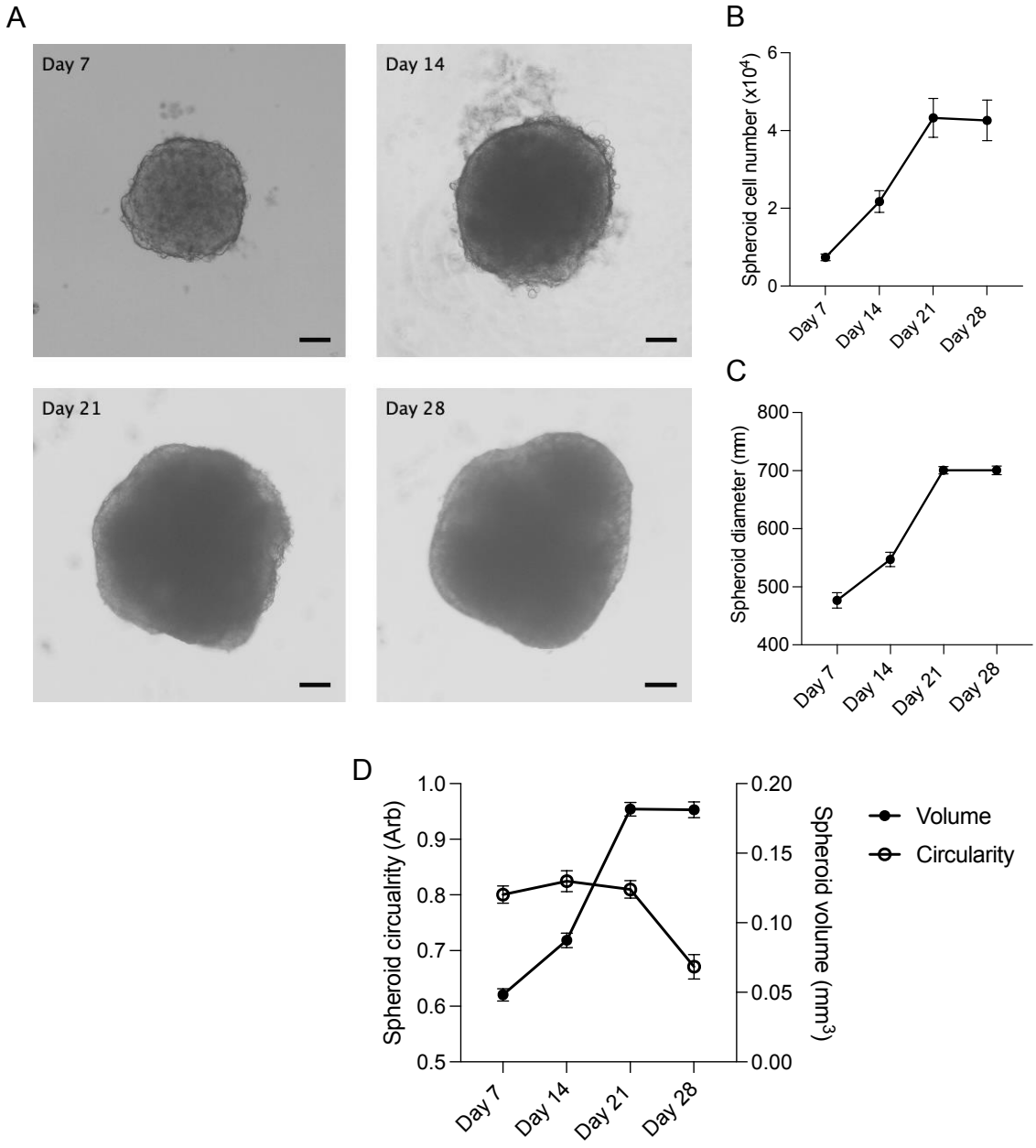

Figure 5.1. HepG2/C3A spheroids continue to proliferate up to 21 days of cultivation but maintain round morphology. *(A) representative phase contrast images of spheroids with data collected for spheroid diameter (B) extracted cell number (C) spheroid diameter and (D) calculated spheroid volume and relative circularity. Scale bar is 100 μm. Data presented is ± SEM mean of 15 spheroids collected across n=4 independent experiments, with 4 technical replicates within each experiment.*

5.3.2. Viability and histological analysis of spheroids grown over 28 days

Contrary to our previous crude method of using trypan blue, assessment of annexin V and PI binding to disaggregated spheroids by flow cytometry (Figure 5.2A)., revealed that spheroid viability gradually declined over the culture period, compared to gated controls and the positive apoptosis control, etoposide at 10 μM over 12 h (Figure 5.2B). The percentage of viable cells was maintained between 87.40 – 89.48 % between days 7 – 21 and continued to decline to day 28, however viability was still maintained ≤ 75 %. Monolayer viability was maintained close to 90 %. Between day 7 and 21, most non-live cells were clustered in quadrants representing late apoptosis/necrosis whereas by day 28 the majority of non-viable cells were found to be in early apoptosis. Internal spheroid structure was determined in sections prepared by paraffin-embedding and tissue processing across the time course and haematoxylin and eosin used to stain sections to assess the morphology and augmentation of cells within HepG2/C3A spheroid structures (Figure 5.2C). The compaction of spheroids increased across the time course, in-line with phase contrast microscopy but the peripheral submembrane maintained. Inter-cellular spacing appeared to be maintained across spheroids structures but at later time points condensations of cells appeared to expand out the outer perimeter, commensurate with a thickening of spheroid membrane and deposition of ECM evidenced by eosin staining. Up to 28 days of culture, spheroids appeared devoid of classical necrotic cores as previously evidenced in other studies (Riffle et al., 2017, Riffle and Hegde, 2017, Gaskell et al., 2016). However, haematoxylin staining revealed evidence of enhanced nuclear condensation in the centre of day 21 and day 28 spheroids however this was not widespread. Combined with flowcytometric analysis using the annexin V probe, this suggests that a small population of cells of between 10-25 % of

total spheroid population at later timepoints (day 21-28) appear to re-enter the normal cell-cycle and enter controlled-apoptotic cell death, potentially because of impaired penetration of nutrients and oxygen, but not cell death associated with necrosis.

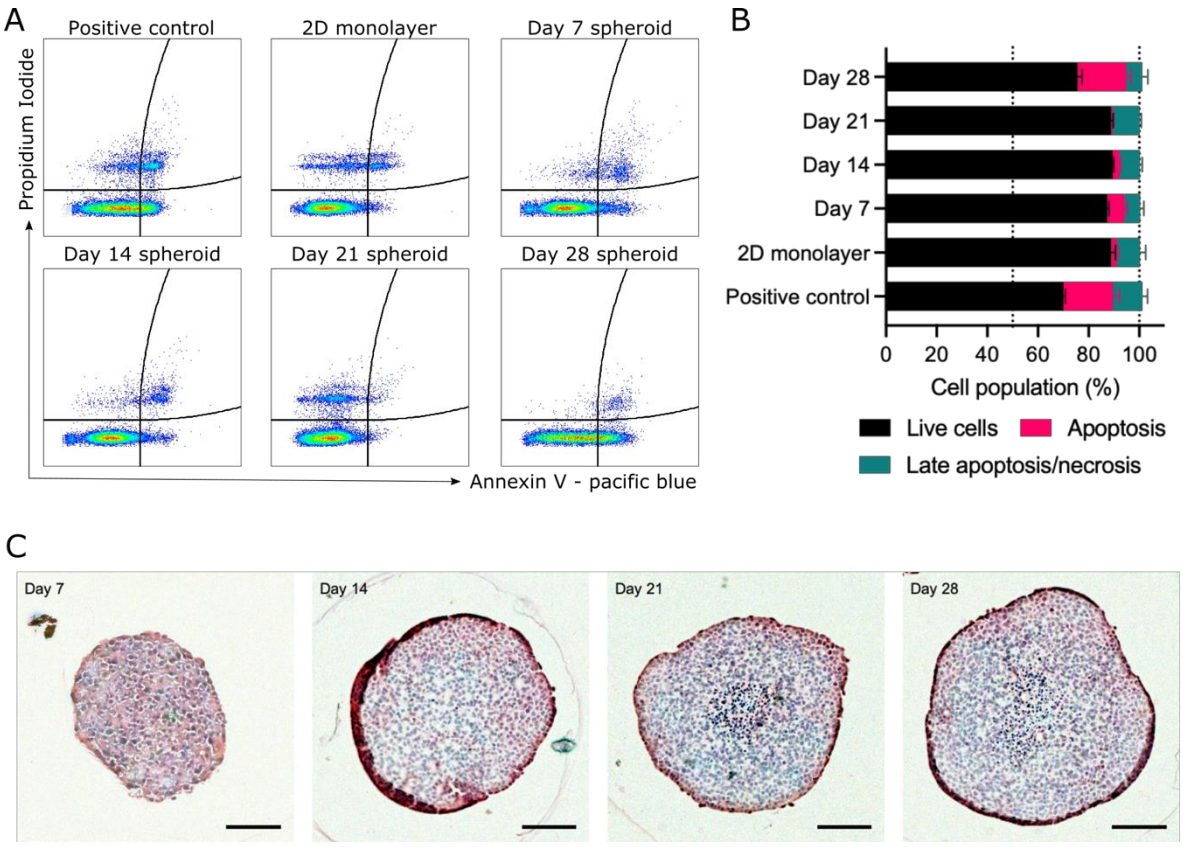

Figure 5.2. HepG2/C3A spheroid viability is maintained over 21 days of proliferative cultivation but begins to decline after 28*. Flow cytometry used to acquire gated populations of Annexin V and propidium iodide positive cells (A) to determine percentage populations of disaggregated cells from HepG2/C3A monolayers or spheroids compared to etoposide-treated apoptosis control. (B) HepG2/C3A spheroids were collected over 28 days of growth and nuclei stained with haematoxylin (blue) and extracellular matrix stained with eosin (red-pink). Scale bar = 100 μm.*

5.3.3. Overall secretion of albumin is enhanced in HepG2/C3A spheroids

Serum albumin was measured in cell culture medium, 72 h after medium refreshment as part of general cell culture methods (Figure 5.3A). Overall, albumin concentrations were found to be significantly enriched in HepG2/C3A spheroids compared to 2D monolayers and were maintained at between 8 and 18-fold higher concentrations than 2D monolayers. Normalised albumin secretion was 0.49 $\pm$ 0.016 ng/mL from monolayer cells. Overall albumin secretion from spheroids increased steadily over the spheroid culture period from 312 $\pm$ 4.99 ng/mL (day 7) to 452.32 $\pm$ 12.70 ng/mL at day 28. However, to correct for spheroid size and cell number, data were normalised to dsDNA content to reveal that spheroids at day 7 had the highest secretion of albumin of 9.31 $\pm$ 0.15 ng/mL (day 7) which was gradually reduced to 6.21 $\pm$ 0.17 (day 14) but this downwards trend appeared to reduce between days 21 (5.18 $\pm$ 0.14) and 28 (4.40 $\pm$ 0.12) suggesting stabilised albumin secretion.

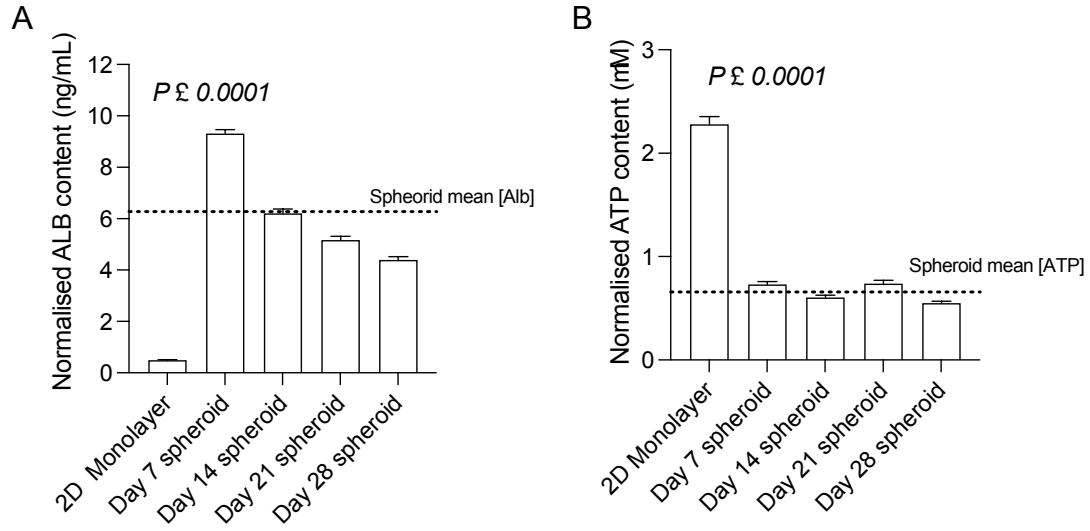

Figure 5.3. Albumin secretion is enhanced in HepG2/C3A spheroids, but production of intracellular ATP content is repressed in spheroids compared to proliferative monolayers. *(A) Serum albumin was quantified from cell culture media by ELISA, collected from HepG2/C3A monolayers and spheroids grown over 28 days. Albumin secreted into cell culture media was significantly enriched in HepG2/C3A spheroids compared to monolayers. In parallel, spheroids were lysed using the CellTiter GLO assay kit and intracellular ATP was quantified against a standard curve. Both datasets were normalised to dsDNA content to*

correct for spheroid size and cell number. Data is mean ± SEM (n=10 independent datapoints); P values were obtained one-way ANOVA.

5.3.4. Normalised ATP content of HepG2/C3A spheroids appeared stabilised versus rapidly proliferating monolayers.

Commensurate with an overall decrease in HepG2/C3A cell doubling time when grown as spheroids, normalised spheroid ATP content was found to be significantly lower compared to highly proliferative monolayers (Figure 5.3B). Normalised ATP content from HepG2/C3A monolayers (2.28 ± 0.071 μM ATP) was approximately 3.4-fold greater than in spheroids whereas spheroidal ATP content was maintained between 0.73 ± 0.026 μM (day 7) to 0.55 ± 0.017 μM (day 28). Interestingly normalised ATP content from spheroids were all closely clustered around the spheroid mean (0.66 μM ATP) where day 14 spheroid responses were highly representative of the mean for both secreted albumin and total ATP content assays.

5.3.5. Metabolic profiling of HepG2/C3A monolayers and spheroids by extracellular flux analysis

To compare the metabolic phenotypes of HepG2/C3A cells grown as monolayers and spheroids the XF24 analyser was used to acquire respiratory data, and again normalised to total cellular dsDNA content, denoted by kinetic mitostress test profiles (Figure 5.4A-B). Despite the heterogeneity associated with spheroid sample versus monolayers, the inter-sample variability with the assay was comparably low. Overall OCR was reduced in all parameters in spheroid models by comparison to 2D monolayers of cells. The basal respiratory rate (Figure 5.4C) of spheroids was more than 2-fold less than that observed in

monolayers (0.07 $\pm$ 0.01 versus 0.17 $\pm$ 0.02 pmol/min/well O_2) suggesting a lower rate of metabolic turnover. Monolayers immediately responded to the addition of the ATP synthase inhibitor, oligomycin, depleting the oxygen consumption rate by approximately 50 % within one cycle whereas this response was retarded in the spheroids requiring 10 assay cycles to reach a similar steady state of OCR kinetics (Figure 5.4A-B) however this could not be maintained and OCR began to increase again in spheroids suggesting incomplete inhibition of cellular ATP synthase activity of spheroids, in-line with Figure 5.4B where ATP content was much lower in spheroids. This suggests metabolic re-routing in the spheroid models to redirect respiration attributed to ATP synthesis which was significantly reduced in spheroids (Figure 5.4D); indeed significant proton leakage was also induced in HepG2/C3A spheroids by more than 5 times that of monolayers suggesting enhanced regulation of mitochondrial ATP synthesis, derived from incomplete inhibition of ATP-synthase activity. Basal extracellular acidification could not be discriminated statistically between the spheroids and monolayers, but the overall pattern of change was in favour in spheroids having a greater ECAR than monolayers, i.e., spheroids have an increased glycolytic rate.

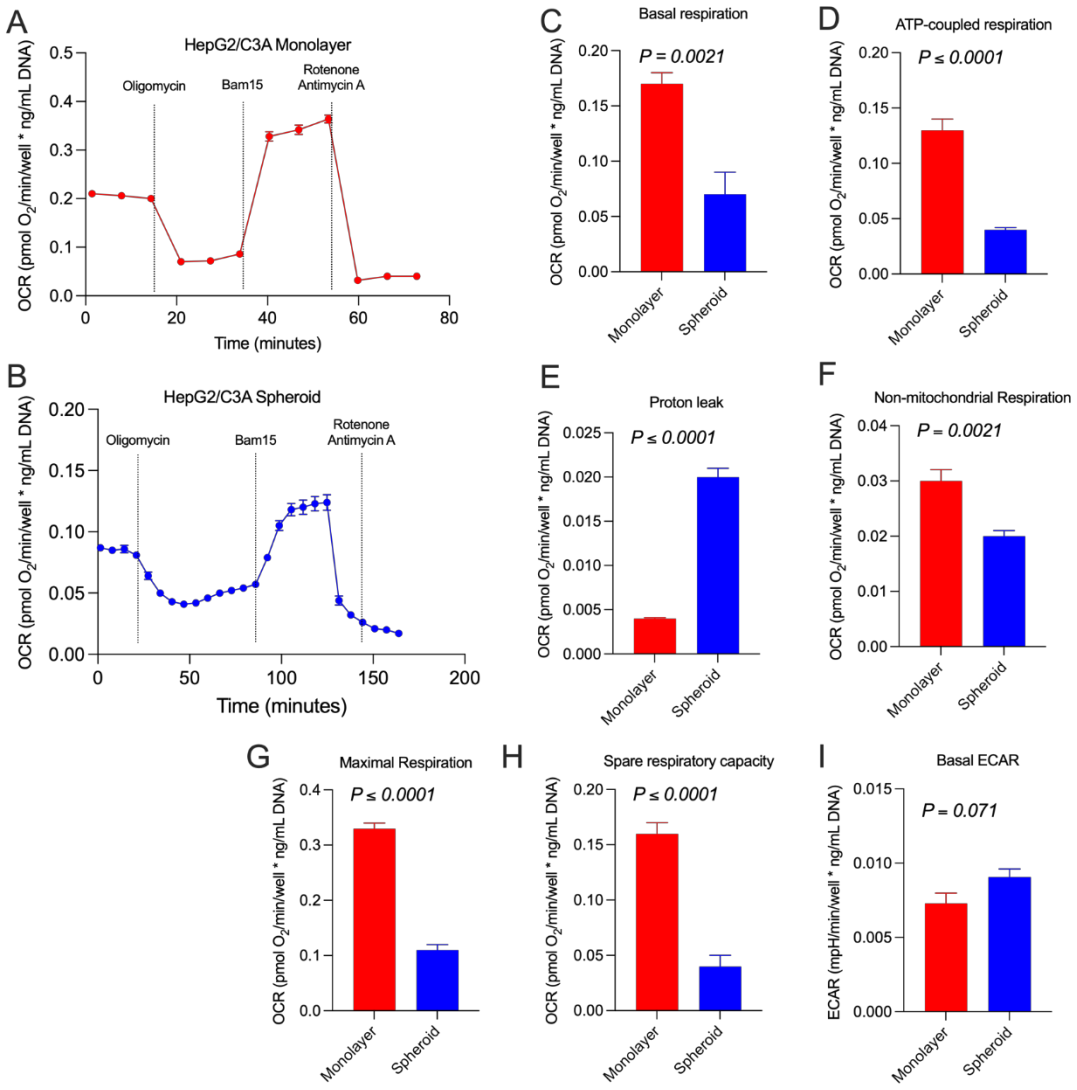

Figure 5.4. Mitochondrial metabolism of Day 7 HepG2/C3A spheroids is diverted from 2D monolayers. *The Agilent Seahorse XF24 was used to acquire respirometry data from pooled HepG2/C3A spheroids and monolayers, and used to derive (A -B) kinetic profiles of mitochondrial stress test performed in monolayers and cells after the addition of oligomycin, Bam 15 and rotenone-Antimycin A in combination. Oxygen consumption rate fluctuations were used to derive a range of functional mitochondrial metabolism parameters (C-G) or extracellular rate used to calculate basal glycolytic rate (I). Data presented is of n=5 independent biological sample, error bars are ±SEM; P values were obtained by unpaired two-tailed t-test.*

5.3.6. Chronological profiling of HepG2/C3A spheroids by extracellular flux metabolic analysis

Interestingly, for all datasets collected, spheroids cultured for between 14-28 days appeared to cluster together and were easily discriminated from parameters acquired in single day 7 spheroids; in line with other datasets gathered in this thesis and further exemplified in **Chapter 6** transcriptomic profiling. This therefore suggests that perhaps metabolic changes in HepG2/C3A spheroids are dynamic to a point and then begin to further stabilise after 2-weeks of culture, before reaching full enrichment after 28 days. This would align with our previous observations that cellular proliferation appears to significantly slow within this culture period. Accordingly, basal respiration, maximum and spare respiratory capacity were all increased (Figure 5.5A, G and H), commensurate with enhanced metabolic requirements of spheroid differentiation. Indeed, proton leakage attributed to incomplete inhibition of ATP synthase activity continued to increase in HepG2/C3A spheroids, significantly by between 5.7 and 10-fold that of day 7 spheroids. Again, although not fully possible to derive a glycolytic rate from this assay type as described in **Chapter 4**, basal extracellular acidification rate, as a proxy for glycolytic spheroid rate, appeared to continue to diverge from day 7 spheroids, and therefore beyond that of monolayers (Figure 5.5E). Unlike Figure 5.4F in which non-mitochondrial respiration was lower in the spheroid versus monolayers, we found that this parameter continued to increase across spheroid cultured for up to 28 days.

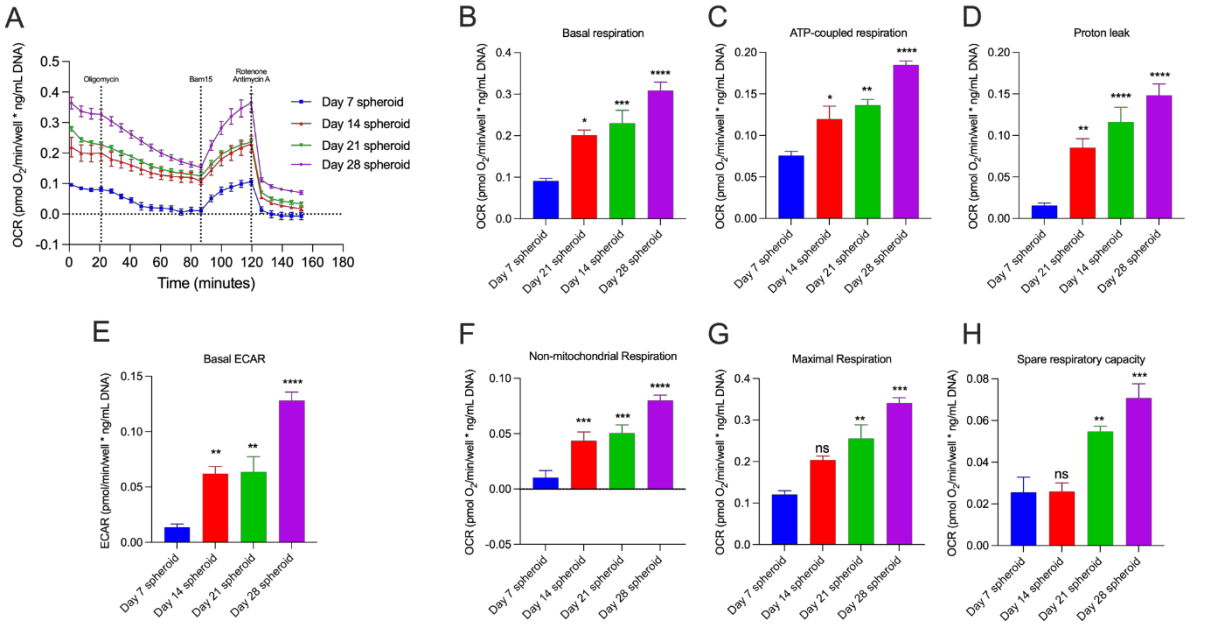

Figure 5.5. Mitochondrial metabolism measured by XF96 extracellular flux analysis of single HepG2/C3A spheroids cultured over time. *The Agilent Seahorse XF96 was used to acquire respirometry data from single HepG2/C3A spheroids grown over 28 days, and used to derive (A) kinetic profile of mitochondrial stress test performed in spheroids after the addition of oligomycin, Bam 15 and rotenone-Antimycin A in combination. Oxygen consumption rate fluctuations were used to derive a range of functional mitochondrial metabolism parameters (B-H) or extracellular rate used to calculate basal glycolytic rate (E). Data presented is of n=5 independent biological spheroid samples, error bars are ±SEM; P values were obtained one-way ANOVA by comparison to day 7 spheroid: ****, P<0.0001; ***, P<0.001; **, P<0.01; *, P<0.05.*

5.3.7. Repeated-dose exposure enhances the sensitivity of HepG2/C3A spheroids to some hepatotoxic compounds versus single-dose exposure in monolayers or spheroids over 48 h

A total of 12 compounds with clinical ranking in terms of drug-induced hepatotoxicity were screened in monolayers over 48 h, and spheroids of varying maturity with a repeated-dose regime (Table 5.1). Clinical C_{max} was recorded for each compound, defined from literature recorded values. Viability, as a percentage of the DMSO vehicle control, was calculated for

all compounds, exposed to monolayers and day 7 spheroids in a single dose 48 h regime; the same compounds were also exposed to spheroids cultured for 7, 14, 21 and 28 days, with repeat dosing every 2 days. Cytotoxic responses were determined by intracellular and intra-spheroidal ATP content. Overall, the maturity of the spheroid models used had limited influence on cytotoxic response to the compounds screened however repeat-dosed spheroids had greater sensitivity to 10/12 compounds tested versus monolayers treated over 48 h. Dose-response curves were constructed for all models using a four-parameter logistical model, and IC50 values (concentration required to reduce viability of respective model by 50 %). Table 5.1 presents data acquired form hepatotoxicity screen, representative plots are appended to this thesis as **Appendix 5**. Of the 12 compounds selected, 7 presented activities in at least one model, with IC50 values at or close to clinically relevant C_{max} values. Compound toxicity towards 2D monolayers was minimal at the concentrations tested however AMD and SLD were active in both monolayers and spheroids, but with significantly supressed activity. Of those active compounds, a repeat dose spheroid model had greater sensitivity to those compounds over 5 days compared to a single-dose 48 h model. For AMD, KETO, TGZ, TRV and VER, there was a difference of $\geq$ 2-fold IC50 change between spheroids exposed over 48 h and those exposed over 7 days, with repeat dosing. At the concentrations tested, dose-response curves did not fully converge for TCR and VPA were in deemed inactive, although at the maximum dose in spheroids, activity was enhanced versus 2D monolayers indicating that activity could be enhanced with increased dose. Similarly, constraining 4PL curve fitting revealed that ATRV and ISZ were both active at the highest concentrations tested, but inactive in HepG2/C3A monolayers.

Table 5.1. Hepatotoxicity screening data derived from repeat and single-dose studies in HepG2/C3A spheroids and monolayers

Compound	Clinical DILI ranking	C_{max} (μM)	Titration range (μM)	Single dose model (48 h)		Repeat dose spheroid model			
				Monolayer IC_{50} (μM)	Day 7 spheroid IC_{50} (μM)	Day 7 IC_{50} (μM)	Day 14 IC_{50} (μM)	Day 21 IC_{50} (μM)	Day 28 IC_{50} (μM)
Acetaminophen	Low	165	1000 - 10	N.C	N.C	N.C	N.C	N.C	N.C
Amiodarone	Severe	5.27	500 – 0.5	48.29 ± 2.53	23.02 ± 0.97	8.19 ± 0.56	14.87 ± 0.25	11.45 ± 1.09	10.62 ± 0.64
Atorvastatin	High	0.45	100 – 0.1	N.C	N.C	N.C	N.C	N.C	N.C
Diclofenac	High	10.1	500 – 0.5	N.C	62.55 ± 3.11	52.98 ± 4.02	89.19 ± 6.81	70.41 ± 6.63	69. 43 ± 5.06
Ketoconazole	Severe	11.3	500 – 0.5	N.C	N.C	28.10 ± 2.89	35.12 ± 3.41	38.12 ± 3.78	28.13 ± 3.75
Isoniazid	Severe	76.6	1000 - 10	N.C	N.C	N.C	N.C	N.C	N.C
Sulindac	High	32	1000 – 10	332.6	210.2 ± 57.98	135.04 ± 11.20	176.50 ± 33.38	161.29 ± 25.72	168 ± 29.64
Tacrine	High	0.08	50 – 0.05	N.C	N.C	N.C	N.C	N.C	N.C
Troglitazone	Severe	6.39	500 – 0.5	N.C	130.4 ± 7.22	70.25 ± 8.80	83.63 ± 8.55	64.90 ± 8.51	74.22 ± 10.95
Trovafloxacin	Severe	4.078	500 – 0.5	N.C	N.C	20.67 ± 0.92	23.39 ± 2.38	29.13 ± 3.37	31.37 ± 3.56
Valproic acid	Severe	693.4	1000 – 10	N.C	N.C	N.C	N.C	N.C	N.C
Verapamil	Low	0.55	100 – 0.1	N.C	13.96 ± 1.96	2.94 ± 0.48	5.89 ± 0.93	6.84 ± 1.25	4.87 ± 0.54

N.C = *curve not converged, IC50 not determined, greater than max dose tested*

= standard error of mean, n=4

5.3.8. Utility of HepG2/C3A spheroids in 7-day repeat genotoxicity exposure studies

HepG2/C3A spheroids were cultured for 7 days and subjected to repeated-dose exposure to model genotoxicants that had previously been screened in **Chapter 3**, **Coltman et al., 2021a.** Repeated -exposure allowed for significantly lower concentrations (10-fold lower) of compounds to be assessed, than were previously determined by use of the alkaline comet assay. In the first instance, the effects of repeat-exposure on spheroid viability were assessed by quantification of intracellular ATP levels (**Figure 5.6**A). The direct acting mutagen 4-NQO appeared to induce modest cytotoxicity in a dose dependant fashion, reducing viability from 92.6 % (0.3 μM) to 80.18 % at the highest concentration. The pro-genotoxicants, B[a]P, PhIP and 2-AA all reduced cell viability by between 10 – 15 % at the maximum tested concentrated (3 μM) however overall viability prior to comet assay analysis was maintained above 85 % under standard comet assay guidelines (Collins, 2004), allowing DNA damage to be distinguished from cytotoxicity-induced cell death. Next, the comet assay was performed on HepG2/C3A spheroids subjected to the same exposure regime (**Figure 5.6**B). The overall ranking of compounds mirrored that of data presented in **Chapter 3**, Coltman et al., 2021a in both the comet assay performed in day 7 and day 10 single-dose exposure studies: 4-NQO > B[a]P > PhIP > 2-AA. For all compounds there was a generalised dose-response trend, however all failed to induced DNA strand breaks at lowest concentration tested (0.3 μM) versus vehicle control. 4-NQO and B[a]P appeared equipotent at 1 μM, with % DNA in comet tail of between 16.4 – 16.07 %, respectively. However, at 3 μM repeated-exposure, 4-NQO increased % of DNA in tail by more than 31.5 %. At 1 μM, PhiP and 2-AA failed to increase DNA damage above that of vehicle control however the length of comet tails were significantly enhanced on increased exposure does to 3 μM.

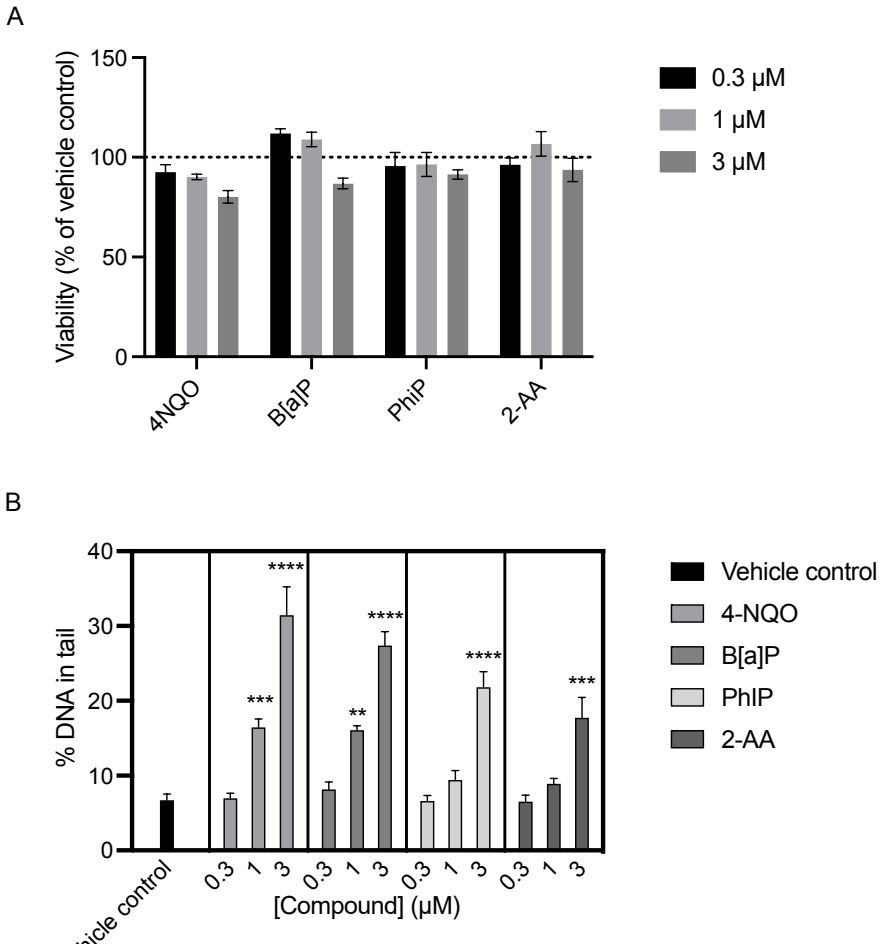

Figure 5.6. Repeat dose genotoxicity testing in HepG2/C3A spheroids. HepG2/C3A cells were cultured as spheroids for 7 days. *At day 7, spheroids were exposed to model genotoxicants at concentrations shown. Every 2 days, a half-volume medium exchange was performed and genotoxicants added again until 7 days of total exposure. Cells were collected and submitted for alkaline comet assay analyses or endpoint ATP viability analyses. (A) cytotoxicity assessment and (B) the percentage DNA in comet tail were determined following repeat-dose genotoxicant exposure in HepG2/C3A spheroids. One-hundred nuclei were scored per experimental unit, in 3 independent experiments and collected as median values. Data is presented as the mean of experimental median values ± SEM. Dotted line in panel A represents maximal viability, data compared to the vehicle control. Statistical significance was determined by comparisons between compound concentrations and vehicle control by one-way ANOVA: ****, P<0.00001; ***, P<0.0001; **, P<0.001; *, P<0.05; ns, P>0.05.*

5.4. Discussion

In line with **Chapter 3, Coltman et al., 2021a** and other studies, long-term cultivation of HepG2/C3A spheroids reveals structures that continue to proliferate, albeit that cell doubling time is significantly reduced across 28 days of culture (Coltman et al., 2021a, Gaskell et al., 2016, Wrzesinski et al., 2013), but compaction, extracellular matrix deposition and overall morphology of HepG2/C3A spheroids does appear to be better maintained than HepG2 parent cells (**Chapter 2**) – and compared to literature sources (Ellero et al., 2021, Elje et al., 2019, Shah et al., 2018b). It is therefore hypothesised that this maintenance of spheroid structure allows for longer-term stability of HepG2/C3A spheroids and this makes them more-readily deployable in toxicological studies, giving rise to increased sensitivity of genotoxicants (Coltman et al., 2021a, Stampar et al., 2020) and hepatotoxicants (Basharat et al., 2020, Fey et al., 2020, Gaskell et al., 2016). HepG2/C3A spheroid vitality was maintained above 75 % for up to 28 days of culture, however proliferation continued to be repressed across this period. We revealed an induction of apoptosis in 28-day old spheroids but only a marginal condensation of nuclei within spheroid centres. Despite these observations, HepG2/C3A spheroids continued to be responsive at all timepoints tested in the battery of assays presented in this chapter, exemplifying their suitability for deployment in longer term toxicity studies than has previously been observed in the literature.

In line with previous studies, albumin secretion was greater in HepG2/C3A spheroids than monolayers (Shah et al., 2018b, Nishikawa et al., 2017, Gaskell et al., 2016) and also evidenced by enhanced mRNA transcription over time (**Chapter 3, Coltman et al., 2021a**) Hepatocyte albumin production rates were found to align with the normalised spheroid

values reported here of between 10-20 pg/cell (Riede et al., 2021). However, the average levels of albumin secretion, when normalised to dsDNA content to take account of spheroid size and cell number, it was found that albumin secretion appeared reduced over the spheroid culture period. Many publications fail to normalise datasets of this kind such as Gaskell et al., 2016, and hence it is difficult to know whether such observations are due to spheroid size or other factors. For example, Nishikawa et al., 2017 showed that albumin secretion and CYP1A1 and 1A2 expression was controlled by HepG2 spheroid size; similarly, we showed that spheroid size controlled for other metabolic events such as oxygen consumption rate (**Chapter 4, Coltman et al. (2021b)**) thus permeability and spheroid size are of course important parameters to consider in studies of this kind and could explain other events elsewhere in the literature, e.g., poor compound diffusivity (Eilenberger et al., 2019).

It would seem plausible that serum albumin in older spheroids could be being harvested for other processes (Spinella et al., 2016), for example in **Chapter 6** we reveal that several pathways relating to the production of other serum proteins, plasminogens and lipoproteins are transcriptionally-upregulated in HepG2/C3A spheroids over 28 days however analysis of these targets at the proteomic level were beyond the current study here. Wrzesinski et al. (2014b) showed that cells extracted from HepG2/C3A spheroids had a much lower protein density compared to DNA content, versus cells taken from highly proliferative monolayers. This would support our observations in that cellular proliferation is repressed across this continuum (Monolayer – Day 7 – Day 14 – Day 21 – Day 28 spheroids). Commensurate with this, it was observed that ATP content extracted form HepG2/C3A monolayers and spheroids, normalised to cell number, was significantly higher in proliferative monolayers

than slowing growing spheroids. In line with observations made by Wrzesinski et al. (2014a), normalised ATP content was stabilised in spheroids between 7-28 days of culture suggesting maximum physiological levels had been reached however it should be noted that this only represents a single endpoint and window of time. Therefore, kinetic metabolic flux analysis was performed in HepG2/C3A monolayer cells and spheroids grown from day 7 – 28. Given that many intracellular metabolic events occur within the order of seconds to minutes, real-time functional approaches such as these applied, were considered paramount for understanding changes in cellular metabolic fluxes, providing information as to the function and overall vitality of the two HepgG2/C3A models.

Understanding phenotypic oxygen profiles of models such as these has significant implications in hepatotoxicity testing pipelines where mode-of-action is potentially impacted by cellular oxygen gradients or the ability of HepG2/C3A to respond to induction of oxidative stress accordingly; dysfunction of active mitochondria is a major cause of hepatotoxicity of xenobiotics such as the cardiotoxin perhexiline and diclofenac (Ren et al., 2020, Syed et al., 2016) as well as having major implications in several disease aetiologies, for example oncological drug-resistance (Hirpara et al., 2019). As such, it was hypothesised that taking HepG2/C3A cells from a monolayer formation into spheroids across a time course would trigger metabolic networks to be redesigned according to spheroid growth, to support the demands of bioenergesis and biosynthesis, away from a cancer phenotype and towards that of phenotypic liver function which would support some of the observations made at the mRNA transcription level in terms of a gain in xenobiotic function and expression of mature hepatic markers such as *HNF4A* and *ALB*.

Overall OCR was decreased in HepG2/C3A spheroids, including reducing spare respiratory capacity – likened to a cellular insurance policy that would allow HepG2/C3A cells to respond to increased energy demand or oxidative stress. However, we previously observed that *NRF2* and *HIF1A* and *NQO1* were induced on genotoxicant exposure in HepG2/C3A spheroids (**Chapter 3, (Coltman et al., 2021a))** suggesting that cells in 3D were perhaps more redox sensitive than those in 2D. This overall reduction in OCR parameters could be because of cells in 3D being forced into a non-proliferative, quiescent state and hence may be better placed to respond to mitochondrial insults. Extracellular acidification rate (ECAR) did appear to be enhanced in spheroids although this could not be confirmed statistically. Due to the geometry of the XF24 cell culture plates we were able to directly compare HepG2/C3A monolayers and spheroids within the same assay. However, in order to compare multiple spheroids across a time course (7-28 days) with several replicates per sample, the XF96 spheroid microplate technology was performed in single spheroids according to **Chapter 4, (Coltman et al., 2021b)** and used to derive respiratory parameters relative to the addition of mitochondrial respiratory modulator compounds, as in Figure 5.4.

Given that HepG2/C3A spheroids cultured for 7 days have been utilised in both assays, and extensively in **Chapter 4, (Coltman et al., 2021b),** it would seem suitable to use this as a control to compared between the two datasets. In-line with data presented in **Chapter 4,** all parameters associated with OCR increased commensurately with HepG2/C3A spheroid age and size (Figure 5.5). However, even after normalisation to dsDNA this still held to be true, indicating that extracellular flux responses were not because of spheroid size as seen previously in HepG2/C3A spheroids of varying cell number (**Chapter 4, Coltman et**

al.,2021b), but more one of distinct metabolic changes, enriched across the spheroid time course. Furthermore, the observation that non-mitochondrial respiration was continually enhanced across the spheroid time course potentially aligns with our original hypothesis that xenobiotic metabolism would be significantly improved in HepG2/C3A spheroids, and continue to be enriched across a spheroid time course as seen by (Fey et al., 2020, Biazi et al., 2020) it is hypothesised that this observation could be as a direct-result of non-mitochondrial oxygen consuming processes, particularly those attributed to CYP450 and flavin monooxygenases metabolism, and NADPH oxidases. In **Chapter 6**, we reveal that several gene pathways are upregulated across the spheroid time course, to this end.

We saw no evidence of there being an induction of a 'necrotic core' by histological analysis. Previous studies have suggested that spheroids with particularly large radii, exceeding some 200 micrometres, how low oxygen porosity due to lack of vasculature, and over cellular compaction, leading to zones of hypoxia (Leedale et al., 2019, Sharifi et al., 2019). However, despite continued expansion in HepG2/C3A spheroid size, we found limited evidence to suggest that that this was the case in our spheroid model. Clearly, those cells throughout our largest (day 28) spheroids are less likely to be exposed to the quantity of nutrients and oxygen that are afforded those cells from day 7 spheroids, and this may explain the gradual decline in spheroid proliferation over the time points described but does not necessarily explain the extracellular flux rates gathered in this study. Interestingly Wrzesinski et al. (2014a) found in HepG2/C3A spheroids cultured over 21 days that these spheroids were potentially able to overcome to this issue relating to poor oxygen transport across the large spheroid diameter by utilising alternative (non-erythrocyte) forms of haemoglobin. Indeed,

as highly sensitive redox sensors, neither *NQO1* or *NRF2* were induced in non-treated spheroids versus monolayers, suggesting that a redox switch was not derived from the switch of culture paradigm. Increasing the oxygen content available to HepG2/C3A spheroids in bioreactor cultures (Stampar et al., 2020, Fey and Wrzesinski, 2012) or a perfused microfluidic device (Tostoes et al., 2012, Domansky et al., 2010) appeared to improve hepatic function. For example, maintenance of oxygen concentration is a principal component of hepatic homeostasis and metabolic flux (Farzaneh et al., 2020, Scheidecker et al., 2020) and hence alternations to the oxygen gradient across spheroids could be an important parameter in determining hepatic-like function in HepG2/C3A spheroid and divergence from monolayers such as inducibility of CYP450 enzymes and differentiation markers, e.g., albumin production, such as would be *in vivo* where oxygen gradients differ between portal and central regions.

It is well regarded that many cancer cells in general, but specifically HepG2 or HepG2/C3A cells in 2D, can circumvent the Crabtree effect (Marroquin et al., 2007, Kamalian et al., 2015). The data presented here supports this notion and suggests that HepG2/C3A spheroids are more readily reliant on mitochondrial respiration and OXPHOS but glycolysis continues to emerge to drive hepatic metabolism as seen in Figure 5.5. In line with similar observations made in PHHs and HepG2/C3A spheroids, it is hypothesised that cells within HepG2/C3A spheroids begin to polarise and in doing so utilise OXPHOS to drive ATP synthesis before switching to glycolysis post-polarisation and maturation (Wrzesinski et al., 2014b, Fu et al., 2013). This data therefore provides compelling evidence that HepG2/C3A spheroid metabolism may be more akin to that of PHHs or the human liver *in vivo*.

Zonal models of HepaRG spheroids revealed that APAP and bromobenzene, but not tamoxifen cytotoxicity was observed in 'perivenous zones' with markedly increased *CYP2E1* expression compared to other zones across the spheroid (Ahn et al., 2019); this could not be modelled in day 7 spheroids which may in part explain a lack of sensitivity to APAP throughout this thesis. Regulation of localised oxygen gradients and spheroid size/age may therefore be important factors when considering the use of hepatic models for modelling molecular initiating events requiring the expression of CYP450 enzymes.

Despite overall differences in the sensitivity to DILI compounds in spheroids (7/12 compounds with measured activity) versus monolayers (2 compounds with some activity), the maturity of the spheroid models tested, had limited influence on the cytotoxic response to the compounds screened. Lack of potency divergence from spheroid maturity indicates that for these compounds, the intrinsic mechanism of action does not differ with spheroid culture period but is more likely to be reflected in the phenotypic changes exhibited by 2D monolayer to 3D spheroid, transformations. However, our panel of compounds presented here represent only a small subset to some of those larger screens presented elsewhere, hence such observations could be subject to change. A larger recent study concluded that HepG2/C3A spheroids were more sensitive to a panel of 150 hepatotoxicants than HepaRG spheroids in a 5-day, repeat dose regime (Basharat et al., 2020) whereas Shin et al. (2018) reported CYP3A4-linked hepatotoxic response in HepaRG spheroids to be only marginally greater than that recorded in HepG2 3D, or even PHH studies ; thus suggesting that hepatotoxic response in those *in vitro* cytotoxicity studies was driven by xenobiotic metabolism propensity. Many of the compounds tested in this chapter are substrates and/or

inhibitors for xenobiotic metabolism enzymes however it is not clear if metabolism-linked cytotoxicity could be attributed to the responses observed in these datasets, however we hypothesise that enhance drug-metabolism capacity exemplifies the differences in hepatotoxicant potencies between HepG2/C3A monolayers and spheroids.

Given that results from this chapter indicate that the maturity of the spheroid had overall limited impact on hepatotoxicity sensitivity and in **Chapter 3, Coltman et al., (2021a)** we showed that cultivation of HepG2/C3A spheroids for 10 days and then the comet assay performed, did not necessarily confer heightened sensitivity to genotoxicants, we chose to perform repeat-dose genotoxicity testing in a 7-day old HepG2/C3A spheroid.
Combined with repeat-dose studies used to screen hepatoxic compounds in HepG2 spheroids (Basharat et al., 2020, Ramaiahgari et al., 2014), this study has therefore further highlighted that HepG2/C3A spheroids could be suitably employed in long-term repeat dose studies, for exposure to more realistic daily concentrations to those experienced *in vivo*. In **Chapter 3, Coltman et al., 2021a**, the lowest concentration of genotoxic molecules represented the maximum tested concentration in this chapter (3 μM).

Repeated dosing of HepG2/C3A spheroids with 3 μM 4-NQO (a direct acting mutagen which forms covalent lesions with DNA) marginally increased DNA damage versus acute dosing. In line with (Štampar et al., 2021) over 96 h of exposure, we found that B[a]P and PhIP induced significant DNA damage in repeatedly-exposed spheroids versus acute dosing by almost 2-fold. However, in an earlier publication (Stampar et al., 2020) demonstrated that exposure to PhIP at 3μM in HepG2 spheroids did not induce DNA strand breaks measured by the

micronuclei assay in a 5-day repeat dose model and did not decrease spheroid proliferation, suggesting that our HepG2/C3A model may be more sensitive to PhIP induced toxicological mechanisms. Both B[a]P and PhIP are metabolised to their active form via CYP1A1/1A2 enzymes and 2-AA metabolism is conferred via both CYP and BAT pathways. In **Chapter 3** and Shah et al. (2018a) it is demonstrated that these enzymes were transcriptionally induced on exposure to these compounds over 24h of exposure.

5.5. Conclusion

In **Chapter 3 and 5** of this thesis, we have identified that HepG2/3A cells are capable of forming spheroids with stabilised structures and functionality up to 28 days of culture. We have identified a number of metabolic processes that are stabilised or expanded over this culture period which includes the enriched expression of hepatic nuclear factors, continued secretion of serum albumin at significantly higher concentrations than in monolayers and dynamic changes in mitochondrial respiratory metabolism in favour of hepatic maturations processes. In **Chapter 2** HepG2/C3A spheroids were found to be more sensitive to acute exposure of 3/4 hepatotoxicants and sensitivity was further enhanced in a repeat dose study (**Chapter 5)**. In **Chapter 3** we implemented the HepG2/C3A spheroid into a detailed genotoxicity study and identified spheroids as being significantly more sensitive to pro-genotoxicants requiring metabolism and that sensitivity to these same compounds were further enhanced in a repeat-dose, low exposure concentration study (**Chapter 5**).

Commensurate with these observations, the basal mRNA expression of key ADME proteins were found to be significantly enhanced in the HepG2/C3A spheroids versus monolayers

(e.g., CYP450s, UGTs), and further induced on exposure to small molecule genotoxicants (**Chapter 3**). It is therefore hypothesised that the improved sensitivity to small molecule toxicants throughout this study is as a result of HepG2/C3A spheroids presenting improved xenobiotic functionality and that the basal gene expression in HepG2/C3A spheroids may represent a time course or hepatic maturation continuum. In the final (**Chapter 6**) of this thesis, genome-wide RNA-seq is used to transcriptionally monitor HepG2/C3A cells as they diverge from monolayers to spheroids of 7, 14, 21 and 28 days of growth, as applied in this study (**Chapter 5**). It is hypothesised that an assessment of this potential continuum in spheroids in terms of transcriptional cues, driving endogenous changes in hepatic spheroid metabolism, would have important implications to future model selection in toxicity screening and could support some of our observations made in throughout this thesis and elsewhere in the literature.

5.6. References

Agilent Technologies Inc (2017) *Islet Assay Using the Agilent Seahorse XF24 Islet Capture Microplate*. Available at: https://www.agilent.com/cs/library/technicaloverviews/public/5991-7155EN.pdf (Accessed: 01 Jan 2021.

Ahn, J., Ahn, J. H., Yoon, S., Nam, Y. S., Son, M. Y. and Oh, J. H. (2019) 'Human three-dimensional in vitro model of hepatic zonation to predict zonal hepatotoxicity', *J Biol Eng,* 13, pp. 22.

Basharat, A., Rollison, H. E., Williams, D. P. and Ivanov, D. P. (2020) 'HepG2 (C3A) spheroids show higher sensitivity compared to HepaRG spheroids for drug-induced liver injury (DILI)', *Toxicol Appl Pharmacol,* 408, pp. 115279.

Bavli, D., Prill, S., Ezra, E., Levy, G., Cohen, M., Vinken, M., Vanfleteren, J., Jaeger, M. and Nahmias, Y. (2016) 'Real-time monitoring of metabolic function in liver-on-chip microdevices

tracks the dynamics of mitochondrial dysfunction', *Proc Natl Acad Sci U S A,* 113(16), pp. E2231-40.

Biazi, B. I., Zanetti, T. A., Marques, L. A., Baranoski, A., Coatti, G. C. and Mantovani, M. S. (2020) 'mRNAs biomarker related to the control of proliferation and cell death in HepG2/C3A spheroid and monolayer cultures treated with piperlongumine', *Applied Cancer Research,* 40(1), pp. 2.

Calitz, C., Hamman, J. H., Fey, S. J., Viljoen, A. M., Gouws, C. and Wrzesinski, K. (2019) 'A sub-chronic Xysmalobium undulatum hepatotoxicity investigation in HepG2/C3A spheroid cultures compared to an in vivo model', *J Ethnopharmacol,* 239, pp. 111897.

Chen, M., Suzuki, A., Thakkar, S., Yu, K., Hu, C. and Tong, W. (2020) 'Food and Drug Administration. Drug Induc'.

Cho, C. H., Park, J., Nagrath, D., Tilles, A. W., Berthiaume, F., Toner, M. and Yarmush, M. L. (2007) 'Oxygen uptake rates and liver-specific functions of hepatocyte and 3T3 fibroblast co-cultures', *Biotechnol Bioeng,* 97(1), pp. 188-99.

Collins, A. R. (2004) 'The Comet Assay: A Sensitive Genotoxicity Test for the Detection of DNA Damage and Repair', *Molecular Biotechnology,* 26, pp. 249-261.

Coltman, N. J., Coke, B. A., Chatzi, K., Shepherd, E. L., Lalor, P. F., Schulz-Utermoehl, T. and Hodges, N. J. (2021a) 'Application of HepG2/C3A liver spheroids as a model system for genotoxicity studies', *Toxicol Lett,* 345, pp. 34-45.

Coltman, N. J., Rochford, G., Hodges, N. J., Ali-Boucetta, H. and Barlow, J. P. (2021b) 'Optimised protocols to expore mitochondrial energy metabolism in spheorids using Agilent Seahorse Extracellular Flux Analysis', *Journal of Visualized Experiments,* n/a(e63346).

Conway, G. E., Shah, U. K., Llewellyn, S., Cervena, T., Evans, S. J., Al Ali, A. S., Jenkins, G. J., Clift, M. J. D. and Doak, S. H. (2020) 'Adaptation of the in vitro micronucleus assay for genotoxicity testing using 3D liver models supporting longer-term exposure durations', *Mutagenesis,* 35(4), pp. 319-330.

Domansky, K., Inman, W., Serdy, J., Dash, A., Lim, M. H. and Griffith, L. G. (2010) 'Perfused multiwell plate for 3D liver tissue engineering', *Lab Chip,* 10(1), pp. 51-8.

Eilenberger, C., Rothbauer, M., Ehmoser, E. K., Ertl, P. and Kupcu, S. (2019) 'Effect of Spheroidal Age on Sorafenib Diffusivity and Toxicity in a 3D HepG2 Spheroid Model', *Sci Rep,* 9(1), pp. 4863.

Elje, E., Hesler, M., Rundén-Pran, E., Mann, P., Mariussen, E., Wagner, S., Dusinska, M. and Kohl, Y. (2019) 'The comet assay applied to HepG2 liver spheroids', *Mutation Research/Genetic Toxicology and Environmental Mutagenesis*.

Ellero, A. A., van den Bout, I., Vlok, M., Cromarty, A. D. and Hurrell, T. (2021) 'Continual proteomic divergence of HepG2 cells as a consequence of long-term spheroid culture', *Sci Rep,* 11(1), pp. 10917.

Farzaneh, Z., Abbasalizadeh, S., Asghari-Vostikolaee, M. H., Alikhani, M., Cabral, J. M. S. and Baharvand, H. (2020) 'Dissolved oxygen concentration regulates human hepatic organoid formation from pluripotent stem cells in a fully controlled bioreactor', *Biotechnol Bioeng,* 117(12), pp. 3739-3756.

Feng, J., Li, J., Wu, L., Yu, Q., Ji, J., Wu, J., Dai, W. and Guo, C. (2020) 'Emerging roles and the regulation of aerobic glycolysis in hepatocellular carcinoma', *Journal of Experimental & Clinical Cancer Research,* 39(1), pp. 126.

Fey, S. J., Korzeniowska, B. and Wrzesinski, K. (2020) 'Response to and recovery from treatment in human liver-mimetic clinostat spheroids: a model for assessing repeated-dose drug toxicity', *Toxicol Res (Camb),* 9(4), pp. 379-389.

Fey, S. J. and Wrzesinski, K. (2012) 'Determination of drug toxicity using 3D spheroids constructed from an immortal human hepatocyte cell line', *Toxicol Sci,* 127(2), pp. 403-11.

Fu, D., Mitra, K., Sengupta, P., Jarnik, M., Lippincott-Schwartz, J. and Arias, I. M. (2013) 'Coordinated elevation of mitochondrial oxidative phosphorylation and autophagy help drive hepatocyte polarization', *Proc Natl Acad Sci U S A,* 110(18), pp. 7288-93.

Gaskell, H., Sharma, P., Colley, H. E., Murdoch, C., Williams, D. P. and Webb, S. D. (2016) 'Characterization of a functional C3A liver spheroid model', *Toxicology research,* 5(4), pp. 1053-1065.

Gehre, C., Flechner, M., Kammerer, S., Kupper, J. H., Coleman, C. D., Puschel, G. P., Uhlig, K. and Duschl, C. (2020) 'Real time monitoring of oxygen uptake of hepatocytes in a microreactor using optical microsensors', *Sci Rep,* 10(1), pp. 13700.

Hirpara, J., Eu, J. Q., Tan, J. K. M., Wong, A. L., Clement, M.-V., Kong, L. R., Ohi, N., Tsunoda, T., Qu, J., Goh, B. C. and Pervaiz, S. (2019) 'Metabolic reprogramming of oncogene-addicted cancer cells to OXPHOS as a mechanism of drug resistance', *Redox Biology,* 25, pp. 101076.

Hurrell, T., Lilley, K. S. and Cromarty, A. D. (2019) 'Proteomic responses of HepG2 cell monolayers and 3D spheroids to selected hepatotoxins', *Toxicology Letters,* 300, pp. 40-50.

Kamalian, L., Chadwick, A. E., Bayliss, M., French, N. S., Monshouwer, M., Snoeys, J. and Park, B. K. (2015) 'The utility of HepG2 cells to identify direct mitochondrial dysfunction in the absence of cell death', *Toxicol In Vitro,* 29(4), pp. 732-40.

Kietzmann, T. (2017) 'Metabolic zonation of the liver: the oxygen gradient revisited', *Redox Biol,* 11, pp. 622-30.

Kyffin, J. A., Sharma, P., Leedale, J., Colley, H. E., Murdoch, C., Harding, A. L., Mistry, P. and Webb, S. D. (2019) 'Characterisation of a functional rat hepatocyte spheroid model', *Toxicology in Vitro,* 55, pp. 160-172.

Leedale, J., Colley, H. E., Gaskell, H., Williams, D. P., Bearon, R. N. and Chadwick, A. E. (2019) 'In silico-guided optimisation of oxygen gradients in hepatic spheroids', *Comput Toxicol*.

Li, F., Cao, L., Parikh, S. and Zuo, R. (2020) 'Three-Dimensional Spheroids With Primary Human Liver Cells and Differential Roles of Kupffer Cells in Drug-Induced Liver Injury', *J Pharm Sci,* 109(6), pp. 1912-1923.

Marroquin, L. D., Hynes, J., Dykens, J. A., Jamieson, J. D. and Will, Y. (2007) 'Circumventing the Crabtree effect: replacing media glucose with galactose increases susceptibility of HepG2 cells to mitochondrial toxicants', *Toxicol Sci,* 97(2), pp. 539-47.

Nelson, L. J., Morgan, K., Treskes, P., Samuel, K., Henderson, C. J., LeBled, C., Homer, N., Grant, M. H., Hayes, P. C. and Plevris, J. N. (2017) 'Human Hepatic HepaRG Cells Maintain an Organotypic Phenotype with High Intrinsic CYP450 Activity/Metabolism and Significantly Outperform Standard HepG2/C3A Cells for Pharmaceutical and Therapeutic Applications', *Basic & clinical pharmacology & toxicology,* 120(1), pp. 30-37.

Nishikawa, T., Tanaka, Y., Nishikawa, M., Ogino, Y., Kusamori, K., Mizuno, N., Mizukami, Y., Shimizu, K., Konishi, S., Takahashi, Y. and Takakura, Y. (2017) 'Optimization of Albumin Secretion and Metabolic Activity of Cytochrome P450 1A1 of Human Hepatoblastoma HepG2 Cells in Multicellular Spheroids by Controlling Spheroid Size', *Biol Pharm Bull,* 40(3), pp. 334-338.

Ramaiahgari, S. C., den Braver, M. W., Herpers, B., Terpstra, V., Commandeur, J. N., van de Water, B. and Price, L. S. (2014) 'A 3D in vitro model of differentiated HepG2 cell spheroids with improved liver-like properties for repeated dose high-throughput toxicity studies', *Arch Toxicol,* 88(5), pp. 1083-95.

Ren, Z., Chen, S., Seo, J.-E., Guo, X., Li, D., Ning, B. and Guo, L. (2020) 'Mitochondrial dysfunction and apoptosis underlie the hepatotoxicity of perhexiline', *Toxicology in vitro : an international journal published in association with BIBRA,* 69, pp. 104987-104987.

Riede, J., Wollmann, B. M., Molden, E. and Ingelman-Sundberg, M. (2021) 'Primary Human Hepatocyte Spheroids as an In Vitro Tool for Investigating Drug Compounds with Low Hepatic Clearance', *Drug Metabolism and Disposition,* 49(7), pp. 501.

Riffle, S. and Hegde, R. S. (2017) 'Modeling tumor cell adaptations to hypoxia in multicellular tumor spheroids', *J Exp Clin Cancer Res,* 36, pp. 102.

Riffle, S., Pandey, R. N., Albert, M. and Hegde, R. S. (2017) 'Linking hypoxia, DNA damage and proliferation in multicellular tumor spheroids', *BMC Cancer,* 17(1), pp. 338.

Scheidecker, B., Shinohara, M., Sugimoto, M., Danoy, M., Nishikawa, M. and Sakai, Y. (2020) 'Induction of in vitro Metabolic Zonation in Primary Hepatocytes Requires Both Near-Physiological Oxygen Concentration and Flux', *Front Bioeng Biotechnol,* 8, pp. 524.

Shah, U. K., Mallia, J. O., Singh, N., Chapman, K. E., Doak, S. H. and Jenkins, G. J. S. (2018a) 'Reprint of: A three-dimensional in vitro HepG2 cells liver spheroid model for genotoxicity studies', *Mutat Res Genet Toxicol Environ Mutagen,* 834, pp. 35-41.

Shah, U. K., Mallia, J. O., Singh, N., Chapman, K. E., Doak, S. H. and Jenkins, G. J. S. (2018b) 'A three-dimensional in vitro HepG2 cells liver spheroid model for genotoxicity studies', *Mutat Res Genet Toxicol Environ Mutagen,* 825, pp. 51-58.

Sharifi, F., Firoozabadi, B. and Firoozbakhsh, K. (2019) 'Numerical Investigations of Hepatic Spheroids Metabolic Reactions in a Perfusion Bioreactor', *Front Bioeng Biotechnol,* 7, pp. 221.

Shin, D.-S., Seo, H., Yang, J. Y., Joo, J., Im, S. H., Kim, S. S., Kim, S. K. and Bae, M. A. (2018) 'Quantitative Evaluation of Cytochrome P450 3A4 Inhibition and Hepatotoxicity in HepaRG 3-D Spheroids', *International Journal of Toxicology,* 37(5), pp. 393-403.

Spinella, R., Sawhney, R. and Jalan, R. (2016) 'Albumin in chronic liver disease: structure, functions and therapeutic implications', *Hepatol Int,* 10(1), pp. 124-32.

Stampar, M., Sedighi Frandsen, H., Rogowska-Wrzesinska, A., Wrzesinski, K., Filipic, M. and Zegura, B. (2020) 'Hepatocellular carcinoma (HepG2/C3A) cell-based 3D model for genotoxicity testing of chemicals', *Sci Total Environ*, pp. 143255.

Štampar, M., Žabkar, S., Filipič, M. and Žegura, B. (2021) 'HepG2 spheroids as a biosensor-like cell-based system for (geno) toxicity assessment', *Chemosphere*, pp. 132805.

Syed, M., Skonberg, C. and Hansen, S. H. (2016) 'Mitochondrial toxicity of diclofenac and its metabolites via inhibition of oxidative phosphorylation (ATP synthesis) in rat liver mitochondria: Possible role in drug induced liver injury (DILI)', *Toxicol In Vitro,* 31, pp. 93-102.

Tenen, D. G., Chai, L. and Tan, J. L. (2021) 'Metabolic alterations and vulnerabilities in hepatocellular carcinoma', *Gastroenterol Rep (Oxf),* 9(1), pp. 1-13.

Thakkar, S., Li, T., Liu, Z., Wu, L., Roberts, R. and Tong, W. (2020) 'Drug-induced liver injury severity and toxicity (DILIst): binary classification of 1279 drugs by human hepatotoxicity', *Drug Discovery Today,* 25(1), pp. 201-208.

Tostoes, R. M., Leite, S. B., Serra, M., Jensen, J., Bjorquist, P., Carrondo, M. J., Brito, C. and Alves, P. M. (2012) 'Human liver cell spheroids in extended perfusion bioreactor culture for repeated-dose drug testing', *Hepatology,* 55(4), pp. 1227-36.

Wikstrom, J. D., Sereda, S. B., Stiles, L., Elorza, A., Allister, E. M., Neilson, A., Ferrick, D. A., Wheeler, M. B. and Shirihai, O. S. (2012) 'A novel high-throughput assay for islet respiration reveals uncoupling of rodent and human islets', *PloS one,* 7(5), pp. e33023.

Wrzesinski, K., Magnone, M. C., Hansen, L. V., Kruse, M. E., Bergauer, T., Bobadilla, M., Gubler, M., Mizrahi, J., Zhang, K., Andreasen, C. M., Joensen, K. E., Andersen, S. M., Olesen, J. B., Schaffalitzky de Muckadell, O. B. and Fey, S. J. (2013) 'HepG2/C3A 3D spheroids exhibit stable physiological functionality for at least 24 days after recovering from trypsinisation', *Toxicology Research,* 2(3), pp. 163-172.

Wrzesinski, K., Rogowska-Wrzesinska, A., Kanlaya, R., Borkowski, K., Schwämmle, V. and Dai, J. (2014a) 'The cultural divide: exponential growth in classical 2D and metabolic equilibrium in 3D environments'.

Wrzesinski, K., Rogowska-Wrzesinska, A., Kanlaya, R., Borkowski, K., Schwammle, V., Dai, J., Joensen, K. E., Wojdyla, K., Carvalho, V. B. and Fey, S. J. (2014b) 'The cultural divide: exponential growth in classical 2D and metabolic equilibrium in 3D environments', *PLoS One,* 9(9), pp. e106973.

Yokoyama, Y., Sasaki, Y., Terasaki, N., Kawataki, T., Takekawa, K., Iwase, Y., Shimizu, T., Sanoh, S. and Ohta, S. (2018) 'Comparison of Drug Metabolism and Its Related Hepatotoxic Effects in HepaRG, Cryopreserved Human Hepatocytes, and HepG2 Cell Cultures', *Biol Pharm Bull,* 41(5), pp. 722-732.

Zhang, J. H., Chung, T. D. and Oldenburg, K. R. (1999) 'A Simple Statistical Parameter for Use in Evaluation and Validation of High Throughput Screening Assays', *J Biomol Screen,* 4(2), pp. 67-73.

Chapter 6. GLOBAL TRANSCRIPTOMIC PROFILING OF HEPG2/C3A SPHEROIDS BY RNA-SEQUENCING ANALYSIS

Declaration

This research forms a manuscript that is currently being prepared for peer-reviewed journal submission.

Author declarations

N.J.C was involved in all facets of this research and conducted all experimental design, data collection and analyses described. Throughout this research, N.J.C was supported by P.F. Lalor and N. J. Hodges

Acknowledgements and funding sources

N.J.C was supported by a BBSRC MIBTP CASE studentship award (BB/M01116X/1, 1940003). Thanks are given to Ms Hannah Dixon for their bioinformatics opinion and guidance.

6.1. Abstract

HepG2/C3A spheroids are a powerful tool for use in toxicological and pharmacological studies, with a more normal liver like phenotype compared to 2D monolayers, allowing their application for example in longer-term toxicity studies. Despite this, a comprehensive understanding as to how a more liver phenotype arises in 3D culture over time, is unclear. In this study we investigated how these models diverge over time using whole-genome transcriptional profiling by RNA-sequencing. RNA from pooled spheroids grown for 7, 14, 21 and 28 days, or monolayers were harvested and submitted for paired-end RNA-sequencing and their transcriptomic profiles compared by differential gene expression analysis. Global transcriptional analysis revealed clear divergence of HepG2/C3A spheroids from monolayers revealing differentially expressed genes (DEGs), of over 500 (Day 7:↑260, ↓244); 1024 DEGs (Day 14:↑811, ↓213); 1298 DEGs (Day 21:↑904, ↓2394) to over 1500 (Day 28:↑1040, ↓486), where inter-spheroid divergence continued across the time course. Upregulated gene clusters directly related to an enrichment of a normal hepatocyte-like phenotype which included prominent pathways pertaining to cholesterol metabolism and bile acid synthesis; xenobiotic metabolism and pathways related to the remodelling of extracellular matrices. Conversely, downregulated genes clustered related to cell-cycle progression, DNA repair and attenuation of apoptosis. These time-lapse analyses demonstrate a transcriptional transformation dependant on the dimensionality of HepG2/C3A cells, towards a more normal hepatic-like phenotype, and an overall divergence away from a hepatic cancer phenotype, evident in HepG2/C3A monolayers.

6.2. Introduction

A widely accepted notion amongst researchers in various communities including toxicology, drug metabolism and disease modelling, is that culturing hepatic cells in three dimensions allows the remodelling of cellular, and moreover molecular processes, towards the recapitulation of an *in vivo* liver phenotype (Kanebratt et al., 2021, Bell et al., 2020); HepaRG (Mandon et al., 2019, Ramaiahgari et al., 2017) , and carcinoma-derived hepatic cells such as HepG2 (Wang et al., 2021b, ter Braak et al., 2021, Gupta et al., 2021); Huh7 (Jung et al., 2017, Terashima et al., 2015), and HepG2/C3A (Coltman et al., 2021a, Stampar et al., 2020, Biazi et al., 2020, Wrzesinski et al., 2013). Despite the striking paradigm shift observed in the phenotype of hepatic cells grown in 3D, a comprehensive understanding of the transcriptional changes underpinning these phenotypic changes remains unclear. Across models using immortalised cell lines, primary human tissue and stem cells, there appears a paucity in datasets defining the molecular events that bring advanced hepatic models closer to the human liver phenotype; in particular, those phenotypic changes that occur in hepatic models cultured over time are poorly understood.

Although hepatocytes at best represent up to three—quarters of total liver cells *in vivo (Zhou et al., 2016, Kmiec, 2001, Aizarani et al., 2019)*, an understanding as to how HepG2/C3A spheroids may be promoted towards a hepatic phenotype away from monolayers, would be beneficial. One area this may serve benefit is with regard to understanding the key molecular cues that underpin hepatic regeneration as a part of disease or toxic insult; for example, advanced HepG2/C3A and HepaRG cell models have shown promise as critical components of bioartificial livers for transplantation and hepatic

regeneration therapies (van Wenum et al., 2016, Chen et al., 2014, Chan et al., 2004). Furthermore, the ability to expose hepatic spheroids to xenobiotics over a prolonged period is one of the principal benefits not possible with the classical 2D monolayer paradigm. In addition, in 2D monolayers many key ADME related genes are either inherently repressed or repressed during extended cell culture. This is particularly true for PHHs which when cultured on stiff matrices such as plastic, rapidly dedifferentiate (Sun et al., 2019, Guo et al., 2017). For many xenobiotics, the time required to biotransform or clear such molecules into active or inactive moieties may often extend beyond such timeframes (Riede et al., 2021). In other fields, the long-term culture of hepatic cells could be particularly important for studying dynamic events such progressive hepatic disease modelling, e.g., insulin resistance (Kozyra et al., 2018), induction of cholestasis (Rose et al., 2021, Nudischer et al., 2020) or the establishment of bile canaliculi (Reif et al., 2015). Alternatively, the typical concentrations of compounds used in *in vitro* toxicology studies often exceed clinical Cmax/plasma concentrations. Therefore, chronic long-term toxicity studies in spheroids may prove particularly useful for modelling low-dose compound concentrations over time (Llewellyn et al., 2021). Gaining an understanding as to the molecular changes in such spheroid models over an extended time course is therefore important.

Although transcriptional changes do not necessarily confer direct translation to a functionally active proteome (Ellero et al., 2021), RNA and proteins are typically-well correlated in hepatic models (Messner et al., 2018), making transcriptional analysis of HepG2/C3A spheroids relevant. Although HepG2/C3A, and their parental counterpart, HepG2, have been probed at the transcriptional level these analyses have been done by

qPCR and hence only generally consider single gene results, with selective biased towards key gene sets, for example xenobiotic metabolism or DNA damage response. We have previously shown high viability and reproducibility of HepG2/C3A spheroids including transcriptional upregulation of key hepatic genes such as *ALB* and CYP450 genes (Coltman et al., 2021a), as well as efficient energy production via oxidative phosphorylation (Coltman et al., 2021b) over time. Transcriptional monitoring of spheroids over an extended period of culture would allow for a detailed time-resolved genome-wide quantification of gene expression.

In this chapter we apply unbiased RNA-sequencing and systematic pathway analyses to gain knowledge about the molecular processes driving the divergence of the phenotype in HepG2/C3A models. These data will therefore be useful for researchers transforming their hepatic cell culture practice from two-dimensions, to three. We show that HepG2/C3A spheroids at all timepoints between 7 – 28 days of culture, significantly diverge from 2D monolayers. We reveal differentially expressed genes in clusters pertaining to a recapitulation of hepatic function, including cholesterol metabolism and bile acid synthesis; the transcriptional control of key hepatic proteins such as plasminogen, albumin, and apolipoproteins; xenobiotic metabolism and pathways related to the remodelling of extracellular matrices. Critically we show that down regulated pathways in HepG2/C3A spheroids relate to cell-cycle progression, DNA repair, attenuation of apoptosis, commensurate with spheroid growth and proliferation between 7 and 28 days of culture, previously observed in **Chapter 5**. Taken together, culture of HepG2/C3A spheroid a across a time course continuum suggests a transcriptional transformation towards a hepatic-like phenotype, and an overall divergence away from the hepatocellular carcinoma tissue from

which cells were derived suggesting transcriptional transformations that are dependent on the dimensionality of HepG2/C3A cells in culture.

6.3. Materials and methods

6.3.1. RNA Extraction

To minimise contamination and degradation of samples, nuclease-free water (Qiagen) and high-quality, sterile laboratory plasticware such as pipette tips and microcentrifuge tubes (Greiner Bio-One) were used. Total RNA was extracted from HepG2 C3A cells cultured as monolayers (2D), and 60 pooled spheroids (3D) over 7-28 days of cultivation, with 5 independent biological samples collected for each sample type using the forced-aggregate approach, agarose liquid-overlay technique, as previously described (Coltman et al., 2021a). The RNEasy Mini extraction kit (Qiagen) was also used as previously described including additional steps for the removal of genomic DNA and quality control. Pure RNA samples were stored at – 80 ^{o}C for subsequent analyses. Figure 6.1 presents an overview of the RNA-seq study from sample collection through to gene set enrichment analysis.

6.3.2. Quality control of RNA samples

Quality and concentration of RNA was assessed by both the Nanodrop N800 spectrophotometer and Qubit Fluorometer (Thermo Fisher Scientific). RNA quality was accepted if the 260/280 and 260/230 ratios was between 1.8 and 2.0 on the Nanodrop N800 prior to high-accuracy quantification using the Qubit RNA High-sensitivity Kit. Quality control and preparation of libraries was performed by the Environmental Omics Group, University of Birmingham. Aliquots of each sample were diluted to 5 ng/μL and analysed using the Agilent

Tapestation 2200 (#G2964AA, Agilent Technologies) with High Sensitivity RNA Screentapes (#5067-5579, Agilent Technologies); RNA Integrity Number (RIN) was determined ≥ 8.0.

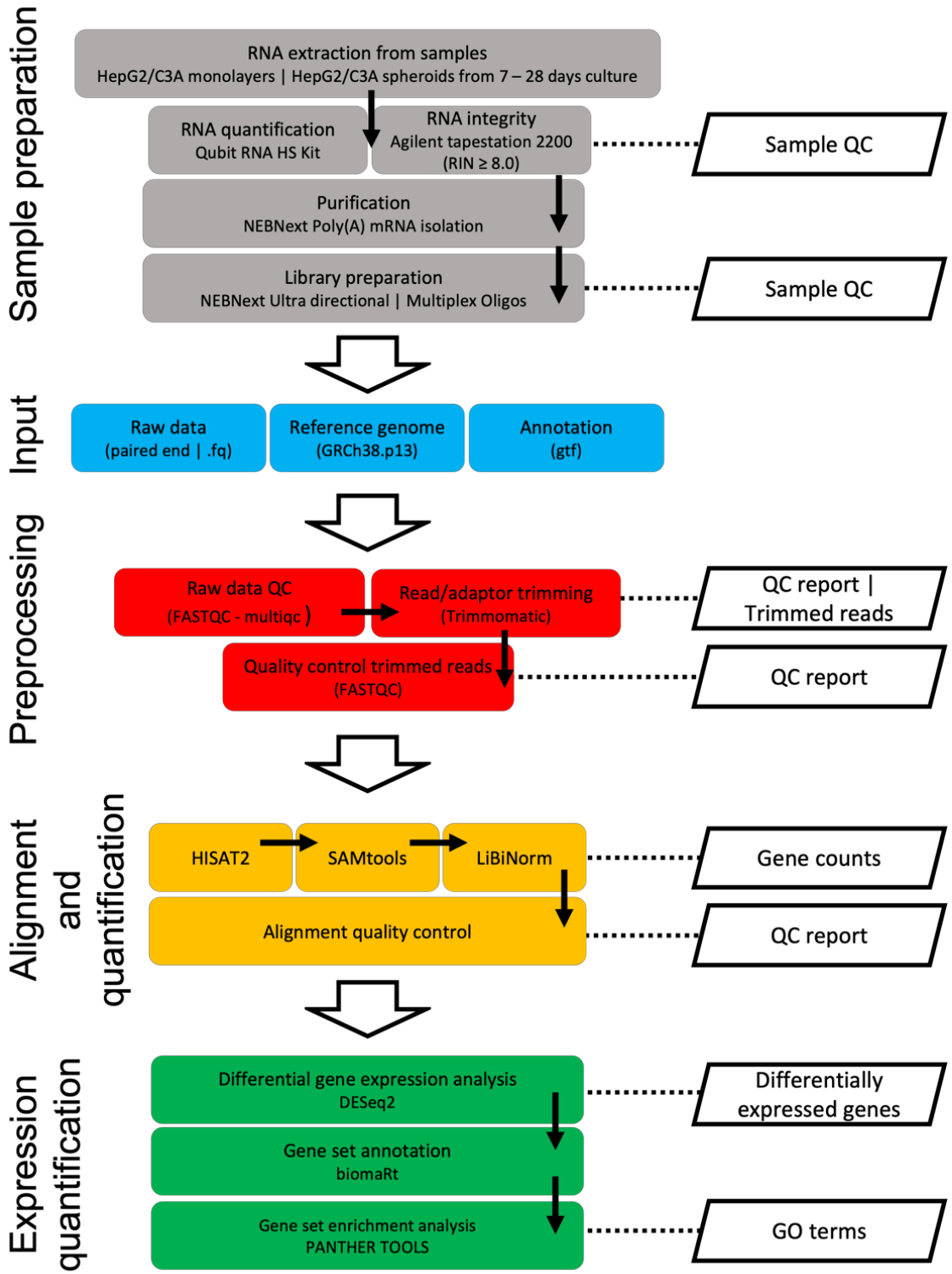

Figure 6.1. Overview of RNA-seq pipeline from sample collection to gene set enrichment. *Overview of RNA-seq pipeline from sample collection to gene set enrichment. Overview of RNA-seq pipeline from sample collection to gene set enrichment. RNA was extracted from HepG2/C3A cells growth as monolayers or as three-dimensional spheroids for 7, 14, 21 or 28 days. Multiplexed cDNA libraries were prepared and subjected to paired-end sequencing before alignment to the GRCh38.013 human reference genome. Differential gene expression was performed from gene-counts data and functional gene set enrichment analysis performed for all samples.*

6.3.3. Preparation of RNA libraries and data acquisition

Sample purification was performed by use of the NEBNext® Poly(A) mRNA Magnetic Isolation Module (#E7490L, New England Biolabs) before progressing to library construction. RNA libraries were produced using 500 ng of total RNA, using the Biomek FxP (#A31842, Beckman Coulter) with NEBNext Ultra II Directional RNA Library Prep Kit (#E7420L, New England Biolab) and NEBNext Multiplex Oligos for Illumina, consisting of 96 unique dual-index primer pairs (#E6440L, New England Biolabs). After library construction, RNA library quality was assessed using the Agilent Tapestation with High Sensitivity D1000 DNA screentapes (#5067-5584, Agilent Technologies). Multiplex library clustering and sequencing was performed with a Paired-End 100bp run upon the DNBseq sequencing platform (BGI Genomics, Shenzen, China), to achieve an average read depth of 10Mb reads per sample, with data being delivered as FASTQ format files.

6.3.4. Pre-processing of data

All subsequent computations for pre-processing and analyses were performed using the BlueBEAR HPC and CaStLeS resources from the University of Birmingham (Thompson et al., 2019). Raw FASTQ files were analysed using FASTQC – v.0.11.9 (Andrews, 2010) and MultiQC – v.1.9 (Ewels et al., 2016). Poor-quality reads and adaptor sequences were removed by Trimmomatic – v.0.39 (Bolger et al., 2014) with default paired-end parameters. Reads were

trimmed where phred score fell below threshold of 33, with average base quality ($q \leq 15$). Read lengths less than 36 bp were excluded from analyses. Sequences were aligned to the GRCh38 human reference genome from Ensembl (Zerbino et al., 2018) using HISAT2 – v.2.2.1. Indexed BAM files were generated using SAMtools – v.0.1.19 (Li et al., 2009), discarding unmapped reads.

6.3.5. Obtaining gene counts

Gene counts files were generated using the LiBiNorm tool (Dyer et al., 2019) in a HTSeq-count compatible format from aligned indexed BAM files, using default bias compensation according to Smart-seq2 protocols, using the reference gene transfer file (GTF, v-104.p13) file from Ensembl. HISAT2, SAMtools and LiBiNorm was performed using a looped custom script with the BlueBEAR environment. Quality control and inspection of files throughout the pipelines was performed using FastQC & MultiQC, Picard tools – v.2.17.8 (Broad Institute, 2018) and Qualimap – v.2.2.1 (Okonechnikov et al., 2016).

6.3.6. Identification of differentially expressed genes

All further steps in the RNA-seq analysis pipeline were computed from within the *R'* environment (R Core Team, 2019). Differential gene expression analysis was performed by DESeq2 – v.1.31 (Love et al., 2014) using counts files for the normalised expression of gene reads for each respective sample as transcripts per million (TPM), generated from the LiBiNorm tool. Exploration and visualisation of data was performed using the *Tidyverse* (Wickham et al., 2019) and *Bioconductor* (Huber et al., 2015) collection of packages, including ggplot2 (Wickham et al., 2016), *ViDGER (Monier et al., 2021)*, *enhancedvolcano*

(Blighe et al., 2019) and pheatmap (Kolde, 2012). Gene annotation was performed using data collected from Ensemble by the *BioMart package (Smedley et al., 2009),* and subjected to gene ontology analysis (GO analysis) using *PANTHER* (Ashburner et al., 2000, Gene Ontology, 2021). Differentially expressed genes were stringently defined as having adjusted *P* value (padj, benjamini-Hochberg correction) ≤ 0.05, and log2 fold change of gene count ≥ 2 or ≤ -2 for up – or downregulated genes, respectively.

6.4. Results from RNA-seq transcriptomic study in HepG2/C3A models

6.4.1. Pre-processing results

Stringent quality control was applied therefore due to technical reasons and quality control threshold, some replicates were removed from the analysis pipeline. All remaining samples passed the initial quality control after the removal of poor-quality reads and adapter sequences using Trimmomatic (Table 6.1).The mean average guanine-cytosine content (GC content) was 49.68 % $\pm$ 0.33 across all samples, with an average per base quality phred score (100 bp) of 34.97 $\pm$ 0.13. For all samples an average of 97.3 $\pm$ 0.63 % of reads aligned to at least one region of the human reference genome, with average sequencing depth of 14.92 million reads per sample. Biological replicates were compared by log-normalised counts which were typically concordant between replicates, indicating tight clustering within sample groups. With the exception of 2D monolayers, with *n=3* replicates, sample sizes were a minimum of 4 (day 7 and 14) -5 (day 21 and 28) biological replicates which were carried forward in the analysis pipeline for statistical analyses and differential gene expression analysis.

Table 6.1. Summary of RNA-seq data for all samples before differential gene expression analysis using DESeq2

Sample iD	Condition	Mean GC content (%)	Sequence depth/sample (millions of reads)	Overall genome alignment rate (%)	Per base$_{100}$ sequence quality (phred score)
21	2D_monolayer	49	14	98.59	34.09
23	2D_monolayer	48	22.02	98.04	34.5
24	2D_monolayer	52	14.8	98.61	34.07
26	Day_7_spheroid	49	12.5	98.68	34.31
27	Day_7_spheroid	49	12.8	98.71	34.2
28	Day_7_spheroid	49	11.2	98.86	34.12
29	Day_7_spheroid	49	14.8	98.67	33.96
32	Day_14_spheroid	48	23.8	91.15	35.8
33	Day_14_spheroid	50	23.4	96.13	34.12
34	Day_14_spheroid	50	13.3	96.77	34.24
35	Day_14_spheroid	53	10.9	98.59	33.65
36	Day_21_spheroid	49	13.2	97.62	34.25
37	Day_21_spheroid	49	23.9	98.17	35.7
38	Day_21_spheroid	49	14.7	98.65	34.03
39	Day_21_spheroid	47	9.6	84.96	34.14
40	Day_21_spheroid	49	11.2	93.7	33.67
41	Day_28_spheroid	50	10.1	97.38	33.3
42	Day_28_spheroid	50	15.5	97.76	33.88
43	Day_28_spheroid	50	14.5	98.57	34.18
44	Day_28_spheroid	53	14.5	99.13	33.54
45	Day_28_spheroid	49	18.1	98.73	34.05

6.4.2. Summary of raw and normalised gene expression levels across HepG2/C3A sample types in transcriptomic study

A total of 17,611 genes were successfully annotated against the GRCh38 human reference transcript, within biological replicates over 5 sample groups. To aid graphical visualisation of raw read counts, the mean number of mapped gene counts was determined for each biological sample within each of the 5 groups. Prior to normalisation, the number of mapped gene counts achieved for each biological sample was between 5×10^6 and 1.7×10^7 reads. (Figure 6.2B) For library size compensation, rlog transformation was applied using DESeq2 to obtain gene read counts per million (CPM) allowing for visual representation of all replicates within the 5 sample groups. The distribution of log2 normalised counts was highly comparable across every replicate within each sample group median values in the range of 6.24 – 6.38 gene log2 counts per million. Mean CPM values were in the range 4.70 – 4.75 indicating successful DESeq2 normalisation and removal of mean variance dependence across sample types.

6.4.2.1. Clustering of transcriptomic datasets based on sample condition

Hierarchical clustering by Euclidean distance clearly discriminated between HepG2/C3A monolayers and the four spheroid groups, with strong conservation of distance between biological replicates of the same condition (Figure 6.2A) indicating independence of sample type between HepG2/C3A cell grown as monolayers and those as spheroids. Principal component analysis (PCA) was used to resolve dimensions between sample groups in an unsupervised manner (Figure 6.2C). PCA clearly separated groups firstly by model type (monolayer versus spheroid) and then length of spheroid culture period, with tight clustering

between condition groups. Principal component 1 (PC1) significantly discriminated between groups, contributing 75 % of the total variance in the dataset. Conversely, PC2 only contributed to 9 % of the total variance but still resolved sample groups. Interestingly, in the both the hierarchical clustering and PCA model, there appeared to be close association between spheroids grown between days 14 and 28 which was discriminated from those in the day 7 population indicating a continual transcriptomic divergence between 2D monolayers, day 7 spheroids and spheroids at later timepoints.

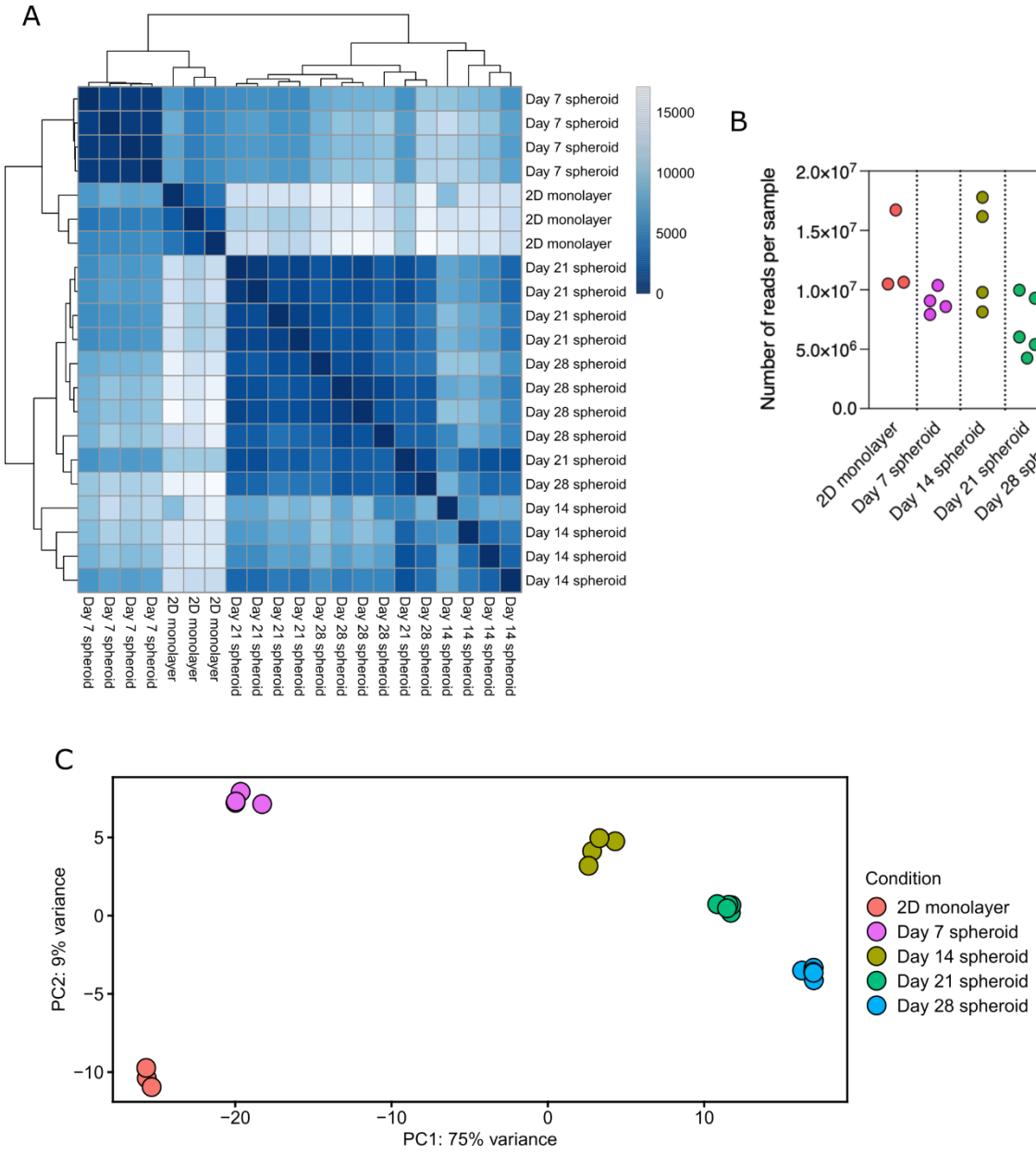

Figure 6.2. RNA-seq dataset summaries for HepG2/C3A monolayers and spheroids grown for 7, 14, 21 and 28 days. *(A) Hierarchical clustering with Euclidean distance used to measure dissimilarity between samples. (B) Number of raw gene count reads recorded for each biological sample type prior to data normalisation. (C) Principal component analysis comparing HepG2/C3A 2D monolayers and spheroid sample types between Component 1 (x-axis) and Component 2 (y-axis).*

6.4.2.2. Comparison of raw gene counts between sample replicates and groups

To investigate the expression levels of individual genes in the 5 sample groups, iterative pairwise comparisons were made (Figure 6.3). DESeq2 normalised gene expression levels were made using $\log_{10}$ of normalised reads per million mapped reads (FPM) and compared Pearson's correlation used to compare the number of gene read counts between different sample groups constituting pools of biological replicates. It was therefore expected that datapoints that aligned with the *x=y* line (*R=1)* between sample comparison were unlikely to be DEGs. Conversely, those that deviated from the *x=y* line could potentially be DEGs or may identify artefacts in datasets. Where pairwise comparisons were made between the 2D monolayer and spheroid groups, there was continuous deviation of transcripts from the *x=y* line with the degree of correlation reducing with each iterative comparison to the monolayer control group: *R = 0.982*, D7*; R = 0.967,* D14*; R = 0.959,* D21 and *R = 0.952,* D28 spheroid. When pairwise comparisons were made using the Day 28 spheroid group as the control, the degree of correlated FPM transcripts was also reduced at each iteration. These observations further highlight a continuous transcriptomic divergence with spheroid culture time where FPM reads between Day 21 and Day 28 were found to be highly similar (*R=0.995*); however, a substantial dissimilarity was seen when compared to the Day 7 spheroid group (*R=0.965*). Taken together, normalised data taken from the DESeq2 object suggests transcriptomic divergence that is clustered across three groups: HepG2/C3A 2D monolayers | Day 7 HepG2/C3Aspheroids | spheroids of later time points (14 -28 days).

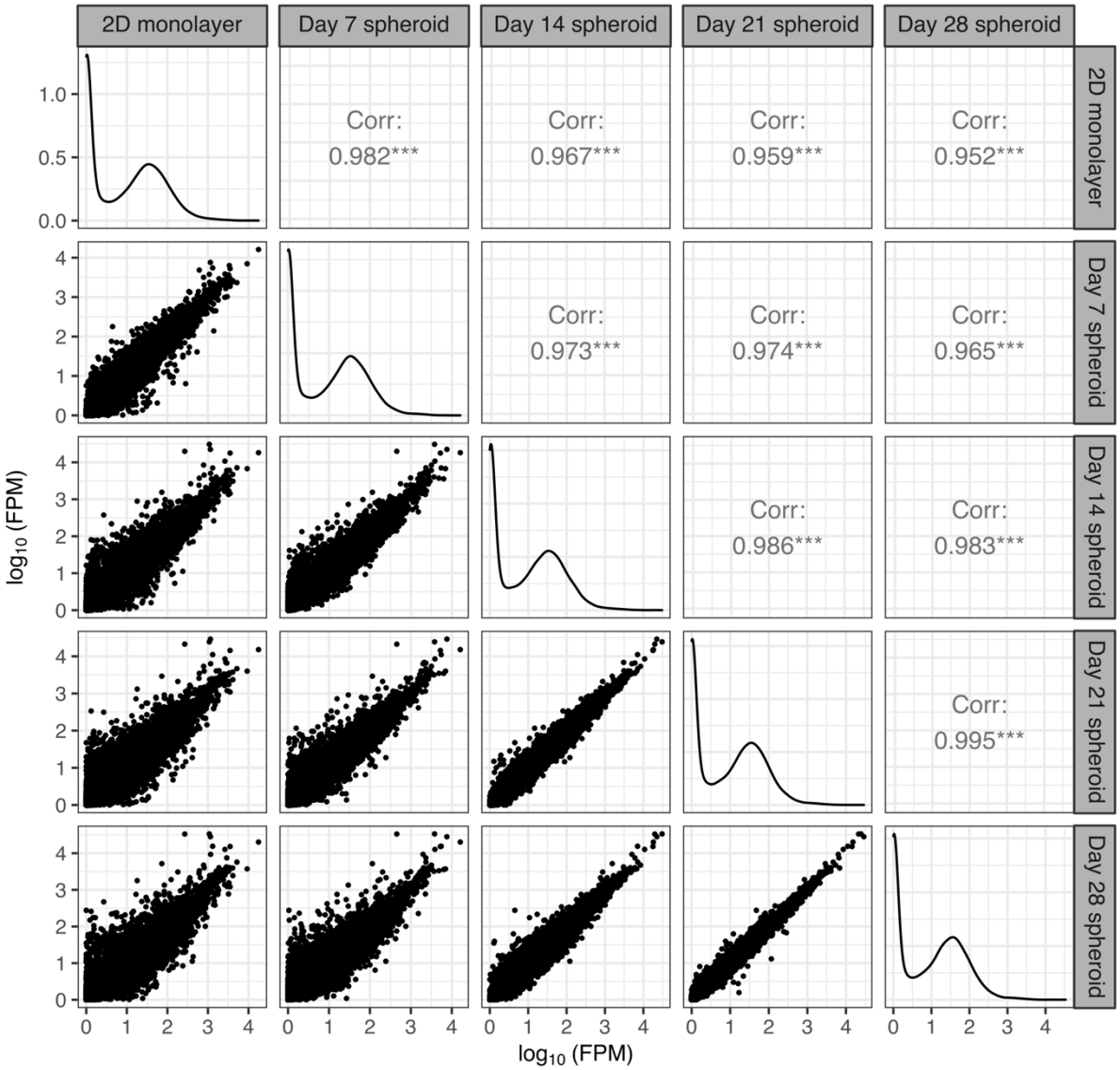

Figure 6.3. Scatter plots showing pairwise comparisons between transcriptomic experiment sample types of normalised gene expression levels*. Expression levels of individual genes was made using log₁₀ of normalised reads per million mapped reads (FPM), with density plots displayed and compared between sample groups by Pearson's correlation.*

6.4.2.3. Obtaining a prediction of human *in vivo* liver similarity of raw transcripts

All HepG2/C3A models, including 2D monolayers, were assessed for degree of human liver similarity at the raw transcript level using the liver-specific gene expression panel algorithm (LiGEP), see Figure 6.4. The LiGEP algorithm has been developed to allow statistical

comparison of raw transcript values (FPKM) from hepatic samples (e.g., liver spheroids, organoids, cells lines), to those of human adult liver (Kim et al., 2017).

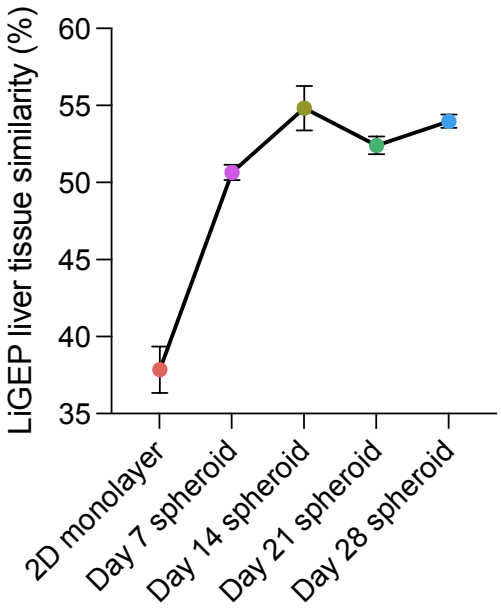

Figure 6.4.Degree of liver similarity score of HepG2/C3A models. *Raw FPKM values were compared for all models, to data embedded within the LiGEP algorithm, against human liver samples (Kim et al., 2017).*

This algorithm has recently been updated to include similar algorithms to yield similarity scores against lung, heart, and stomach tissue (Lee et al., 2021). The algorithm is hosted as a web-based interface (Web-based Similarity Analysis System, https://www.kobic.re.kr/wsas/) and uses a system of functions embedded within an R' script. To derive a score of organ similarity, e.g., percentage liver similarity, the system takes raw RNA-Sequencing transcript data in the form of normalised FPKM, RPKM or TPM values exported from the RNA-seq analysis pipeline. For the LiGEP algorithm, raw FPKM values were calculated for all HepG2/C3A samples using the *countToFPKM* function (Alhendi, 2019) which takes: (1) mean fragment length insert for all transcripts (in the range 193 – 230 bp); (2) feature length of all

genes in aligned transcript and (3) gene counts derived from DESeq2. FPKM values were tabulated alongside a corresponding gene as Ensemble gene ID, uploaded in delimited form and compared by the LiGEP algorithm to FPKM values derived from adult human liver that were embedded within the algorithm, generating percentage liver similarity for all uploaded samples.

Similarity scores are presented in Figure 6.4 . HepG2/C3A 2D monolayers presented a low liver similarity score of 37.86 $\pm$ 1.52 % which was increased to 50.66 $\pm$ 0.51% similarity in spheroids cultured over 7 days. Spheroids cultured for 14 – 28 days were further diverged from 7-day spheroids and monolayers with increased liver similarity scores of between 52.41 $\pm$ 0.58 (day 21) to 53.97 $\pm$ 0.43 % (day 28), with and highest liver similarity in day 14 spheroids (54.82 $\pm$ 1.43 %), indicating further enrichment of LiGEP genes and moreover, a stabilisation in expressed genes controlling hepatic-like differentiation. These results are in-line with HepaRG spheroids compared using the same algorithm (Kim et al., 2017, Mun et al., 2019), and reflects that of a similar study comparing HepG2 spheroids to various advanced liver models including precision cut liver slices and organoids, for degree of liver similarity by RNA-seq. (Gupta et al., 2021). It would seem that although HepG2/C3A spheroids had greater similarity to human liver versus cultured monolayers, a greater degree of liver similarity would perhaps be conferred by the addition of other non-parenchymal hepatic cells types, not incorporated as part of this model but extensively deployed elsewhere in similar *in vitro* toxicological studies (Bell et al., 2020, Kermanizadeh et al., 2019)

6.4.2.4. Fold-change differences in normalised mean counts between sample groups

Pairwise comparisons of all spheroid groups compared to the 2D monolayer baseline control was made for log-transformed mean normalised counts versus log fold-change as a ratio of normalised counts 'signal' intensity using MA plots whereby data was transfored to log ration (M) and mean-average scale (A), (Figure 6.5). In these analyses, a conserved fold-change threshold was set at ≥ 1 and ≤ -1, respectively, controlled for false discovery rate ($P \leq 0.05$). Similarly, divergence from the *M=0* line, where gene counts clustered along the *M=0* line represent non-significant gene expression, increased with spheroid culture time point. A significant number of data points deviated from *M=0* in the monolayer versus Day 7 spheroid group with a relatively even distribution of data points across the *y-axis* (Figure 6.5A) indicating an even dispersion of up – and downregulated genes. This was significantly enhanced in the Day 14 group (Figure 6.5B) and further in the remaining two groups where the dispersion of data points across the *y-axis* became more polarised with each iterative comparison thus indicating an upwards trend of upregulated genes in spheroids of a later timepoint.

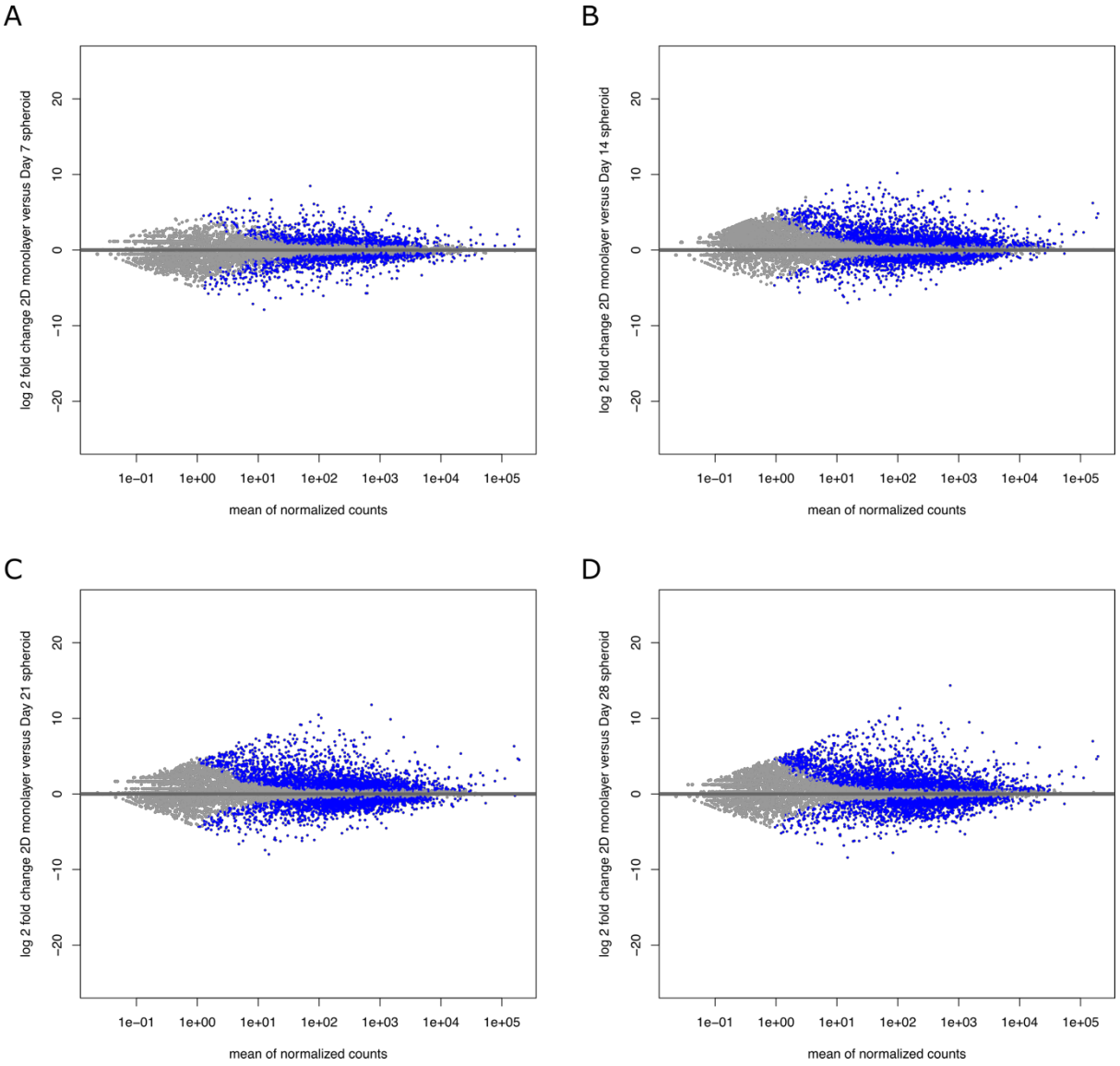

Figure 6.5. MA plots displaying fold change versus mean expression of normalised counts. *Pairwise comparisons were made between HepG2/C3A 2D monolayers and day 7 (A), Day 14 (B), Day 21 (C) and Day 28 spheroids (D). Individual data points represent a single gene with those highlighted in blue exceeding conserved log2 fold-change threshold of ≥1 or ≤-1, FDR corrected (P ≤0.05).*

6.5. Discussion of differential gene expression analysis results

DEGA was applied to obtain the number of DEGs throughout all sample type comparisons to HepG2/C3A monolayers using the DESeq2 package with *R'* (Figure 6.6). HepG2/C3A 2D monolayers were used as the baseline reference group and statistical analyses used to compare the 4 spheroid groups. Using stringent filtering methods of log2 fold-change ≥ 2 or ≤ -2, and Benjamini-Hochberg FDR correction of $P \leq 0.05$, a continual increase in the number of both up- and down-regulated genes at each successive spheroid timepoint was observed using multiple *t-testing*. The number of DEGs between the control monolayer group and spheroids cultured for 7 days was 504 DEGs (2.86 % of total positively identified genes) (Figure 6.6A) with relatively even distribution of those considered up – (260) and downregulated (244). The total number of DEGs increased with each iterative comparison to 1014 (day 14, 5.76 % of total positively identified genes), 1298 (day 21, 7.37 % of total positively identified genes) and was increased approximately 3-fold by day 28 (1526, 8.67 % of total positively identified genes) of which, 1040 exceed the ≥ 2-fold threshold and 486 fell below the ≤ 2-fold threshold indicating downregulated gene expression (Figure 6.6D).

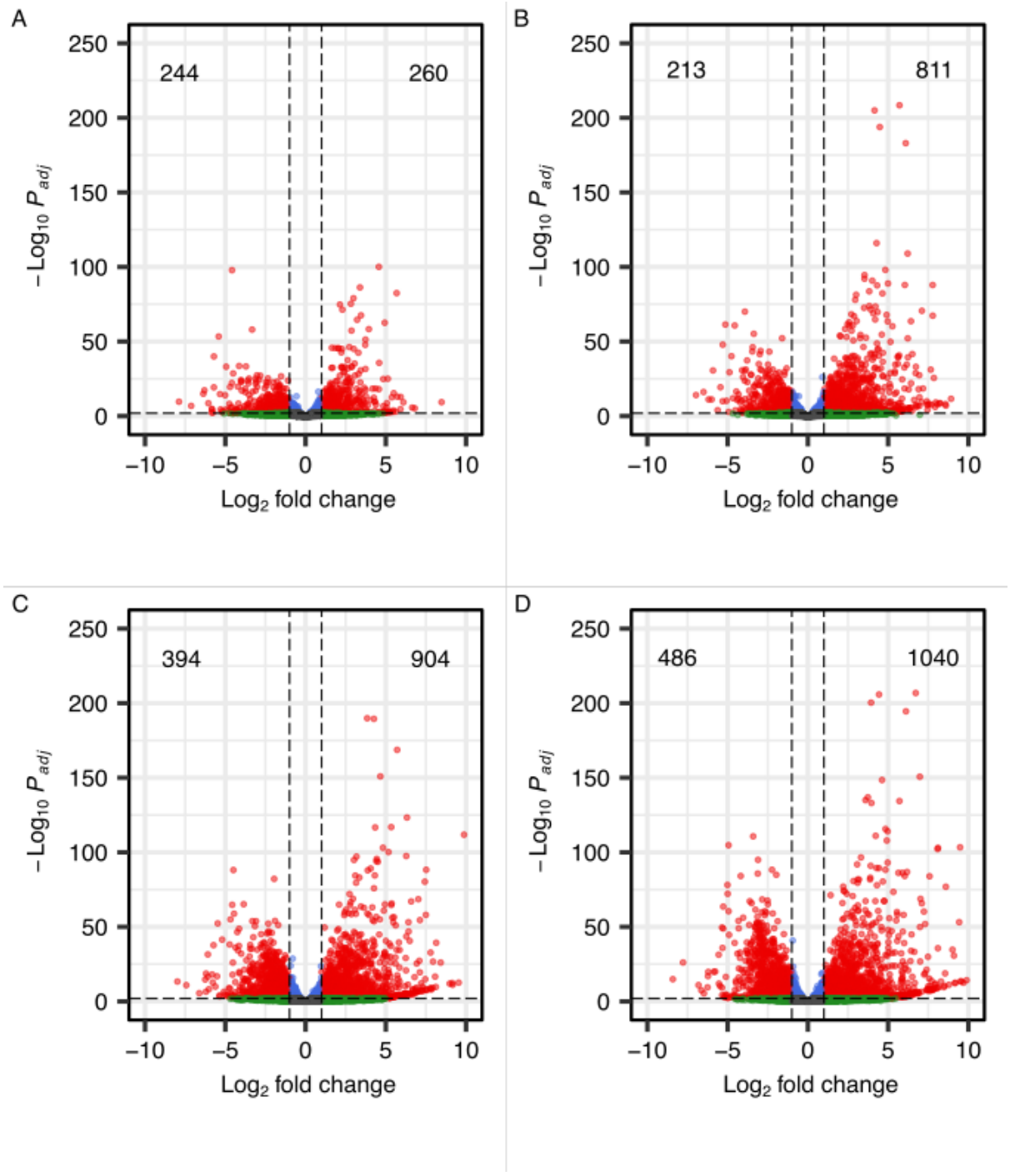

Figure 6.6. Volcano plots revealing differentially expressed genes (DEGs) between experimental groups. *The number of significant DEGs was determined by a two-sided t-test (FDR corrected ≤0.05) and highlighted in red. Dashed lines represent identification boundaries for up or down-regulated genes with the number of DEGs exceeding Log2 fold change (≥2 or ≤-2) displayed, derived from comparisons made between 2D monolayers and Day 7 spheroids (A), Day 14 spheroids (B), Day 21 spheroids (C), and Day 28 spheroids (D).*

6.5.1. Identification of differentially expressed genes in HepG2/C3A spheroids

In general, where specific genes were identified as being differentially expressed between C3A monolayers and spheroids, this pattern continued with spheroid culture period. Cohorts of genes supporting the notion of a transformation towards a hepatic phenotype, were tracked between 2D monolayers and spheroids; the top subsets of DEGs are presented in Figure 6.7. DEGs encoded a variety of hepatic functions including embryonic and developmental hepatic markers such as *AFP*, principle hepatic protein (albumin, *ALB*) and other hepatic plasma proteins such as apolipoproteins. In addition, families of serpins, integrins, tetraspanins, and matrix metalloproteinases, important for hepatic matrix deposition were found to be upregulated in spheroids. In addition, there was evidence of key hepatic metabolic events, both endogenous and exogenous; this included: pathways related to the control of gluconeogenesis; bioprocessing of bile acids and metabolism of lipids and linked moieties, e.g., cholesterol; xenobiotic metabolism including oxidative and conjugative processes as well as hepatic uptake and transport mechanisms. Commensurate with the dynamics of HepG2/C3A spheroid proliferation size over time and a divergence away from the basal cancer phenotype of 2D monolayers, 47 shared DEGs were found to be downregulated in the four spheroid groups. These gene sets were all markers for cellular proliferation, DNA replication and repair pathways including cyclins, tumour suppressor genes and regulators of cell cycle progression and growth which were all concomitantly repressed in spheroids, indicating that cells within HepG2/C3A spheroids were progressively existing the 'normal cell cycle' experienced by cells in monolayer cultures. Compared to HepG2/C3A monolayers, enrichment of these biological pathways suggests that C3A spheroid are more physiologically related to human liver *in vivo*.

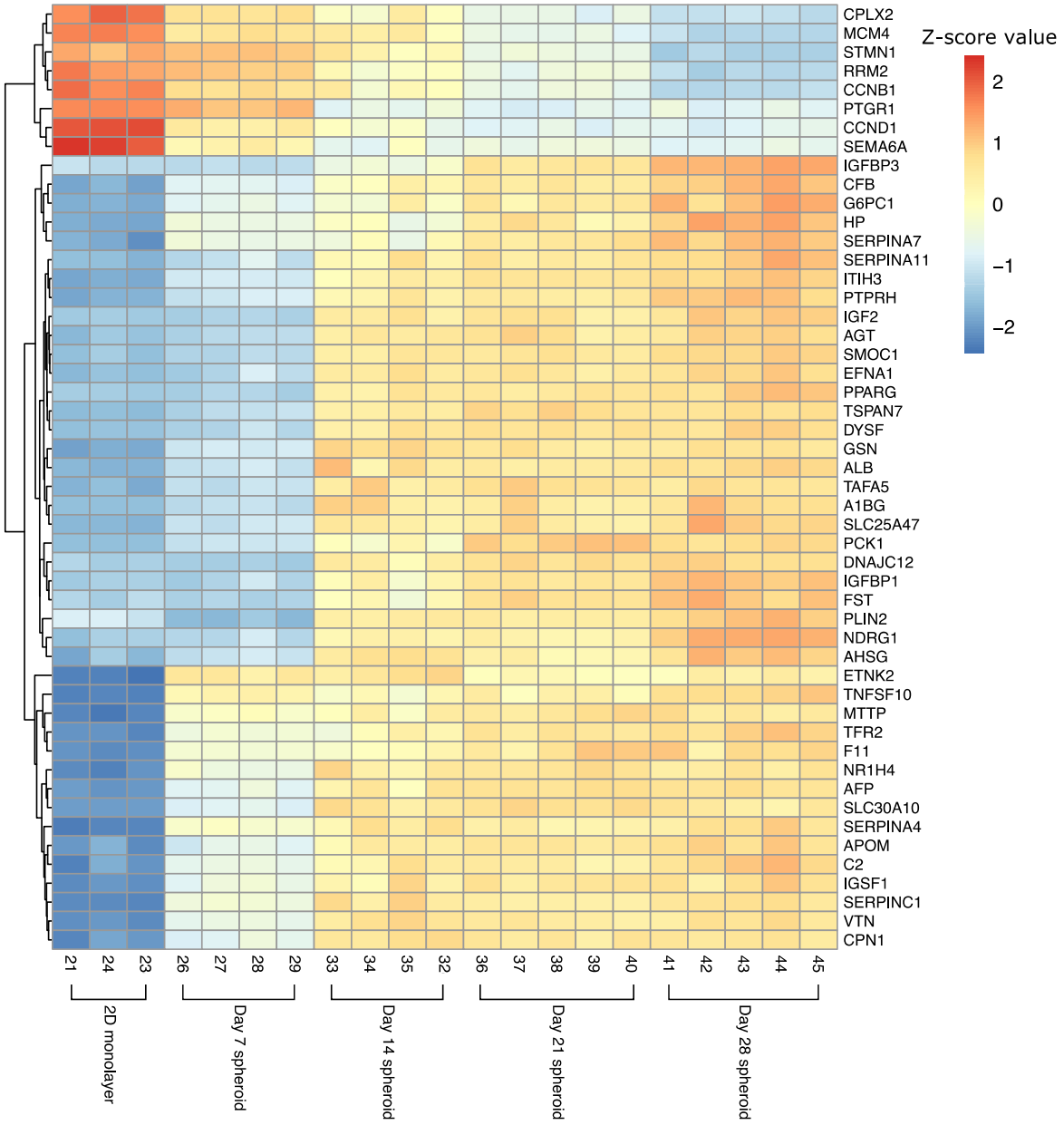

Figure 6.7. Differentially expressed genes are enhanced across spheroid time course continuum. *Comparisons for the top subset of 50 DEGs were derived from 2D monolayer baseline controls compared against spheroids up to 28 days old. Hierarchical clustering indicates those DEGs up – or down-regulated. Expression values are on the log2 scale of transformed gene counts where colour gradient intensity represents Z-score of gene expression across samples.*

6.5.2. Gene set enrichment analysis by gene ontology mapping to identify linked biological processes between spheroids and monolayers of HepG2/C3A cells

Venn diagrams were used to compare DEGs across spheroid sample groups revealing 172 and 47 genes shared between all spheroid timepoints which were up- or down-regulated, respectively (Figure 3A). GO analysis was performed using stringent thresholds to identify enriched gene related pathways (enrichment ≥ 2, FDR corrected $P \leq 0.05$). Positively enriched pathways were centred around organotypic liver function which included regulatory pathways relating to cholesterol metabolism (GO:0008203; GO:0042632; GO:0032376; GO:0033344) as a major precursor to the biosynthesis of bile acids (GO:0070857; GO:0006699) and steroid growth hormones (GO:0010893; GO:0008209; GO:0051384). Other pathways relating to hepatic function and phenotype were significantly enriched according to the metabolism of lipids and products thereof (GO:0016101; GO:0006641); fibrin clot mechanisms (GO:0042730; GO:0031639) and xenobiotic metabolism (GO:0006805). Biological processes were also that might be expected to be involved in the growth dynamics of cellular spheroid structure including cell-matrix adhesion and morphogenesis (GO:0060560; GO:0007160) whereas those down-regulated pathways related to DNA repair and cell-cycle progression mechanisms (GO:0006281; GO:0000075).

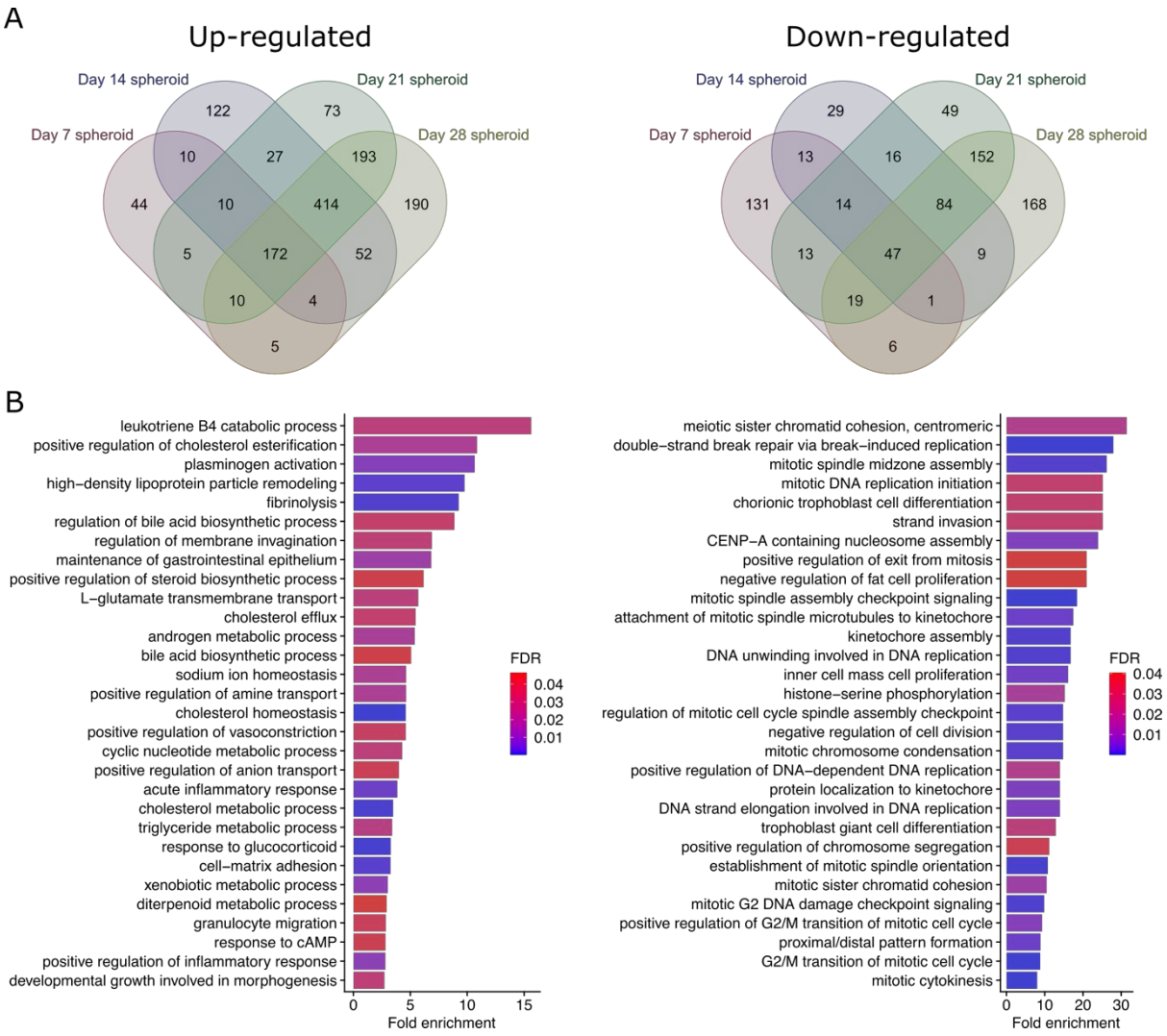

Figure 6.8. Characteristics of DEGs between HepG2/C3A spheroids. *(A) Venn diagram displaying the overlaps of Up (left) and down-regulated (right) genes common to four condition groups compared to 2D monolayer samples. (B) Functional classification of positive (left) and negative (right) DEGs by gene ontology annotation of enriched gene pathways relating to biological processes (FDR corrected P ≤0.05).*

6.5.2.1.1. HepG2/C3A spheroids gain human liver transcriptional similarity

Following the quantitative prediction of similarity to human liver *in vivo* (see Figure 6.4) for liver similarity plot), the expression of DEGs was compared against a panel of 93 liver-specific genes (Figure 6.9) from the liver-specific gene expression panel (LiGEP), encoding proteins relating to the principal organotypic functions critical to the normal function of human liver *in vivo*, including the metabolism of steroids and fatty acids; the synthesis of bile acids; pathways of endogenous liver glucose homeostasis, and xenobiotic metabolism (Kim et al., 2017). From across the four spheroid groups, between 29 % and 48 % of the LiGEP panel were highlighted as DEGs with the total number of upregulated DEGs increasing across the spheroid time course from 27 (day 7) through to 41 (day 14); 36 (day 21) and a total of 45 DEGs at day 28 (Figure 6.9). Only the day 7 spheroid group presented downregulated DEGs which were the liver-produced hormone (*HAMP*, hepcidin preproprotein) and protease, hyaluronan binding protein 2 (*HAMB2*) as part of the hepatic ECM. The abundance of the most significant upregulated DEGs were enhanced with each spheroid time point. These DEGs were found to be proteins synthesised in the liver *in* vivo: inter-alpha trypsin inhibitors (*ITH1, ITH3*); vitronectin (*VTN*); albumin (*ALB*) and alpha-foetal protein (*AFP*) and apolipoprotein families, as well as serine protease inhibitors (*SERPINC1; SERPINA4*) and carboxypeptidase B2(*CPB2*). Similarly, many of the gene targets within the LiGEP panel were highly conserved, and overlapped with, the other curated gene panels. In this way, we therefore also observed high differential expression of genes across the spheroid time course relating to the metabolism of steroids and fatty acids; the synthesis of bile acids; pathways of endogenous liver glucose homeostasis, and xenobiotic metabolism, as part of healthy *in* vivo liver biology at the global transcriptome level.

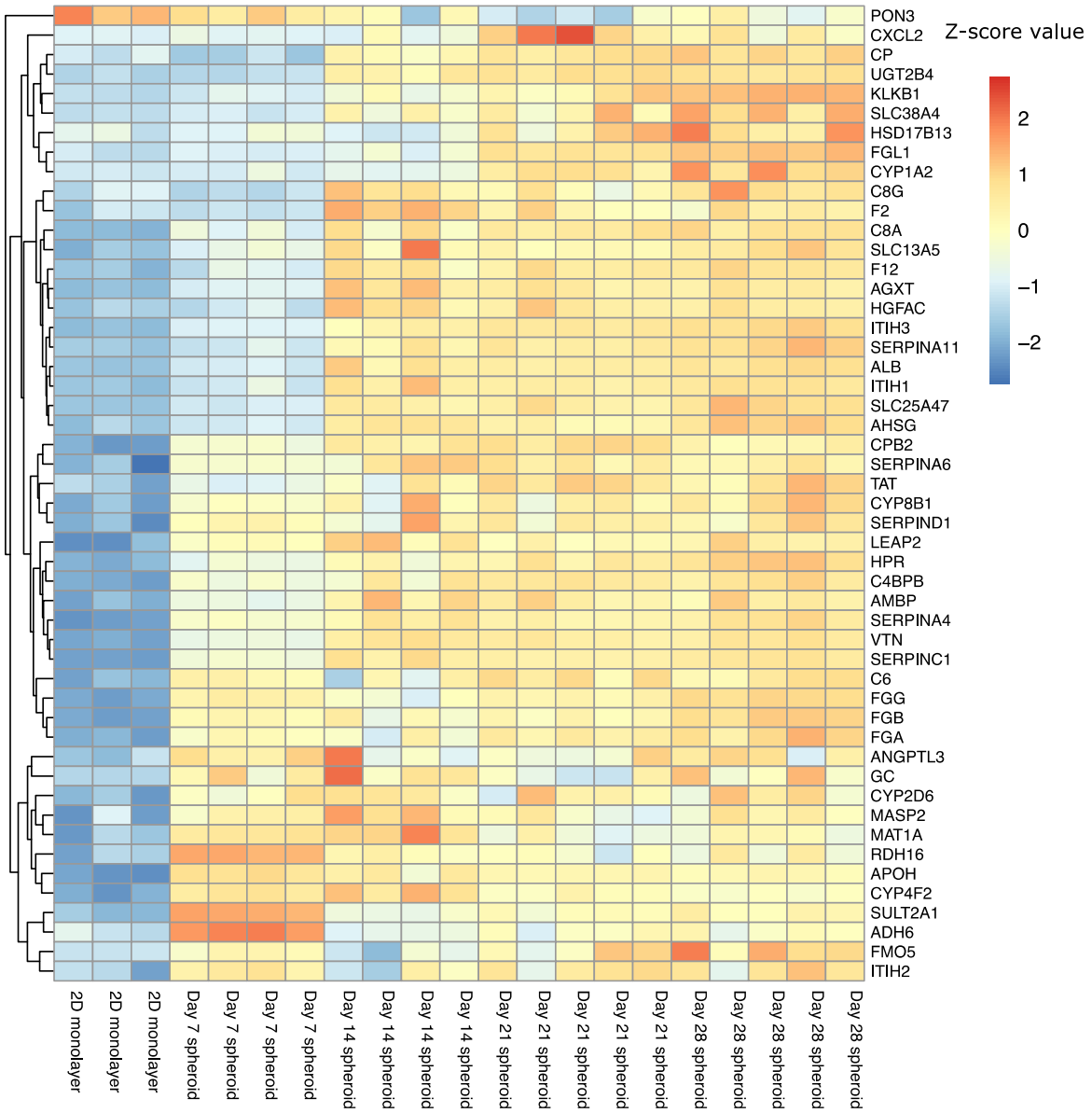

Figure 6.9. Heatmap of differentially expressed genes across HepG2/C3A spheroids and monolayers filtered against from the liver specific LiGEP gene panel. *Comparisons for the top subset of DEGs derived from 2D monolayer baseline controls compared to spheroids. Hierarchical clustering indicates those DEGs up – or down-regulated. Expression values are on the log2 scale of transformed gene counts where colour gradient intensity represents Z-score of gene expression across samples.*

6.5.3. Curation of gene set lists and filtration of DEGs

Considering the large transcriptomic dataset employed for this analysis, it is noted that the statistical thresholding applied to derive DEGs, potentially leads to some biological process pathways being poorly represented and masked in the GO datasets. To further facilitate these observations, all DEGs from each spheroid comparison group were filtered against gene-sets detailing a publicly available panel of xenobiotic metabolism (ADME) gene sets and four manually curated gene sets. These gene sets pertained were:

I. cell-cell and cell-matrix interactions
II. bile acid synthesis via cholesterol metabolic routes
III. hepatic bioenergesis through gluconeogenesis and glycolysis pathways
IV. overexpressed and re-pressed gene sets in hepatocellular carcinoma

Heatmaps to summarise the top DEGs were assembled for all filtered gene sets and an overview of the top differentially expressed genes presented as *Z-score* which was calculated by subtracting the overall average of raw gene counts abundance, divided by the standard deviation of all the measured counts from DESeq2, across all monolayers and spheroid samples.

6.5.4. Expression of ADME related genes is enhanced in HepG2/C3A spheroids

Differentially expressed genes were filtered against the PharmaADME consortium (*www.pharmadme.org*) curated gene list detailing 299 ADME-related genes from the "core" and "extended" lists, relating to nuclear receptor, drug transporter proteins, and phase I/II metabolic enzymes. Representation of the total DEGs derived from spheroid – 2D monolayers comparison groups was low in this gene list, representing a maximum of 19 % coverage (57/299) of ADME-related genes being represented in at least one spheroid group. However, the representation of genes in this list was commensurate with spheroid culture time, increasing from only 27 upregulated DEGs in the day 7 spheroid group, through to a total of 43 at day 28 indicating enriched ADME expression profiles with spheroid culture duration (Figure 6.10), which are known to be significantly deregulated in hepatocellular carcinoma (Hu et al., 2018), indicating a divergence away from the basal HepG2/C3A carcinoma phenotype.

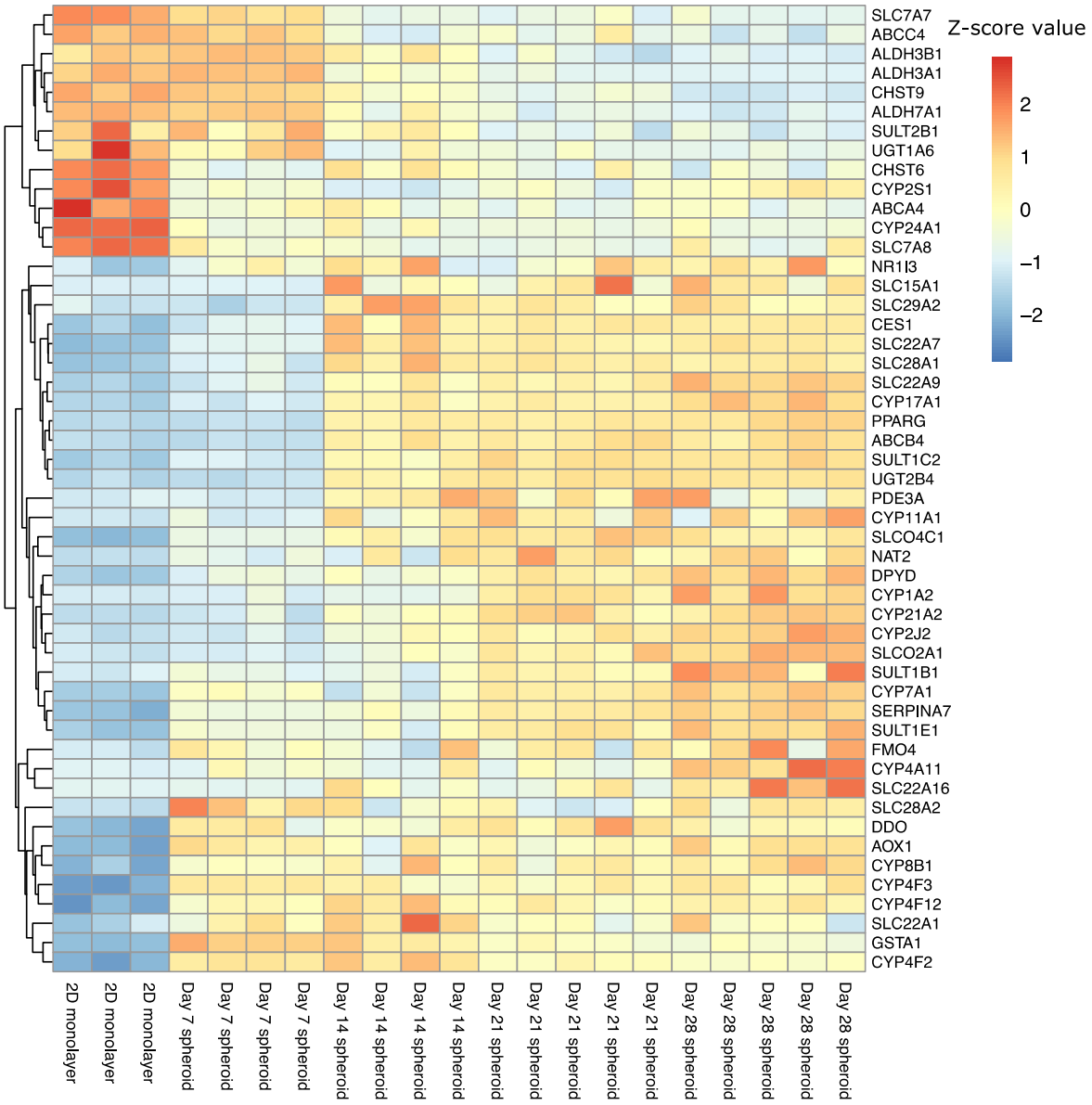

Figure 6.10. Heatmap of differentially expressed genes across HepG2/C3A spheroids and monolayers filtered against from the PharmaADME gene panel. *Comparisons for the top subset of DEGs derived from 2D monolayer baseline controls compared to spheroids. Hierarchical clustering indicates those DEGs up – or down-regulated. Expression values are on the log2 scale of transformed gene counts where colour gradient intensity represents Z-score of gene expression across samples.*

6.5.4.1. Differential expression of hepatic nuclear receptors

Only 2 nuclear receptor genes from the ADME gene panel were found to be differentially expressed in spheroids. Surprisingly, differential expression of liver enriched nuclear factors

such as *HNF4* or *HNF1* could not be determined, neither was the expression of the aryl hydrocarbon receptor (*AHR*) or its nuclear translocator (*ARNT*) yet many target genes downstream of their expression were positively expressed in HepG2/C3A. Both peroxisome proliferator-activated receptor (*PPARγ*) and the constitutive androstane receptor (CAR, *NR1I3*) however, were both stably expressed in spheroids between 14 – 28 days of growth but repressed in day 7 spheroids. We previously observed re-expression of *CAR* and downstream genes such as *CYP1A2,* but not *PXR* or *AhR* in HepG2/C3A spheroids (Coltman et al., 2021a) which was indeed also reflected in this RNA-seq dataset. *CAR* and *PXR* are closely coordinated xenobiotic receptors which function as master sensors of toxic moieties derived from endogenous and exogenous hepatic metabolism (Timsit and Negishi, 2007), with a variety of known ligands. There is a greater evidence for the indirect activation of *CAR* and its ligands, than there is for *PXR* or *AhR;* for example, without ligand binding, e.g., xenobiotic, the expression of *PXR* is silenced (Hendriks et al., 2020, Mackowiak and Wang, 2016), which could explain our findings here. Though not in the PharmaADME core list, when the nuclear receptor gene list was expanded to include other important nuclear receptor proteins, the farnesoid X receptor (FXR, *NRH4*) was found to be differentially expressed in all spheroid models whereas there was no evidence for the expression of liver X receptor (LXR).

6.5.4.2. Differential expression of genes related to phase I xenobiotic metabolism

The major CYP450 superfamilies were represented to varying degrees in the DEGs results, where expression of the major CYP3A family was significantly enriched across all spheroid samples. The principle *CYP3A4* isoform had dynamic expression in 3D spheroids whereas

CYP3A7 (a foetal isoform of 3A4) expression was stabilised. On the contrary, *CYP3A5* expression was significantly enhanced between 2D monolayers and day 7 spheroids but reduced to insignificant levels in day 14 – 28 spheroid samples, indicating transient enrichment of *CYP3A* isoforms across the continuum. *CYP1A2* expression was insignificant in day 7 spheroids but was rapidly enhanced between days 14 to day 28 spheroids, respectively, but not *CYP1A1*. Interestingly, the *CYP2C9* and *CY2C18* isoforms were only found to be significantly expressed in some of the spheroids. Expression of *CYP2D6* did not surpass statistical thresholds in any of the spheroid models, indeed other CYP2 family members such as *CYP2S1* and *CYP2B6* were downregulated. Other CYP450 isoforms were also significantly upregulated across the spheroid time course, for example isoforms *CYP21A2* and *11A1* were not upregulated in day 7 spheroids, but significantly upregulated between days 14 – 28 of spheroid cultivation. The CYP4 family was significantly represented amongst DEGs in spheroid models which included *CYP4F1*, *F2* and *F12* isoforms, as well as *CYP4A11* which was highly abundant in all spheroids other than day 14 spheroids that did not surpass the threshold for analysis. P450 isoforms *7A1* and *17A* were the most upregulated DEGs from the ADME gene expression panel which were significantly enriched in day 7 spheroids and further enriched by day 28, commensurate with time. Other upregulated phase I ADME genes included flavin monooxygenases (*FMO4*) which is typically enriched in human adult liver (Huang et al., 2021) and carboxylesterase, *CES1*. Gene counts abundance for enzymes involved in retinoid signalling, and for the detoxification of alcohol and peroxidation of lipids, the aldehyde dehydrogenase family, were significantly repressed or downregulated in spheroids. *ALDH3A1* and *ALDH3B1,* responsible for the detoxification of aldehydes expression were stably downregulated in the spheroids whereas ALDH3B1 is

typically overexpressed in cancer (Marchitti et al., 2010). Related gene, aldehyde oxidase (*AOX1*) differential expression was stable in all spheroid models.

6.5.4.2.1. Differential expression of genes related to phase II xenobiotic metabolism

The UGT enzyme, *UGTB4* had stabilised expression between days 14 – 28 whereas *UGT1A6* had a reversed pattern of expression in the same models where the gene was progressively downregulated in contrast to our previous observations; however *UGT1A9* expression was evident in day 7 and day 14 spheroids The *SULT1* family was highly represented amongst DEGs in all spheroid models with *SULT1C2, 1C4, 1E1* and *1B1* were upregulated in spheroids compared to monolayers including *SULT2E1* expression which was enhanced at all timepoints whereas *CAR* regulated gene, *SULT2A1* showed the reverse expression pattern. Related sulfotransferases, *CHST6* and *CHST9* were also significantly downregulated. Similarly, *GSTA1 and GSTA2* were also significantly upregulated in day 7 spheroids but seemingly repressed over the remaining spheroid time course.

6.5.4.3. Differential expression of genes related to phase III xenobiotic metabolism

More than one-dozen *SLC* genes were differentially expressed which included the *SLC22A*, *SLC28* and *SLC7A* family members. *SLC22A1, A7, A9* and *SLCA16* were all significantly upregulated whereas *SLC22A1*, was downregulated alongside *SLC7A7/A8*. Differential expression of all solute carriers was enhanced with spheroid growth, establishing stabilised expression between day 21 and day 28 time points. Related to the export of bile acids and xenobiotics, expression of the bile salt export pump gene (BSEP*, ABCB11*) was apparent in day 14 spheroids only; gene counts for the multidrug resistance-associated protein 2 (MRP2*,*

ABCC2) did not surpass the threshold for differential expression. However, significant down regulation of the bile acid associated transporter (MRP4, *ABCC4*) was evident between days 14 - 28, as was related ABC protein, *ABCA4* in all spheroids. On the other hand, the related p-glycoprotein (MDR4, *ABCB4*) was significantly upregulated across all groups.

Although there was limited evidence of these drug-transporter protein transcripts in the RNA-Seq dataset, there was differential expression of aquaporin protein families (*AQP*), expressed in epithelial cells such hepatocytes and cholangiocytes in the liver (Marinelli et al., 2004, Masyuk and LaRusso, 2006). Though not listed in the pharmaADME or LiGEP panels major hepatic aquaporins *AQP8* and *AQP6* were significantly expressed across the spheroid time course by up to a 5-fold change versus HepG2/C3A monolayers cells, with some evidence of *AQP7* expression in day 28 spheroids only, and *AQP1* in day 14 spheroids which was also seen by Mori and Kida (2020) in a transcriptomic analysis of a perfused 3D HepG2 model. There is some evidence to suggest that AQP control of biliary water secretion is also rate limiting on bile secretion (Masyuk and LaRusso, 2006, Marinelli et al., 2019). For example, liver cholestatic disease is principally defined suppressed hepatic bile secretion for which down-regulation of *AQP8* has been implicated (Boyer, 2013). Given the significant expression of both *AQP6/8*, but absence of BSEP/MRP2 in spheroids could indicate the development of precursory mechanisms for bile-secretory pathways which has been seen previously in HepG2/C3A spheroids (Pluta et al., 2020, Jia et al., 2020, Gaskell et al., 2016) In addition, expression of *AQP4* was down-regulated in day 14 and day 28 spheroids by more than 2-fold which may indicate preferential expression of AQPs over time. However, recently, Jung et al. (2021) highlighted AQP as potential markers for cellular proliferation and

for the formation of stem cell niches which would corroborate with other findings in the dataset such as the enhanced downregulation of *MKI67* as a proliferation marker over time. However, at the transcriptional level, re-expression or repression of hepatic transporter proteins does not necessarily confer increased uptake or excretion of bile acids as it is not known as to the localisation of such proteins across the cell surface area.

6.5.5. Extracellular matrix-linkages are enriched in HepG2/C3A spheroids

A panel of genes was manually curated according to enriched gene pathways highlighted from the GO analysis that took consideration of the basic morphological and phenotypic differences between spheroids and monolayers (Figure 6.11). These included observations as to inter-cellular communication and interactions, e.g., cell signalling, and interactions derived from cell-matrix contacts, e.g., deposition of extracellular matrices. A list of 520 genes was curated based on GO search terms relating to morphogenesis/development (GO:0060560) cell-matrix and cell-cell adhesion (GO:0007160; GO:0098609) and potential extracellular matrix depositions (GO:0031012).

Over 70 genes were differentially expressed in at least one spheroid growth phase compared to HepG2/C3A monolayers; however, DEGs in these groups only represented approximately 14 % of the gene set list (501 genes representing cell-cell and cell-matrix gene ontological terms). Similarly, to representation by the ADME gene panel, the differential expression of genes relating to inter-cellular and cell-matrix interactions was also commensurate with spheroid culture time. The number of upregulated genes was increased from 15 at day 7 through to 50 at day 28, the number of downregulated genes remained relatively stable

between days 7 – 21 (12-14 DEGs) but further increased in day 28 spheroids in which expression of a further 10 genes were enriched.

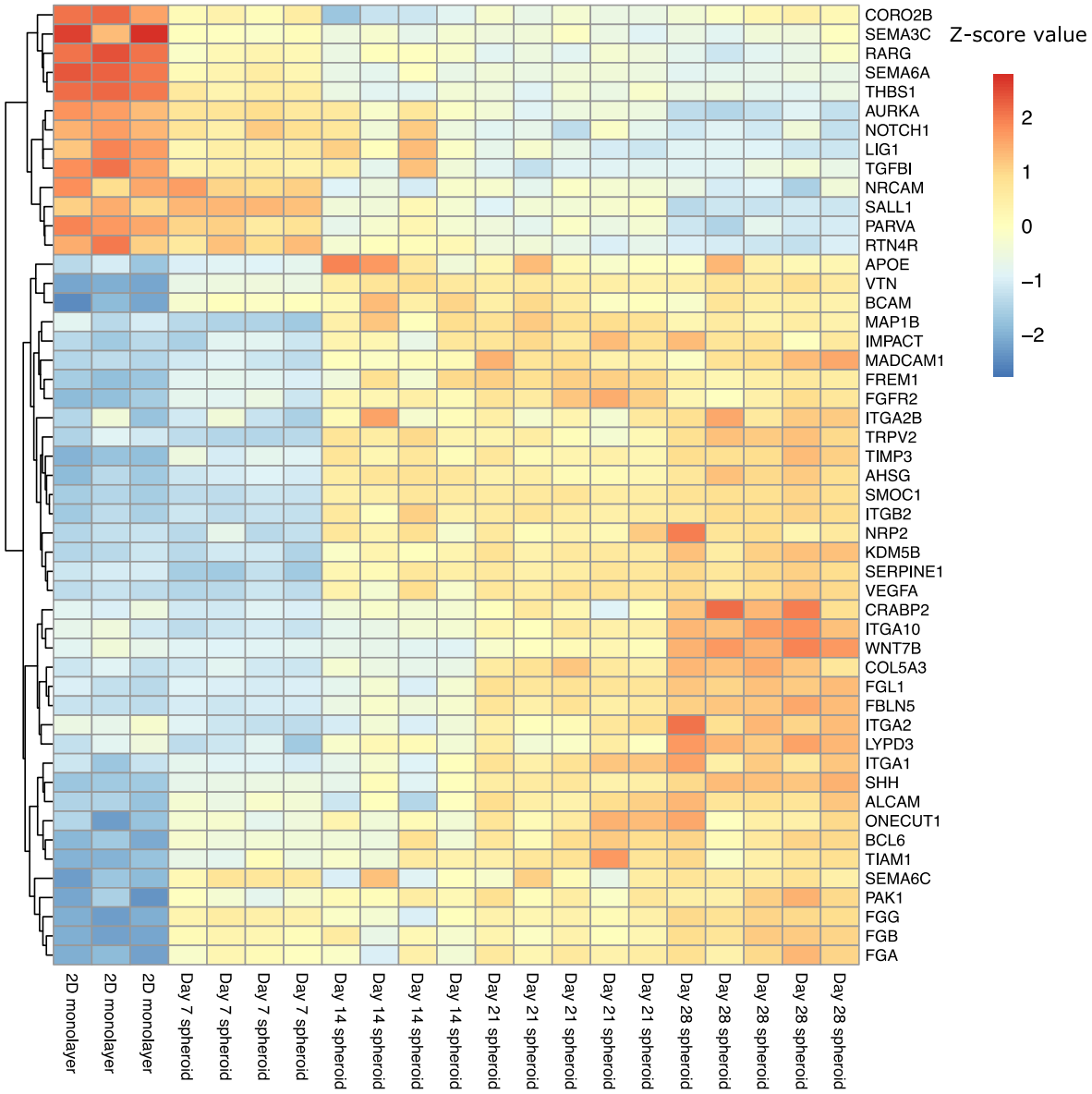

Figure 6.11. Heatmap of differentially expressed genes across HepG2/C3A spheroids and monolayers filtered against a curated list of genes relating to cell-cell and cell-matrix interactions. *Comparisons for the top subset of DEGs derived from 2D monolayer baseline controls compared to spheroids. Hierarchical clustering indicates those DEGs up – or down-regulated. Expression values are on the log2 scale of transformed gene counts where colour gradient intensity represents Z-score of gene expression across samples.*

6.5.5.1. Expression of matrix-linked signalling genes

DEGs derived from comparisons between C3A monolayers and spheroids were all linked to pathways controlling cellular adhesion, inflammation, and wound healing which included

signalling pathways, indicative of a transcriptional cue occurring between 2D monolayers and spheroids. The hepatocyte nuclear factor family was again represented in filtered genes where transcriptional regulator, *ONECUT1* (HNFA-6) was identified in all DEGs groups. Signalling molecules including, sonic hedgehog (*SHH*), notch homolog 1 (*NOTCH1*), and NOTCH ligands, *DLK1/2,* were all found to have upregulated expression with spheroid culture time; known to be critical to the differentiation of hepatic stem cells (Mun et al., 2019, Huang et al., 2019) whereas hepatocyte proliferation marker *WNT7B*, part of the Wnt/beta-Catenin pathway, was downregulated in line with similar studies in differentiating PHH models (Oliva-Vilarnau et al., 2020).

6.5.5.2. Expression of genes related to extracellular matrix remodelling

The hepatic extracellular matrix (ECM) is thought to change concordantly with liver development, e.g., foetal to adult liver transition, and during liver repair processes. Therefore, the differential expression of genes specifically related to hepatocyte ECM were investigated across the spheroid growth period. As one of the principle hepatic adhesion molecules that mediate intercellular and cell-matrix interactions, a total of 8 genes encoding the integrin protein family were differentially expressed in spheroids, but gene counts for most of these genes only surpassed the threshold for significance in day 14, 21 and 28 spheroids (*ITGB2* and *ITGA2B*) and were typically absent in day 7 spheroids. *ITGA3* was downregulated in these spheroids whereas other members of the ITGA family were upregulated but only in day 21 and day 28 spheroids (*ITGA2* and *ITGA1*). Interestingly, *ITGA10* and *ITGB4* were dynamically expressed in C3A spheroids where ITGA10 expression was down regulated in day 7 spheroids but positively expressed by day 21 and 28 of

spheroid culture. Integrin linked proteins such as tenascin (*TNC*), transforming growth factor beta (*TGFB1*), thrombospondin (*THBS1*), were all downregulated at days 21 and 28 of spheroid culture but were absent at earlier timepoints. In addition, expression of *VEGFA* in spheroids was indicative of hepatic vascular development in the spheroid models. The notion of extracellular matrix remodelling is a critical component of liver development and response to injury. Differential expression of *ECM2*, including genes encoding fibronectin receptor proteins (*FLRT1* and *FLRT3*), and laminin gene, netrin-1 (*NTN1*), and *MADCAM1*, a vascular adhesion protein, were all upregulated over time. Collagen genes, *COL5A3* and *COL17A1* were enriched at day 21 and day 28 but specific type- I or type III collagen proteins were absent in the DEGs. In addition, both the inhibitor of metalloproteinase (*TIMP3*) and matrix metalloproteinase linked proteins, *LYPD3*, were significantly upregulated across the spheroid time course whereas the linked transmembrane proteins (*SEMA6A, SEMA3C*), and regulatory protein, insulin growth factor (*IGFBP7*) were all down regulated. Hepatically synthesised glycoproteins, fibrinogens (*FGB, FGA* and *FGC*) were also upregulated in spheroids compared to monolayers. Evidence for the expression of genes related to hyaluronans – a critical component of the ECM, were not evident, however its ligand binding protein, the cell adhesion molecule, *CD44*, was expressed abundantly although there was limited evidence for the expression of other linked genes such as those encoding sulphate proteoglycans or laminins beyond netrin-1 or a larger suite of collagen markers, were not evident.

6.5.6. Expression pathways for bile acid synthesis via cholesterol metabolic routes are enhanced in HepG2/C3A spheroids

A panel of genes was manually curated pertaining to the metabolism of cholesterol (GO:0008203) and bile acid synthesis (GO:0070857) yielding a list spanning some 158 unique genes. Approximately 25 % of these genes were identified at least once in the spheroid differentially expressed gene sets (41 genes identified) with the number of differentially expressed genes increasing with time from 12 at day 7 through 29 by day 28, which were mostly upregulated in spheroids with very few downregulated genes, see Figure 6.12. Low-density lipoprotein receptor (*LDLRAP1*), *SULT2B1* and *CYP39A*1, all had decreasing gene abundance from monolayers to spheroids whereas other P450 isoforms had enriched expression over time (*CYP11A1, CYP51A1, CYP7A1* and *CYP8B1*). Gene sets of apolipoproteins (*APOA1, APOA4* and *APOE*), and hydroxymethylglutaryl-CoA synthases (*HMGCS1* and *HMGCS2*) were also upregulated in spheroids as were genes encoding key conjugative oxysterol (*OSBPL6*), cholesterol (*SOAT2*) and bile (*BAAT, day 28*) proteins, and the cholesterol transporter protein (*ABCA5*).

Combined with differentially expressed CYP isoforms from other filtered datasets, CYP*11A1*, *17A* and *21A*, *CYP3A7* forms a family of steroidogenic enzymes that are found in high abundance during foetal liver development through to the human adult liver (O'Shaughnessy et al., 2013), as part of a large suite of enzymes responsible for the synthesis of bile acid conjugates from steroid precursors (Russell, 2009, Miller and Auchus, 2011). For example, *CYP11A1* catalyses the metabolism of cholesterol to pregnenolone – the precursor to all steroid hormones and a critical component of the foetal liver development. These initial reactions then trigger a cascade of other reactions whereby *CYP17A* typically bio-transforms steroids to androgens and *CYP21A2* converts progesterone to corticosteroid molecules.

Further support for this mechanism is offered by the high differential expression of *CYP7A1, CYP8B1, CYP51A1* and *FXR* in spheroids versus monolayers. Interestingly, REV-ERBα (*NR1D1*), a nuclear receptor related to hepatic circadian rhythm (Ikeda et al., 2019), was found to be stably expressed from day 14 onwards and is thought to regulate the transcription of genes in the bile acid synthesis pathways such as *CYP7A1* (Duez et al., 2008).*CYP7A1* is thought to be rate limiting in bile acid synthesis through the metabolic conversion of cholesterol towards its termination as cholic acid (Zhang et al., 2009) and is frequently repressed by *PXR* (Zhang et al., 2004), whereas *CYP51A1* appears much earlier in the pathway, responsible for the conversion of lanosterol (Režen et al., 2017). In addition, *AKR1D1 and AKR1C4*), responsible for the third steps in the conversion of cholesterol (Bale et al., 2014), were also upregulated in spheroids. Thus, these CYP isoforms are likely be to occupy a position in a negative feedback loop between bile acids, *FXR* and other functional proteins with HepG2/C3A spheroids. Taken together, the progressive transcriptional abundance of these steroidogenic CYP isoforms supports the notion of a developing hepatic phenotype across the spheroid sample types, as key components of the cholesterol-steroid-bile acid synthesis axis (Russell, 2009), and as major regulatory mechanisms that drive the functional change between HepG2/C3A monolayers and spheroids.

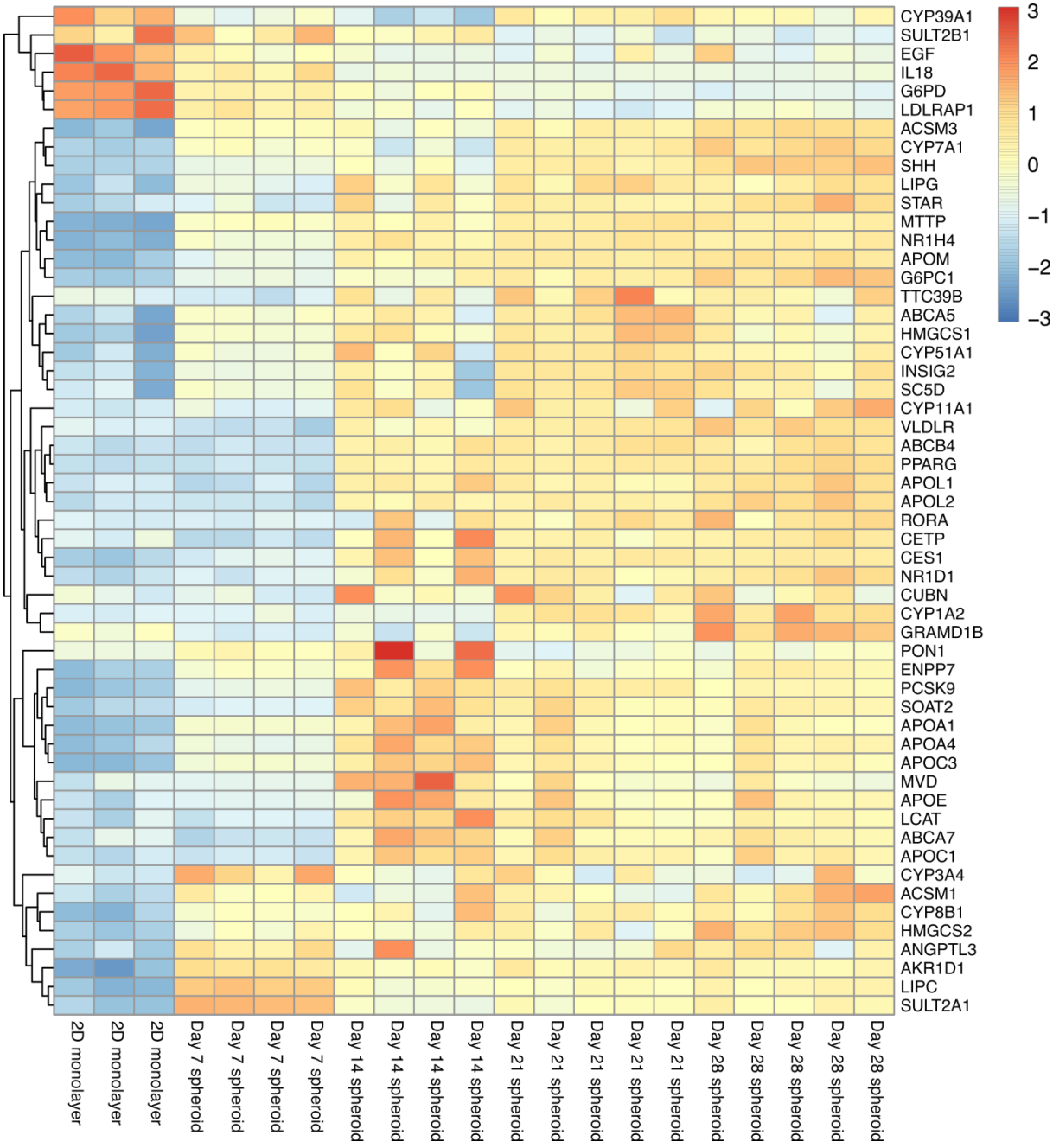

Figure 6.12. Heatmap of differentially expressed genes across HepG2/C3A spheroids and monolayers filtered against a gene panel relating to the Sterol-Cholesterol-Bile acid metabolism axis in liver. *Comparisons of DEGs derived from 2D monolayer baseline controls compared to spheroids. Hierarchical clustering indicates those DEGs up – or down-regulated. Expression values are on the log2 scale of transformed gene counts where colour gradient intensity represents Z-score of gene expression across samples.*

6.5.7. Expression of genes relating to hepatic bioenergesis through gluconeogenesis and glycolysis pathways

A further panel of 198 genes (Figure 6.13) was curated to cover the principal pathways of hepatic bioenergesis, gluconeogenesis (GO:0006111) and glycolysis (GO:0006096). By comparison to some of the other filtered datasets, very few differentially expressed genes appeared in this gene set, where only approximately 12 % of genes were identified at least once in the spheroid comparison groups (24 genes total). However, like the other filtered gene sets the number of DEGs contributing to gluconeogenesis or glycolytic processes was enhanced with spheroid culture period. Phosphofructokinase (*PFKP*) was downregulated in all spheroid time points whereas fibroblast growth factor 19 (*FGF19*) was only downregulated in day 28 spheroids and absent in other filtered gene sets. Key genes in the gluconeogenesis pathway for the regulation of hepatic glucose levels were all upregulated in spheroids in line with data presented in **Chapter 5** that functional respiratory metabolism is enriched in HepG2/C3A spheroids, across a time course linked to hepatocyte maturation, an increase in glycolysis and non-respiratory metabolic pathways linked to enriched expression of CYP450 and FMO enzyme pathways. The differential expression of genes Glucose-6-phosphatase (*G6PC*) and pyruvate kinase (*PCK1*) were successively upregulated across the spheroid time course whereas as the preceptor for *PCK1* (*PKLR1*) was stably expressed in day 14 – 28 spheroids.

Hepatic regulators of glycogen metabolism, the hepatic protein phosphatase family (*PPPR3*) were differentially expressed where *PPPR3B* was upregulated in all spheroids, furthermore, variants *PPPR3C* and *PPPR3G* were only upregulated in day 21 and 28 spheroids. Similarly,

the key regulators of hepatic glucose homeostasis (*PPARG1CA*), hepatic lipid accumulation (*IGF2*), and phosphofructokinase (*PFKB1*) were also only upregulated in 21 and 28 spheroids, whereas the hepatocyte nuclear factor-6 and regulator of hepatic differentiation (*ONECUT1*) was expressed in all samples after day 7. The majority of DEGs were preferentially clustered around gluconeogenesis and hepatic differentiation but also some towards hepatic glycolysis. During hepatocyte differentiation, polarisation of cells forces cells to upregulated pro-glycolytic pathways (Fu et al., 2013, Wrzesinski et al., 2014). Together, enrichment of such genes and diversion from monolayer datasets, suggests that this principal mechanism of hepatic bioenergesis could be progressively tracked across HepG2/C3A spheroid timepoints, and may indicate and an augmentation of the metabolism axis in spheroids away from the malignant metabolism form assumed of monolayer HepG2/C3A cells and closer to that of hepatocytes undergoing differentiation towards a mature phenotype.

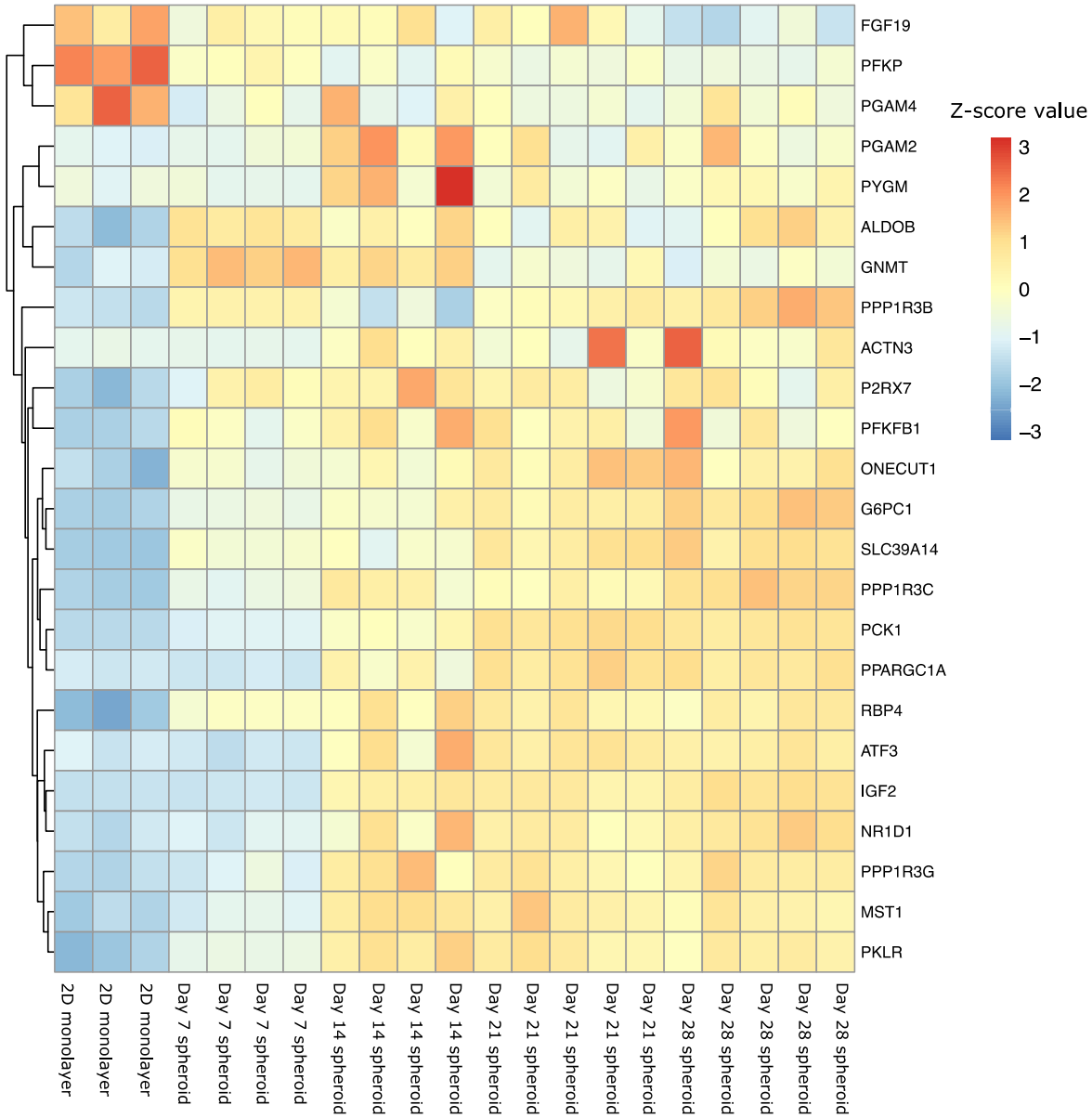

Figure 6.13. Heatmap of differentially expressed genes across HepG2/C3A spheroids and monolayers filtered against a gene panel relating to hepatic bioenergesis via gluconeogenesis and glycolysis. *Comparisons of DEGs derived from 2D monolayer baseline controls compared to spheroids. Hierarchical clustering indicates those DEGs up – or down-regulated. Expression values are on the log2 scale of transformed gene counts where colour gradient intensity represents Z-score of gene expression across samples.*

6.5.8. HepG2/C3A spheroids diverge from cancer-related phonotype

Considering that HepG2/C3A cells are derived from hepatocellular carcinoma (HCC), we prudently assessed how well global transcriptome changes supported the notion of a cancer

phenotype being gained in 3D spheroids over time. A series of target genes were manually curated from the literature (Wang et al., 2021a, Tao et al., 2021, Feng et al., 2020, Song et al., 2020, Zhou et al., 2020, Nwosu et al., 2017), identified to be typically over-expressed (210 genes, Figure 6.14) or repressed (211 genes, Figure 6.15) in HCC tissues *in vivo,* supporting poor patient prognosis and disease progression. Those genes typically found to be upregulated in HCC were related to cell-division cycle control, regulation of metastasis and attenuation of apoptosis; including pathways related to metabolism switching events such as glycolysis, away from oxidative phosphorylation.

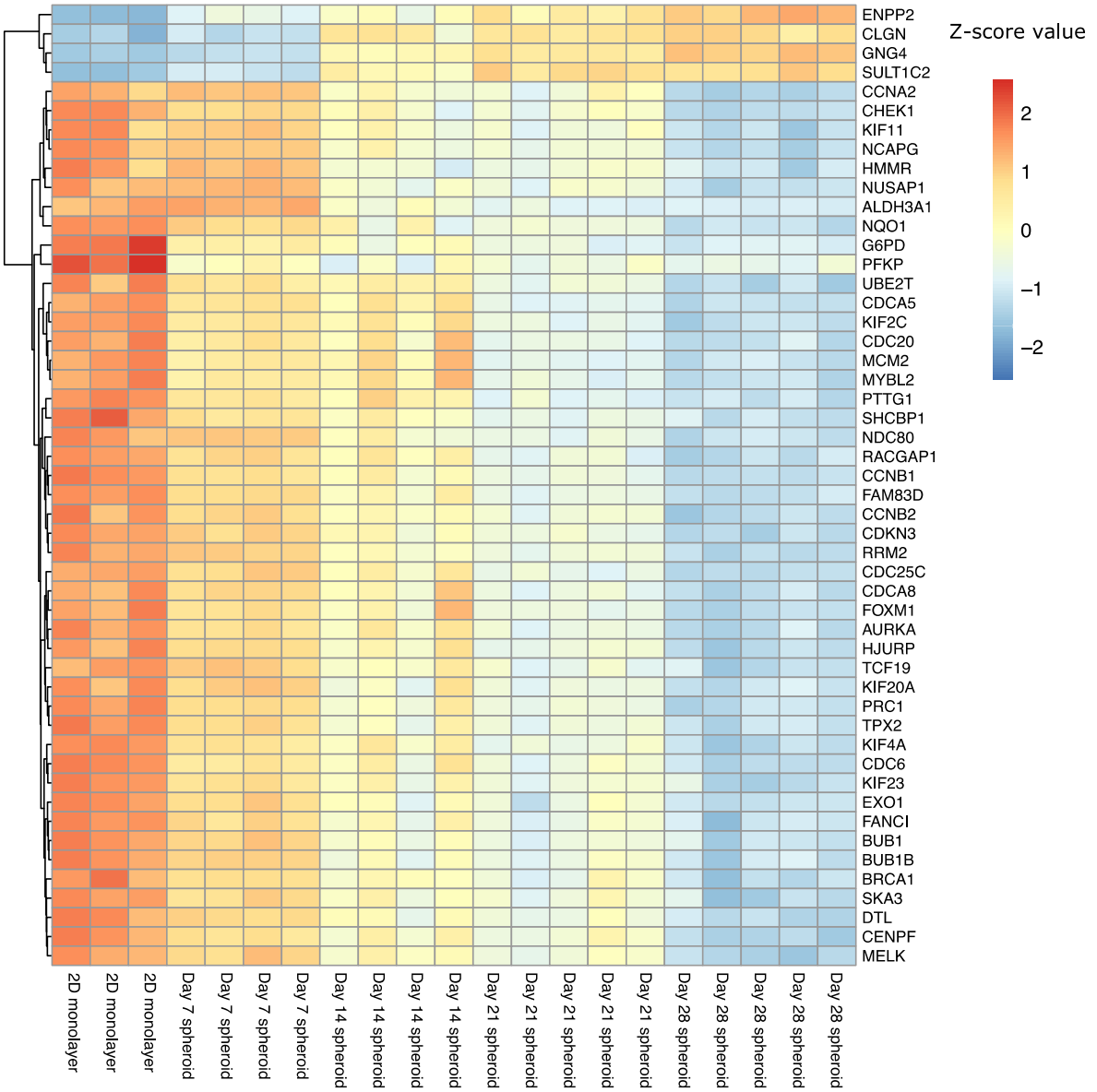

Figure 6.14. Genes typically overexpressed in hepatocellular carcinoma are downregulated in HepG2/C3A spheroids. *Comparisons of DEGs derived from 2D monolayer baseline controls compared to spheroids. Hierarchical clustering indicates those DEGs up – or down-regulated. Expression values are on the log2 scale of transformed gene counts where colour gradient intensity represents Z-score of gene expression across samples.*

Many of those genes and pathways highlighted to be typically downregulated in HCC related to the metabolism of xenobiotics, fatty acids, and amino acids. HepG2/C3A spheroid transcriptomes were found to progressively promote a non-cancerous phenotype by comparison to 2D monolayer cells. Despite HepG2/C3A spheroids presenting reduced viability at day 28 of culture (**Chapter 5**), there was limited evidence for the upregulation of pro-apoptotic pathways. Of those 210 genes typically found to be expressed in HCC, a maximum of 7 genes were positively differentially expressed in spheroids whereas between 75 - 14 of these genes were down regulated between days 28 and 14. These included tumour suppressor and DNA replication genes (*BRCA1*, *FANC1*, *MCM2)*, evidence of checkpoint inhibition (*BUB1* and *BUB1B*) and regulation of cell cycle progression and growth (*CDKN3, CDCA8, CDC6, CCNB1, FOXM1 and MELK*). Conversely, most of those genes repressed in HCC were upregulated across the spheroid time course with 27 – 40 positively identified DEGs, such as ADME related genes (*NAT2, CYP4A11, CES1* and *SULT2A1*), regulation of hepatic glucose synthesis, (*PCK1* and *PFKFB1*), and carrier proteins (*SLC7A2, SLC38A** and *SLC39A14*). Taken together, this suggests that the malignant phenotype associated with the HepG2/C3A cell lineage is lost when cultured as spheroids. How this relates or tracks to spheroids grown from the parental HepG2 cell line would therefore warrant attention as to whether such signatures are conserved between the two models commonly deployed in toxicological studies.

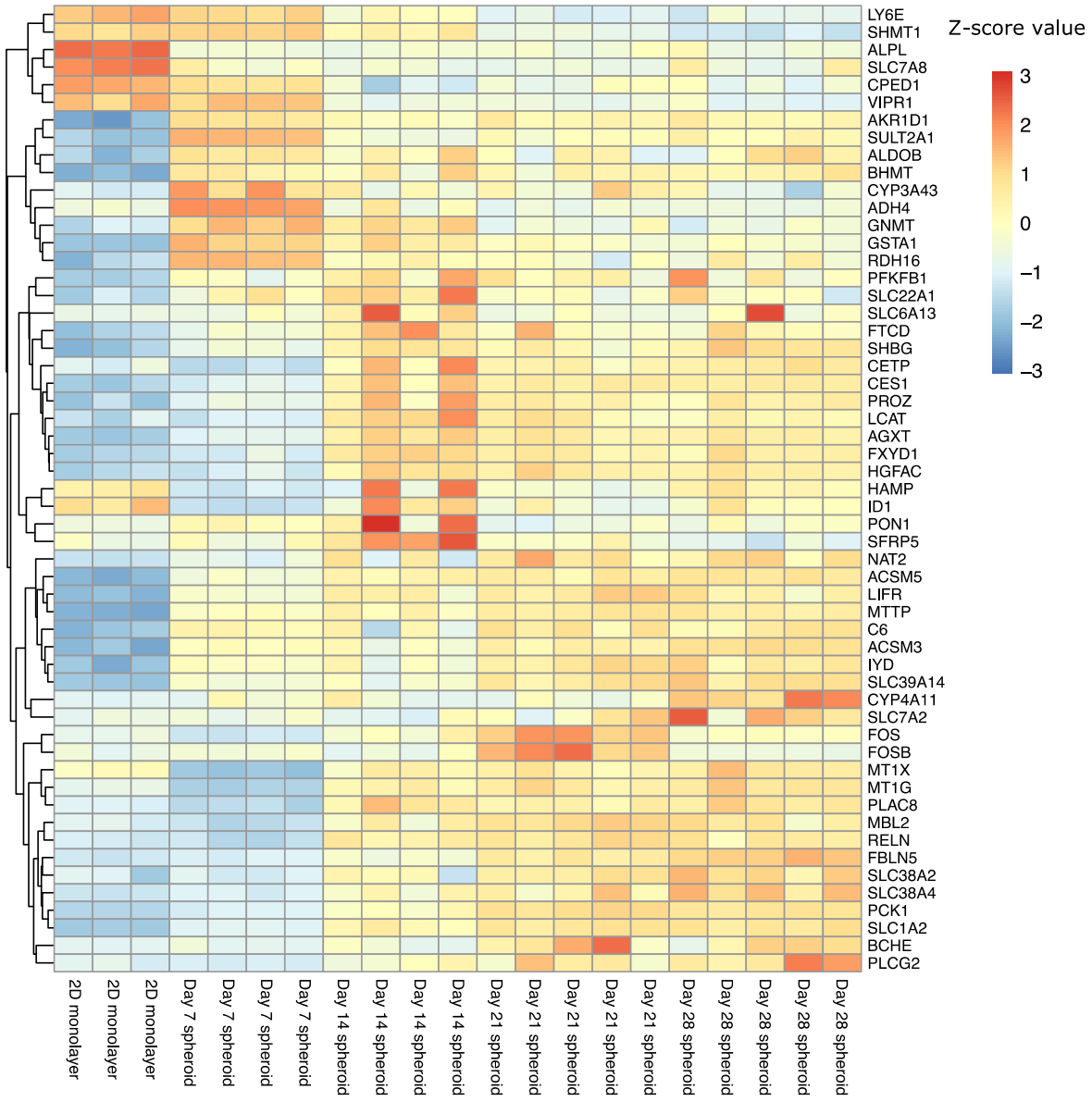

Figure 6.15. Genes typically repressed in hepatocellular carcinoma are re-expressed in HepG2/C3A spheroids. *Comparisons of DEGs derived from 2D monolayer baseline controls compared to spheroids. Hierarchical clustering indicates those DEGs up – or down-regulated. Expression values are on the log2 scale of transformed gene counts where colour gradient intensity represents Z-score of gene expression across samples.*

6.6. Conclusion

In line with our original hypothesis at the beginning of this thesis, culturing HepG2/C3A as spheroids, force cells to undergo a transcriptional and morphological transformation towards a hepatic phenotype, away from its highly proliferative and malignant monolayer progenitor and continue to transcriptomically diverge across a continuum of spheroid growth and maturation, up to 28 days. In this study we identify significant transcriptional divergence of HepG2/C3A spheroids away from monolayers by RNA-seq analysis to reveal clusters of DEGs that are attributed to various elements of hepatic physiology. Several core hepatic transcriptome groups were differentially expressed pertaining to a recapitulation of hepatic function including the sterol-cholesterol-bile acid axis; the transcriptional control of key hepatic proteins such as plasminogen, albumin, and apolipoproteins; remodelling of extracellular matrix proteins, and ADME.

Conversely, down regulated genes were mostly related to cell cycle progression, cellular proliferation, DNA replication and an attenuation of hepatic carcinogenesis. It is therefore likely that the down-regulated genes across this study could be related to key differences in contact inhibition, cell doubling time (proliferation) and HepG2/C3A cell dynamically exiting and re-entering the normal cell-cycle throughout their period of growth. We have noted that the velocity of HepG2/C3A doubling rate is significantly reduced over time versus 2D monolayers for up to 4-5 weeks of culture (**Chapter 3, Coltman et al., 2021a).** In addition, the attenuation of processes relating to apoptosis, tumour suppression or DNA repair, may in part explain the continued growth of HepG2/C3A spheroids and progressively reduced viability beyond 4 weeks of culture (**Chapter 5**), as well as the paradigm that exists between

PHHs lacking proliferative capacity (Zhang et al., 2018) and immortalised hepatic cells lines often being over-proliferative. For example, pathways related to *p53* and Wnt/beta-catenin signalling were found to repressed in our dataset and similarly confirmed between monolayers and spheroids of PHHs (Oliva-Vilarnau et al., 2020), but seemingly reversed in HCC spheroids (Pomo et al., 2016). Combined with metabolic data in **Chapter 5**, and the functional attributes paid to HepG2/C3A spheroids in terms of enhanced genotoxic and ADME responses (**Chapter 3 and Chapter 5**), it is therefore hypothesised that cells within rapidly-diving monolayers have repressed several attributes that make HepG2/C3A spheroids favourable model for study in this thesis, in favour of pure cellular replication.

In conclusion, our transcriptomic analyses suggests that cells grown as monolayers or spheroids grown over time, occupy a space somewhere on the continuum between developing foetal hepatocytes and mature adult hepatocytes. To our knowledge, this is the first time that genome-wide RNA-seq has been applied to extensively characterise a hepatic model of this kind, in parallel to a suite of *in* vitro toxicological studies. Combined with other datasets presented throughout this thesis, the results we present here provide evidence for important transcriptional differences in HepG2/C3A dimensionality between 2D and 3D culture and are an important contribution to those selecting models for deployment in future toxicological or pharmacological studies.

6.7. References

Aizarani, N., Saviano, A., Sagar, Mailly, L., Durand, S., Herman, J. S., Pessaux, P., Baumert, T. F. and Grün, D. (2019) 'A human liver cell atlas reveals heterogeneity and epithelial progenitors', *Nature,* 572(7768), pp. 199-204.

Alhendi, A. S. N. (2019) 'countToFPKM: Convert Counts to Fragments per Kilobase of Transcript per Million (FPKM).', *R package version 1.0.0*.

Andrews, S. (2010) *FastQC: a quality control tool for high throughput sequence data*. Available at: http://www.bioinformatics.babraham.ac.uk/projects/fastqc.

Ashburner, M., Ball, C. A., Blake, J. A., Botstein, D., Butler, H., Cherry, J. M., Davis, A. P., Dolinski, K., Dwight, S. S., Eppig, J. T., Harris, M. A., Hill, D. P., Issel-Tarver, L., Kasarskis, A., Lewis, S., Matese, J. C., Richardson, J. E., Ringwald, M., Rubin, G. M. and Sherlock, G. (2000) 'Gene ontology: tool for the unification of biology. The Gene Ontology Consortium', *Nat Genet,* 25(1), pp. 25-9.

Bale, S. S., Vernetti, L., Senutovitch, N., Jindal, R., Hegde, M., Gough, A., McCarty, W. J., Bakan, A., Bhushan, A., Shun, T. Y., Golberg, I., DeBiasio, R., Usta, B. O., Taylor, D. L. and Yarmush, M. L. (2014) 'In vitro platforms for evaluating liver toxicity', *Exp Biol Med (Maywood),* 239(9), pp. 1180-1191.

Bell, C. C., Chouhan, B., Andersson, L. C., Andersson, H., Dear, J. W., Williams, D. P. and Soderberg, M. (2020) 'Functionality of primary hepatic non-parenchymal cells in a 3D spheroid model and contribution to acetaminophen hepatotoxicity', *Arch Toxicol,* 94(4), pp. 1251-1263.

Biazi, B. I., Zanetti, T. A., Marques, L. A., Baranoski, A., Coatti, G. C. and Mantovani, M. S. (2020) 'mRNAs biomarker related to the control of proliferation and cell death in HepG2/C3A spheroid and monolayer cultures treated with piperlongumine', *Applied Cancer Research,* 40(1), pp. 2.

Blighe, K., Rana, S. and Lewis, M. (2019) 'EnhancedVolcano: Publication-ready volcano plots with enhanced colouring and labeling', *R package version,* 1(0).

Bolger, A. M., Lohse, M. and Usadel, B. (2014) 'Trimmomatic: a flexible trimmer for Illumina sequence data', *Bioinformatics,* 30(15), pp. 2114-20.

Boyer, J. L. (2013) 'Bile formation and secretion', *Compr Physiol,* 3(3), pp. 1035-78.

Author (2018) *Picard Tools* (Version 2.17.8). Available at: http://broadinstitute.github.io/picard/.

Chan, C., Berthiaume, F., Nath, B. D., Tilles, A. W., Toner, M. and Yarmush, M. L. (2004) 'Hepatic tissue engineering for adjunct and temporary liver support: critical technologies', *Liver Transpl,* 10(11), pp. 1331-42.

Chen, Y., Yu, C., Lv, G., Cao, H., Yang, S., Zhang, Y., Yu, J., Pan, X. and Li, L. (2014) 'Rapid large-scale culturing of microencapsulated hepatocytes: a promising approach for cell-based hepatic support', *Transplant Proc,* 46(5), pp. 1649-57.

Coltman, N. J., Coke, B. A., Chatzi, K., Shepherd, E. L., Lalor, P. F., Schulz-Utermoehl, T. and Hodges, N. J. (2021a) 'Application of HepG2/C3A liver spheroids as a model system for genotoxicity studies', *Toxicol Lett,* 345, pp. 34-45.

Coltman, N. J., Rochford, G., Hodges, N. J., Ali-Boucetta, H. and Barlow, J. P. (2021b) 'Optimised protocols to expore mitochondrial energy metabolism in spheorids using Agilent Seahorse Extracellular Flux Analysis', *Journal of Visualized Experiments,* n/a(e63346).

Duez, H., Van Der Veen, J. N., Duhem, C., Pourcet, B., Touvier, T., Fontaine, C., Derudas, B., Baugé, E., Havinga, R. and Bloks, V. W. (2008) 'Regulation of bile acid synthesis by the nuclear receptor Rev-erbα', *Gastroenterology,* 135(2), pp. 689-698. e5.

Dyer, N. P., Shahrezaei, V. and Hebenstreit, D. (2019) 'LiBiNorm: an htseq-count analogue with improved normalisation of Smart-seq2 data and library preparation diagnostics', *PeerJ,* 7, pp. e6222.

Ellero, A. A., van den Bout, I., Vlok, M., Cromarty, A. D. and Hurrell, T. (2021) 'Continual proteomic divergence of HepG2 cells as a consequence of long-term spheroid culture', *Sci Rep,* 11(1), pp. 10917.

Ewels, P., Magnusson, M., Lundin, S. and Kaller, M. (2016) 'MultiQC: summarize analysis results for multiple tools and samples in a single report', *Bioinformatics,* 32(19), pp. 3047-8.

Feng, J., Li, J., Wu, L., Yu, Q., Ji, J., Wu, J., Dai, W. and Guo, C. (2020) 'Emerging roles and the regulation of aerobic glycolysis in hepatocellular carcinoma', *Journal of Experimental & Clinical Cancer Research,* 39(1), pp. 126.

Fu, D., Mitra, K., Sengupta, P., Jarnik, M., Lippincott-Schwartz, J. and Arias, I. M. (2013) 'Coordinated elevation of mitochondrial oxidative phosphorylation and autophagy help drive hepatocyte polarization', *Proc Natl Acad Sci U S A,* 110(18), pp. 7288-93.

Gaskell, H., Sharma, P., Colley, H. E., Murdoch, C., Williams, D. P. and Webb, S. D. (2016) 'Characterization of a functional C3A liver spheroid model', *Toxicology research,* 5(4), pp. 1053-1065.

Gene Ontology, C. (2021) 'The Gene Ontology resource: enriching a GOld mine', *Nucleic Acids Res,* 49(D1), pp. D325-D334.

Guo, R., Xu, X., Lu, Y. and Xie, X. (2017) 'Physiological oxygen tension reduces hepatocyte dedifferentiation in in vitro culture', *Sci Rep,* 7(1), pp. 5923.

Gupta, R., Schrooders, Y., Hauser, D., van Herwijnen, M., Albrecht, W., Ter Braak, B., Brecklinghaus, T., Castell, J. V., Elenschneider, L., Escher, S., Guye, P., Hengstler, J. G., Ghallab, A., Hansen, T., Leist, M., Maclennan, R., Moritz, W., Tolosa, L., Tricot, T., Verfaillie, C., Walker, P., van de Water, B., Kleinjans, J. and Caiment, F. (2021) 'Comparing in vitro human liver models to in vivo human liver using RNA-Seq', *Arch Toxicol,* 95(2), pp. 573-589.

Hendriks, D. F. G., Vorrink, S. U., Smutny, T., Sim, S. C., Nordling, A., Ullah, S., Kumondai, M., Jones, B. C., Johansson, I., Andersson, T. B., Lauschke, V. M. and Ingelman-Sundberg, M. (2020) 'Clinically Relevant Cytochrome P450 3A4 Induction Mechanisms and Drug Screening in Three-Dimensional Spheroid Cultures of Primary Human Hepatocytes', *Clin Pharmacol Ther*.

Hu, D. G., Marri, S., McKinnon, R. A., Mackenzie, P. I. and Meech, R. (2018) 'Deregulation of the Genes that Are Involved in Drug Absorption, Distribution, Metabolism, and Excretion (ADME genes) in Hepatocellular Carcinoma', *Journal of Pharmacology and Experimental Therapeutics*, pp. jpet.118.255018.

Huang, J., Zhao, X., Wang, J., Cheng, Y., Wu, Q., Wang, B., Zhao, F., Meng, L., Zhang, Y., Jin, M. and Xu, H. (2019) 'Distinct roles of Dlk1 isoforms in bi-potential differentiation of hepatic stem cells', *Stem Cell Research & Therapy,* 10(1), pp. 31.

Huang, S., Howington, M. B., Dobry, C. J., Evans, C. R. and Leiser, S. F. (2021) 'Flavin-Containing Monooxygenases Are Conserved Regulators of Stress Resistance and Metabolism', *Frontiers in Cell and Developmental Biology,* 9(151).

Huber, W., Carey, V. J., Gentleman, R., Anders, S., Carlson, M., Carvalho, B. S., Bravo, H. C., Davis, S., Gatto, L., Girke, T., Gottardo, R., Hahne, F., Hansen, K. D., Irizarry, R. A., Lawrence, M., Love, M. I., MacDonald, J., Obenchain, V., Oleś, A. K., Pagès, H., Reyes, A., Shannon, P., Smyth, G. K., Tenenbaum, D., Waldron, L. and Morgan, M. (2015) 'Orchestrating high-throughput genomic analysis with Bioconductor', *Nature Methods,* 12(2), pp. 115-121.

Ikeda, R., Tsuchiya, Y., Koike, N., Umemura, Y., Inokawa, H., Ono, R., Inoue, M., Sasawaki, Y., Grieten, T., Okubo, N., Ikoma, K., Fujiwara, H., Kubo, T. and Yagita, K. (2019) 'REV-ERBα and REV-ERBβ function as key factors regulating Mammalian Circadian Output', *Scientific Reports,* 9(1), pp. 10171.

Jia, Z., Cheng, Y., Jiang, X., Zhang, C., Wang, G., Xu, J., Li, Y., Peng, Q. and Gao, Y. (2020) '3D Culture System for Liver Tissue Mimicking Hepatic Plates for Improvement of Human Hepatocyte (C3A) Function and Polarity', *BioMed Research International,* 2020, pp. 6354183.

Jung, H. J., Jang, H.-J. and Kwon, T.-H. (2021) 'Aquaporins implicated in the cell proliferation and the signaling pathways of cell stemness', *Biochimie,* 188, pp. 52-60.

Jung, H. R., Kang, H. M., Ryu, J. W., Kim, D. S., Noh, K. H., Kim, E. S., Lee, H. J., Chung, K. S., Cho, H. S., Kim, N. S., Im, D. S., Lim, J. H. and Jung, C. R. (2017) 'Cell Spheroids with Enhanced Aggressiveness to Mimic Human Liver Cancer In Vitro and In Vivo', *Sci Rep,* 7(1), pp. 10499.

Kanebratt, K. P., Janefeldt, A., Vilén, L., Vildhede, A., Samuelsson, K., Milton, L., Björkbom, A., Persson, M., Leandersson, C., Andersson, T. B. and Hilgendorf, C. (2021) 'Primary Human Hepatocyte Spheroid Model as a 3D In Vitro Platform for Metabolism Studies', *Journal of Pharmaceutical Sciences,* 110(1), pp. 422-431.

Kermanizadeh, A., Brown, D. M., Moritz, W. and Stone, V. (2019) 'The importance of inter-individual Kupffer cell variability in the governance of hepatic toxicity in a 3D primary human liver microtissue model', *Sci Rep,* 9(1), pp. 7295.

Kim, D. S., Ryu, J. W., Son, M. Y., Oh, J. H., Chung, K. S., Lee, S., Lee, J. J., Ahn, J. H., Min, J. S., Ahn, J., Kang, H. M., Kim, J., Jung, C. R., Kim, N. S. and Cho, H. S. (2017) 'A liver-specific gene expression panel predicts the differentiation status of in vitro hepatocyte models', *Hepatology,* 66(5), pp. 1662-1674.

Kmiec, Z. (2001) 'Cooperation of liver cells in health and disease', *Adv Anat Embryol Cell Biol,* 161, pp. III-XIII, 1-151.

Kolde, R. (2012) 'Pheatmap: pretty heatmaps', *R package version,* 1(2), pp. 726.

Kozyra, M., Johansson, I., Nordling, A., Ullah, S., Lauschke, V. M. and Ingelman-Sundberg, M. (2018) 'Human hepatic 3D spheroids as a model for steatosis and insulin resistance', *Sci Rep,* 8(1), pp. 14297.

Lee, M.-O., Lee, S.-G., Jung, C.-R., Son, Y. S., Ryu, J.-W., Jung, K. B., Ahn, J.-H., Oh, J.-H., Lee, H.-A., Lim, J. H., Kim, J., Jang, I., Choi, J., Jung, J., Park, K., Lee, B., Kim, D.-S., Son, M.-Y. and Cho, H.-S. (2021) 'Development of a quantitative prediction algorithm for target organ-specific similarity of human pluripotent stem cell-derived organoids and cells', *Nature Communications,* 12(1).

Li, H., Handsaker, B., Wysoker, A., Fennell, T., Ruan, J., Homer, N., Marth, G., Abecasis, G., Durbin, R. and Genome Project Data Processing, S. (2009) 'The Sequence Alignment/Map format and SAMtools', *Bioinformatics,* 25(16), pp. 2078-9.

Llewellyn, S. V., Conway, G. E., Zanoni, I., Jørgensen, A. K., Shah, U.-K., Seleci, D. A., Keller, J. G., Kim, J. W., Wohlleben, W. and Jensen, K. A. (2021) 'Understanding the impact of more realistic low-dose, prolonged engineered nanomaterial exposure on genotoxicity using 3D models of the human liver', *Journal of nanobiotechnology,* 19(1), pp. 1-24.

Love, M. I., Huber, W. and Anders, S. (2014) 'Moderated estimation of fold change and dispersion for RNA-seq data with DESeq2', *Genome Biol,* 15(12), pp. 550.

Mackowiak, B. and Wang, H. (2016) 'Mechanisms of xenobiotic receptor activation: Direct vs. indirect', *Biochim Biophys Acta,* 1859(9), pp. 1130-1140.

Mandon, M., Huet, S., Dubreil, E., Fessard, V. and Le Hegarat, L. (2019) 'Three-dimensional HepaRG spheroids as a liver model to study human genotoxicity in vitro with the single cell gel electrophoresis assay', *Sci Rep,* 9(1), pp. 10548.

Marchitti, S. A., Orlicky, D. J., Brocker, C. and Vasiliou, V. (2010) 'Aldehyde dehydrogenase 3B1 (ALDH3B1): immunohistochemical tissue distribution and cellular-specific localization in normal and cancerous human tissues', *The journal of histochemistry and cytochemistry : official journal of the Histochemistry Society,* 58(9), pp. 765-783.

Marinelli, R. A., Gradilone, S. A., Carreras, F. I., Calamita, G. and Lehmann, G. L. (2004) 'Liver aquaporins: Significance in canalicular and ductal bile formation', *Annals of Hepatology,* 3(4), pp. 130-136.

Marinelli, R. A., Vore, M. and Javitt, N. B. (2019) 'Hepatic Bile Formation: Canalicular Osmolarity and Paracellular and Transcellular Water Flow', *J Pharmacol Exp Ther,* 371(3), pp. 713-717.

Masyuk, A. I. and LaRusso, N. F. (2006) 'Aquaporins in the hepatobiliary system', *Hepatology,* 43(2 Suppl 1), pp. S75-81.

Messner, S., Fredriksson, L., Lauschke, V. M., Roessger, K., Escher, C., Bober, M., Kelm, J. M., Ingelman-Sundberg, M. and Moritz, W. (2018) 'Transcriptomic, Proteomic, and Functional Long-Term Characterization of Multicellular Three-Dimensional Human Liver Microtissues', *Appl In Vitro Toxicol,* 4(1), pp. 1-12.

Miller, W. L. and Auchus, R. J. (2011) 'The Molecular Biology, Biochemistry, and Physiology of Human Steroidogenesis and Its Disorders', *Endocrine Reviews,* 32(1), pp. 81-151.

Monier, B., McDermaid, A., Zhao, J. and Ma, Q. J. (2021) *vidger: Create rapid visualizations of RNAseq data in R*. Available at: https://bioconductor.org/packages/release/bioc/html/vidger.html.

Mori, N. and Kida, Y. S. (2020) 'Expression of genes involved in drug metabolism differs between perfusable 3D liver tissue and conventional 2D-cultured hepatocellular carcinoma cells', *FEBS open bio,* 10(10), pp. 1985-2002.

Mun, S. J., Ryu, J.-S., Lee, M.-O., Son, Y. S., Oh, S. J., Cho, H.-S., Son, M.-Y., Kim, D.-S., Kim, S. J., Yoo, H. J., Lee, H.-J., Kim, J., Jung, C.-R., Chung, K.-S. and Son, M. J. (2019) 'Generation of

expandable human pluripotent stem cell-derived hepatocyte-like liver organoids', *Journal of Hepatology,* 71(5), pp. 970-985.

Nudischer, R., Renggli, K., Hierlemann, A., Roth, A. B. and Bertinetti-Lapatki, C. (2020) 'Characterization of a long-term mouse primary liver 3D tissue model recapitulating innate-immune responses and drug-induced liver toxicity', *PLoS One,* 15(7), pp. e0235745.

Nwosu, Z. C., Megger, D. A., Hammad, S., Sitek, B., Roessler, S., Ebert, M. P., Meyer, C. and Dooley, S. (2017) 'Identification of the Consistently Altered Metabolic Targets in Human Hepatocellular Carcinoma', *Cellular and Molecular Gastroenterology and Hepatology,* 4(2), pp. 303-323.e1.

O'Shaughnessy, P. J., Monteiro, A., Bhattacharya, S., Fraser, M. J. and Fowler, P. A. (2013) 'Steroidogenic enzyme expression in the human fetal liver and potential role in the endocrinology of pregnancy', *Molecular Human Reproduction,* 19(3), pp. 177-187.

Okonechnikov, K., Conesa, A. and García-Alcalde, F. (2016) 'Qualimap 2: advanced multi-sample quality control for high-throughput sequencing data', *Bioinformatics (Oxford, England),* 32(2), pp. 292-294.

Oliva-Vilarnau, N., Vorrink, S. U., Ingelman-Sundberg, M. and Lauschke, V. M. (2020) 'A 3D Cell Culture Model Identifies Wnt/β-Catenin Mediated Inhibition of p53 as a Critical Step during Human Hepatocyte Regeneration', *Advanced Science,* 7(15), pp. 2000248.

Pluta, K. D., Samluk, A., Wencel, A., Zakrzewska, K. E., Gora, M., Burzynska, B., Ciezkowska, M., Motyl, J. and Pijanowska, D. G. (2020) 'Genetically modified C3A cells with restored urea cycle for improved bioartificial liver', *Biocybernetics and Biomedical Engineering,* 40(1), pp. 378-387.

Pomo, J. M., Taylor, R. M. and Gullapalli, R. R. (2016) 'Influence of TP53 and CDH1 genes in hepatocellular cancer spheroid formation and culture: a model system to understand cancer cell growth mechanics', *Cancer Cell Int,* 16, pp. 44.

R Core Team (2019) *R: A language and environment for statistical computing.*: R Foundation for Statistical Computing, Vienna, Austria. Available at: https://www.R-project.org/.

Ramaiahgari, S., Waidyanatha, S., Dixon, D., DeVito, M., Paules, R. and Ferguson, S. (2017) 'From the cover: three-dimensional (3D) HepaRG spheroid model with physiologically relevant xenobiotic metabolism competence and hepatocyte functionality for liver toxicity screening', *Toxicol Sci,* 159, pp. 124-36.

Reif, R., Karlsson, J., Günther, G., Beattie, L., Wrangborg, D., Hammad, S., Begher-Tibbe, B., Vartak, A., Melega, S., Kaye, P. M., Hengstler, J. G. and Jirstrand, M. (2015) 'Bile canalicular dynamics in hepatocyte sandwich cultures', *Archives of Toxicology,* 89(10), pp. 1861-1870.

Režen, T., Ogris, I., Sever, M., Merzel, F., Golic Grdadolnik, S. and Rozman, D. (2017) 'Evaluation of Selected CYP51A1 Polymorphisms in View of Interactions with Substrate and Redox Partner', *Frontiers in Pharmacology,* 8(417).

Riede, J., Wollmann, B. M., Molden, E. and Ingelman-Sundberg, M. (2021) 'Primary Human Hepatocyte Spheroids as an In Vitro Tool for Investigating Drug Compounds with Low Hepatic Clearance', *Drug Metabolism and Disposition,* 49(7), pp. 501.

Rose, S., Cuvellier, M., Ezan, F., Carteret, J., Bruyère, A., Legagneux, V., Nesslany, F., Baffet, G. and Langouët, S. (2021) 'DMSO-free highly differentiated HepaRG spheroids for chronic toxicity, liver functions and genotoxicity studies', *Archives of Toxicology*.

Russell, D. W. (2009) 'Fifty years of advances in bile acid synthesis and metabolism', *J Lipid Res,* 50 Suppl, pp. S120-5.

Smedley, D., Haider, S., Ballester, B., Holland, R., London, D., Thorisson, G. and Kasprzyk, A. (2009) 'BioMart – biological queries made easy', *BMC Genomics,* 10(1), pp. 22.

Song, H., Ding, N., Li, S., Liao, J., Xie, A., Yu, Y., Zhang, C. and Ni, C. (2020) 'Identification of Hub Genes Associated With Hepatocellular Carcinoma Using Robust Rank Aggregation Combined With Weighted Gene Co-expression Network Analysis', *Front Genet,* 11, pp. 895.

Stampar, M., Sedighi Frandsen, H., Rogowska-Wrzesinska, A., Wrzesinski, K., Filipic, M. and Zegura, B. (2020) 'Hepatocellular carcinoma (HepG2/C3A) cell-based 3D model for genotoxicity testing of chemicals', *Sci Total Environ*, pp. 143255.

Sun, P., Zhang, G., Su, X., Jin, C., Yu, B., Yu, X., Lv, Z., Ma, H., Zhang, M., Wei, W. and Li, W. (2019) 'Maintenance of Primary Hepatocyte Functions In Vitro by Inhibiting Mechanical Tension-Induced YAP Activation', *Cell Rep,* 29(10), pp. 3212-3222 e4.

Tao, Q., Chen, S., Liu, J., Zhao, P., Jiang, L., Tu, X., Tang, X., Liu, Z., Yasheng, A., Tuerxun, K. and Zheng, Y. (2021) 'The roles of the cell division cycle-associated gene family in hepatocellular carcinoma', *Journal of gastrointestinal oncology,* 12(2), pp. 781-794.

ter Braak, B., Niemeijer, M., Wolters, L., Le Dévédec, S., Bouwman, P. and van de Water, B. (2021) 'Towards an advanced testing strategy for genotoxicity using image-based 2D and 3D HepG2 DNA damage response fluorescent protein reporters', *Mutagenesis*.

Terashima, J., Goto, S., Hattori, H., Hoshi, S., Ushirokawa, M., Kudo, K., Habano, W. and Ozawa, S. (2015) 'CYP1A1 and CYP1A2 expression levels are differentially regulated in three-dimensional spheroids of liver cancer cells compared to two-dimensional monolayer cultures', *Drug Metab Pharmacokinet,* 30(6), pp. 434-40.

Thompson, S. J., Thompson, S. E. M. and Cazier, J.-B. (2019) 'CaStLeS (Compute and Storage for the Life Sciences): a collection of compute and storage resources for supporting research at the University of Birmingham', *Zenodo*.

Timsit, Y. E. and Negishi, M. (2007) 'CAR and PXR: the xenobiotic-sensing receptors', *Steroids,* 72(3), pp. 231-246.

van Wenum, M., Adam, A. A., Hakvoort, T. B., Hendriks, E. J., Shevchenko, V., van Gulik, T. M., Chamuleau, R. A. and Hoekstra, R. (2016) 'Selecting Cells for Bioartificial Liver Devices and the Importance of a 3D Culture Environment: A Functional Comparison between the HepaRG and C3A Cell Lines', *Int J Biol Sci,* 12(8), pp. 964-78.

Wang, J., Peng, R., Zhang, Z., Zhang, Y., Dai, Y. and Sun, Y. (2021a) 'Identification and Validation of Key Genes in Hepatocellular Carcinoma by Bioinformatics Analysis', *BioMed Research International,* 2021, pp. 6662114.

Wang, Z., Karkossa, I., Grosskopf, H., Rolle-Kampczyk, U., Hackermuller, J., von Bergen, M. and Schubert, K. (2021b) 'Comparison of quantitation methods in proteomics to define relevant toxicological information on AhR activation of HepG2 cells by BaP', *Toxicology,* 448, pp. 152652.

Wickham, H., Averick, M., Bryan, J., Chang, W., McGowan, L., François, R., Grolemund, G., Hayes, A., Henry, L., Hester, J., Kuhn, M., Pedersen, T., Miller, E., Bache, S., Müller, K., Ooms, J., Robinson, D., Seidel, D., Spinu, V., Takahashi, K., Vaughan, D., Wilke, C., Woo, K. and Yutani, H. (2019) 'Welcome to the Tidyverse', *Journal of Open Source Software,* 4(43).

Wickham, H., Sievert, C. and SpringerLink (2016) 'ggplot2 : Elegant Graphics for Data Analysis', *Use R!*

Wrzesinski, K., Magnone, M. C., Hansen, L. V., Kruse, M. E., Bergauer, T., Bobadilla, M., Gubler, M., Mizrahi, J., Zhang, K., Andreasen, C. M., Joensen, K. E., Andersen, S. M., Olesen, J. B., Schaffalitzky de Muckadell, O. B. and Fey, S. J. (2013) 'HepG2/C3A 3D spheroids exhibit stable physiological functionality for at least 24 days after recovering from trypsinisation', *Toxicology Research,* 2(3), pp. 163-172.

Wrzesinski, K., Rogowska-Wrzesinska, A., Kanlaya, R., Borkowski, K., Schwämmle, V. and Dai, J. (2014) 'The cultural divide: exponential growth in classical 2D and metabolic equilibrium in 3D environments'.

Zerbino, D. R., Achuthan, P., Akanni, W., Amode, M. R., Barrell, D., Bhai, J., Billis, K., Cummins, C., Gall, A. and Girón, C. G. (2018) 'Ensembl 2018', *Nucleic acids research,* 46(D1), pp. D754-D761.

Zhang, J., Huang, W., Qatanani, M., Evans, R. M. and Moore, D. D. (2004) 'The constitutive androstane receptor and pregnane X receptor function coordinately to prevent bile acid-induced hepatotoxicity', *Journal of Biological Chemistry,* 279(47), pp. 49517-49522.

Zhang, K., Zhang, L., Liu, W., Ma, X., Cen, J., Sun, Z., Wang, C., Feng, S., Zhang, Z., Yue, L., Sun, L., Zhu, Z., Chen, X., Feng, A., Wu, J., Jiang, Z., Li, P., Cheng, X., Gao, D., Peng, L. and Hui, L. (2018) 'In Vitro Expansion of Primary Human Hepatocytes with Efficient Liver Repopulation Capacity', *Cell Stem Cell,* 23(6), pp. 806-819 e4.

Zhang, L., Huang, X., Meng, Z., Dong, B., Shiah, S., Moore, D. D. and Huang, W. (2009) 'Significance and mechanism of CYP7a1 gene regulation during the acute phase of liver regeneration', *Mol Endocrinol,* 23(2), pp. 137-45.

Zhou, T., Cai, Z., Ma, N., Xie, W., Gao, C., Huang, M., Bai, Y., Ni, Y. and Tang, Y. (2020) 'A Novel Ten-Gene Signature Predicting Prognosis in Hepatocellular Carcinoma', *Frontiers in Cell and Developmental Biology,* 8(629).

Zhou, Z., Xu, M. J. and Gao, B. (2016) 'Hepatocytes: a key cell type for innate immunity', *Cell Mol Immunol,* 13(3), pp. 301-15.

Chapter 7. GENERAL DISCUSSION

7.1. Introduction

The need to adequately assess human risk exposure to small molecule chemicals is an ever-growing task as novel chemical entities continue to be synthesised for a wide-array of utilities including those for pharmaceutical, agricultural or industrial use. Therefore, as the number of chemicals increases, so too does human xenobiotic toxicological risk if not properly understood. Hence, the need to assess chemicals for variety of toxicological risks including those relating to genetic-toxicology or drug-induced liver injury is not just one of a regulatory requirement but also one that can be implemented early in pre-clinical and basic research. This need to expand toxicological knowledge and improve research efficiency is of course neatly exemplified by commonly cited articles reviewing chemical safety as being a primary reason for the early termination of drug development and research programmes. (Waring et al., 2015, Hay et al., 2014), particularly those attributed to drug-induced liver injury. Despite, a better understanding of toxicological potential of chemicals, the models available and our knowledge-pool and to undertake *in vitro-in silico* toxicological experiments, has increased significantly in the past 10 years (Anklam et al., 2021, Fischer et al., 2020).

The use of advanced 3D hepatic models has introduced a paradigm-shift in the way that *in vitro* pharmacological and toxicological experiments are undertaken; that is that 3D models are able to correct some of the shortcomings and pitfalls associated with traditional models such as monolayers of cells or even sandwich-cultures, to regain metabolic competency and *in vivo*-like status. Despite advances in 3D cell culture models, the most probable position that such models could occupy under current guidelines is within the nonclinical safety

evaluation space for the safety assessment of novel chemical entities, e.g., pharmaceuticals for human use. In order to take the next step, regulatory bodies such as the FDA, have defined fundamental questions need to be addressed in order to pitch these models for regulatory use with regards to human toxicity prediction studies, more than current models used (Wang et al., 2021). Therefore, there is still a need to understand the 'valued-added' of such approaches in the regulatory or pre-clinical context. To this end, a deeper understanding as to the potential use of hepatic 3D cell culture models in toxicological practise is still required and represents an ever-evolving body of work from multiple researchers, world-wide.

Therefore, the specific goals of this thesis were to:

vi. Undertake a critical assessment of the requirements needed to develop a simple HepG2/C3A spheroid model and deploy it in a series of proof-of-concept studies (**Chapter 2**)

vii. Implement a HepG2/C3A spheroid model in a battery of *in* vitro assays to assess the genotoxic potential of chemical carcinogens (**Chapter 3**)

viii. Develop a robust methodology for the measurement of cellular-mitochondrial respiration in single spheroids of varying sizes and cell lineage (**Chapter 4**)

ix. Evaluate the longevity of HepG2/C3A spheroids through a series of approaches and their applicability to repeat-dose assays to assess genotoxic and hepatotoxic potential of chemicals (**Chapter 5**)

x. Undertake a transcriptomic comparison on HepG2/C3A cells across a continuum from monolayers to spheroids cultured for up to 28 by use of paired-end RNA-seq (**Chapter 6**)

7.2. Summary of major thesis findings

Despite a growing body of evidence for the development and deployment of hepatic spheroid models, there remains a lack of coherent protocols or studies that have demonstrated reproducibility of HepG2 spheroid models using simple *in vitro* cell culture techniques. Therefore, in **Chapter 2** we attempted the development of a HepG2/C3A spheroid model using evidence from the literature by exploring the liquid agarose overlay technique (Costa et al., 2014). Here we have extensively evaluated a range of different agarose types (low – high gelling point) and their ability to form cell-repellent layers within tissue culture plates for the formation of HepG2/C3A spheroids (Figure 2.1), compared to commercially available alternatives. Contrary to previous studies (Gaskell et al., 2016, Kyffin et al., 2019b), we found that the use of specialised agaroses was unnecessary and instead normal, molecular biology grade agarose, commonly found in most laboratories, was highly suited to the generation of reproducible HepG2/C3A spheroids (expanded in **Chapter 3**). In a simplified study, we demonstrated that HepG2/C3A cells are capable of generating spheroids with significant superiority to the parent HepG2 cell line, in-line with a running commentary in the common literature that HepG2/3A cells possess contact-inhibition properties making them more suited to forming spheroids (Gaskell et al., 2016, Wrzesinski et al., 2013) versus highly proliferative HepG2 parent cells. This theme is one that requires urgent attention as HepG2 and HepG2/C3A models continue to be employed within toxicology studies and a empirical comparison of the two cell lines is currently lacking in the literature. One of the main concerns with use of the agarose LOT to produce spheroids versus commercial alternatives which is not assessed in the literature, is the ability of the agarose hydrogels to perform as molecular sinks for subsequent chemical exposures, and

cell growth medium. To this end, **Chapter 2** presents a study using fluorescein as a trackable small molecule, and the mutagen 4-NQO. We show that these small molecules reach an equilibrium of partition between the cell culture medium and agarose within 24-72 h of incubation. Future expansions to this thesis would therefore look to clarify the concentration of small molecules within spheroid cell culture mediums, analytically using this approach.

7.2.1. Implementation of HepG2/C3A spheroids *in vitro* toxicological studies

We implemented a simplified *in vitro* screen for hepatotoxicity and found that spheroids were more sensitive versus their monolayer counterparts on exposure to APAP and TRV, but not DCF or the NSAID cinchophen, in line with previous studies (Ramaiahgari et al., 2014, Gaskell et al., 2016). Similarly, we presented [at the time of research] a novel use for the alkaline comet assay in an acute genotoxicity assay study and identified that spheroids were more sensitive to the pro-mutagen, B[a]P which is typically bio-transformed by CYP1A metabolism (Park et al., 2006).

In **Chapter 3**, we expanded this study and further optimised the development of HepG2/C3A, to form spheroids that were devoid of the classic 'hypoxic/necrotic' core and could be maintained over 28 days under standard tissue culture conditions. **Chapter 3** further developed the use of the comet assay to measure single-stranded DNA breaks in disaggregated spheroids to ensure maximal viability, and developed an additional assay to study the induction of double-strand breaks using gamma-H2AX as a proxy. Consistent with the initial datasets gathered in **Chapter 2, Coltman et al. (2021a)**, compared to monolayer cultured cells, we found that HepG2/C3A spheroids cultured for 7 days, were significantly

more sensitive on exposure to three model genotoxicants (B[a]P, PhIP and 2-AA) requiring xenobiotic metabolism to form DNA-reactive metabolites, initiating the DNA damage response, without the induction of cytotoxicity. Furthermore, analysis of basal mRNA transcripts by qPCR revealed that the upregulation of hepatic nuclear factors such as *HNF4A* and *CAR* drove the induction several CYP450 enzymes including *1A1/1A2, 3A4, 2C9* and *2C19*, in spheroids compared to monolayers (**Chapter 3 and Addendum**); in addition to phase II conjugative enzymes (*UGT1A1/1A3/1A6*; *SULTs* and *NATs*), and gene sets linked to improved 'hepatic-like' function in HepG2/C3A spheroids, such as *ALB* and *CPS1*, in line with previous studies (Gaskell et al., 2016). In response to the three pro-genotoxicants, further transcriptional upregulation of ADME related genes occurred including *CYP1A1/1A2, NAT1/2, SULT1A2* and *UGT1A* family members, commensurate with the induction of genes pertaining to cell-cycle arrest, DNA damage response such as *GADD45A* and *CDKN1A.* In this study we also reveal a potentially novel role for B[a]P, which to the best of our knowledge, has not been seen elsewhere, suggesting that B[a]P may be able to induce metabolic alterations in HepG2/C3A spheroids through the Warburg-effect, via *HIF1A* activation (Hardonniere et al., 2016).

At the time of publishing **Chapter 3**, we were the first to implement the use of HepG2/C3A spheroids in an *in vitro* genotoxicity study and one of only a few articles that have assessed the impact of hepatic spheroids within this new space (Shah et al., 2018, Elje et al., 2019b, Elje et al., 2019a). In **Chapter 2 and 3**, in support of our hypotheses, we present HepG2/C3A 3D spheroids as a sensitive model for *in vitro* genotoxicity assessment and recapitulate

hepatotoxicity studies commonly exemplified in the literature, as a result of prolonged culture.

7.2.2. Metabolism switching in HepG2/C3A models

Hepatocytes are one of the most energetic cell types within the human body and dynamically switch their metabolism according to their distribution throughout the zones of the liver *in vivo,* between OXPHOS and glycolysis (Jungermann and Kietzmann, 1997, Gebhardt, 1992). Hepatocytes when grown as spheroids have been shown to be capable of forming both apical and basolateral membranes (Kyffin et al., 2019a, Bell et al., 2018, Terashima et al., 2015), in support of cellular polarisation and the formation of bile canaliculi (HepG2/C3A, (Gaskell et al., 2016)), and utilise OXPHOS to a significant extent during this processes. However, at the point of maturation, hepatocyte metabolism is switched towards glycolysis (Fu et al., 2013). In **Chapter 4**, we therefore looked to test our hypothesis that mitochondrial metabolism was altered when cells were grown within a different spatial arrangement (i.e., in 3D), by use of Seahorse extracellular flux analysis to measure real-time bioenergetics of intact singular spheroids, and provide a substantial set of protocols and considerations that are not present in the current literature considering metabolic flux analysis of *in vitro* spheroid models. In **Chapter 4** we cultivated spheroids from four different cancer derived cell lines which were A-549 (lung), HepG2/C3A (liver), MCF-7 (breast) and SK-OV-3 (ovarian) and compared their relative oxygen consumption rates (OCR) at various seeding densities (1, 2, 4 or 8 x 10^3 cells per well) and therefore spheroid sizes (Figure 4.3), using MCF-7 spheroids as a control subject. In-keeping with mathematical predictions, we found that average OCR for all spheroids tested in this study, were directly correlated with

spheroid size (Leedale et al., 2019). Interestingly, despite significant differences in spheroid sizes, we found that the basal OCR of HepG2/C3A spheroids cultured over 7 days was equal to MCF-7 spheroids of a much smaller size and cell number cultured only over 3 days, we therefore hypothesised that this was likely a result of extensive cellular replication in MCF-7 cell line versus HepG2/C3A which had obtained a more quiescent phenotype by direct comparison - a repression of cell doubling rate as seen in **Chapter 3**. We demonstrate and discuss that the function between spheroid size (volume, initial cell seeding number) and OCR could impact total oxygen diffusion across the spheroid core and give rise to gradients thereof, which could have important implications when studying metabolism in spheroids over prolonged periods of culture; to the best of our knowledge we do not believe the extensive observations or guidance of Chapter 4, Coltman et al. (2021b), have been considered elsewhere in the literature before. Accordingly, the limitations of extracellular flux analyses for measurement of cellular bioenergetics is discussed extensively in **Chapter 4** and in the subsequent publication: Coltman et al., 2021b**.** Furthermore, **Chapter 4 section 4.5.2.4** extensively reviews common practices in spheroid culture techniques including handling, and the importance of data normalisation, to which the reader is directed.

7.2.3. Chronological profiling of HepG2/C3A models

A major aim of this thesis was to monitor functional changes in HepG2/C3A spheroids over time and how these observations may help ascertain has to why sensitivity towards hepatotoxicants (**Chapter 2**) or genotoxicants (**Chapter 3**) was improved in HepG2/C3A spheroids when compared to monolayers. **Chapter 5** therefore presents a study in which HepG2/C3A spheroids are chronologically profiled for up to 28 days of culture alongside cell

2D monolayers. Contrary to the literature, we found that HepG2/C3A cells continue to proliferate when cultured as spheroids (Figure 5.1) but the doubling rate is substantially reduced compared to rapidly-dividing monolayers (**Chapter 3**) in accordance with Wrzesinski et al. (2014) and in line with Gaskell et al. (2016), monitoring the expression of Ki67 in HepG2/C3A spheroids. In **Chapter 5** we found that HepG2/C3A spheroids continued to proliferate up to approximately 21 days of culture before viability was reduced by up to 10 % by day 28 of culture by an induction of apoptosis and not necrosis, but spheroid structure was maintained throughout, revealing spheroids that were devoid of the common 'hypoxic-necrotic core' seen by Gaskell et al., 2016 and others (Riffle et al., 2017). Throughout the 28-day culture period, albumin secretion continued to be increased compared to monolayers, and supported by the continued mRNA expression of the *ALB* gene target in **Chapter 3**, but downregulated on exposure to genotoxicant (Coltman et al., 2021a).

Furthermore, we undertook extensive examination of HepG2/C3A mitochondrial metabolism according to established parameters in **Chapter 4**, compared between monolayers and spheroids of all time points. Results from **Chapter 5**, undertaking comprehensive extracellular flux analysis, supports of our hypothesis that the phenotypic transformation of HepG2/C3A from monolayers to spheroids triggers rewiring of metabolic networks as previously described in HepG2/C3A (Iyer et al., 2010, Fey et al., 2020). Spheroid metabolism was gradually directed towards a glycolysis and a reduction in OXPHOS across the spheroid time course to support ATP synthesis. We postulate that these observations in **Chapter 5** support the notion that HepG2/C3A cells are undergoing rapid differentiation and polarisation within spheroid structures, likened to similar observations made in primary

human hepatocytes (Fu et al., 2013, Wrzesinski et al., 2014). Intriguingly, we found that oxygen consumption linked to non-mitochondrial processes, was progressively enhanced in all spheroids, and argue that this could be attributed to enhanced monooxygenase function in spheroids versus monolayers seen in **Chapter 3**, such as those provided by CYP450 and FMO xenobiotic metabolism (Foti and Dalvie, 2016, Huang et al., 2021, Krueger and Williams, 2005).

Considering their suitability for long-term growth, we looked to assess the utility of HepG2/C3A spheroids in repeated exposure studies. Compared to day 7 spheroids and monolayers offered an acute 48 h exposure, HepG2/C3A spheroids repeatedly exposed to 12 common hepatotoxicants over 1 week, proved significantly more sensitive. However, the maturation of HepG2/C3A spheroid (i.e., 7-28 days of growth), had little to no impact, in line with our previous observation **in Chapter 3, Coltman et al., 2021a**, that a 10-day old spheroid offered no further sensitivity to the panel of genotoxicants, than that of the 7-day HepG2/C3A. Owing to results presented in **Chapter 3**, that ADME related gene pathways were further induced on exposure to pro-genotoxic molecules, it would seem probable that prolonged exposure of HepG2/C3A spheroids continue to induce xenobiotic metabolism enzymes to levels above those in monolayers cells, promoting the biotransformation of selected hepatotoxicants to reactive intermediates (Fey et al., 2020). Alternatively, of course they could prove useful for assessing the metabolism of low-turnover compounds as a novel application. Similarly, we implemented a repeat-dose genotoxicity assay in HepG2/C3A over 7-days exposed to the four model compounds used previously but at significantly lower concentrations (3 – 0.3 μM) used in **Chapter 3**, or elsewhere in similar studies (Stampar et

al., 2020, Elje et al., 2019b) and reveal single DNA strand breaks are significantly induced in HepG2/C3A spheroids but at more realistic physiological doses, again supporting the notion that both basal and induced-ADME responses are enhanced in HepG2/C3A spheroids over time.

7.2.4. Transcriptional changes in HepG2/C3A models

Finally, in **Chapter 6** we undertake global transcriptomic profiling of the HepG2/C3A spheroid models and monolayers, in parallel to studies described in **Chapter 5.** Despite the chapters throughout this thesis describing phenotypic responses that appear to favour the HepG2/C3A spheroid as a more promising model for deployment in toxicological studies versus traditionally grown monolayers, it is unclear as to the molecular cues that promote the behaviour seen. Therefore **Chapter 6** monitors the divergence of these models over time using whole-genome transcriptional profiling by paired-end RNA-seq. Transcriptomic profiling was able to clearly discriminate between all models (Figure 6. 2), whereby the number of differentially expressed genes was found to increase across the spheroid continuum, as a function of growth period, which concurs with a recently published proteomic study in HepG2 spheroids (Ellero et al., 2021) and transcriptomic-metabolomics study conducted in PHH spheroids (Vorrink et al., 2017), concluding that stability of hepatocyte spheroids is enhanced over time to yield a favourable hepatic phenotype compared to that offered by cells grown in 2D. HepG2/C3A spheroids cultured over 28 days revealed striking evidence that key clusters of genes related to hepatocyte-like phenotype were incrementally upregulated, pertaining to the functional enrichment of prominent pathways including cholesterol metabolism, bile acid synthesis, xenobiotic metabolism and

remodelling of hepatic ECM. Whereas downregulated gene clusters supported the notion observed in **Chapter 3** and **Chapter 5** that HepG2/C3A cells within spheroids exit the normal cell cycle and instead focus bioenergesis towards hepatocyte functionalisation. To the best of our knowledge, this is the first time a study of this extent has been applied in HepG2/C3A spheroids. Taken as one, and in support of other basic research discussed, the datasets presented throughout this thesis suggest that HepG2/C3A cells undergo a transcriptomic and proteomic transformation which is dependent on dimensionality and spatial organisation of cells which diverges away from the malignant hepatic carcinoma phenotype of HepG2/C3A monolayers, towards obtaining a more hepatocyte-like phenotype.

7.3. Future work and perspectives on 3D liver models

Although the use of hepatic spheroid models has become widespread in recent years, particularly the use of HepG2 3D spheroids, there are several experimental elements that would help strengthen the research outputs of this thesis. One of the future outlooks for my work and utility of HepG2/C3A spheroids would be further implementation into screening paradigms for genetic-toxicology but also a broader-range of molecules of varying physico-chemistry. For example, most of the small molecules presented in **Chapter 3** and **Chapter 5** of this thesis share similar moieties or routes of metabolism and toxicity; inclusion of non-genotoxic carcinogens or nanomaterials would provide another line of interesting research.

An original aim of this thesis was to undertake extensive characterisation of the xenobiotic metabolism capacity of HepG2/C3A spheroids across the time continuum studied in **Chapter 5 and 6**, using both targeted and untargeted approaches by LC-MS/MS, and map these to

the other datasets collected, for an integrated assessment of cytotoxicity, biotransformation, and potential transcriptomic assessment of chemically-induced cytotoxicity – e.g., biotransformation of benzo[a]pyrene in the HepG2/C3A over prolonged exposure. However, due to the COVID-19 pandemic this body of work awaits final LC-MS/MS data acquisition. A smaller study has therefore been proposed and is presented in **Appendix 3,** to assess the 5 principle CYP450 enzymes in spheroids undergoing a kinetic regimen. All samples and analytical standards have been prepared and they await immanent submission to LC-MS/MS.

RNA-seq analysis is a powerful and sensitive technique and has been used in HepG2/C3A spheroids to reveal a broad-dataset that could be probed further where spheroids represent an enriched i*n* vitro environment not found in monolayers of cells (**Chapter 6**). A combination of multi-omics techniques would serve to further investigate these pathways. For example, proteomics would allow the discrimination between events that are purely transcriptional and those in which proteins are translated and may help confer both protein conformation and functionality (Ellero et al., 2021, Tascher et al., 2019, Bruderer et al., 2015). Furthermore, novel mass spectrometry imaging and ionisation modalities such as nano-DESI or MALDI may allow the distribution of key proteins to spatially resolved in complete and sectioned spheroids, in support of the paradigm that HepG2/C3A spheroids recapitulated zonation of the *in vivo,* and similarly applied for both targeted and untargeted metabolomics (Xie et al., 2020).

Most notably, lipidomics may help further elucidate the role of steroid and cholesterol metabolism in the longevity of HepG2/C3A spheroids, which could be further enhanced by

use of tracer-metabolomics used radiolabelled isotopes by LC-MS/MS and NMR, e.g., radio-labelled glucose uptake studies (Knitsch et al., 2021), to gain insight as to real-time metabolic changes in single spheroids , although currently achieved resolution by mass spectrometry imaging probably precedes single-cell resolution but could allow zones throughout the spheroid to be analysed.

The stability of the HepG2/C3A genome when grown as spheroids would benefit from investigation. Epigenetic events are known to control stem cell fate during hepatic maturation (Park et al., 2015) and DNA hypomethylation has been deployed for the reversal a hepatocellular malignancy in HepG2 cells (Raggi et al., 2014). Therefore, understanding the epigenetic mechanisms that HepG2/C3A spheroids undergo during long-term cultivation studies would be beneficial and may further aid in model selection for inclusion to toxicology studies.

Finally, in this thesis we have attempted to further characterise the use of HepG2/C3A cells in both monolayer and spheroid form toxicological assays. However, despite the efforts made here and, in the literature, there remains a significant lack of transparency as to the profile of HepG2/C3A cells and how these compare to the HepG2 parental cell line in terms of baseline genetic variation. Future work should therefore rigorously compare HepG2 and HepG2/C3A cells from the bottom-up using next-generation sequencing modalities, particularly where phenotypic assays, e.g., response to hepatotoxicants, cannot necessarily differentiate the two.

7.4. Concluding statement

The implementation of 3D hepatic spheroid models is now a mainstay for use on the pharmaceutical research sector but also gathering momentum in other industries. To this end I conclude that a spheroid model borne from HepG2/C3A cells would also serve those concerned with identifying potentially genotoxic or carcinogenic chemicals and would be of value when modelling long-term exposure, thereof. Furthermore, given the utility of the 3D spheroid models reviewed throughout this literature I have demonstrated that prolonged cultivation, distributes the phenotypes of HepG2/C3A spheroids across a time continuum. Although HepG2 spheroid models have been particularly well-studied in the literature owing to extensive accessibility and ease of use, there have been no studies that have investigated spheroid respiratory metabolism over time or have extensively profiled the transcriptional journey of HepG2/C3A cells from monolayers to spheroids over several weeks of growth and show that spheroids continue to transcriptomically diverge from their original monolayers, and gain a transcriptional profile more-closely mimicking human liver tissue. Combined with other datasets entailing repeat dosing of both genotoxic and hepatotoxic compounds, this research demonstrates as series of approaches that could be used to aid in model selection for inclusion in toxicological studies.

7.5. References

Anklam, E., Bahl, M. I., Ball, R., Beger, R. D., Cohen, J., Fitzpatrick, S., Girard, P., Halamoda-Kenzaoui, B., Hinton, D., Hirose, A., Hoeveler, A., Honma, M., Hugas, M., Ishida, S., Kass, G. E., Kojima, H., Krefting, I., Liachenko, S., Liu, Y., Masters, S., Marx, U., McCarthy, T., Mercer, T., Patri, A., Pelaez, C., Pirmohamed, M., Platz, S., Ribeiro, A. J., Rodricks, J. V., Rusyn, I., Salek, R. M., Schoonjans, R., Silva, P., Svendsen, C. N., Sumner, S., Sung, K., Tagle, D., Tong, L., Tong, W., Eijnden-van-Raaij, J. V. D., Vary, N., Wang, T., Waterton, J., Wang, M., Wen, H., Wishart, D., Yuan, Y. and Slikker, W., Jr. (2021) 'Emerging technologies and their impact on regulatory science', *Exp Biol Med (Maywood)*, pp. 15353702211052280.

Bell, C. C., Dankers, A. C. A., Lauschke, V. M., Sison-Young, R., Jenkins, R., Rowe, C., Goldring, C. E., Park, K., Regan, S. L., Walker, T., Schofield, C., Baze, A., Foster, A. J., Williams, D. P., van de Ven, A. W. M., Jacobs, F., Houdt, J. V., Lahteenmaki, T., Snoeys, J., Juhila, S., Richert, L. and Ingelman-Sundberg, M. (2018) 'Comparison of Hepatic 2D Sandwich Cultures and 3D Spheroids for Long-term Toxicity Applications: A Multicenter Study', *Toxicol Sci,* 162(2), pp. 655-666.

Bruderer, R., Bernhardt, O. M., Gandhi, T., Miladinovic, S. M., Cheng, L. Y., Messner, S., Ehrenberger, T., Zanotelli, V., Butscheid, Y., Escher, C., Vitek, O., Rinner, O. and Reiter, L. (2015) 'Extending the limits of quantitative proteome profiling with data-independent acquisition and application to acetaminophen-treated three-dimensional liver microtissues', *Mol Cell Proteomics,* 14(5), pp. 1400-10.

Coltman, N. J., Coke, B. A., Chatzi, K., Shepherd, E. L., Lalor, P. F., Schulz-Utermoehl, T. and Hodges, N. J. (2021a) 'Application of HepG2/C3A liver spheroids as a model system for genotoxicity studies', *Toxicol Lett,* 345, pp. 34-45.

Coltman, N. J., Rochford, G., Hodges, N. J., Ali-Boucetta, H. and Barlow, J. P. (2021b) 'Optimised protocols to expore mitochondrial energy metabolism in spheorids using Agilent Seahorse Extracellular Flux Analysis', *Journal of Visualized Experiments,* n/a(e63346).

Costa, E. C., Gaspar, V. M., Coutinho, P. and Correia, I. J. (2014) 'Optimization of Liquid Overlay Technique to Formulate Heterogenic 3D Co-Cultures Models', *Biotechnology and Bioengineering,* 111(8), pp. 1672-1685.

Elje, E., Hesler, M., Runden-Pran, E., Mann, P., Mariussen, E., Wagner, S., Dusinska, M. and Kohl, Y. (2019a) 'The comet assay applied to HepG2 liver spheroids', *Mutat Res Genet Toxicol Environ Mutagen,* 845, pp. 403033.

Elje, E., Hesler, M., Rundén-Pran, E., Mann, P., Mariussen, E., Wagner, S., Dusinska, M. and Kohl, Y. (2019b) 'The comet assay applied to HepG2 liver spheroids', *Mutation Research/Genetic Toxicology and Environmental Mutagenesis*.

Ellero, A. A., van den Bout, I., Vlok, M., Cromarty, A. D. and Hurrell, T. (2021) 'Continual proteomic divergence of HepG2 cells as a consequence of long-term spheroid culture', *Sci Rep,* 11(1), pp. 10917.

Fey, S. J., Korzeniowska, B. and Wrzesinski, K. (2020) 'Response to and recovery from treatment in human liver-mimetic clinostat spheroids: a model for assessing repeated-dose drug toxicity', *Toxicol Res (Camb),* 9(4), pp. 379-389.

Fischer, I., Milton, C. and Wallace, H. (2020) 'Toxicity testing is evolving!', *Toxicology Research,* 9(2), pp. 67-80.

Foti, R. S. and Dalvie, D. K. (2016) 'Cytochrome P450 and Non-Cytochrome P450 Oxidative Metabolism: Contributions to the Pharmacokinetics, Safety, and Efficacy of Xenobiotics', *Drug Metab Dispos,* 44(8), pp. 1229-45.

Fu, D., Mitra, K., Sengupta, P., Jarnik, M., Lippincott-Schwartz, J. and Arias, I. M. (2013) 'Coordinated elevation of mitochondrial oxidative phosphorylation and autophagy help drive hepatocyte polarization', *Proc Natl Acad Sci U S A,* 110(18), pp. 7288-93.

Gaskell, H., Sharma, P., Colley, H. E., Murdoch, C., Williams, D. P. and Webb, S. D. (2016) 'Characterization of a functional C3A liver spheroid model', *Toxicology research,* 5(4), pp. 1053-1065.

Gebhardt, R. (1992) 'Metabolic Zonation of the Liver - Regulation and Implications for Liver-Function', *Pharmacology & Therapeutics,* 53(3), pp. 275-354.

Hardonniere, K., Saunier, E., Lemarie, A., Fernier, M., Gallais, I., Helies-Toussaint, C., Mograbi, B., Antonio, S., Benit, P., Rustin, P., Janin, M., Habarou, F., Ottolenghi, C., Lavault, M. T., Benelli, C., Sergent, O., Huc, L., Bortoli, S. and Lagadic-Gossmann, D. (2016) 'The environmental carcinogen benzo[a]pyrene induces a Warburg-like metabolic reprogramming dependent on NHE1 and associated with cell survival', *Sci Rep,* 6, pp. 30776.

Hay, M., Thomas, D. W., Craighead, J. L., Economides, C. and Rosenthal, J. (2014) 'Clinical development success rates for investigational drugs', *Nature biotechnology,* 32(1), pp. 40-51.

Huang, S., Howington, M. B., Dobry, C. J., Evans, C. R. and Leiser, S. F. (2021) 'Flavin-Containing Monooxygenases Are Conserved Regulators of Stress Resistance and Metabolism', *Frontiers in Cell and Developmental Biology,* 9(151).

Iyer, V. V., Yang, H., Ierapetritou, M. G. and Roth, C. M. (2010) 'Effects of glucose and insulin on HepG2-C3A cell metabolism', *Biotechnol Bioeng,* 107(2), pp. 347-56.

Jungermann, K. and Kietzmann, T. (1997) 'Role of oxygen in the zonation of carbohydrate metabolism and gene expression in liver', *Kidney Int,* 51(2), pp. 402-12.

Knitsch, R., AlWahsh, M., Raschke, H., Lambert, J. and Hergenroder, R. (2021) 'In Vitro Spatio-Temporal NMR Metabolomics of Living 3D Cell Models', *Anal Chem,* 93(40), pp. 13485-13494.

Krueger, S. K. and Williams, D. E. (2005) 'Mammalian flavin-containing monooxygenases: structure/function, genetic polymorphisms and role in drug metabolism', *Pharmacol Ther,* 106, pp. 357-87.

Kyffin, J. A., Cox, C. R., Leedale, J., Colley, H. E., Murdoch, C., Mistry, P., Webb, S. D. and Sharma, P. (2019a) 'Preparation of Primary Rat Hepatocyte Spheroids Utilizing the Liquid-Overlay Technique', *Curr Protoc Toxicol,* 81(1), pp. e87.

Kyffin, J. A., Sharma, P., Leedale, J., Colley, H. E., Murdoch, C., Harding, A. L., Mistry, P. and Webb, S. D. (2019b) 'Characterisation of a functional rat hepatocyte spheroid model', *Toxicology in Vitro,* 55, pp. 160-172.

Leedale, J., Colley, H. E., Gaskell, H., Williams, D. P., Bearon, R. N. and Chadwick, A. E. (2019) 'In silico-guided optimisation of oxygen gradients in hepatic spheroids', *Comput Toxicol*.

Park, H. J., Choi, Y. J., Kim, J. W., Chun, H. S., Im, I., Yoon, S., Han, Y. M., Song, C. W. and Kim, H. (2015) 'Differences in the Epigenetic Regulation of Cytochrome P450 Genes between Human Embryonic Stem Cell-Derived Hepatocytes and Primary Hepatocytes', *PLoS One,* 10(7), pp. e0132992.

Park, S.-Y., Lee, S.-M., Ye, S.-K., Yoon, S.-H., Chung, M.-H. and Choi, J. (2006) 'Benzo[a]pyrene-induced DNA damage and p53 modulation in human hepatoma HepG2 cells for the identification of potential biomarkers for PAH monitoring and risk assessment', *Toxicology Letters,* 167(1), pp. 27-33.

Raggi, C., Factor, V. M., Seo, D., Holczbauer, A., Gillen, M. C., Marquardt, J. U., Andersen, J. B., Durkin, M. and Thorgeirsson, S. S. (2014) 'Epigenetic reprogramming modulates malignant properties of human liver cancer', *Hepatology,* 59(6), pp. 2251-62.

Ramaiahgari, S. C., den Braver, M. W., Herpers, B., Terpstra, V., Commandeur, J. N. M. and van de Water, B. (2014) 'A 3D in vitro model of differentiated HepG2 cell spheroids with improved liver-like properties for repeated dose high-throughput toxicity studies', *Arch Toxicol,* 88, pp. 1083-95.

Riffle, S., Pandey, R. N., Albert, M. and Hegde, R. S. (2017) 'Linking hypoxia, DNA damage and proliferation in multicellular tumor spheroids', *BMC Cancer,* 17(1), pp. 338.

Shah, U. K., Mallia, J. O., Singh, N., Chapman, K. E., Doak, S. H. and Jenkins, G. J. S. (2018) 'Reprint of: A three-dimensional in vitro HepG2 cells liver spheroid model for genotoxicity studies', *Mutat Res Genet Toxicol Environ Mutagen,* 834, pp. 35-41.

Stampar, M., Sedighi Frandsen, H., Rogowska-Wrzesinska, A., Wrzesinski, K., Filipic, M. and Zegura, B. (2020) 'Hepatocellular carcinoma (HepG2/C3A) cell-based 3D model for genotoxicity testing of chemicals', *Sci Total Environ*, pp. 143255.

Tascher, G., Burban, A., Camus, S., Plumel, M., Chanon, S., Le Guevel, R., Shevchenko, V., Van Dorsselaer, A., Lefai, E., Guguen-Guillouzo, C. and Bertile, F. (2019) 'In-Depth Proteome Analysis Highlights HepaRG Cells as a Versatile Cell System Surrogate for Primary Human Hepatocytes', *Cells,* 8(2).

Terashima, J., Goto, S., Hattori, H., Hoshi, S., Ushirokawa, M., Kudo, K., Habano, W. and Ozawa, S. (2015) 'CYP1A1 and CYP1A2 expression levels are differentially regulated in three-dimensional spheroids of liver cancer cells compared to two-dimensional monolayer cultures', *Drug Metab Pharmacokinet,* 30(6), pp. 434-40.

Vorrink, S. U., Ullah, S., Schmidt, S. F., Nandania, J. T., Velagapudi, V., Beck, O., Ingelman-Sundberg, M. and Lauschke, V. M. (2017) 'Endogenous and xenobiotic metabolic stability of primary human hepatocytes in long-term 3D spheroid cultures revealed by a combination of targeted and untargeted metabolomics', *Faseb Journal,* 31(6), pp. 2696-2708.

Wang, H., Brown, P. C., Chow, E. C. Y., Ewart, L., Ferguson, S. S., Fitzpatrick, S., Freedman, B. S., Guo, G. L., Hedrich, W., Heyward, S., Hickman, J., Isoherranen, N., Li, A. P., Liu, Q., Mumenthaler, S. M., Polli, J., Proctor, W. R., Ribeiro, A., Wang, J. Y., Wange, R. L. and Huang, S. M. (2021) '3D cell culture models: Drug pharmacokinetics, safety assessment, and regulatory consideration', *Clin Transl Sci,* 14(5), pp. 1659-1680.

Waring, M. J., Arrowsmith, J., Leach, A. R., Leeson, P. D., Mandrell, S., Owen, R. M., Pairaudeau, G., Pennie, W. D., Pickett, S. D. and Wang, J. (2015) 'An analysis of the attrition of drug candidates from four major pharmaceutical companies', *Nature reviews Drug discovery,* 14(7), pp. 475-486.

Wrzesinski, K., Magnone, M. C., Hansen, L. V., Kruse, M. E., Bergauer, T., Bobadilla, M., Gubler, M., Mizrahi, J., Zhang, K., Andreasen, C. M., Joensen, K. E., Andersen, S. M., Olesen, J. B., Schaffalitzky de Muckadell, O. B. and Fey, S. J. (2013) 'HepG2/C3A 3D spheroids exhibit stable physiological functionality for at least 24 days after recovering from trypsinisation', *Toxicology Research,* 2(3), pp. 163-172.

Wrzesinski, K., Rogowska-Wrzesinska, A., Kanlaya, R., Borkowski, K., Schwammle, V., Dai, J., Joensen, K. E., Wojdyla, K., Carvalho, V. B. and Fey, S. J. (2014) 'The cultural divide: exponential growth in classical 2D and metabolic equilibrium in 3D environments', *PLoS One,* 9(9), pp. e106973.

Xie, P., Liang, X., Song, Y. and Cai, Z. (2020) 'Mass Spectrometry Imaging Combined with Metabolomics Revealing the Proliferative Effect of Environmental Pollutants on Multicellular Tumor Spheroids', *Anal Chem,* 92(16), pp. 11341-11348.

Chapter 8. APPENDICES

1. GENERAL MATERIALS AND METHODS

PCR primer selection criteria

Properties of ideal primers

- qPCR primers require an annealing temperature of between 50 – 65˚C. The Tm is defined as the temperature at which 50% of primers molecule will be disassociated from the parent strand at any point. The annealing temperature is normally set at 2-5˚C below the melting temperature or Tm (with WT taq) and a Tm-2˚C for highly efficient polymerase such as Phusion. An annealing temperature based on the above, is sufficiently stringent to confer specific (i.e. single site) binding but at the same time relaxed enough to enable adequate priming and thus efficient amplification of product. If primers incorporate 50 – 60 % GC, the above equates to a primer length of between 18 – 25 bases.
- Primers with AT rich sequences will need to be longer in order to preserve the Tm value.
- Primer up to 25bp can be synthesised at 50 n mole scale and desalted. However, for primers longer than 30 bp, HPLC will be needed in their production, as a significant population of the primer during production will have their chain terminated prematurely, which will interfere with your PCR.
- The middle region of the primers should be GC biased in order to confer binding ("GC Clamp")

Guidelines for design

1. Go to: http://primer3plus.com/cgi-bin/dev/primer3plus.cgi OR
2. Pick primer location in such that GC clamp is in the middle or towards the 3' end of the primer
3. On average, make primers 18-22 bps and incorporate 50-60% GC: average Tm of ~ 60 ˚C
4. Avoid runs of 3 or more of the same bases, particularly G's & C's or consecutive G's
5. Keep primer Tm's in an optimal window of 55-65 ˚C
6. Ensure that primer pairs have Tm's within 2 ˚C of one another

Pay attention to the last 5 bases:

- Preferably terminate with either a 'G' or 'C' residue preceded by a 'C' or 'T'
- Double purine termination, i.e. 'GG'; 'GC' or 'CC' is acceptable constituting a so called 'GC clamp'
- Avoid terminating with 'T' residues
- Avoid > 2 G/C residues in last 3' bases
- If primer must end in 2-3 'G' or 'C' residues due to restricted placement, terminate with an 'A' residue

- With candidate primers, verify their Tm by using calculators such as https://eu.idtdna.com/pages/tools/oligoanalyzer
- Screen for secondary structures (e.g. hairpin loops)
- Screen for self-annealing (e.g. primer dimer formation)
- Screen for inter-primer binding (e.g. dimer formation)

BLAST primer to confirm sequence match to target:
(https://blast.ncbi.nlm.nih.gov/Blast.cgi?PAGE_TYPE=BlastSearch**)**

Key resources tables

Chemical and biological reagents

Reagent	Source	Identifier
2-aminoanthracene	Merck Life Sciences	Cat#A38800
4-nitroquioniline-1-oxide	Merck Life Sciences	Cat#N8141
Acetaminophen	Cayman Chemical	Cat#10024
amino-1-methyl-6-phenylimidazo[4,5-b]pyridine	Cayman Chemical	Cat#22590
Annexin binding buffer	Thermo Fisher Scientific (Invitrogen)	Cat#BMS500BB
Benzo[a]pyrene	Merck Life Sciences	Cat#B1760
Beta mercaptoethanol	Merck Life Sciences	Cat#M3148
Bovine Serum Albumin	Fisher Scientific	Cat#BP9702-10E
Calcein AM	Biotium	Cat##80011
CellTracker green CMFDA	Thermo Fisher Scientific (Molecular probes)	Cat#C2925
Cinchophen	Alfa Aeser	Cat#A18734
Diclofenac	Cayman Chemical	Cat#70680
dimethylsulphoxide	Merck Life Sciences	Cat#473201
DPX mounting medium	CellPath Ltd	Cat#SEA-1304-00A
Draq7	BioStatus Ltd	Cat#DR71000
Eosin staining solution	PFM medical	Cat#PRC/66/1
Ertythrosine B stain	Merck Life Sciences	Cat#E8886
Haematoxylin staining solution	PFM medical	Cat#PRC/R/51
Hoescht 33342	Merck Life Sciences	Cat#62249
Low melting agarose	Merck Life Sciences	Cat#A9414
LPS from E.coli	Merck Life Sciences	Cat#L4391
Molecular Biology Grade Agarose	Merck Life Sciences	Cat#A9539
Paraformaldehyde	Alfa Aeser	Cat#J61899
Phalloidin-565	Biotium	Cat#00040
Phorbol myristate acetate	Cayman Chemicals	Cat#10008014
ProLong Gold Anti-fade mountant	Thermo Fisher Scientific (Life Technologies Ltd)	Cat#P36930
Propidium Iodide	Merck Life Sciences	Cat#P3566
Recombinant human Interleukin-10	Peprotech EC Ltd	Cat#200-10
Recombinant human Interleukin-4	Peprotech EC Ltd	Cat#200-04
Recombinant Human IFN-y	Peprotech EC Ltd	Cat#300-02
Recombinant Human IL-13	Peprotech EC Ltd	Cat#200-13
Ribolock Rnase Inhibitor	Thermo Fisher Scientific (Life Technologies Ltd)	Cat#EO0381
SYBR Gold Nucleic acid stain	Thermo Fisher Scientific (Life Technologies Ltd)	Cat#S11494
Tissue-Tek OCT cutting compound	Sakura Finetek Europe B.V.	Cat#4583
Triton X-100	Merck Life Sciences	Cat#X100-1L

Trovafloxacin	Cayman Chemical	Cat#9000303
Type I agarose	Merck Life Sciences	Cat#A0169
Type VII agarose	Merck Life Sciences	Cat#A4018
Van Geison staining solution	PFM medical	Cat#PRC/R/54

Cell culture

Item	Source	Identifier
Human hepatocellular carcinoma cells	American Type Culture Collection	HepG2/C3A Cat#ATCC CRL-10741
Human hepatic stellate cells	Friedman Group, Icahn School of Medicine at Mount Sinai, New York, USA	LX-2
Human acute monocytic leukaemia cells	Khanim Group, School of Biomedical Sciences, University of Birmingham	THP-1
Human dermal endothelial cells	American Type Culture Collection	hMEC-1 Cat#ATCC CRL-3243
Cultrex Poly-D-Lysine	R&D Systems a biotechne brand	Cat#3439-100-01
Dexamethasone	Thermo Fisher Scientific (Gibco)	Cat#11965092
Dulbeccos' Modified Eagles Medium	Thermo Fisher Scientific (Gibco)	Cat#21875091
Foetal Bovine Serum	Merck Life Sciences	Cat#F7524
Human Recombinant EGF	Thermo Fisher Scientific (Gibco)	Cat#12604-021
Hydrocortisone	Merck Life Sciences	Cat#G7513
ITS Liquid	Thermo Fisher Scientific (Gibco)	Cat#15140122
L-glutamine	Merck Life Sciences	Cat#M8537-1L
MCB131 Medium	Merck Life Sciences	Cat#13146-5ml
Penicilin – streptomycin (10,000 U/mL)	Merck Life Sciences	Cat#D4902
RPMI 1640	Peprotech EC Ltd	Cat#AF-10015-100
TrypLExpress	Merck Life Sciences	Cat#H0888

Molecular probes

Probe	Source	Identifier	Use
Alexafluor 488 secondary Ab (anti-Ms)	Thermo Fisher Scientific (Life Technologies Ltd)	Cat#A31574	1/200
Alexafluor 594 secondary Ab (anti-Rb)	Thermo Fisher Scientific (Life Technologies Ltd)	Cat#A11012	1/200
MKI67 Ab	Origine	Cat#TA500265	1/50
CK18 Ab	Abcam	Cat#ab133263	1/50
HNF4A Ab	Cell Signalling	Cat#3113s	1/500
EPCAM Ab	Progen	Cat#61004	1/50
Gamma H2AX Ab	Merck-Milipore	Cat#05-636	1/200

Primers for quantitative PCR

Gene symbol	Gene ID	Forward primer	Reverse primer
18S	18S RNA	GTAACCCGTTGAACCCCATT	CCATCCAATCGGTAGTAGCG
ACTB	beta actin	ACTCTTCCAGCCTTCCTTCC	GTTGGCGTACAGGTCTTTGC
AFP	alpha foetal protein	TTTTGGGACCCGAACTTTCC	CATCCTGCAGACAATCCAGC
AHR	aryl hydrocarbon receptor	ATCCATACCGAAGACCGAGC	GACCAGTGGCTTCTTCAATTCC
ALB	albumin	AAAGCATGGGCAGTAGCTCG	GCATTCCGTGTGGACTTTGG
ARNT	aryl hydrocarbon receptor nuclear translocator	CTACTGCCAACCCCGAAATG	CCGCTTAATAGCCCTCTGGA
BRACA2	breast cancer type 2 susceptibility gene	GTTTCCACACCTGTCTCAGC	GGTGGAGGTAAAGGCAGTCT
BSEP	bile salt export pump	TGAGTAAGATTCAGCATGGGC	AAGAGCTTGATTTCCCTGGC
CAR	constitutive androstane receptor	CACAAAACTTCCTCTGCGGG	GTAACTCCAGGTCGGTCAGG
CASP3	caspase 3	GCCTCTTCCCCCATTCTCAT	CTTCCATGTATGATCTTTGGTTCC
CDK2	cyclin dependant kinase 2	CATCTTTGCTGAGATGGTGACT	ACTTGGCTTGTAATCAGGCAT

CDK7	cyclin dependant kinase 7	CTCGGGCAAAGCGTTATGAG	CTCTGGCCTTGTAAACGGTG
CDKN1A	cyclin-dependent kinase inhibitor 1	GCCGAAGTCAGTTCCTTGTG	CATGGGTTCTGACGGACATC
CPS1	carbamoyl phosphate synthetase I	CGCAAGGAGCCATTGTTTGG	TGATTCTGCCCTCTGTTGGC
CYP1A1	cytochromes P450 1A1	CGACACTCTTCCTTCGTCCC	ACCCATAGCTTCTGGTCATGG
CYP1A2	cytochromes P450 1A2	GAGGTTCCTGTGGTTCCTGC	GACTGTGTCAAATCCTGCTCC
CYP2C19	cytochromes P450 2C19	GCAGCTGACTTACTTGGAGC	TGTATCTCTGGACCTCGTGC
CYP2C9	cytochromes P450 2C9	CAGAGACGACAAGCACAACC	TGTATCTCTGGACCTCGTGC
CYP2D6	cytochromes P450 2D6	CATCACCAACCTGTCATCGG	GCAGGGAGGTGAAGAAGAGG
CYP2E1	cytochromes P450 2E1	AATTGACAGGGTGATTGGGC	AAAATGGTGTCTCGGGTTGC
CYP3A4	cytochromes P450 3A4	CTGGCTATGAAACCACGAGC	TGAGCGTTTCATTCACCACC
E2F1	E2F transcription factor 1	CTTCGTAGCATTGCAGACCC	TATGGTGGCAGAGTCAGTGG
EPHX	epoxide hydrolase	GTTTCGGGAGGTTTCTTGGC	ATTCAGAGCAGAGCCTACGG
ERCC4	excision repair cross-complementing rodent repair deficiency, complementation 4	GGCCAAGGTTCCATGTAGCA	TCAAGCGATGGGTTATGGCA
GADD45A	growth Arrest and DNA Damage Inducible Alpha	CACTGTCGGGGTGTACGAAG	CCTGGATCAGGGTGAAGTGG
GAPDH	glyceraldehyde 3-phosphate dehydrogenase	CACTAGGCGCTCACTGTTCT	GCCCAATACGAC CAAATCCGT
GSTM1	glutathione s-transferase mu-1	TGGACTTTCCCAATCTGCCC	ATCTTCTCCTCTTCTGTCTCCC
HIF1A	hypoxia inducing factor 1	GACAAGCCACCTGAGGAGAG	ACGCGGAGAAGAGAAGGAAA
HNF1A	hepatocyte nucelar factor 1	CTTGGCTAGTGGGGTTTTGG	CTGGATCAGTGCCTCTTTGC
HNF4A	hepatocyte nucelar factor 4	AAGAATGGTGTGGGAGAGGG	AGCCTCATTACTCTCACCCG
HUS1	checkpoint protein HUS1	GACTTGGTGTAGTAGCCAGAA	CGGGGTGAACACACTGAAAT
MDM2	mouse double minute 2 homolog	CGAGCTTGGCTGCTTCTG	GTACGCACTAATCCGGGGAG
MGST1	microsomal glutathione s-transferase -1	TAGAACGTGTACGCAGAGCC	GTGGTAGATCCGTGCTCCG
MKI67	antigen KI67	ACTCCAAAGAAGCCTGTGGG	AGTTGTTGAGCACTCTGTAGGG
MRP2	multidrug resistance-associated protein 2	AGCCATAGAGCTGGCCC	AACCAGGAGCCATGTGCC
NAT1	N-acetyltransferase 1	AATACAGCACTGGCATGATTCAC	GGAAGATACAAGGCACCTGAGG
NAT2	N-acetyltransferase 2	GGCCAAAGGGATCATGGACA	CTTCTCAAAGGGAACAGCCCG
NFKB1	nuclear factor kappa B	CTTAGGAGGGAGAGCCCAC	CTTCTGCCATTCTGAAGCCG
NQO1	NAD(P)H dehydrogenase [quinone] 1	GGACTGCACCAGAGCCAT	TCCTTTCTTCTTCAAAGCCG
NRF2	nuclear factor erythroid 2-related factor 2	ACCAAAACCACCCTGAAAGC	AGGCCAAGTAGTGTGTCTCC
PXR	pregnane X receptor	ACTTCAGTGGGAATCTCGGC	CCTCTTGGACTGCTTGGTGG
RBBP8	retinoblastoma-binding protein 8	CTCAGAAAGTGCTCGCTTCC	TCTGCAGAGTTAGGGCTTCC
SERTAD1	SERTA domain-containing protein 1	GCCGTTTCCTGATTGGTTGT	AGACCCTTGCTCAGCATCTT
SULT1A1	sulfotransferase 1A1	AAGGTGGTCTATGTTGCCCG	GATCCGTAGGACACTTCTCCG
SULT1A2	sulfotransferase 1A2	CAAAGGATGTGGCGGTTTCC	CCCATAGGACACTTCTCCAGC
TP53	tumour protein 53	GTGACACGCTTCCCTGGATT	ACAGTCAGAGCCAACCTCAG
TP63	tumour protein 63	GCTTATCAACCCTCAGCAGC	ACAATGCTGCAATCTGTGGG
TP73	tumour protein 73	GACGGAATTCACCACCATCC	CCTCATCAGCTTTTCGGTCG
UGT1A1	UDP -glucuronosyltransferase 1A1	CAAAACGATCTGCTTGGTCAC	TCCAGCTCCCTTAGTCTCCA
UGT1A3	UDP -glucuronosyltransferase 1A3	ACCCGACCATCGAATCTTGC	GCATGGGTGATAAAGGCACG
UGT1A6	UDP -glucuronosyltransferase 1A6	ACTTGTCTCAGGAATTTGAAGCC	AGATTCGATGGTCGGGTTCC

Commercial assay kits

Item	Source	Identifier
CELLSTAR Cell-Repellent 96-well plates	Greiner Bio-One	Cat#650970
CellTiter-Glo 3D Luminescent Cell Viability Assay	Promega	Cat#G9681
EZ-PCR Mycoplasma test kit	Biological Industries	Cat#K1-0210
High-Capacity cDNA Reverse Transcription Kit	Applied Biosystems	Cat#4368813
High Sensitivity DNA screentapes	Agilent Technologies Inc.	Cat#5067-5584
High Sensitivity RNA screentapes	Agilent Technologies Inc.	Cat#5067-5579
High Sensitivity RNA quantification kit	Agilent Technologies Inc.	Cat#Q32852
NEBNext Multiplex Oligos for Illumina Primer Pairs	New England Biolabs	Cat#E6440L
NEBNext Poly(A) mRNA Magnetic Isolation Module	New England Biolabs	Cat#E7490L
NEBNext Ultra II Directional RNA Library Prep Kit	New England Biolabs	Cat#E7420L
PowerUP SYBR Green Master Mix	Applied Biosystems	Cat#A25741
RNAeasy Mini Kit	Qiagen	Cat#74106
RNase-Free DNase Set	Qiagen	Cat#79254
Roche LightCycler PCR plates	Greiner Bio-One	Cat#652285
Seahorse Xfe96 Spheroid microplate	Agilent Technologies Inc.	Cat#102978-100
Seahorse Xffe96 Extracellular flux assay kit	Agilent Technologies Inc.	Cat#W23720
Seahorse Xfe24 islet capture flux pak	Agilent Technologies Inc.	Cat#103518-100

Seahorse Xfe24 microplate	Agilent Technologies Inc.	Cat# 100867 100
Black-walled microplate	Greiner Bio-One	Cat#655076
White walled microplate		
Standard 96 well TC plate	Greiner Bio-One	Cat#650160
Tissue culture flask	Greiner Bio-One	Cat#658175

Software and packages

Software/package	Source	Identifier/reference
GraphPad Prism 9	GraphPad Software	Version 9.1.0: https://www.graphpad.com/
Comet Assay IV imaging system	Instem Ltd	Version 4.3.1: https://www.instem.com/solutions/genetic-toxicology/comet-assay.php
FIJI ImageJ	ImageJ	Version 2.0.0-rc-68/1.52g: https://fiji.sc
FlowJo Software	FlowJo, LLC	Version 10.6.2: https://www.flowjo.com
PrimerBlast Tool	National Center for Biotechnology Information, USA	https://www.ncbi.nlm.nih.gov/tools/primer-blast/
RStudio (packages defined in thesis text)	RStudio, Inc	Version 1.0.153: https://www.rstudio.com
SeaHorse Analytics	Agilent Technologies, Inc	Cloud license: https://seahorseanalytics.agilent.com

Equipment

Instrument	Source	Identifier
A1R Inverted Confocal Microscope	Nikon Instruments, Inc.	-
Automated Tissue Processor	INTELSINT Srl	Cat#906.004
Axiovert 10 epifluorescence microscope	Carl Zeiss Ltd	-
DNBSeq NGS platform	BGI, China	Cat#DNBSeq
Inifinite Pro 200 microplate reader	Tecan Trading AG	Cat#INF-FPLEX
LightCycler 480 PCR instrument	Roch Diagnostics GmbH	Cat#04545885001
Nanodrop-8000 Spectrophotometer	Thermo Fisher Scientific (Applied biosytems)	Cat#NG-8000-GL
NxT Attune Flow Cytometer	Thermo Fisher Scientific (Applied biosytems)	
Tapstation 2200	Agilent Technologies, Inc	Cat#G2964AA
Thermal Cycler	Eppendorf Ltd	Cat#5331
Qubit 4 fluoremeter	Thermo Fisher Scientific	Cat#Q33238

2. METHODS PROTOCOLS AS PART OF CHAPTER 4 OF THESIS (Coltman et al., 2021b)

Description of appendix contents

A series of methods protocols which append thesis **Chapter 4** and are published in Journal of Visualised Experiments (Coltman, N. J et al., 2021, DOI: 10.3791/63346)

Materials list

Name of Material/ Equipment	Company	Catalog Number	Comments/Description
A549	**ECACC**	#86012804	Lung carcinoma cell line
Agilent Seahorse XF RPMI Medium, pH 7.4	Agilent Technologies Inc.	103576-100	XF assay medium with 1mM HEPES, without phenol red, sodium bicarbonate, glucose, L-glutamine, and sodium pyruvate
Agilent Seahorse XFe96 Extracellular Flux Analyzer	Agilent Technologies Inc.	-	Instrument for measuring rates of spheroid oxygen uptake in single spheroids
Antimycin A	Merck Life Science	A8674	Mitochondrial respiratory complex III inhibitor
BAM15	TOCRIS bio-techne	5737	Mitochondrial protnophore uncoupler
Black-walled microplate	Greiner Bio-One	655076	For fluorescence-based assays
CELLSTAR cell-repellent surface 96 U well microplates	Greiner Bio-One	650970	Microplates for generating spheroids
CellTiter-Glo 3D Cell Viability Assay	Promega	G9681	Assay for the determination of cell viability in 3D microtissue spheroids
Cultrex Poly-D-Lysine	R&D Systems a biotechne brand	3439-100-01	Molecular cell adhesive for coating XFe96 spheroid microplates to facillitate attachment of spheroids
D-(+)-Glucose	Merck Life Sciences	G8270	Supplement for cell culture growth and XF assay medium
Dulbecco's Modified Eagles Medium (DMEM)	Gibco	11885084	Culture medium for HepG2/C3A spheroids
EVOS XL Core Imaging System	Thermo Fisher Scientific	AMEX1000	Phase contrast iamging microscope
EZ-PCR Mycoplasma test kit	Biological Industries	20-700-20	Mycoplasma screening in cell cultures
FIJI Is Just Image J			Analysis of collated images
Foetal bovine serum	Merck Life Science	F7524	Supplement for cell culture medium
HepG2/C3A	ATCC	#CRL-10741	Hepatic carcinoma cell line, a clonal derivative of the parent HepG2 cell line
Lactate-Glo	Promega	J5021	Assay for measurement of lactate within spheorid culture medium
L-glutamine (200 mM solution)	Merk Life Sciences	G7513	Supplement for cell culture growth and XF assay medium
M50 Stereo microscope	Leica Microsytems	LEICAM50	Stereo dissection micrscope; used for spheorid handling
MCF-7	ECACC	#86012803	Breast adenocarcinoma cell line
Oligomycin from *Streptomyces diastatochromogenes*	Merck Life Science	O4876	ATP Synthase Inhibitor
Penicilin-Streptomycin	Gibco	15140122	Antibiotics added to cell culture medium
Quant-iT PicoGreen dsDNA Assay Kit	Initrogen	P7589	Analysis of dsDNA in spehroids
Rotenone	Merck Life Science	R8875	Mitochondrial Respiratory Complex I Inhibitor
RPMI 1640	Gibco	21875091	Culture medium for A549, MCF7, and SK-OV-3 spheroids
Seahorse Analytics	Agilent Technologies Inc.	Build 421	https://seahorseanalytics.agilent.com
Seahorse XFe96 Spheroid FluxPak	Agilent Technologies Inc.	102905-100	Each Seahorse XFe96 Spheroid FluxPak contains: 6 Seahorse XFe96 Spheroid Microplates (102978-100), 6 XFe96 sensor cartridges, and 1 bottle of Seahorse XF Calibrant Solution 500 mL (100840-000)
Serological pipette: 5, 10, and 25 mL	Greiner Bio-One	606107; 607107; 760107	Consumables for cell culture
SK-OV-3	ECACC	#HTB-77	Ovarian adenocarcinoma cell line
Sodium pyruvate (100 mM solution)	Merck Life Science	S8636	Supplement for cell culture growth and XF assay medium
T75 cm^2 cell culture flask	Greiner Bio-One	658175	Tissue culture treated flasks for maintaining cell cultures
TrypLExpress	Gibco	12604-021	Cell dissociation reagent
Wave controller software	Agilent Technologies Inc.	-	
Wide orifice tip	STARLAB International GmbH	E1011-8400	Pipette tips with wide opening for spheroid handling

1.1. Cultivation of cancer cell lines as 3D *in vitro* spheroids

Table 1. Cancer cell line media and XF media compositions

Cell line	Description	Culture medium	Source
A549	Lung carcinoma cell line	RPMI 1640	European Collection of Authenticated Cell Cultures (ECACC)
		Sodium pyruvate (1 mM)	
		Penicillin- Streptomycin - (100 U/mL – 100 mg/mL)	
		10 % (v/v) FBS	
HepG2/C3A	Hepatic carcinoma cell line, a clonal derivative of the parent HepG2 cell line	DMEM	American Tissue Culture Collection (ATCC)
		Penicillin- Streptomycin - (100 U/mL – 100 mg/mL)	
		10 % (v/v) FBS	
MCF7	Breast adenocarcinoma cell line	RPMI 1640	European Collection of Authenticated Cell Cultures (ECACC)
		Sodium pyruvate (1 mM)	
		Penicillin- Streptomycin - (100 U/mL – 100 mg/mL)	
		10 % (v/v) FBS	
SK-OV-3	Ovarian adenocarcinoma cell line	RPMI 1640	European Collection of Authenticated Cell Cultures (ECACC)
		Sodium pyruvate (1 mM)	
		Penicillin- Streptomycin - (100 U/mL – 100 mg/mL)	
		10 % (v/v) FBS	

Component	**RPMI assay medium (50 mL final volume)**
Base Medium	Agilent Seahorse XF RPMI, pH 7.4
Glucose (1M sterile stock)	11 mM (0.55 mL stock solution)
L-glutamine (200 mM sterile stock)	2 mM (0.5 mL of stock solution)
Sodium pyruvate (100 mM sterile stock)	1 mM (0.5 mL of stock solution)

1.1. Culture all cell lines using standard aseptic tissue culture technique and confirm that they are free of mycoplasma using a suitable assay kit.

1.2. Culture the cell lines in T75 tissue culture flasks or equivalent, using the recommended medium (**Table 1**). Culture the cell lines to 65–80% confluency and passage them regularly up to a maximum of 25 passages.

1.3. Rinse the cell culture flasks twice in Dulbecco's modified phosphate-buffered saline (DBPS).

1.4. Detach the cells from the flasks with 3 mL of the cell dissociation reagent (see the **Table of Materials**) for 5 min at 37 °C and confirm the detachment by microscopy.
1.5. Aspirate the detached cell suspension gently to ensure a single-cell suspension and deactivate the cell dissociation reagent with 7 mL of complete tissue culture medium.
1.6. Collect the cells by centrifugation at 300 × *g* for 5 min, discard the supernatant, and resuspend the cells in complete medium.
1.7. Count the cells using a hemocytometer or an automated cell counter and titrate to the desired cell density required for seeding.
NOTE: To seed an entire 96-well plate at 100 µL/well at 4×10^3 cells/well, cells should be titrated to 4×10^4 cells/mL in a recommended volume of 12 mL.
1.8. Decant the cell suspension into a sterile reservoir and dispense 100 µL of the cell suspension into each well of a cell-repellent microplate using a multichannel pipettor.
NOTE: Only the inner 60 wells of a microplate should be seeded and the remainder filled with DPBS. This will form an evaporation barrier, ensure spheroid homogeneity across the plate, and minimize plate edge effects.
1.9. Centrifuge spheroid microplates at 300 x *g* for 15 min to force the cells into loose aggregates.
1.10. Incubate the plates at 37 °C, 5% CO_2 for a minimum of 3 days to ensure spheroid formation.
1.11. Perform phase contrast microscopy using standardized laboratory practices to monitor the growth of spheroids. Replenish the cell culture medium every 3 days or twice weekly by performing a half-volume medium exchange.

2. Probing mitochondrial energy metabolism of single spheroids using Extracellular Flux (XF) Technology

2.1. Assay preparation (one day prior)
2.1.1. Check spheroid viability using an inverted light microscope with phase contrast at 4x magnification to ensure intact spheroid structure, morphology, and overall uniformity between samples.
2.1.2. Hydrate the sensor cartridge.
2.1.2.1. Aliquot ~20 mL of the calibrant into a conical tube.
2.1.2.2. Place the conical tube containing the calibrant in a non-CO_2 37 °C incubator overnight.
2.1.2.3. Open the assay kit and remove the contents.
2.1.2.4. Remove the sensor cartridge from the utility plate and place it upside down on the worktop next to the utility plate.

2.1.2.5. Pipette 200 µL of sterile ddH_2O into each well of the sensor cartridge utility plate using a multichannel P300 pipette.
2.1.2.6. Place sensor cartridge on top of utility plate.
2.1.2.7. Check that the water level in each well is high enough to submerge the sensor probes.

2.1.2.8. Transfer the assembled sensor cartridge to a non-CO2 37 °C incubator and leave it overnight.

NOTE: This step can be performed 12–72 h prior to assay commencement.

2.2. Coat spheroid assay microplate

2.2.1. Using aseptic technique, add 30 µL/well of sterile Poly-D-Lysine (0.1 mg/mL) solution to the spheroid microplate and incubate it for 30 min at room temperature.

2.2.2. Aspirate the solution from each well of the spheroid microplate, invert the plate, and tap it firmly onto tissue paper to remove any residual solution.

2.2.3. Wash the plate twice with 200 µL/well of sterile ddH_2O.

2.2.4. After the final wash, invert the microplate and tap it firmly onto tissue paper to remove any residual water.

2.2.5. Allow the plate to air-dry for 30 min before using or storing it at 4 °C for future use.

NOTE: The spheroid assay microplate should be coated with a molecular adhesive to ensure that the spheroids are fixed at the bottom of the microplate. Without a molecular adhesive, spheroids can become dislodged and interfere with assay results. Other molecular adhesives can also be used as an alternative to Poly-D-Lysine for precoating plates. Precoated plates can be stored at 4 °C but should be left to equilibrate to room temperature before assay commencement.

2.3. Prepare XF Assay medium

2.3.1. Prepare XF RPMI medium, as detailed in **Table 1**, and sterile-filter with a 0.22 µm syringe filter

2.4. Assay preparation (1 h prior to assay)

2.4.1. Prewarm the supplemented XF RPMI assay medium to 37 °C.

2.4.2. Prewarm the coated spheroid assay microplate in a non-CO_2 37°C incubator or dry bath.

2.4.3. Prepare the sensor cartridge.

2.4.3.1. Take out the conical tube containing the calibrant and the sensor cartridge from the air incubator.

2.4.3.2. Remove the sensor cartridge from the utility plate and place it upside down on the worksurface.

2.4.3.3. Using a P300 multichannel pipette, aspirate the water from the utility plate and discard it.

2.4.3.4. Pour the calibrant solution into a sterile reagent reservoir and add 200 µL/well of the prewarmed calibrant to the utility plate using a P300 multichannel pipette.

2.4.3.5. Pick up the sensor cartridge and place it back on top of the utility plate, making sure the sensors are well submerged in the calibrant.

2.4.3.6. Transfer the assembled sensor cartridge back into the non-CO_2 37 °C incubator until ready to load the port injection solutions.

2.5. Wash the spheroids with the assay medium.

2.5.1. Remove the spheroid culture plate from the 37 °C, 5% CO_2 incubator and observe the spheroids under the microscope to ensure their integrity prior to the spheroid transfer steps.

2.5.2. Load all wells of the spheroid plate with 180 µL/well of prewarmed assay medium, including any background correction wells.

2.5.3. Partially-fill a 7 cm Petri dish with 3 mL of the assay medium.

2.5.4. Using a multichannel pipette loaded with wide orifice pipette tips, transfer the spheroids from the 96-well culture plate into 7 cm Petri dishes by setting the pipettor at an aspiration volume of 10–50 µL.

2.6. Seed spheroids into the pre-coated spheroid assay microplate

2.6.1. Using a dissection microscope and a light-box apparatus, transfer the spheroids from the Petri dish to the spheroid assay microplate as detailed below.

2.6.1.1. Set the volume of a single-channel pipettor fitted with a wide orifice pipette tip to 20 µL and carefully aspirate a single spheroid. Place the tip directly in the center of each well of the spheroid assay microplate and allow gravity to elute a single spheroid into the center of each well, i.e., do not expel any medium from the pipette tip and allow capillary action to withdraw the spheroid from the pipette tip. To confirm elution, the contents of the pipettor can be pipetted back into the 7 cm Petri dish under the microscope. NOTE: Gravity elution of a single spheroid typically takes 15–30 s depending on spheroid size/density. During this time, the pipettor should not be removed. Any background correction wells should be free of spheroids and only contain assay medium. Under the microscope, confirm the position of each spheroid. Each spheroid should ideally be positioned within the centre of each well.

2.6.1.2. Once all the spheroids have been transferred to the spheroid assay microplate, transfer to a non-CO_2 incubator at 37 °C for a minimum of 1 h prior to the assay.

3. Preparation and loading of compounds into the sensor cartridge for XF assays

Table 2 . Mitochondrial compound concentrations for probing mitochondrial energy metabolism of single 3D spheroids using the XFe96 Analyzer.

Injection Strategy	Compound (Port)	XFe96 microwell starting volume (µL)	Desired final well concentration	Port Volume (µL)	Final XFe96 microwell volume post injection (µL)	Working stock concentration
1	Oligomycin (A)	180	3 ug/mL	20	200	30 µg/mL
	Rotenone (B)	200	2 µM	20	220	22 µM
	Antimycin A (B)	200	2 µM	20	220	22 µM
2	BAM 15 (A)	180	5 µM	20	200	50 µM
	Rotenone (B)	200	2 µM	20	220	22 µM
	Antimycin A (B)	200	2 µM	20	220	22 µM

3.1. Prepare working stock concentrations of each compound as noted in **Table 1** using fully supplemented, prewarmed XF RPMI assay medium.
3.2. Orient the cartridge plate (coupled to the utility plate) column-wise, 1–12 from left to right.
3.3. If using a loading guide, place it atop the cartridge plate according to the well-loading procedure, e.g., if port A is be loaded first, ensure that **A** is visible in the upper-left corner of the guide.
3.4. Transfer the working solution of each compound into a suitable reservoir and using a calibrated P100 multichannel pipette, dispense 20 µL into all corresponding ports. Repeat for each compound into the remaining ports.
NOTE: If any ports are not being used on the sensor cartridge plate, these can be left empty or filled with assay medium. If only a selection of a specific port letter is being used, ensure that the other ports corresponding to that letter are loaded with assay medium; otherwise, air will be injected into the well, compromising the results in those wells.
3.5. After port loading, remove the plate-loading guides (if used) and prepare the analyzer for loading the sensor cartridge.
NOTE: If the assay is not being run immediately after loading the ports, place the lid back on the sensor cartridge and put the plate back in the 37 °C air incubator until ready to load into the machine.

4. Assay design, injection strategies, and data acquisition

4.1. Running the assay
4.1.1. Power on the analyzer and connect to controller (computer).
NOTE: This can be verified by the instrument connection status in the widget panel of the Wave Controller software.
4.1.2. Navigate to the **templates** page in the WAVE software, find the assay template file for the experiment and double-click to open it.
NOTE: If the assay template does not appear on the displayed **Templates** view, import the template file into the template folder from a shared network drive or USB flash drive.
4.1.3. To start the assay, click the **Run Assay** tab.
NOTE: If the group definitions have been allocated within the plate map correctly, the assay will be ready to be run as indicated by the green tick on the right-hand side of the page. At this stage, any additional information can be input on the assay summary page or the page left blank; proceed to the next step. Due to the delayed penetration of mitochondrial modulators in 3D microtissue spheroids (**Chapter 3, Figure 2**), use the measurement protocol information described in **Table 3**.

Table 3: Protocol setup for probing mitochondrial energy metabolism of single 3D spheroids using the XFe96 Analyzer.

Measurement Period	Injection Number and Port	Measurement Details	Period Duration (h:min:s)

Calibration	Not applicable	XF analysers always perform this calibration to make sure measurements are accurate	00:20:00 (this is an average and can vary between machines)
Equillibration	Not applicable	Equilibration occurs after Calibration and it is recommended.	00:10:00
Basal	Not applicable	Cycles = 5 Mix = 3:00 Wait = 0:00 Measure = 3:00	00:30:00
Oligomycin / BAM 15	Injection 1 (Port A)	Cycles = 10 Mix = 3:00 Wait = 0:00 Measure = 3:00	01:00:00
Rotenone + antimycin A	Injection 2 (Port B)	Cycles = 10 Mix = 3:00 Wait = 0:00 Measure = 3:00	01:00:00
Total Time:			**03:00:00**

4.1.4. Click **start run** to bring up the **save location** dialog box.
4.1.5. Enter the **save location** for the result file, and place the assembled sensor cartridge onto the thermal tray that appears from the door on the side of the analyzer. Wait for the thermal tray to open automatically and the screen to display the message **Load Calibrant Utility Plate**. Before following the on-screen prompts, ensure i) the sensor cartridge fits properly on the Utility plate, ii) the lid is removed from the sensor cartridge, and iii) proper orientation (direction) of the sensor cartridge on the Utility plate.

4.1.6. Follow the on-screen commands to initiate sensor cartridge calibration.
NOTE: The time taken to complete calibration is approximately 10–20 min (for assays at 37 °C).
4.1.7 After sensor cartridge calibration, load the spheroid microplate into the analyzer by following the on-screen instructions on the Wave Controller to initiate the 12 min equilibration step.
NOTE: Green boxes with white ticks indicate a ‘good’ calibration for that well. If any wells fail to provide a ‘good’ calibration, they will be indicated with a red box and white cross. Such wells should be noted and excluded from any analysis after the assay is completed using the **modification assay** tab.

4.1.8 Wait for the analyzer to automatically begin acquiring baseline measurements after the machine has completed the equilibration step (as outlined in the instrument protocol).
4.1.9 To complete the experiment, follow the onscreen commands on the WAVE controller.
NOTE: Once the spheroid microplate has been removed from the analyzer, discard the sensor cartridge and set aside the spheroid plate for further analysis if necessary (e.g., double-stranded (ds) DNA quantification). If the microplate is not required for any further analysis, it can be discarded along with the sensor cartridge.
4.1.10 Wait for the assay dialog to appear and view the results or return to **templates** view.

5. Data normalization and analysis strategies—post assay normalization and downstream assays (optional steps)

5.1. Data normalization
5.1.1. To normalize spheroid data, refer to the series of protocols pertinent to data normalization strategies for the calculation of spheroid size and volume and the quantification of dsDNA within spheroid assays. (These are also included below).
5.2. Data analysis
5.2.1. To export data into one of the automated analysis generators, follow the data export commands on the WAVE controller and select the export generator that matches the assay type. Alternatively, export the data result file and upload into Seahorse analytics.
NOTE: The downside of report generators and Seahorse analytics is that data analysis is limited to the way in which the XF assay is designed and does not allow for averages to be taken across measurement cycles. Manual export of datasets from the instrument software allows for user preference in this regard. Given that the injection strategy for assessing mitochondrial respiration of 3D spheroids will likely differ to that of a typical 'MitoStress' test, a series of spreadsheet templates have been developed to help aid in the analysis of these datasets, specific to 3D cell cultures and will be provided upon request. These data template files will provide data on the key mitochondrial respiratory parameters detailed and explained in **Chapter 4, Figure 2** only.
5.2.2. To analyze the data, export the data as a spreadsheet report from the WAVE controller software and use an independent spreadsheet template for analysis.

6. Analysis of spheroid size and volume

The following protocol assumes access to a phase-contrast microscope capable of image acquisition and a basic user knowledge of ImageJ. Proficient users can automate the following steps by creating an analysis script.

6.1. Collect photomicrographs of spheroids by phase contrast microscopy, ensuring the same objective lens is used throughout. Images can also be used to confirm stability of spheroids throughout the XFe assay, e.g., spheroids dislodged during the assay may yield erroneous data (see **Chapter 4, Figure 7)**.

NOTE: Typically, a 2–4X objective lens is suitable for most 100–1,000 mM diameter spheroids.

6.2. Collect photomicrographs of a known image scale.

NOTE: A simple cell culture haemocytometer is suitable as it is manufactured to known dimensions.

6.3. Open ImageJ and import the haemocytometer image.

6.4. Using the **Straight** annotation tool, draw a line between two known points on the haemocytometer image, e.g., each of the 16 squares within the 4 haemocytometer counting areas measures 250 µm x 250 µm (1 mm^2total quadrant) on the typical Neubauer-type haemocytometer.

6.5. Go to **Analyse/Set scale** and set **Known distance: 250** and **Unit of length: µm.** Click to set to **Global.**

6.6. Import spheroid images into ImageJ.

6.7. Using the **Freehand selection** tool, draw around the circumference of each spheroid and collect data by going to **Analyse/Measure** for each spheroid.

6.8. Copy **Measurement table** to clipboard and import into R', Microsoft excel, or equivalent.

6.9. Use **Feret diameter** to estimate spheroid volume (mm^3) using **Feret** and **MinFeret** values according to the following equation:

((0.5) × (Feret value) × (MinFeret value^2))

NOTE: A true spheroid would have Feret/MinFeret value equal to 1; thus these values can also be used to estimate 'roundness' of spheroids.

7. Quantification of dsDNA from spheroids in an XFe96 spheroid microplate

The following steps describe a protocol for quantifying intra-spheroidal dsDNA using the Quant-iT PicoGreen dsDNA Assay Kit. As nuclear dsDNA in spheroids is linearly correlated with cell seeding density or spheroid volume (**Chapter 4, Figure 9**), nuclear dsDNA content is a possible approach to normalize XF data. dsDNA is preferred over protein normalization, particularly where spheroid adhesion to assay culture plates is aided by poly-D-lysine and where pre-treatments may impact protein synthesis. This protocol assumes the final XFe assay well volume to be ~ 240 µL. Adjust the protocol as necessary for other volumes, e.g., spheroids within cell culture growth plates. Users may wish to prepare a standard curve of monolayer cells for DNA quantification to allow estimation of cell number within spheroids.

7.1. Carefully aspirate 190 µL of XF assay medium from each well of the XFe96 spheroid microplate, leaving ~50 µL of assay medium/well.

7.2. Add 50 µL/well of spheroid lysis buffer (supplemented with 20 mg/mL proteinase K), place the plate on ice, and leave to lyse for a minimum of 10–30 min.

NOTE: Shake the assay plate on a plate shaker, if necessary, to help enhance lysis. Larger spheroids may require elongated incubation, and lysis can be confirmed under the microscope. The process of freeze-thawing will also help aid spheroid lysis.

7.3. Add an equal volume (100 µL/well) of 1x Tris-EDTA buffer (10 mM Tris-HCl + 1 mM EDTA, pH 7.4) to reduce sample viscosity.

7.4. Carefully mix lysates within wells by pipette aspiration. Alternatively, use a plate shaker set at 500 rpm.

7.5. Generate a standard curve of lambda DNA in 100 µL of XF assay medium from 2 mg/mL–2 ng/mL DNA.

7.6. Add 100 µL of spheroid lysis buffer to match sample volumes and mix.

NOTE: Final standard curve will be in the range of 1 mg/mL–1 ng/mL after dilution.

7.7. Transfer 20 µL of the spheroid lysate and standards into separate wells of a suitable 96-well microplate for recording fluorescence (preferably black).

7.8. Dilute PicoGreen DMSO stock solution 200-fold to achieve final volume required to complete assay e.g., to achieve analysis of 10 samples at 100 µL final volume, dilute 4 µL of PicroGreen DMSO stock solution in 796 µL of 1x TE buffer.

7.9. Add 80 µL/well of PicoGreen working solution and incubate at room temperature for 2–5 min, protected from light, with gentle intermittent shaking to equilibrate.

7.10. Measure well fluorescence on a fluorescent-based microplate reader with an excitation wavelength of 485nm and emission wavelength of 520nm (485_{EX}–520_{EM}).

8. Recommendations for the number of replicates required to obtain reliable XF assay datasets

We have shown that spheroid positioning within the XF spheroid assay microplates can impact overall values in the final datasets. As with all biological datasets, with enough replicates, such values may have limited impact on the total outcome if it is captured by the standard deviation within the assay; however, this might not always be the case. The Z' prime equation is a form of statistical analysis that compares two groups of data performing as samples or negative control. Users should therefore consider applying the Z' prime equation to subset groups of the XF data for comparison. Unlike other statistical test such as standardized mean difference (SSMD)(Zhang et al., 2007), the Z' primes formula is not robust to outliers (Zhang et al., 1999) and is therefore ideally placed to help users identify erroneous XF assay datapoints or datapoints that do not fit the dispersion of other replicates within the group, as might be the case with the misalignment of spheroids in the assay microplate .

Derivation of the Z' primes equation.

$$Z' = 1 - \frac{3\sigma_{positive\ control\ values} + 3\sigma_{negative\ control\ values}}{|\mu_{positive\ control\ values} - \mu_{negative\ control\ values}|}$$

$3\sigma_{positive\ control\ values} = 3 * \text{standard deviation of sample values in XF assays}$
$3\sigma_{negative\ control\ values} = 3 * \text{standard deviation of control wells values in XF assays}$
$\mu_{positive\ control\ values} = \text{mean of sample values in XF assays}$
$\mu_{negative\ control\ values} = \text{mean of control wells values in XF assays}$

The above equation states that good Z' values can only be obtained when all values, representing both upper and lower, are sufficiently different from each other. In this way, applied to XF data, the 'signal' intensity of both value sets should be significant enough to separate them and the standard deviation should be as low as possible. For example, a strong Z' prime value could be achieved with a large signal discrimination or with tight dispersion of values attributed to the standard deviation.

8.1. Collect values for sample replicate wells (representing positive control values) and for the background correction wells (representing negative control values).

8.2. Derive the mean average and standard deviation for both data groups.

8.3. Apply the Z' primes equation.

Interpretation of Z' prime values.

Z' primes value (z-factor)	**Data interpretation**
1.0	Ideal value but should not exceed
≥ 0.5 - ≤ 1.0	Good discrimination between data groups
≥ 0 - ≤ 0.5	Questionable separation between groups
> 0	The overlap between the control and sample wells is too great.

8.4. To determine the impact of a particular well on the overall dataset, users should omit those values of interest and see how Z' primes is altered. For example, outliers in either data group will affect the Z' primes output.

Using power analysis, Yépez et al. highlight the ideal number of replicates in the XFe96 format to be 12 per sample type (Yepez et al., 2018). Within the context of 3D cell culture, which is often limited by the amount of material available (e.g., cost of 3D cell culture; maintenance of samples), we believe this to be unrealistic and recommend 5–8 samples per condition measured.

3. FUTURE WORK: METHODOLOGY FOR THE PHENOTYPIC SCREENING OF XENOBIOTIC METABOLISM POTENTIAL IN HEPG2/C3A SPHEROIDS AND MONOLAYERS

Disclaimer

Due to the impact of covid-19, prohibiting lack of access to facilities this work has only been partially completed for this thesis and is therefore not presented in the results **Chapter 3**. All samples have been extracted and collected from HepG2/C3A models, including standards, and the analytical workflow completed. We are therefore currently awaiting LC-MS/MS analysis and hope these samples will be ready soon.

Study overview

Building from our initial observations in Chapter 3 concerning the use of a coumarin pro-fluorescent substrate for measuring CYP450 activity in spheroids we looked to develop a high-sensitivity LC-MS/MS assay to monitor xenobiotic biotransformation in HepG2/C3A spheroids. To determine the xenobiotic transformation capacity of HepG2/C3A cells as monolayers or spheroids cultured over time, a 5-CYP dosing cassette regime was developed to assess the metabolic activity of CYP1A, CYP2C9, CYP2C19, CYP2D6 or CYP3A4 using Liquid chromatography mass spectrometry (LC-MS/MS). The choice of CYP450 substrates was optimised from literature searches to seek CYP substrates suitable for the cocktail approach: (Berger et al., 2016, Chen et al., 2016, Pillai et al., 2013, Valicherla et al., 2019), which represent the 5 major Human CYP450 isoforms, responsible for the metabolism of most pharmaceuticals and common xenobiotics. The final choice of substrates is highlighted in Table 1. These substrates also represent those that are considered 'FDA accepted' for use in regulator ADME studies and are exposed to HepG2/C3A models within the range of their approximate K_m values (within isolated microsomal systems, or PHH assay).

1.1.1. Sample preparation and dosing

For each spheroid model, 15 spheroids were pooled into 135 μL of complete phenol red-free DMEM; a monolayer model was established in the same way by seeding HepG2/C3A cells at 1 x 10^5 cells/well. Fifteen microliters of a dosing cassette was titrated into the culture medium according to Table 2. At designated time points (0, 8, 24 or 48 h) 100 μL of culture medium supernatant was sampled and stored at -80 ^oC in sealed polypropylene V-bottomed plates (Greiner Bio-One). The resulting sample pellets were snap-frozen and stored at -80 ^oC for data normalisation using dsDNA content quantification, as in Chapter 5.

Table 1. Five-CYP450 dosing cassette used for xenobiotic biotransformation studies

CYP target	Substrate	10X cassette concentration (μM)	1X final assay concentration (μM)	Expected Metabolite/standards
CYP1A2	Tacrine	50	5	1-hydroxytacrine
CYP2C9	Diclofenac	50	5	4-hydroxydiclofenac
CYP2C19	S-mephenytoin	500	50	4-hydroxymephenytoin
CYP2D6	Bufuralol	100	10	Hydroxybufuralol

CYP3A4	Midazolam	50	5	1-hydroxymidazolam
DMSO	Vehicle buffer	3 %	0.3 %	-

1.1.2. Methodology for bioanalysis

Frozen supernatant samples were thawed and crashed by addition of 50 μL methanol to 50 μL supernatant and mixed at 2000 rpm; incubated at -20 ^{o}C for 2 h and then centrifuged at 3400 rpm over 20 min. Ahead of LC-MS/MS analysis: Standards for the expected metabolites (Table 1) were prepared and titrated in methanol. Standards were prepared by diluting 10 μL of standard with 50 μL of cell culture medium awaiting the addition of methanol containing a specific LC-MS/MS internal standard (TBC), internal standards were also added to all samples and standards. Matched metabolite-standard dosing caseates were created by titrating all standards to achieve a final matrix concentration of 5000 to 1 ng/mL over 12 titration points.

Samples and standards now await analysis by LC-MS/MS

4. REPRESENTATIVE FOUR-PARAMETER LOGISTIC (4PL) CURVES FITTED FROM HEPATOTOXICITY SCREEN IN HEPG2/C3A SPHEROIDS

Description of appendix contents

Representative 4PL curves from hepatotoxicity study in **Chapter 5**